Elaboration of nanofibrous biomimetic scaffolds based on poly(glycerol sebacate) for cardiac tissue engineering

Florence Flaig

UNIVERSITÉ DE STRASBOURG

ÉCOLE DOCTORALE DE PHYSIQUE ET CHIMIE PHYSIQUE

Institut de Chimie et Procédés pour l'Énergie, l'Environnement et la Santé

(ICPEES – UMR 7515)

THÈSE présentée par :

Florence FLAIG

soutenue le **03 décembre 2019**

pour obtenir le grade de **Docteur de l'université de Strasbourg**

Discipline / Spécialité : Chimie des polymères

Élaboration de matériaux nanofibreux biomimétiques à base de poly(sébaçate de glycérol) pour l'ingénierie tissulaire cardiaque

THÈSE dirigée par :
M. Guy SCHLATTER — Professeur des universités, université de Strasbourg

RAPPORTEURS :
Mme Catherine AMIEL — Professeur des universités, université Paris-XII
M. Bernard MARTEL — Professeur des universités, université de Lille

---

AUTRES MEMBRES DU JURY :
Mme Cécile LEGALLAIS — Directeur de recherche, université de technologie de Compiègne
Mme Anne HÉBRAUD — Maître de conférences, université de Strasbourg

TABLE OF CONTENTS

Remerciements

Je tiens tout d'abord à remercier les membres de mon jury, les professeurs Catherine Amiel, Bernard Martel et le docteur Cécile Legallais d'avoir accepté de juger ces travaux de thèse et de me faire l'honneur de leur présence pour ma soutenance. Je remercie également les directeurs de l'Institut de chimie et procédés pour l'énergie, l'environnement et la santé (ICPEES – UMR7515) où a été réalisée cette thèse, de m'avoir accueillie dans leur unité.

Si ces trois années de travail ont pu aboutir à cette thèse, c'est grâce à la contribution de nombreuses personnes et en particulier celle de mes encadrants : le professeur Guy Schlatter, mon directeur de thèse, ainsi que le docteur Anne Hébraud. Alors merci à Guy d'avoir su trouver le temps, malgré son travail de direction, pour me guider, me conseiller, et aussi me corriger et me permettre de progresser. Merci aussi à Anne pour tous les conseils prodigués : des conseils scientifiques, mais aussi des conseils utiles pour la vie d'enseignant-chercheur. Ils me sont très précieux.

Ces travaux ont pu être menés grâce au financement ANR du projet MimHeart. Merci donc à l'ANR et à tous les participants au projet. Merci d'abord au professeur Onnik Agbulut pour avoir coordonné ce projet du point de vue de la biologie et pour m'avoir accueillie dans son laboratoire afin que je découvre comment étaient utilisées les membranes que je leur confiais. Merci à tous les autres biologistes de l'équipe "Cellules souches et biothérapies" de l'Institut de Biologie Paris-Seine avec qui j'ai pu collaborer. En particulier, merci au docteur Hélène Ragot qui a beaucoup travaillé pour révéler le potentiel thérapeutique de mes matériaux ainsi que pour rédiger notre article commun, à Alexandre Simon qui m'a si bien accueillie et expliqué toutes les étapes de la culture cellulaire, à Gaëlle Revet qui m'a démontré ses talents avec les souris, et aussi à Lisa Kitasato et Maria Kitsara. Échanger avec des scientifiques d'un autre domaine a été très enrichissant.

Je voudrais également remercier Damien Favier et Christian Gauthier de l'Institut Charles Sadron grâce à qui j'ai pu ajouter de belles images obtenues par tomographie à la toute fin de ma thèse.

À l'ICPEES, je tiens à remercier tous ceux qui ont pu m'aider, en particulier les membres de l'axe polymères. Merci aux enseignants-chercheurs, le docteur Éric Pollet et le professeur Luc Avérous pour leurs conseils et surtout merci au docteur Nicolas Leclerc qui m'a gentiment prêté une paillasse à mon arrivée. J'ai été accueillie par de nombreuses personnes très serviables. D'abord, merci à Chheng Ngov qui m'a permis de me lancer au laboratoire de chimie. Un grand merci à Christophe Mélart pour avoir su régler tous mes problèmes de rhéomètre et autres machines et d'avoir supervisé la fabrication de pièces qui m'ont été indispensables. À ce sujet, merci aussi à Thierry Djekrif qui les a soigneusement fabriquées. Mille mercis à Christophe Sutter, qui a toujours fait preuve d'une grande patience pour me sauver lorsque j'avais des problèmes informatiques ou autres, en particulier avec mon ordinateur capricieux. Merci à Céline Piras pour sa formidable énergie qui la rend toujours prête à rendre service et indispensable pour l'équipe. Merci à Géraldine Layrac d'avoir passé quelques mois avec moi au laboratoire

d'electrospinning, et merci aussi pour son aide lors des commandes, pour ses conseils de rédaction et pour les viennoiseries ! Merci à Stéphanie Ferry pour les discussions de ces derniers mois, et pour ses efforts pour maintenir une bonne tenue du laboratoire. Un très grand merci à Catherine Kientz pour toute son aide administrative, mais aussi pour son implication dans la vie de l'étage qui nous permet de bénéficier d'un coin cuisine en bon état et de petits-déjeuners communs réguliers.

Les journées de thésards sont souvent égayées par la présence des collègues qui vivent la même expérience ; je tiens donc aussi à remercier les étudiants et post-doctorants que j'ai pu croiser pendant mon séjour à l'ICPEES. D'abord, merci à celles qui étaient là à mon arrivée et qui m'ont donc servi de modèle : les docteurs Morgane Séon-Lutz et Domitille Mailley. À Domitille, merci de m'avoir poussée à faire du sport, et merci d'avoir égayé le bureau pendant ces deux années de cohabitation ! Merci à Meng Liang, pour nos échanges réguliers sur nos conditions de thésards français et chinois et courage à lui pour les derniers mois ! Merci à Mohammad Rammal d'avoir été un sympathique voisin de bureau et surtout d'avoir partagé avec moi cette année de monitorat à l'IUT Robert Schuman. Merci particulièrement aux biologistes qui ont séjourné dans notre bureau et qui m'ont beaucoup éclairée sur les aspects biologiques de mon projet : d'abord, merci au docteur Manon Allais qui a toujours incroyablement su me remonter le moral. Merci au docteur Lisa Terranova qui est venue apporter une touche féminine indispensable à notre bureau, et qui m'a prodigué beaucoup de conseils très utiles sur la rédaction de ma thèse et de mes articles. Et bien-sûr, merci à mon rayon de soleil brésilien, le docteur Caroline Bellani, pour sa joie de vivre qui a illuminé la grisaille strasbourgeoise à chacune de ses venues. C'est un honneur de partager des publications avec une scientifique aussi énergique et volontaire !

Je dois aussi remercier les stagiaires que j'ai supervisés, pour les résultats de leur travail, mais surtout pour m'avoir permis de progresser comme encadrante et enseignante. Alors merci aux « stagiaires labo » Alfred, Mathilde, Océane et Justin, à Zion, et surtout à Özgün qui a travaillé avec moi pendant près d'un an. Et merci aux autres stagiaires, doctorants, post-doctorants ou autres que j'ai croisés, en particulier Thibaud, Ouassim, Lìza, Wassim, Chengzhang, Martin, Rodolphe, Yunhui, Mariana et tous ceux du N2.

Enfin, merci à tous mes proches qui ont été là dans les moments de doute. En particulier, merci à mon mari Théodore pour son soutien quotidien, à mon frère pour m'avoir montré l'exemple, et à mes parents qui nous ont toujours encouragés à poursuivre nos études en nous apportant tout le soutien nécessaire.

Résumé de la thèse en français

1. Contexte et choix du matériau et procédé

1.1. Contexte

Les maladies cardiovasculaires représentent aujourd'hui l'une des principales causes de mortalité. Parmi elles, les infarctus du myocarde sont responsables de 24% des décès en Europe. Les patients qui survivent à ces attaques souffrent d'insuffisance cardiaque qui dégrade leur qualité de vie. En effet, les infarctus conduisent à la destruction d'une partie du muscle cardiaque, qui subit alors une plus forte contrainte. La mortalité reste donc élevée dans les années qui suivent un diagnostic d'insuffisance cardiaque. Pour soigner les patients, la solution la plus radicale est la greffe d'un cœur sain. Malheureusement, les dons d'organes sont insuffisants, et le risque de rejet est élevé. Une autre solution serait de régénérer les tissus lésés.

Cette approche est celle de l'ingénierie tissulaire. Le principe de cette méthode repose sur la promotion de la croissance cellulaire sur une matrice bio-inspirée qui mime la matrice extra-cellulaire du tissu à réparer. Concrètement, un support adapté aux cellules est fabriqué puis implanté, déjà cellularisé ou non. Cette matrice artificielle va aider les cellules du tissu à proliférer, afin de le reformer ou le réparer. Elle doit donc posséder certains attributs. D'abord, le matériau qui la constitue doit être biocompatible : il ne doit pas provoquer de réaction inflammatoire trop importante une fois implanté dans le corps, mais il doit aussi permettre aux cellules d'y adhérer. D'autre part, il doit être biorésorbable. En effet, une fois le tissu reformé, il doit se dégrader et être éliminé sous la forme de sous-produits non toxiques. Enfin, ses propriétés mécaniques doivent être adaptées au tissu : il a été montré que les cellules sont sensibles à la rigidité du substrat sur lequel elles se trouvent. Par exemple, des cellules souches mésenchymateuses auront tendance à se différencier en cellules du cerveau sur un substrat très souple et en cellules osseuses sur un substrat rigide [1]. La matrice doit aussi avoir une structure proche de la matrice extra-cellulaire du tissu à régénérer, qui est fibreuse. Elle doit être assez poreuse pour laisser passer le sang, les nutriments et les déchets, ainsi que pour permettre l'infiltration cellulaire. En résumé, il faut mettre au point une matrice qui imite le tissu à réparer à la fois du point de vue des propriétés physico-chimiques du matériau qui la composent et du point de vue de sa structure.

Dans le cas du cœur, on cherche à fabriquer une matrice souple, puisque le module du muscle cardiaque est de 10-20 kPa au début de la diastole (quand le cœur commence à se relâcher) et de 200-500 kPa à la fin de la diastole [2]. Par ailleurs, le myocarde se déforme de manière cyclique et réversible. Le matériau choisi doit donc être un élastomère. En outre, la matrice extra-cellulaire du muscle cardiaque se présente comme une structure hiérarchisée formée de fibres de collagène alignées qui délimitent des pores (Figure R1). Ces pores correspondent en

fait à l'espace où se trouvent les cardiomyocytes – les cellules du muscle cardiaque – et les vaisseaux sanguins.

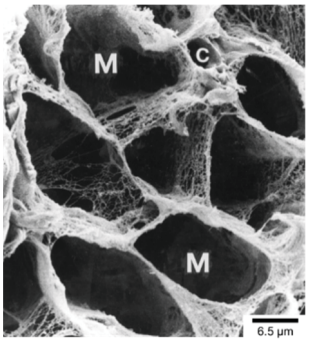

Figure R1. Section d'un cœur de lapin après élimination des cellules : seules les fibres de collagène restent. Les pores marqués M correspondent aux emplacements des cardiomyocytes et ceux marqués C aux capillaires [3].

1.2. Choix du matériau

Pour le projet présenté dans cette thèse, l'élastomère choisi comme matériau de base pour fabriquer la matrice est le poly(sébaçate de glycérol) (PGS). Il s'agit d'un polyester thermodurcissable synthétisé par polycondensation en masse du glycérol et de l'acide sébacique [4]. Cette synthèse est généralement décrite en deux étapes : la prépolymérisation qui conduit à des oligomères solubles et le recuit qui permet la réticulation de l'élastomère. Le PGS est biocompatible et se dégrade par hydrolyse en composés naturellement présents dans l'organisme. Son module d'Young a été rapporté entre 0.025 et 1.2 MPa pour une élongation à rupture pouvant atteindre 330% [5], ce qui convient pour des applications en ingénierie tissulaire des tissus mous. Plusieurs exemples de son utilisation pour l'ingénierie cardiaque peuvent être trouvés dans la littérature [6–8]. Ses propriétés sont modulables grâce aux modifications que l'on peut apporter aux paramètres de synthèse.

1.3. Procédé

Pour imiter la structure fibreuse de la matrice extra-cellulaire du cœur, il a été décidé de mettre le PGS en œuvre par électrofilage. Il s'agit d'une méthode qui permet de fabriquer une fibre ultra-fine par étirement d'une solution de polymère sous l'effet d'un champ électrique important. La fibre obtenue est déposée aléatoirement sur le collecteur, avec un diamètre pouvant atteindre 30 nm à 3 µm. Pour y parvenir, il faut que la solution soit en régime semi-dilué enchevêtré. Sans enchevêtrements, le jet se rompt en particules : on parle d'électrospray. On peut aisément fabriquer des fibres composites, soit en mélangeant les composants, soit en fabriquant des fibres coaxiales. Ces matériaux nanofibreux ont un réel intérêt pour l'ingénierie tissulaire, puisqu'ils sont fibreux comme la matrice extra-cellulaire, ils sont poreux, et offrent une grande surface à fonctionnaliser. Néanmoins, leurs pores sont souvent trop petits pour laisser les cellules s'y infiltrer aisément.

Le matériau et le procédé de fabrication de la matrice synthétique étant choisis, un défi reste à relever. En effet, l'objectif est d'électrofiler un élastomère. Néanmoins, ce dernier est insoluble puisque réticulé. La consultation de la littérature nous a permis d'identifier plusieurs stratégies existantes pour réaliser l'électrofilage d'élastomères. Tout d'abord, la mise en œuvre des élastomères thermoplastiques (TPE) ne pose pas de problèmes majeurs dans la mesure où ils sont

solubles. On trouve surtout des exemples de nanofibres de TPE styréniques [9–11] ou à base de polyuréthane [12–14]. Mais bien que ces derniers soient très prisés dans le domaine biomédical, ils ne sont pas biodégradables. En revanche, dans le cas des élastomères thermodurcissables, il faut procéder à l'électrofilage avant formation du réseau réticulé pour pouvoir préparer les solutions. La réaction de réticulation peut ensuite avoir lieu soit pendant la formation de la fibre, soit après électrofilage. On peut trouver plusieurs exemples d'électrofilage de solutions de macromères comportant des liaisons C=C : ils sont réticulés *in situ* ou post-électrofilage sous rayonnement ultraviolet [15–17]. Des élastomères tels que les silicones peuvent aussi être réticulés pendant la formation de la fibre si le polymère et l'agent réticulant sont mélangés juste avant l'injection de la solution d'électrofilage [18,19]. Il faut néanmoins dans ce cas que la réaction ne soit pas trop rapide : une solution trop visqueuse ne peut pas être électrofilée. Enfin, les polyesters réticulés peuvent être électrofilés sous la forme de prépolymères, c'est-à-dire d'oligomères ramifiés mais solubles. Les fibres doivent ensuite être recuites afin de poursuivre l'estérification afin de former le réseau réticulé insoluble. Malheureusement, la faible masse molaire des prépolymères les empêche de former des enchevêtrements en solution, ce qui les rend difficiles à électrofiler. D'autre part, ces prépolymères ont souvent une viscosité très faible à la température de recuit. Il faut donc les mélanger à un polymère porteur, capable de fournir les enchevêtrements nécessaires à l'électrofilage mais aussi d'empêcher le prépolymère de s'écouler hors des fibres lors du recuit. C'est cette stratégie qui est choisie pour l'électrofilage du PGS.

Le PGS a par exemple été électrofilé avec des protéines telles que du collagène [20] ou de la gélatine [21]. Après réticulation de ces protéines, des fibres élastomères sont obtenues. Néanmoins, les protéines ne supportant pas des températures trop élevées, le PGS contenu dans ces fibres ne peut pas être réticulé. D'autre part, si les protéines offrent l'avantage d'avoir une bonne affinité avec les cellules, elles aussi ont l'inconvénient d'avoir des propriétés variables en fonction de leur source d'extraction. L'utilisation de polymères synthétiques résout ce problème. Différents polymères synthétiques biocompatibles ont été utilisés comme polymères porteurs pour le PGS : un polyuréthane thermoplastique (TPU) [22], ou encore des polyesters tels que l'acide poly(lactique-*co*-glycolique) (PLGA) [23], la polycaprolactone (PCL) [24] ou l'acide polylactique (PLA) [25]. L'avantage de ce dernier est que contrairement aux autres, il ne fond pas aux températures de recuit et permet donc la réticulation du PGS. À l'issue du recuit, le PLA peut être éliminé par solubilisation dans le chloroforme afin de garder des fibres de PGS [26]. Cette stratégie peut être améliorée si l'on utilise un polymère soluble dans un solvant moins toxique, si possible l'eau. L'alcool polyvinylique a été utilisé comme polymère porteur dans ce cadre [27].

Pour résumer l'objectif de ces travaux de thèse, il s'agissait de préparer une matrice biocomaptible, biorésorbable, élastomère et nanofibreuse avec une structure hiérarchisée adaptée aux cardiomyocytes. Pour cela, le poly(sébaçate de glycérol) a été synthétisé et l'effet de certains paramètres de synthèse a été étudié. Le PGS a ensuite été électrofilé afin de fabriquer soit des fibres composites, soit des fibres élastomères. Enfin, les matrices fibreuses ont été structurées à l'aide de méthodes électrostatiques ou mécaniques pour mieux ressembler à la matrice extracellulaire.

2. Synthèse du poly(sébaçate de glycérol)

La synthèse du PGS se fait en deux étapes : la prépolymérisation et la réticulation. La prépolymérisation conduit à l'obtention d'oligomères solubles, ce qu'on appelle prépolymère (pPGS), par polycondensation du glycérol et de l'acide sébacique (Figure R2). Il est important de déplacer l'équilibre de cette estérification par élimination de l'eau. Pour caractériser le pPGS, le degré d'estérification (DE) peut être mesuré. Il est défini en fonction du nombre d'acides carboxyliques initiaux et d'esters finaux de la manière suivante pour les cas où les acides carboxyliques ne sont pas en excès (comme dans les exemples présentés ici) :

$$DE = \frac{n_{esters}^{fin}}{n_{acides}^{init}} \times 100$$

Le DE peut être déterminé par RMN du proton ou par dosage des fonctions acides. Le dosage après gonflement de l'élastomère dans le solvant est la seule méthode possible une fois le PGS réticulé.

Plusieurs paramètres ont une influence sur le DE et sur les propriétés du prépolymère synthétisé. Parmi ces paramètres, on trouve la température, le type de chauffage ou encore le ratio glycérol/acide sébacique (G/SA) introduit. Les proportions stœchiométriques correspondent à un ratio G/SA égal à 2/3, c'est-à-dire quand le nombre de –OH est égal au nombre de –COOH (Figure R2). Le glycérol comporte deux alcools primaires pour un alcool secondaire, ce dernier étant moins réactif. Pour cette raison, au début de la réaction, les alcools secondaires peuvent ne pas réagir, ce qui conduit à la synthèse de segments linéaires. Les ramifications latérales apparaissent lorsque les alcools secondaires sont forcés à réagir parce que peu d'alcool primaires subsistent.

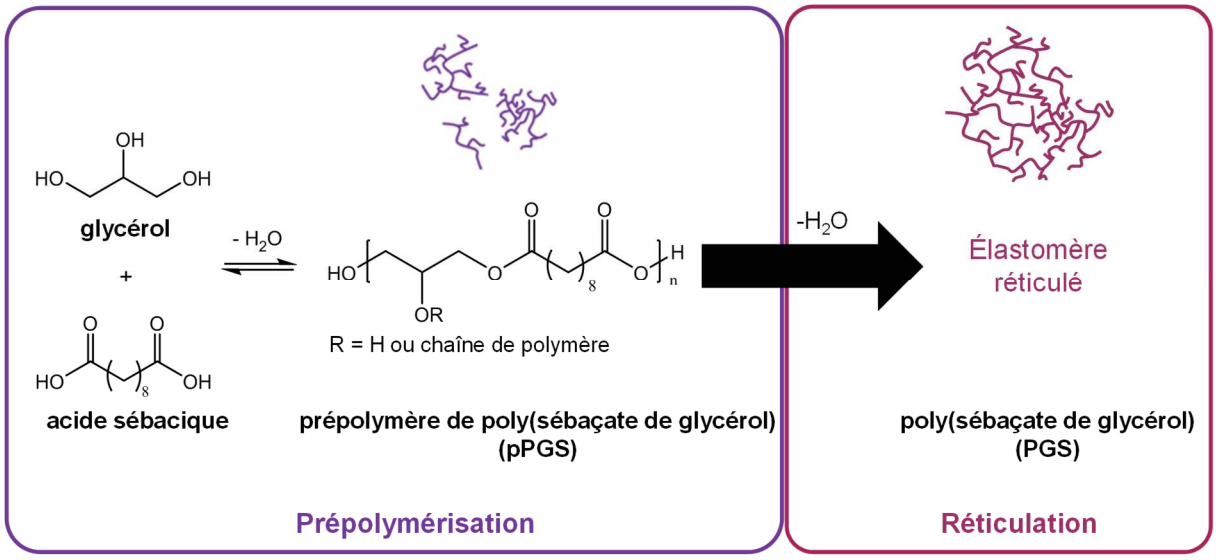

Figure R2. Schéma décrivant la synthèse du PGS.

La seconde étape est l'étape de réticulation, lorsque les prépolymères ramifiés se lient entre eux en un réseau 3D insoluble (Figure R2). Pour atteindre ce résultat, la réticulation a lieu par chauffage à 120-170°C sous vide, afin d'extraire l'eau du milieu réactif et de forcer l'estérification.

2.1. Etude de la prépolymérisation

Le premier paramètre étudié a été le mode de chauffage. Il a été vérifié que le chauffage par irradiation micro-onde dans un réacteur de laboratoire permet d'accélérer la réaction avec une bonne reproductibilité.

L'influence de la température de prépolymérisation a ensuite été testé pour des températures comprises entre 120°C et 180°C. On a pu montrer que des DE plus élevés étaient atteints plus vite à plus haute température.

L'effet du ratio glycérol/acide sébacique a aussi été analysé. Il a été montré que le DE augmente plus lentement pour le ratio stœchiométrique (2/3). Cela est aisément compréhensible dans la mesure où le ratio stœchiométrique impose la réaction des alcools secondaires, puisqu'ils sont plus nombreux. En revanche, le degré de polymérisation évolue différemment. En effet, le DE peut être relié au degré de polymérisation moyen en nombre théorique grâce à l'équation de Carothers adaptée pour des monomères polyfonctionnels :

$$\overline{DP_n} = \frac{2}{2 - \frac{DE}{100} f_{moy}}$$

avec f_{moy} la fonctionnalité moyenne du mélange de monomère. Elle est égale à deux fois le nombre total de groupes fonctionnels en défaut divisé par le nombre total de molécules. On s'aperçoit alors que le degré de polymérisation théorique des prépolymères préparés à partir d'un ratio 2/3 augmente plus vite. En effet, ce ratio stœchiométrique conduit à un point de gel pour un degré d'estérification de seulement 83%, contre 100% dans le cas 1/1. En réalité, comme les alcools secondaires sont forcés de réagir plus tôt dans le cas 2/3, les prépolymères synthétisés sont plus ramifiés. Cela a été vérifié par DSC, les températures et enthalpies de fusion étant plus faibles.

2.2. Etude de l'élastomère

La comparaison de certaines propriétés d'élastomères synthétisés à partir de différents ratios glycérol/acide sébacique a permis de confirmer que le ratio stœchiométrique (2/3) conduit à des élastomères plus réticulés. En effet, ces derniers ont une fraction en parties solubles plus faible et gonflent moins dans l'eau que dans le cas 1/1. D'autre part, des tests de tractions ont montré qu'ils sont plus rigides. De la même manière, un élastomère recuit plus longtemps est plus rigide car plus réticulé.

L'étude de la synthèse du PGS nous a donc permis de déterminer quel sont les paramètres de réaction à choisir pour obtenir les propriétés du matériau final voulues. Ainsi, pour avoir un matériau plus souple comportant plus de –OH disponibles, on utilisera un pPGS préparé à partir d'un ratio 1/1. Pour avoir un prépolymère proche de son point de gel, on utilisera un pPGS 2/3 de DE élevé.

3. Elaboration de fibres composites PLA/PGS

Nous avons vu ci-dessus que le pPGS ne peut pas être électrofilé et réticulé sans la présence d'un polymère porteur. L'acide polylactic (PLA), qui est un biopolymère souvent utilisé dans le domaine biomédical [28] est un bon candidat : il est biocompatible, peut être électrofilé, et garde sa tenue mécanique à la température de recuit du PGS. En revanche, il est rigide et hydrophobe, ce qui constitue des inconvénients pour des applications en ingénierie cardiaque. Il peut donc être fonctionnalisé par mélange avec le PGS. Pour contrebalancer les inconvénients du PLA, on choisit ici un PGS plus hydrophile et plus souple, le prépolymère utilisé étant préparé à partir d'un ratio 1/1 avec un DE de 85%. Des membranes avec différentes teneurs en PGS (0%, 30% ou 40%) ont été électrofilées en utilisant différents solvants afin de faire varier le diamètre des fibres. Elles ont ensuite été recuites pendant deux jours à différentes températures (90 ou 120°C). Leur hydrophilie et leurs propriétés mécaniques et thermiques (DSC) ont été comparées. Elles ont été utilisées pour des tests *in vitro* comme substrats de culture de cellules cardiaques après imprégnation par du Matrigel, un mélange de protéines qui permet d'améliorer l'adhésion des cellules. Elles ont aussi été employées dans le cadre de tests *in vivo*, greffées sur des cœurs de souris. Leur potentiel thérapeutique a été comparé en fonction des paramètres de procédé.

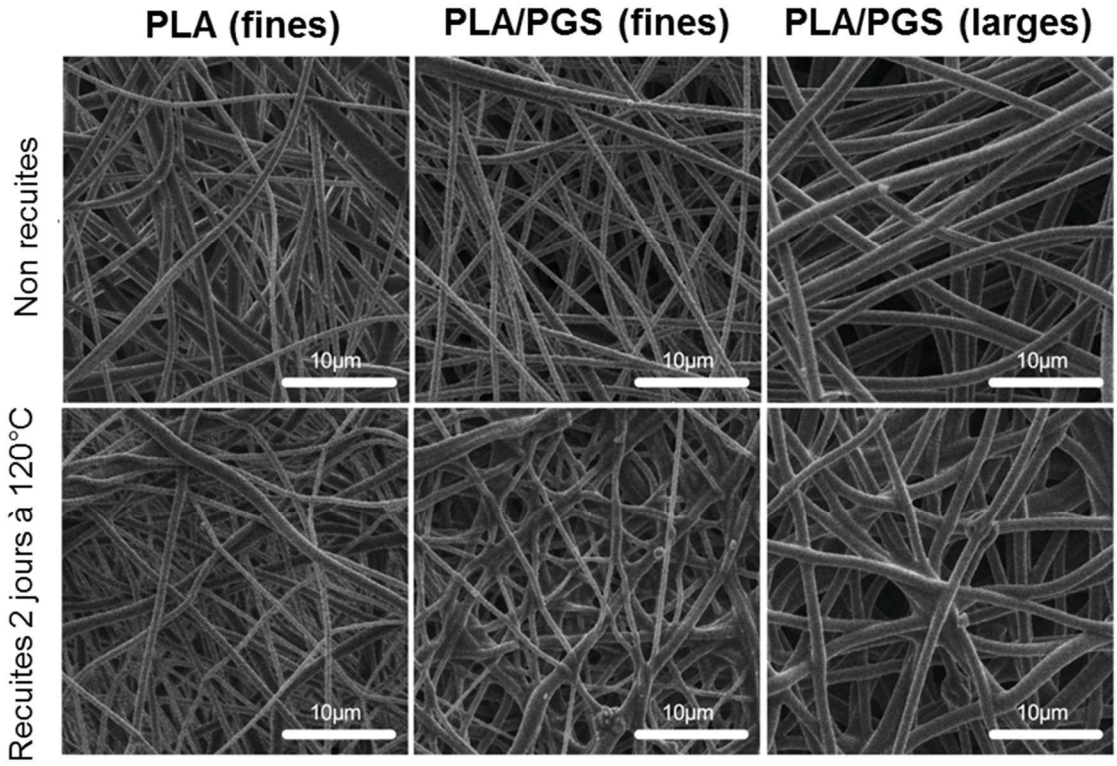

Figure R3. Images MEB de fibres PLA et PLA (70%)/PGS (30%), fines et larges, avant et après recuit.

L'utilisation d'un solvant plus volatil (dichlorométhane/diméthylformamide 7/3 au lieu de 6/4) a permis d'électrofiler des fibres plus épaisses, avec un diamètre moyen proche de 1500 nm contre 500 nm pour les plus fines (voir Figure R3). En effet, si le solvant s'évapore plus vite lors de l'étirement de la fibre, elle sera moins allongée. Il a été observé que les cardiomyocytes prolifèrent mieux sur des membranes fabriquées avec des fibres fines (500 nm de diamètre).

Le recuit rend les fibres plus rigides, à cause de la réticulation du PGS, de la cristallisation du PLA et de la fusion des fibres au niveau des points de contact (voir Figure R3). Cette fusion

est due à un écoulement partiel du pPGS hors des fibres lors du chauffage. En revanche, un recuit à plus haute température (120°C) permet de diminuer la cytotoxicité des membranes contenant du PGS. On explique cela par le fait qu'à plus haute température, la réaction est plus aboutie. Or, la toxicité du PGS est liée aux fonctions acides carboxyliques qu'il porte. Après recuit à plus haute température, moins d'acides restent libres. Mais ces membranes recuites à 120°C sont trop rigides pour l'application cardiaque visée, avec un module d'Young mesuré après hydratation à 54±9 MPa pour des fibres de PLA pur et une élongation à la rupture de 50±5%. Les membranes de fibres de PLA/PGS (avec 30% de PGS) fines ont un module d'Young de 278±98 MPa pour une élongation à la rupture de 60±14% et celles avec les fibres épaisses ont un module de 216±48 MPa avec une élongation à la rupture de 123±5%. Néanmoins, ces mesures correspondent la déformation globale des membranes et donc au mouvement des fibres entre elles, et non à la rigidité que ressentent les cellules localement.

L'ajout du PGS dans les fibres permet d'augmenter leur hydrophilie et donc d'améliorer l'imprégnation du Matrigel. En revanche, on ne peut pas identifier de différences notables selon qu'il y ait 30% ou 40% de PGS, que ce soit du point de vue de l'hydrophilie ou des propriétés mécaniques. Le procédé de fabrication des fibres à 30% étant plus facile, ces dernières seront privilégiées.

Après greffes de patchs cardiaques composés de fibres fines PLA ou PLA/PGS 30%, il a été trouvé que ces dernières favorisent la capillarisation des tissus régénérés et provoquent une inflammation moindre. Ces sont donc les meilleurs candidats pour l'application visée.

Cette étude comparative de fibres PLA et PLA/PGS de différents diamètres et recuites à différentes températures a permis d'identifier les fibres contenant 30% de PGS, avec un diamètre d'environ 500 nm et recuites à 120°C pendant deux jours comme les meilleures candidates pour la régénération cardiaque parmi les membranes testées. Ces membranes ne sont pas élastomères, à cause du PLA, mais elles semblent néanmoins très prometteuses.

4. Elaboration de fibres élastomères

Les matériaux à base de PLA et de PGS présentés ci-dessus ne remplissent pas les spécifications concernant les propriétés mécaniques pour une application cardiaque à cause de la présence du PLA. Pour améliorer ce point, il faudrait éliminer le polymère porteur. Malheureusement, le PLA n'est soluble que dans des solvants toxiques tels que le chloroforme ou le dichlorométhane. On préférerait utiliser un polymère hydrosoluble que l'on éliminerait facilement dans l'eau, afin d'éviter un risque de toxicité supplémentaire. Ici, nous avons choisi un mélange de polyvinylpyrrolidone (PVP) et d'hydroxypropyl-β-cyclodextrine (HPβCD) comme matériau porteur. Le PVP est soluble dans l'eau, approuvé par la *Food and Drugs Administration* américaine pour des applications biomédicales, et garde une bonne tenue mécanique aux températures de recuit. La HPβCD est un oligosaccharide biocompatible ayant une température de dégradation de 278°C. Elle est connue pour aider à stabiliser le procédé d'électrofilage [29–31]. D'autre part, elle comporte une cavité hydrophobe qui peut être exploitée pour l'encapsulation de médicaments par complexes d'inclusion [32]. Enfin, elle peut réagir avec les –COOH du PGS grâce aux nombreux –OH qu'elle comporte. Dans cette stratégie, le pPGS a été électrofilé mélangé avec le matériau porteur. Les fibres ont ensuite été recuites afin de réticuler le PGS, puis le polymère porteur a été éliminé par lavage dans l'eau pour obtenir des fibres élastomères. Pour

cette partie, on a voulu comparer les membranes obtenues avec des membranes fabriquées par un procédé identique mais employant de l'alcool polyvinylique (PVA) comme polymère porteur.

Diverses stratégies visant le co-électrofilage du pPGS, du PVP et de la cyclodextrine ont été expérimentées. Après optimisation, la méthode suivante a été sélectionnée : le PVP et la cyclodextrine ont été mélangés en solution avec le pPGS. Ce dernier était synthétisé à partir d'un ratio G/SA égal à 2/3 avec un degré d'estérification de 72%. De cette manière, le prépolymère employé est proche du point de gel. Cela limite les risques d'écoulement du pPGS hors des fibres lors du recuit. Après électrofilage de la solution, les fibres sèches contenaient 50% de pPGS, 25% de PVP et 25% de HPβCD. Elles ont été recuites sous vide 24h à 120°C puis 48h à 140°C. Une dernière étape de 24h à 170°C a été ajoutée pour certaines membranes afin d'étudier l'effet d'un recuit plus poussé. Enfin, elles ont été immergées dans l'eau pendant 24h pour éliminer le matériau porteur.

La Figure R4 montre que les fibres préparées à partir du PVA sont plus larges et résistent mieux aux post-traitements. Les fibres fabriquées à partir de PVP et de HPβCD ont plus tendance à avoir fusionné entre elles. De la matière fondue bouche les pores, surtout après le lavage qui suit le recuit le plus court. On peut en déduire qu'une meilleure réticulation du PGS permet d'avoir une meilleure tenue des fibres et donc une meilleure morphologie de membrane.

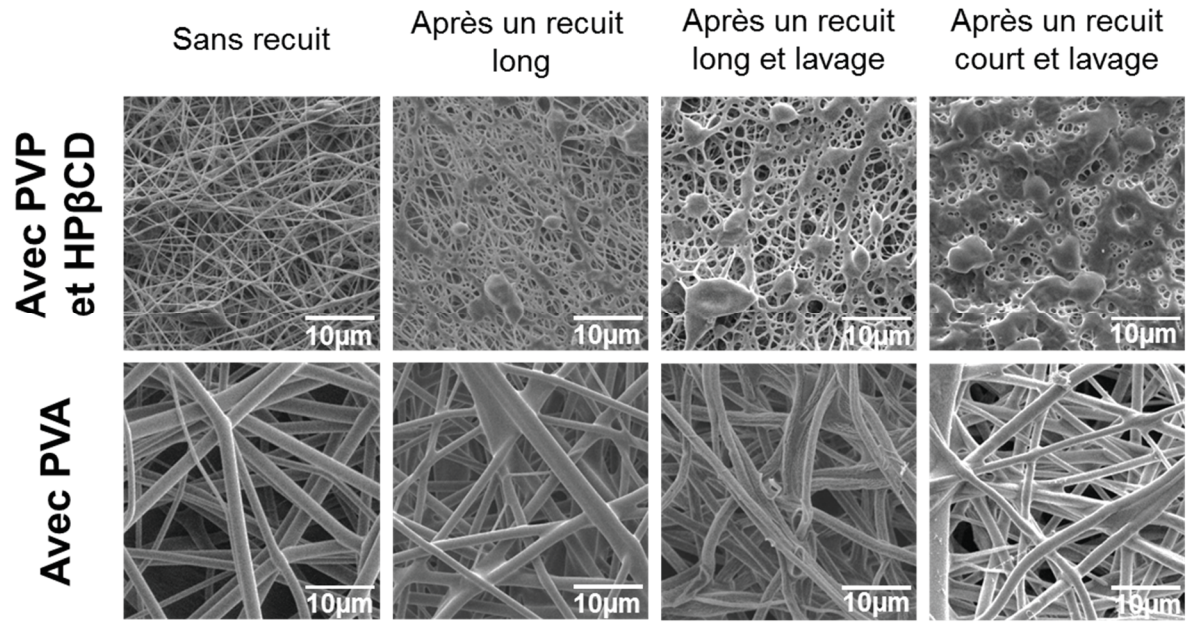

Figure R4. Images MEB des fibres préparées à l'aide de PVP/HPβCD ou de PVA.

Une comparaison des masses des membranes avant et après lavage ainsi que des analyses infra-rouge indiquent que les fibres lavées ne contiennent pas que du PGS, sans que la quantité de polymère porteur restante n'ait pu être quantifiée.

Les propriétés mécaniques ont été comparées avant et après lavage, à l'état sec et hydraté, pour les deux types de recuit et les deux types de formulation. Pour les deux formulations, il a à nouveau été observé que plus les membranes sont recuites, plus leur module est élevé puisque le PGS est plus réticulé. En revanche, le lavage permet de diminuer le module, ce qui confirme qu'une partie du matériau porteur a bien été éliminé. Ainsi, à l'état sec, le module d'Young des

membranes fabriquées à partir de PVP et de HPβCD est situé entre 2 et 6 MPa, selon l'intensité du recuit ; l'élongation à la rupture atteint 390% pour le recuit le plus court, contre 111% pour le recuit le plus long. Le module d'Young des membranes fabriquées à l'aide de PVA est situé entre 56 et 81 MPa et leur élongation à la rupture entre 157% et 138%. L'hydratation des membranes permet de diminuer fortement leur module mais aussi leur élongation à la rupture. Cela est dû à la dissipation des forces de frottement par l'eau qui gonfle le matériau. Toutes les membranes ont ainsi un module d'Young proche de 200 kPa, ce qui est intéressant pour une utilisation dans le domaine cardiaque, et une élongation à la rupture entre 50 et 60%. Cette dernière valeur est assez faible mais néanmoins suffisante pour le muscle cardiaque qui n'est pas étiré à plus de 15% lors de son activité [8].

Les membranes ont également été testées mécaniquement par traction répétée entre 0 et 15% d'élongation, afin d'évaluer la dissipation d'énergie qui a lieu lors de leur déformation. A l'état sec, tous les matériaux testés (avec PVP/HPβCD ou PVA) récupèrent environ 40% de l'énergie, mais à l'état hydraté, la dissipation d'énergie est presque nulle, ce qui montre que le matériau est bien élastique. Ainsi, il ne subit pas de modifications irréversibles lors d'une sollicitation répétée qui imite les battements du cœur.

Il n'a pas été possible de prouver que la cyclodextrine peut potentiellement être exploitée dans les membranes fabriquées à partir de PVP et de HPβCD pour l'encapsulation de principes actifs. En effet, il a bien été vérifié que ces membranes sont capables d'adsorber du bleu de méthylène par immersion dans une solution de colorant. Néanmoins, la même faculté a été trouvée pour les membranes fabriquées à l'aide de PVA, montrant que le bleu de méthylène s'adsorbe en réalité sans doute sur le PGS.

Enfin, les membranes fabriquées à l'aide de PVP et de HPβCD n'ont pas montré une bonne affinité avec les cellules. En effet, malgré une imprégnation de ces membranes par du Matrigel, les cellules ensemencées s'allongent peu et adhèrent mal. Cela serait dû à une trop forte acidité induise par ces matériaux dans le milieu de culture. Cette acidité pourrait être réduite si un pPGS préparé à partir d'un ratio G/SA égal à 1/1 était employé. En effet, ce dernier contient une plus faible proportion de fonctions –COOH. Il faudrait néanmoins utiliser un pPGS 1/1 avec un DE très élevé, afin d'être proche du point de gel et éviter ainsi la perte de la structure fibreuse. En effet, les premiers essais avec un pPGS 1/1 ont conduit à la fusion totale des fibres. Cette perspective pourrait encore être approfondie.

Le défi que constitue la préparation de membranes fibreuses élastomères par électrofilage a donc été relevé. Pour cela, un matériau porteur résistant à la température de recuit et soluble dans l'eau a été utilisé. Ces membranes ont des propriétés mécaniques intéressantes à l'état hydraté pour l'application cardiaque visée. Leur potentiel thérapeutique doit encore être prouvé.

5. Membranes structurées avec des fibres organisées

Les membranes décrites dans les parties précédentes imitent le caractère fibreux de la matrice extra-cellulaire sans imiter sa structure hiérarchisée. En particulier, leurs pores sont trop petits pour laisser les cellules pénétrer et les fibres étant déposées de manière aléatoire, l'anisotropie des tissus cardiaques n'est pas reproduite. La dernière partie de cette thèse a donc pour objectif de donner des méthodes de structuration de ces membranes.

5.1. Structuration par combinaison d'électrofilage et d'électrospray

Une méthode basée sur la combinaison de l'électrofilage et de l'électrospray de particules permet d'organiser le dépôt de la fibre afin de former de larges pores très peu denses en fibres. Cette méthode repose sur les interactions électrostatiques. En effet, le dépôt par électrofilage d'une fibre chargée sur un collecteur structuré (comportant des creux et des bosses) va créer des zones attractives, là où la fibre peut se décharger à travers le collecteur grâce à un bon contact, et des zones répulsives, là où la fibre est suspendue et conserve ses charges, comme cela est représenté sur la Figure R5. Si des particules sont électrosprayées sur des fibres organisées ainsi, elles se déposeront exclusivement sur les zones attractives. Si une nouvelle couche de fibres est déposée, elles se déposeront préférentiellement sur les zones attractives, et resteront tendues au-dessus des zones répulsives afin de minimiser la force de répulsion. Ainsi, en alternant le dépôt de fibres et de particules, on peut construire une membrane organisée en « murs » denses en particules et en fibres et en « trous » ne comportant que quelques fibres. Cela est possible sur un collecteur structuré tel qu'une grille métallique, mais aussi sur un collecteur lisse ; dans ce cas, les premières particules déposées joueront le rôle de « bosses » [33–35].

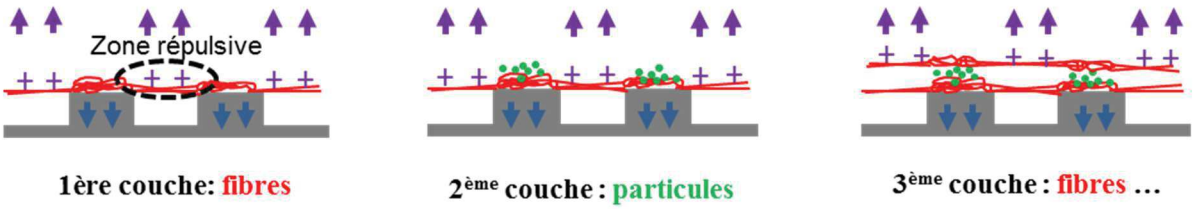

Figure R5. Schéma expliquant le principe de fabrication de membranes à large pores par combinaison de l'électrofilage et de l'électrospray.

Dans le cadre de ces travaux, l'objectif était d'organiser un dépôt de fibres contenant du PGS. Malheureusement, nous avons pu constater que ce n'était pas possible, le PGS rendant les fibres (par exemple PLA/PGS) conductrices. De cette manière, les charges sont évacuées et les zones répulsives et attractives n'apparaissent pas. Le PGS a néanmoins pu être mis en œuvre pour ce type de procédé sous la forme d'électrospray. Ainsi, des membranes organisées constituées de fibres de PLA et de spray de PGS ont été préparées par dépôt alternatif de fibres et de particules sur un collecteur structuré (grille) ou lisse (papier aluminium). La Figure R6.(A) et (C) montre que la structuration est visible à l'œil nu sur la surface supérieure (dernières couches déposées) : elle est couverte de pores peu denses en fibres de large diamètre. En revanche, sur la face inférieure (premières couches déposées), les motifs sont de plus petites dimensions. Certains pores peuvent en effet être perdus lors de la production, lorsque des fibres « enjambent » plusieurs zones répulsives, en les transformant en une grande zone répulsive, donc un grand pore. En outre, les pores ont une forme plus régulière avec l'aide du collecteur structuré, qui guide les fibres et les particules. Lorsque des cellules cardiaques ont été déposées sur ces substrats après réticulation du PGS, on a pu observer qu'elles pénétraient mieux dans la membrane préparée sur une grille métallique, les pores étant plus larges.

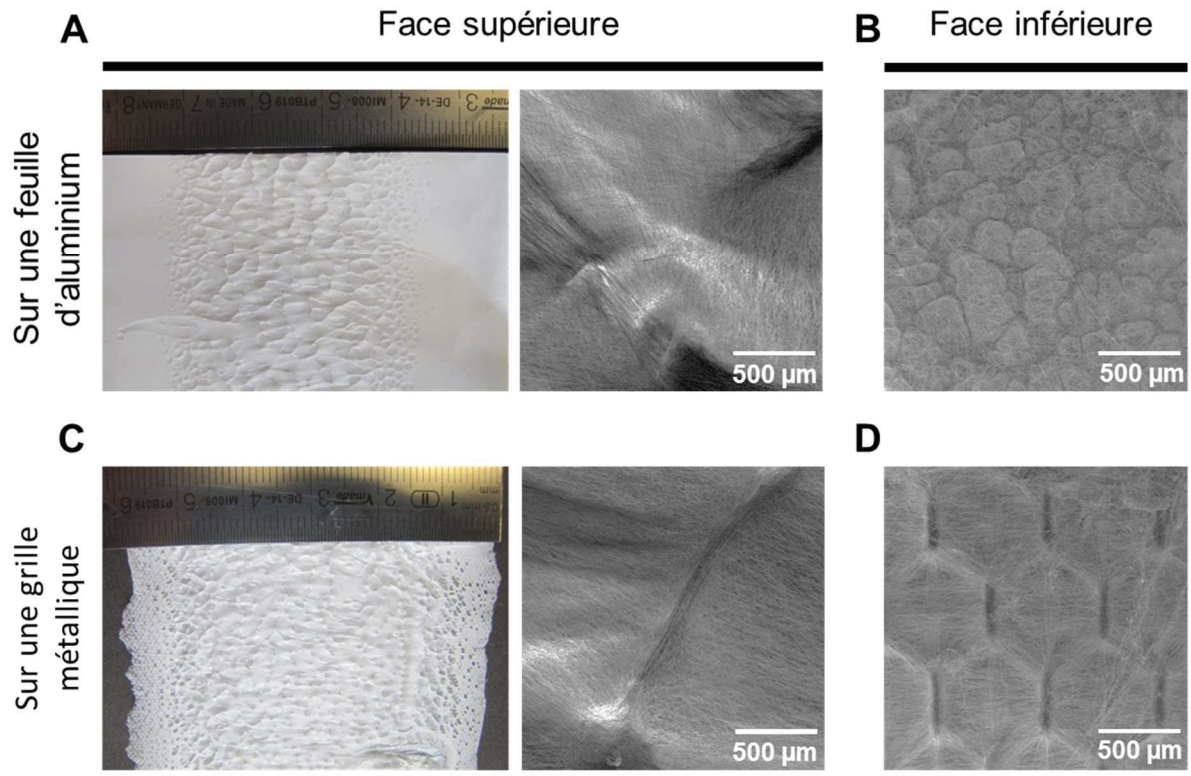

Figure R6. Images de fibres de PLA et de spray de pPGS sur (A-B) un collecteur lisse (feuille d'aluminium) et (C-D) un collecteur structuré (grille métallique) prise avec un appareil photo et le MEB sur (A-C) la face supérieure et (B-D) la face inférieure.

5.2. Alignement des fibres

Afin d'imiter l'anisotropie du tissu cardiaque, il peut être intéressant d'aligner les fibres dans une seule direction. Ce type d'organisation peut aider à améliorer l'alignement des cardiomyocytes pour former le tissu cardiaque [36]. Une méthode pour y parvenir est la rotation à haute vitesse du collecteur cylindrique. En effet, comme cela a été montré par Matthews *et al.* [37], lorsque la vitesse tangentielle du collecteur atteint la vitesse d'atterrissage du jet de polymère, l'alignement de la fibre a lieu perpendiculairement à l'axe de rotation du collecteur cylindrique.

Ici, des fibres de PLA et de PLA/PGS ont ainsi été alignées par rotation à 3000 tr/min d'un collecteur de 13 cm de diamètre. Elles ont ensuite été recuites avant d'être caractérisées mécaniquement. La Figure R7 montre la morphologie des fibres sur ces membranes. Elles sont très denses, les fibres étant proches les unes des autres. Cette proximité provoque la fusion partielle de fibres PLA/PGS entre elles.

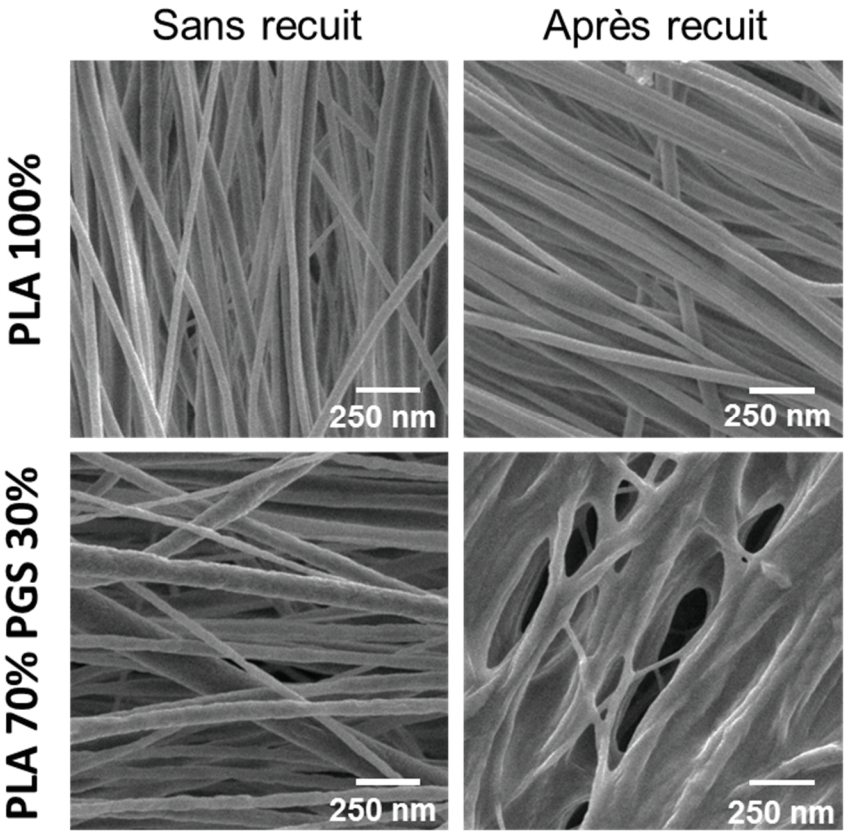

Figure R7. Images MEB des fibres alignées avant et après recuit.

Il résulte de la caractérisation mécanique que les propriétés de ces membranes sont très différentes selon que les membranes soient sollicitées dans la direction longitudinale ou transversale à l'axe des fibres. Dans la direction longitudinale, le module d'Young est élevé, avec une valeur de 746±194 MPa pour le PLA seul, et 493±170 MPa pour les fibres PLA/PGS, le tout après recuit. En effet, lorsque les fibres alignées sont étirées dans leur direction d'alignement, la contrainte correspond à l'étirement du matériau alors que la contribution des forces de friction entre fibres reste faible. Dans la direction transversale, la contrainte mesurée est très faible, parce qu'elle correspond uniquement aux interactions entre fibres, et pas à la déformation du matériau.

Il a été confirmé avec les membranes constituées de fibres de PLA alignées que cette anisotropie favorise l'alignement des cardiomyocytes. Néanmoins, leur faible porosité limite la colonisation des cellules à l'intérieur de la membrane.

5.3. Combinaison de fibres alignées et de particules

Afin d'améliorer la porosité des membranes composées de fibres alignées, une stratégie combinant les deux précédentes a été mise au point. Ici, des fibres alignées et des particules sont déposées alternativement. Les particules sont choisies pour maximiser l'écartement entre les couches de fibres. L'électrospray de pPGS ne produisant pas de particules bien définies mais ayant plutôt tendance à s'étaler en enrobant les fibres, une autre formulation a été choisie : le pPGS a été mélangé à 50% avec de la HPβCD. Les particules sont ainsi plus volumineuses, et les propriétés d'encapsulation de la HPβCD pourront être exploitées. Des couches de particules déposées simultanément avec les fibres de PLA sont alternées avec des couches de particules déposées seules afin d'augmenter la séparation entre couches de fibres. Pour aligner les fibres, le

procédé a lieu avec le collecteur de 13 cm de diamètre tournant à 3000 tr/min. Après l'équivalent d'une heure de dépôt de fibres, les membranes obtenues sont visiblement structurées.

L'observation au MEB montre que les particules se sont organisées en grappes. Des motifs sont apparus au cours du procédé. L'analyse par micro-tomographie par rayons X confirme que les membranes comportent des pores (Figure R8.(B)). On peut aussi constater l'augmentation de la taille de ces pores entre les premières couches déposées et les dernières (Figure R8.(A)). Cette structure alliant l'alignement des fibres et l'incorporation de larges pores imite bien la structure des tissus cardiaques.

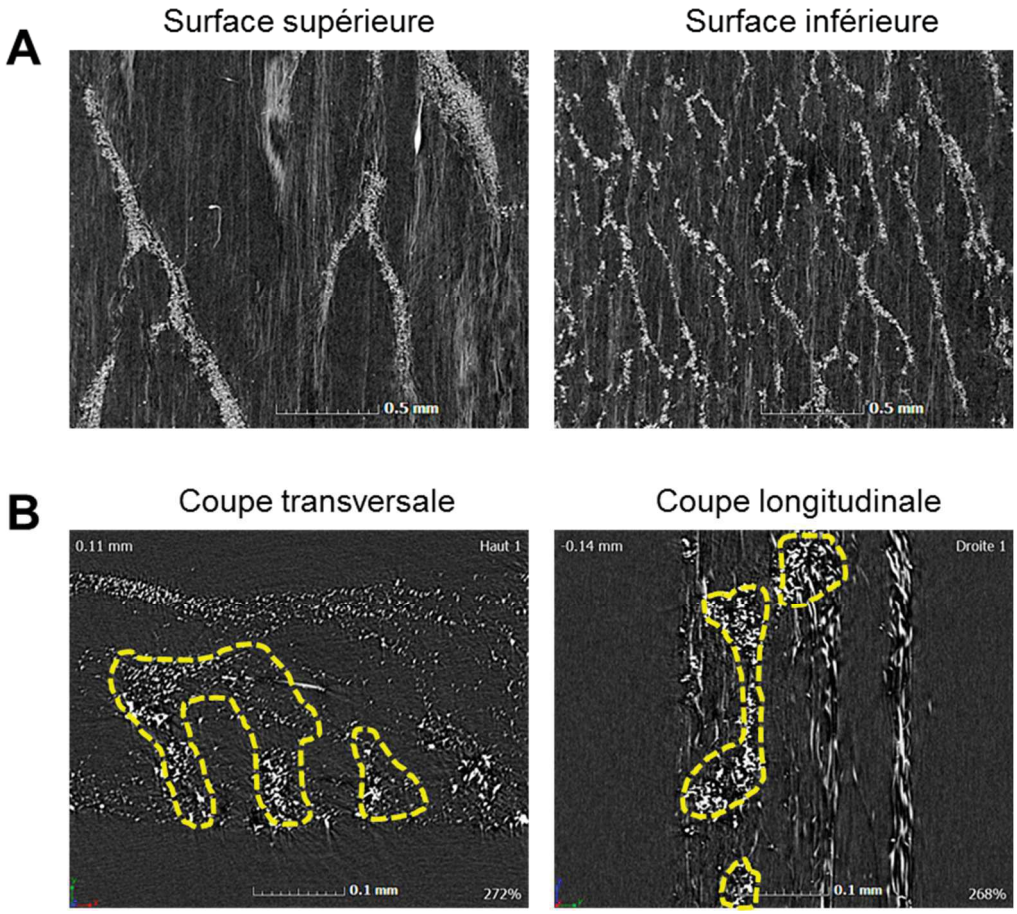

Figure R8. ***Images obtenues par tomographie.*** **(A)** Observation dans un plan parallèle au plan de la membrane. À gauche, une coupe proche de la surface supérieure ; à droite, une coupe proche de la surface inférieure (résolution : 2 µm). **(B)** Vues transversales et longitudinales. Des grappes de particules qui délimitent les pores sont entourées en jaune.

Ces membranes ont été caractérisées mécaniquement avant et après réticulation du PGS pour les comparer aux fibres alignées sans particules. De manière surprenante, malgré la présence locale de PGS réticulé, elles restent très fragiles dans la direction transversale. En outre, elles sont moins rigides que les membranes sans particules dans la direction longitudinale. Leur module d'Young après recuit vaut environ 69 MPa contre 746 MPa en l'absence de particules. Ce résultat pourrait s'expliquer par le fait que la densité des membranes en fibres n'a pas été prise en compte dans le calcul de la contrainte. Or, les membranes comportant des particules sont beaucoup moins denses. En effet, elles sont théoriquement constituées du même nombre de fibres, puisque le temps d'électrofilage était identique. Pourtant, les membranes avec particules sont épaisses d'environ 250 µm après recuit, contre 50 µm sans particules.

Les membranes préparées par cette méthode présentent donc un fort intérêt du point de vue de leur structure. Leur potentiel thérapeutique reste encore à être démontré, mais elles sont très prometteuses et originales.

Pour conclure cette partie portant sur la structuration de matrices fibreuses pour la régénération cardiaque, on peut dire que l'anisotropie offerte par l'alignement des fibres peut avoir un réel intérêt pour l'ingénierie cardiaque. Si le potentiel des membranes PLA et PLA/PGS composées de fibres alignées est confirmée par les résultats de culture cellulaire et de greffe cardiaque, elles pourront éventuellement être greffées cellularisées afin de régénérer un cœur défectueux. L'utilité du point de vue de la biologie des membranes qui comportent des particules en plus doit aussi encore être prouvée. Ces dernières matrices ont l'avantage supplémentaire de pouvoir être utilisées pour la diffusion de médicaments grâce à la présence de la cyclodextrine.

6. Conclusion et perspectives

Ces travaux ont donc d'abord permis de maîtriser la synthèse du PGS et d'identifier quels paramètres donneront les résultats voulus. Le prépolymère synthétisé a été employé afin de préparer des matrices fibreuses composites constituées de PGS et de PLA. Le meilleur candidat parmi tous ceux testés pour la régénération cardiaque a été identifié : il s'agit de membranes composées de 70% de PLA et 30% de PGS de 500 nm de diamètre moyen recuites à 120°C pendant deux jours. Le pPGS a aussi été utilisé pour fabriquer des membranes élastomères obtenues après recuit et lavage du polymère porteur. Leurs propriétés mécaniques à l'état hydraté sont adaptées au tissu cardiaque, avec un module d'Young d'environ 200 kPa et une dissipation d'énergie presque nulle lors de sa déformation à 15%. Ces membranes ne sont pas constituées de PGS pur puisqu'il reste une partie du matériau porteur nécessaire à la l'élaboration des fibres : de la polyvinylpyrrolidone, mais aussi de l'hydroxypropyl-β-cyclodextrine qui leur confère potentiellement des propriétés d'encapsulation. Enfin, diverses pistes de structuration des matrices fibreuses ont été explorées. La combinaison de l'électrofilage et de l'électropray a permis la mise au point de matrices composées de fibres de PLA et de spray de PGS comportant de larges pores favorables à l'infiltration cellulaire. Par ailleurs, l'anisotropie des tissus cardiaques a pu être imitée par alignement de fibres de PLA ou de mélange PLA/PGS. Mais la stratégie la plus originale combine l'alignement des fibres et les particules déposées par électrospray permettant l'apparition de pores larges. Le potentiel thérapeutique de ce type de membrane doit encore être déterminé.

Un aspect qui n'a été qu'effleuré lors de ces travaux est la fonctionnalisation des matrices. En effet, dans la mesure où des matériaux synthétiques ont été utilisés ici, les cellules ont peu d'affinité avec leur substrat. Cette affinité peut être augmentée si des molécules et groupes fonctionnels reconnaissables par les cellules y sont ajoutés. Par exemple, les groupes –OH libres présents sur le PGS peuvent être exploités afin d'y greffer des protéines. Les –OH disponibles sur les cyclodextrines dans les membranes qui en contiennent peuvent être utiles de la même manière, mais les cyclodextrines peuvent aussi être utilisée pour encapsuler des médicaments, des facteurs de croissances ou encore des antimicrobiens.

Références

1. Engler, A.J.; Sen, S.; Sweeney, H.L.; Discher, D.E. Matrix Elasticity Directs Stem Cell Lineage Specification. *Cell* **2006**, *126*, 677–689.
2. Chen, Q.-Z.; Bismarck, A.; Hansen, U.; Junaid, S.; Tran, M.Q.; Harding, S.E.; Ali, N.N.; Boccaccini, A.R. Characterisation of a soft elastomer poly(glycerol sebacate) designed to match the mechanical properties of myocardial tissue. *Biomaterials* **2008**, *29*, 47–57.
3. Macchiarelli, G.; Ohtani, O.; Nottola, S.; Stallone, T.; Camboni, A.; M Prado, I.; M Motta, P. A micro-anatomical model of the distribution of myocardial endomysial collagen. *Histol Histopathol* **2002**, *17*, 699–706.
4. Wang, Y.; Ameer, G.A.; Sheppard, B.J.; Langer, R. A tough biodegradable elastomer. *Nat Biotech* **2002**, *20*, 602–606.
5. Rai, R.; Tallawi, M.; Grigore, A.; Boccaccini, A.R. Synthesis, properties and biomedical applications of poly(glycerol sebacate) (PGS): A review. *Progress in Polymer Science* **2012**, *37*, 1051–1078.
6. Jean, A.; Engelmayr, G.C. Finite element analysis of an accordion-like honeycomb scaffold for cardiac tissue engineering. *Journal of Biomechanics* **2010**, *43*, 3035–3043.
7. Guillemette, M.D.; Park, H.; Hsiao, J.C.; Jain, S.R.; Larson, B.L.; Langer, R.; Freed, L.E. Combined Technologies for Microfabricating Elastomeric Cardiac Tissue Engineering Scaffolds. *Macromolecular Bioscience* **2010**, *10*, 1330–1337.
8. Zhu, C.; Rodda, A.E.; Truong, V.X.; Shi, Y.; Zhou, K.; Haynes, J.M.; Wang, B.; Cook, W.D.; Forsythe, J.S. Increased Cardiomyocyte Alignment and Intracellular Calcium Transients Using Micropatterned and Drug-Releasing Poly(Glycerol Sebacate) Elastomers. *ACS Biomater. Sci. Eng.* **2018**, *4*, 2494–2504.
9. Fong, H.; Reneker, D.H. Elastomeric nanofibers of styrene–butadiene–styrene triblock copolymer. *Journal of Polymer Science Part B: Polymer Physics* **1999**, *37*, 3488–3493.
10. Feng, S.-Q.; Shen, X.-Y.; Fu, Z.-Y.; Ji, Y.-L. Studies on the electrospun submicron fibers of SIS and its mechanical properties. *Journal of Applied Polymer Science* **2009**, *114*, 1580–1586.
11. van der Heijden, S.; De Bruycker, K.; Simal, R.; Du Prez, F.; De Clerck, K. Use of Triazolinedione Click Chemistry for Tuning the Mechanical Properties of Electrospun SBS-Fibers. *Macromolecules* **2015**, *48*, 6474–6481.
12. Lee, K.; Lee, B.; Kim, C.; Kim, H.; Kim, K.; Nah, C. Stress-strain behavior of the electrospun thermoplastic polyurethane elastomer fiber mats. *Macromolecular Research* **2005**, *13*, 441–445.
13. Borg, E.; Frenot, A.; Walkenström, P.; Gisselfält, K.; Gretzer, C.; Gatenholm, P. Electrospinning of degradable elastomeric nanofibers with various morphology and their interaction with human fibroblasts. *Journal of Applied Polymer Science* **2008**, *108*, 491–497.
14. Hunley, M.T.; Pötschke, P.; Long, T.E. Melt Dispersion and Electrospinning of Non-Functionalized Multiwalled Carbon Nanotubes in Thermoplastic Polyurethane. *Macromolecular Rapid Communications* **2009**, *30*, 2102–2106.
15. Thielke, M.W.; Bruckner, E.P.; Wong, D.L.; Theato, P. Thiol-ene modification of electrospun polybutadiene fibers crosslinked by UV irradiation. *Polymer* **2014**, *55*, 5596–5599.
16. Kerr-Phillips, T.E.; Woehling, V.; Agniel, R.; Nguyen, G.T.M.; Vidal, F.; Kilmartin, P.; Plesse, C.; Travas-Sejdic, J. Electrospun rubber fibre mats with electrochemically controllable pore sizes. *J. Mater. Chem. B* **2015**, *3*, 4249–4258.
17. Liu, L.; Zhang, F.; Hu, S.; Zhang, L.; Wen, S. Preparation of Ultrafine Ethylene/Propylene/Diene Terpolymer Rubber Fibers by Coaxial Electrospinning. *Macromolecular Materials and Engineering* **2012**, *297*, 298–302.
18. Lu, S.; Duan, X.; Han, Y.; Huang, H. Silicone rubber/polyvinylpyrrolidone microfibers produced by coaxial electrospinning. *Journal of Applied Polymer Science* **2013**, *128*, 2273–2276.
19. Guarino, V.; Branda, F.; Ausanio, G.; Iannotti, V.; Lanotte, L.; Ambrosio, L. Elastomagnetic NI-PDMS nanofibers via coaxial electrospinning. *Mater. Res. Express* **2018**, *5*, 085029.

20. Ravichandran, R.; Venugopal, J.R.; Sundarrajan, S.; Mukherjee, S.; Ramakrishna, S. Cardiogenic differentiation of mesenchymal stem cells on elastomeric poly (glycerol sebacate)/collagen core/shell fibers. *World Journal of Cardiology* **2013**, *5*, 28–41.
21. Kharaziha, M.; Nikkhah, M.; Shin, S.-R.; Annabi, N.; Masoumi, N.; Gaharwar, A.K.; Camci-Unal, G.; Khademhosseini, A. PGS:Gelatin nanofibrous scaffolds with tunable mechanical and structural properties for engineering cardiac tissues. *Biomaterials* **2013**, *34*, 6355–6366.
22. Jiang, L.; Jiang, Y.; Stiadle, J.; Wang, X.; Wang, L.; Li, Q.; Shen, C.; Thibeault, S.L.; Turng, L.-S. Electrospun nanofibrous thermoplastic polyurethane/poly(glycerol sebacate) hybrid scaffolds for vocal fold tissue engineering applications. *Materials Science and Engineering: C* **2019**, *94*, 740–749.
23. Sfakis, L.; Kamaldinov, T.; Khmaladze, A.; Hosseini, Z.F.; Nelson, D.A.; Larsen, M.; Castracane, J. Mesenchymal Cells Affect Salivary Epithelial Cell Morphology on PGS/PLGA Core/Shell Nanofibers. *International Journal of Molecular Sciences* **2018**, *19*, 1031.
24. Sant, S.; Hwang, C.M.; Lee, S.-H.; Khademhosseini, A. Hybrid PGS–PCL microfibrous scaffolds with improved mechanical and biological properties. *J Tissue Eng Regen Med* **2011**, *5*, 283–291.
25. Yi, F.; LaVan, D.A. Poly(glycerol sebacate) Nanofiber Scaffolds by Core/Shell Electrospinning. *Macromol. Biosci.* **2008**, *8*, 803–806.
26. You, Z.-R.; Hu, M.-H.; Tuan-Mu, H.-Y.; Hu, J.-J. Fabrication of poly(glycerol sebacate) fibrous membranes by coaxial electrospinning: Influence of shell and core solutions. *Journal of the Mechanical Behavior of Biomedical Materials* **2016**, *63*, 220–231.
27. Jeffries, E.M.; Allen, R.A.; Gao, J.; Pesce, M.; Wang, Y. Highly elastic and suturable electrospun poly(glycerol sebacate) fibrous scaffolds. *Acta Biomaterialia* **2015**, *18*, 30–39.
28. Lasprilla, A.J.R.; Martinez, G.A.R.; Lunelli, B.H.; Jardini, A.L.; Filho, R.M. Poly-lactic acid synthesis for application in biomedical devices — A review. *Biotechnology Advances* **2012**, *30*, 321–328.
29. Uyar, T.; Balan, A.; Toppare, L.; Besenbacher, F. Electrospinning of cyclodextrin functionalized poly(methyl methacrylate) (PMMA) nanofibers. *Polymer* **2009**, *50*, 475–480.
30. Séon-Lutz, M.; Couffin, A.-C.; Vignoud, S.; Schlatter, G.; Hébraud, A. Electrospinning in water and in situ crosslinking of hyaluronic acid / cyclodextrin nanofibers: Towards wound dressing with controlled drug release. *Carbohydrate Polymers* **2019**, *207*, 276–287.
31. Kayaci, F.; Uyar, T. Electrospun zein nanofibers incorporating cyclodextrins. *Carbohydrate Polymers* **2012**, *90*, 558–568.
32. Otero-Espinar, F.J.; Torres-Labandeira, J.J.; Alvarez-Lorenzo, C.; Blanco-Méndez, J. Cyclodextrins in drug delivery systems. *Journal of Drug Delivery Science and Technology* **2010**, *20*, 289–301.
33. Lavielle, N.; Hébraud, A.; Schlatter, G.; Thöny-Meyer, L.; Rossi, R.M.; Popa, A.-M. Simultaneous Electrospinning and Electrospraying: A Straightforward Approach for Fabricating Hierarchically Structured Composite Membranes. *ACS Appl. Mater. Interfaces* **2013**, *5*, 10090–10097.
34. Wittmer, C.R.; Hébraud, A.; Nedjari, S.; Schlatter, G. Well-organized 3D nanofibrous composite constructs using cooperative effects between electrospinning and electrospraying. *Polymer* **2014**, *55*, 5781–5787.
35. Nedjari, S.; Hébraud, A.; Eap, S.; Siegwald, S.; Mélart, C.; Benkirane-Jessel, N.; Schlatter, G. Electrostatic template-assisted deposition of microparticles on electrospun nanofibers: towards microstructured functional biochips for screening applications. *RSC Adv.* **2015**, *5*, 83600–83607.
36. Kharaziha, M.; Shin, S.R.; Nikkhah, M.; Topkaya, S.N.; Masoumi, N.; Annabi, N.; Dokmeci, M.R.; Khademhosseini, A. Tough and flexible CNT–polymeric hybrid scaffolds for engineering cardiac constructs. *Biomaterials* **2014**, *35*, 7346–7354.
37. Matthews, J.A.; Wnek, G.E.; Simpson, D.G.; Bowlin, G.L. Electrospinning of Collagen Nanofibers. *Biomacromolecules* **2002**, *3*, 232–238.

TITRE EN ANGLAIS :

Elaboration of nanofibrous biomimetic scaffolds based on poly(glycerol sebacate) for cardiac tissue engineering

Cette thèse de doctorat a été rédigée en anglais conformément à l'autorisation délivrée par le M. Aziz Dinia, professeur des universités à l'Université de Strasbourg et directeur de l'École doctorale de physique et chimie-physique (ED 182).

Introduction

General context:

Today, cardiovascular diseases are ones of the leading causes of mortality in the world. With the ageing population, they represent a growing global health problem. Among them, ischemic cardiomyopathy (heart attack) caused 17% of the deaths in the most developed countries in 2017, and more specifically 24% of the deaths in Europe [1]. Such attacks lead to acute myocardial infarction and chronic heart failures due to irreversible modifications in the cardiac tissue. Survival rate to ischemic cardiomyopathies increases in industrialized countries thanks to an early medical care when an attack occurs. As a consequence, the number of patients suffering from heart failure and having therefore an eroded quality of life increases. The number of new cases of heart failure is estimated at 500.000 per year in the United States and 120.000 in France. Due to the need of repeated hospitalizations, they represent a huge economic burden: 1.9% of the total health care expenditure in France between 1995 and 2002 [2] while their global costs were estimated at $108 billion in 2012 [3]. Moreover, the mortality remains high with 80% of male patients and 70% of female patients dying within 8 years after a diagnostic of heart failure. An efficient therapeutic answer is thus urgently needed to limit these costs in term of (quality of) life and public expenditures.

Heart failure can be treated by the replacement of the defective organ by a healthy one. However, although heart transplantation is the only radical treatment, it raises some issues. Indeed, organ shortage and risks of transplant rejection limit its applications. Another therapeutic way is the regeneration of the damaged cardiac tissue by using the tissue engineering approach. Tissue engineering is an interdisciplinary field emerged in the 1990s that combines material engineering and life sciences with the repair of tissues and organs as the objective. The method relies on the use of a scaffold able to promote cell growth. The material employed to build the scaffold and the structure of the latter should be carefully designed in order to fit the properties of the tissue that should be repaired. In particular, the material should be biocompatible and bioresorbable and have mechanical properties close to the tissue's ones. In addition, the scaffold should mimic, by its structure, the extracellular matrix of the tissue [4].

In this context, the MimHeart ANR project, which includes the work presented in this thesis, aims to develop bio-inspired scaffolds for cardiac tissue engineering. This project comprises two main topics: the preparation of the scaffolds, carried out in Strasbourg at ICPEES, and the evaluation of their therapeutic potential by *in vitro* and *in vivo* experiments performed by the Pr. Onnik Agbulut's team "Cellules souches et biotherapies" at the Institut de Biologie Paris-Seine. The present thesis focuses on the preparation of scaffolds, but all the work was done with strong interactions between the two teams.

Methodology:

The design of the scaffolds was done in accordance with the requirements for cardiac tissue engineering. In particular, an elastomer was needed to mimic the mechanical properties of this soft tissue. Poly(glycerol sebacate) (PGS), which is a biocompatible crosslinked polyester was chosen. Moreover, electrospinning, a process allowing the fabrication of nanofibers from a

polymer solution, was chosen thanks to its potential to mimic the fibrous structure of the extracellular matrix (ECM). Finally, it was intended to mimic the 3D hierarchical organization of the cardiac tissue by using a method combining electrospinning and electrospraying (a technic allowing the deposition of particles). The overall strategy of the present work is represented on Figure 1.

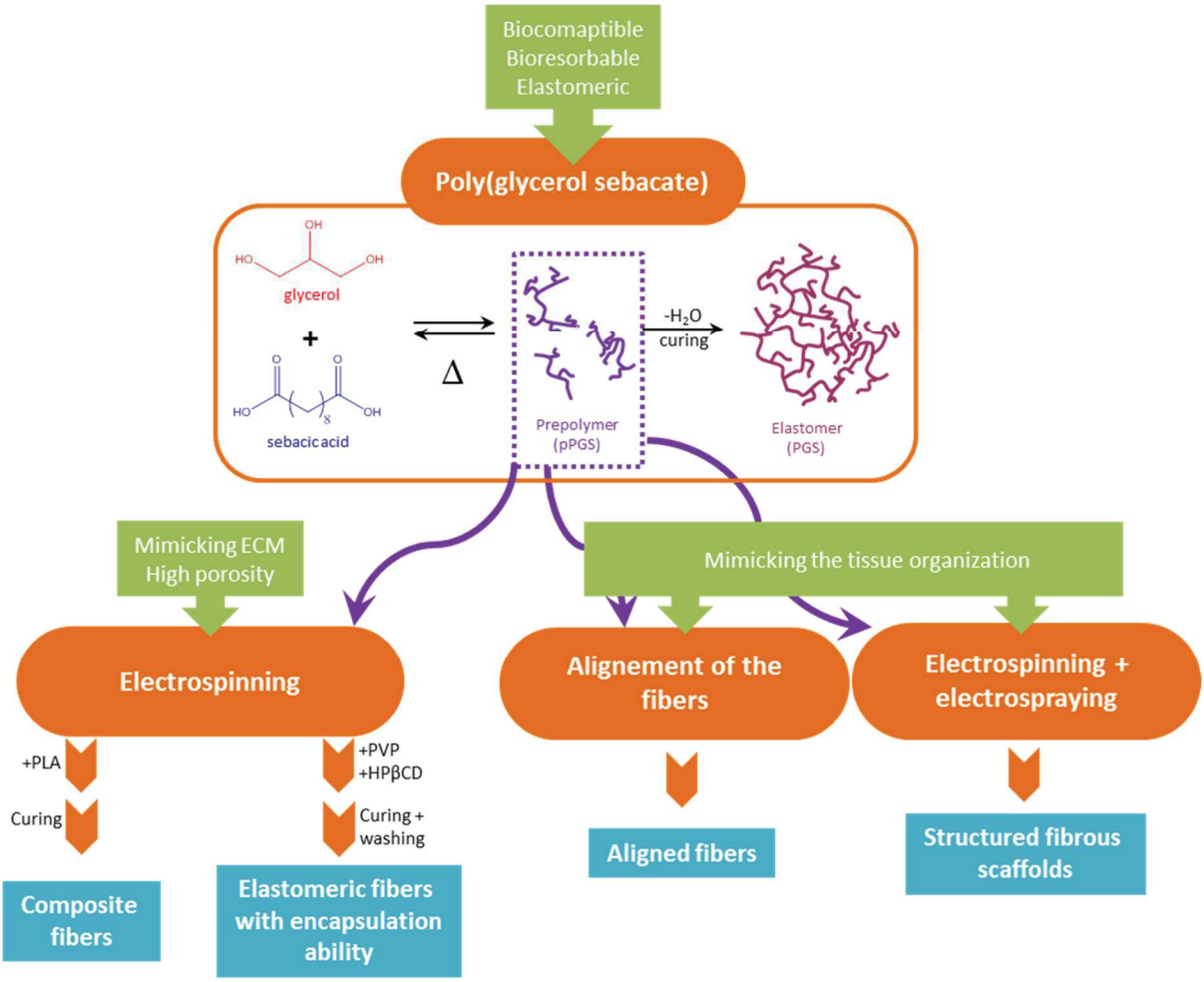

Figure 1. Strategies of elaboration of scaffolds for cardiac engineering. In green : the requirements. In orange: the proposed solutions. In blue: the results.

In a first part (**Chapter 1**), the specifications related to the intended application were identified, which allowed to choose the best material (poly(glycerol sebacate)) and the method (electrospinning). Then (**Chapter 2**), the work was devoted to the synthesis and the characterization of poly(glycerol sebacate). Indeed, it was important to study the effect of the parameters of synthesis on the final properties of the elastomer. The synthesis was divided in two steps: prepolymerization and curing. Prepolymerization leads to a soluble material composed of oligomers with a low molar mass that could be used for electrospinning, while an insoluble crosslinked elastomer was obtained after curing. These first investigations allowed identifying the best reaction conditions to make prepolymers adapted to prepare the desired nanofibrous scaffolds.

The prepolymer (pPGS) was then electrospun with the help of a carrier polymer which is essential to form fibers from molecules with a low molar mass. pPGS was first mixed with poly(lactic acid) (PLA) in order to make composite fibers (**Chapter 3**). These blend fibers were then cured to crosslink PGS. The latter was here useful to enhance the mechanical properties and

the hydrophilicity of PLA. Scaffolds with different compositions and fibers morphology were prepared by this method and their potential for cardiac tissue engineering was compared. In another strategy, pPGS was electrospun with polyvinylpyrrolidone (PVP), a water soluble polymer, and hydroxypropyl-β-cyclodextrin (HPβCD), a biocompatible oligosaccharide that can be exploited to encapsulate drugs by host-guest inclusion complexes (**Chapter 4**). After crosslinking and removal of the carrier polymer by washing in water, elastomeric scaffolds were obtained, with potential interest for drug delivery.

Finally, fibrous structured scaffolds were elaborated from different methods (**Chapter 5**). PGS was processed by electrospraying combined with electrospinning of PLA to make organized fibers deposits. In another method, the high-speed rotation of the collector allowed to fabricate membranes composed of PLA or PLA/PGS aligned fibers. These two last methods were associated to prepare scaffolds composed of aligned PLA fibers and PGS/HPβCD particles. These membranes mimicking the structure of the cardiac tissue, they seem promising to help cell differentiation and migration in the scaffolds.

References

1. The Lancet Global Burden of Disease Visualisations: Compare Available online: https://www.thelancet.com/lancet/visualisations/gbd-compare (accessed on Oct 10, 2019).
2. Lee, W.C.; Chavez, Y.E.; Baker, T.; Luce, B.R. Economic burden of heart failure: a summary of recent literature. *Heart Lung* **2004**, *33*, 362–371.
3. Cook, C.; Cole, G.; Asaria, P.; Jabbour, R.; Francis, D.P. The annual global economic burden of heart failure. *International Journal of Cardiology* **2014**, *171*, 368–376.
4. Langer, R.; Vacanti, J.P. Tissue engineering. *Science* **1993**, *260*, 920–926.

CHAPTER 1

Cardiac tissue engineering: context, materials and process methods

Cardiac tissue engineering is a promising method for the treatment of heart failure. It relies on the promotion of cells growth on a bio-inspired scaffold mimicking the extracellular matrix, the objective being the regeneration the myocardium. This introductive chapter brings the keys to understand the utility of this method and the issues that are raised.

This work starts from two choices. Firstly, poly(glycerol sebacate) was chosen as the material to build the scaffold. Secondly, electrospinning was chosen as the process method in order to make a nanofibrous scaffolds. Arguments for these choices will be provided.

Poly(glycerol sebacate) is suitable for the application because it is an elastomer. However, as a thermoset elastomer, it is difficult to process. Several methods to electrospin elastomers will be reviewed. And finally, examples of electrospinning of poly(glycerol sebacate) taken from the literature will be given.

Cardiac tissue engineering: context, materials and process methods

1. Cardiac tissue engineering: principles and objectives

1.1. A therapy for cardiovascular diseases

Today, cardiovascular diseases are the leading cause of mortality in industrialized countries [1]. For example, myocardial infarctions represent about 20% of the reported deaths in the United States [2]. Such heart attacks are caused by coronary artery occlusions, which lead to a deficient oxygen supply to cardiac cells and subsequently to their death. The loss of cardiomyocytes – the cardiac muscle cells – results in the dilation of the ventricle and in the thinning of the wall of the myocardium – the layer of beating muscle. Moreover, the destroyed tissue is replaced by a non-contractile fibrous scar. As a result, the stress experienced by the muscle increases, inducing a ventricular remodeling expressed by structural and functional changes. Finally, the affected heart becomes less efficient to pump the blood in the body: the patient suffer from heart failure [3]. Unfortunately, the mature myocardium does not have the ability to regenerate by itself [4]. It is thus of great importance to find a therapeutic method to treat heart failure to help the recovery of the heart's vital functions (dioxygen and nutriment supply and waste removal through the blood flow) and to improve the quality of life of the patients.

The first method that can be proposed is a pharmaceutical method where drugs are administrated to limit the production of toxic factors by the body and to decrease the work done by the heart. This method is suitable for mild symptoms [3]. Pacing devices that imposes an electrical stimulation can also be used, but these methods are not enough to tackle the progression of the disease [3]. Today, the ultimate treatment is the transplantation of a healthy heart, but the lack of donors and the issues caused by the immune response limits the applicability of this method.

In new therapeutic methods, researchers intend to decrease the stress in myocardial wall by the use of a biomaterial wrapping the muscle and able to support it. Remodeling can in this way be limited or even reversed [5,6] (Figure 1.1.(A)). Another approach focuses on the lack of cells in the infarcted area, due to the poor regeneration ability of the tissue. In order to tackle this issue, cardiac cells are implanted in the defective area by direct injection of a suspension of cells. Results show that the engraftment of new cardiomyocytes by this method improves contractile functions [3]. However, the engraftment of cells is not efficient by this way because only a few of the injected cells remain in place [4,7].

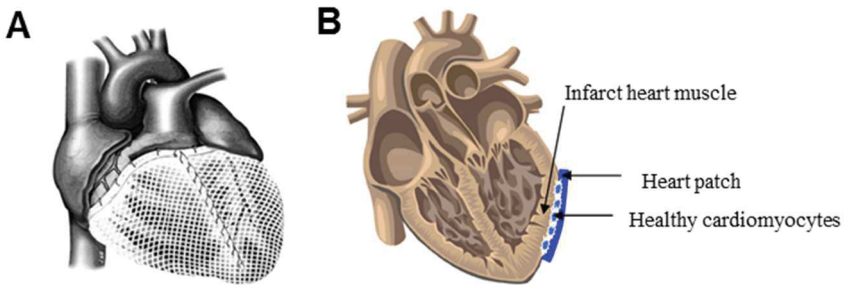

Figure 1.1. (A) Illustration of the use of a commercial mesh used to restrain left ventricle (CorCap Cardiac Support Device (Acorn Cardiovascular, Inc.). **(B)** Illustration of the use of a cardiac patch delivering cardiomyocytes [8].

Tissue engineering was the strategy chosen for the present project and it will be discussed in the following sections. It combines these two last methods. Indeed, in order to improve the engraftment of the cells, they can be delivered with the help of a supporting material providing mechanical support to the muscle (Figure 1.(B)).

1.2. Principle of tissue engineering

Tissue engineering is a relatively new concept emerged in the early 1990s [9]. It is a really interdisciplinary field where material engineering and life sciences are closely associated. As discussed above, the objective is the regeneration instead of the replacing of a tissue [10]. Two different main approaches are possible. In the traditional one, a biological tissue made-up *in vitro* is grafted on the injured part. In the *in vivo* approach, an acellular device able to promote host cells regeneration is implanted. In both cases, to ensure a good success, it is of great importance to draw inspiration from nature. Native tissues are composed of cells, extracellular matrix and signaling molecules. Engineered tissues should thus mimic this "triad". The extracellular matrix, that is intended to support the cells, is replaced in the tissue engineering method by a supporting material named the scaffold. The scaffold should be porous to allow the migration of cells and the nutrients supply. Moreover, in order to improve the therapeutic potential of the tissue construct, it is possible to incorporate signaling molecules like growth factors to enhance the differentiation of the cells, or molecules involved in cell signaling or even adhesion proteins [3,9,10].

Finally, major required features of the device can be identified. Some are related to the material chosen to build the scaffold; others are related to the process of fabrication of the scaffold. The mode of cell seeding and the source of cells are also essential questions researchers should answer to prove that the technique is viable. However, as these last points are not crucial aspects for the present work, they will not be developed here. In summary, it can be mentioned that immature cells like stem cells are usually seeded, possibly associated with supporting cells able to help to recreate the native environment. In particular, it is useful to seed endothelial cells that will allow the formation of capillaries necessary to provide blood in the thickness of the regenerated material.

The first requirement for the material employed to build such scaffold is its biocompatibility. It means that when implanted in the body, it does not trigger a high inflammatory response from the host tissue or any harm [11]. It also implies that before implantation, cells can adhere and proliferate at its surface [10]. Natural polymers like collagen, gelatin, alginate or chitosan are a good choice for this purpose. Indeed, they promote cells

adhesion, growth and differentiation because their surface can be recognized by the cells thanks to chemical cues like ligands [10,12]. However, natural polymers, especially proteins have several drawbacks: risk of immune rejection, properties variability depending on the source, and low mechanical properties [12,13]. For these reasons, synthetic polymers represent also a choice of interest, as some synthetic biopolymers can also be biocompatible. To compensate their biological inactivity, they can be functionalized by coating or grafting chemical functions recognized by the cells.

The material chosen should also be bioresorbable. Indeed, the final objective is to achieve the regeneration of the host tissue. When this task is completed, the scaffold is not necessary anymore. In order to avoid the presence of a foreign material in the body over a long period of time and the resulting long term biocompatibility issues, the degradation of the scaffold is crucial [9,12]. The products of degradation should also be biocompatible and be eliminated by the body. In addition, the rate of degradation is of major importance as the scaffold should not disappear before its supporting mission is fulfilled: the degradation rate should fit the tissue formation rate [10].

The choice of the material should also be driven by its mechanical properties. Of course, the scaffold should be easy to handle for a surgical operation and be able to undergo the same stress than the host tissue without any weakness [9]. It should also be compliant enough to prevent any damage on the surrounding tissues. In addition, cells are sensitives to their environment, in particular to the stiffness of the substrate. Several studies suggest that the differentiation of the cells seeded on a substrate can be enhanced or even oriented differently by the mechanical properties of the substrate. Engler *et al.* [14] published an illustrative example with mesenchymal stem cells (MSCs). MSCs are multipotent stem cells that can potentially differentiate in cells composing various tissues. Here, Engler's team showed that when MSC's are cultured on a soft substrate having a stiffness similar to brain stiffness, they differentiate in neurons-like cells. When the substrate is stiffer like bone, bone cells are obtained. And for a middle stiffness mimicking muscle stiffness, muscle cells develop. These results are illustrated on Figure 1.2.

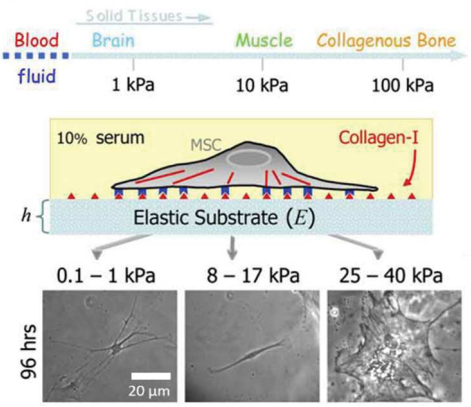

Figure 1.2. Differentiation of the MSCs according to the stiffness of the substrate [14].

Beyond the material itself, the process of fabrication should also be carefully chosen. On the one hand, if we think on the applicability of the method for a large number of patients, the process should be easily scalable up, despite the required high degree of quality (sterilized devices …). On the other hand, the choice of the process method has an impact on the structure of the scaffold and thus on its mechanical properties. In order to get the needed porosity, several techniques are possible. We can cite particulate leaching, solvent casting, freeze drying, phase

separation, foaming, sintering of particles, electrospinning, photolithography and additive manufacturing. The idea is to find a method able to reproduce the extracellular matrix and a surface of substrate with a topography adapted for the cells.

The scaffold can thus be enhanced by the choice of adequate material and structure, but also by functionalization. For example, we can use the material to deliver drugs, growth factors, angiogenesis factors (to induce the generation of capillaries) or genes [10,12]. In these cases, all the fabrication steps must be mild enough to preserve these components. To enhance the cells-substrate interaction, the surface can be functionalized by grafting proteins, plasma treatments, UV irradiation or etching by a base or an acid [9].

1.3. Specification for cardiac tissue engineering

The key parameters related to the scaffold are related to the properties of the tissue which has to be regenerated. In order to design a scaffold adapted for cardiac tissue engineering, it is thus of great importance to consider the myocardium's characteristics.

The first observation we can do relates to the structure of this muscle. Cardiomyocytes are aligned fibrous cells supported by an extracellular matrix composed of aligned collagen fibers embedding honeycomb-like pores hierarchically organized. Smallest pores (8-15 μm) in the tissue are occupied by capillaries, middle-size pores (15-25 μm) are defined to receive the cardiomyocytes and larger pores (40-200 μm) embed blood vessels [15] (Figure 1.3). This observation leads to several conclusions about the requirements for the scaffold. The scaffold should include pores with different sizes, ranging from about 10 μm to 100 or 200 μm to allow the migration of cells and vascularization. Moreover, it should be composed of fibers. And in order to mimic the anisotropy of the organization of the collagen structure, the fibers should be aligned to ensure a good orientation of cells [16]. Indeed, former studies showed that scaffolds with aligned patterns can improve the generated tissue in comparison to randomly organized one. For example, aligned electrospun fibers promote cell organization, attachment, alignment and more mature phenotype [17,18]. All these parameters should also help to choose the process.

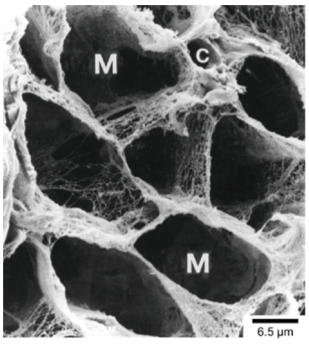

Figure 1.3. Rabbit heart section after removing of the cells: only collagen fibers remains. M marks the pores embedding cardiomyocytes and C the capillaries [15].

A large number of biopolymers were already used for cardiac tissue engineering. Bio-based polymers where used as injectable gel [13] but also as scaffolds. We can find examples of collagen [19], gelatin [20] or alginate [21] porous mesh. Synthetic polymers were also used to build scaffolds, especially polyesters like polycaprolactone [22,23], poly(lactic acid) [24] or its copolymer with poly(glycolic acid) [25,26], poly(glycerol sebacate) [4,27] or poly[(1,8-octanediol)-co-(citric acid)] [28] use. Additionally, polyurethanes, biocompatible polymers popular for their mechanical properties were employed [29–31].

To choose among the variety of biocompatible and bioresorbable materials that are available, the first characteristic we can focus on is the mechanical properties. The tensile stress of the cardiac tissue reaches 3-15 kPa [32] to resist to the pressure in the ventricles (until 140 mmHg for healthy patient [33]). In normal condition, it is elongated until 22% of strain [32]. Moreover, it bears a cyclic deformation over a long period. As it deforms elastically [33], it recovers its shape after each deformation. Indeed, as for many biological tissues, heart tissue does not follow a linear elasticity behavior: the modulus increases when the strain increases. The stress-strain curve is thus convex with a "J shape" [3]. The stiffness of the heart muscle was reported at 10-20 kPa at the beginning of diastole (when the heart starts to relax, with a strain of 0%) and 200-500 kPa at the end (when the heart is full of blood, at a strain of 22%) [8].

As previously mentioned, the phenotype of cells is affected by the stiffness of the substrate. Engler *et al.* [34] seeded embryonic cardiomyocytes on substrates with different stiffness and found that the best phenotype was obtained for a modulus of 11 kPa, whereas on harder substrate mimicking heart scar tissue after infarct, the cells stopped to beat. The same kind of result was found by Bhana *et al.* [35] at the tissue level. However, it was mentioned in the literature that the use of stiffer materials could be beneficial because they can decrease the stress due to the myocardium wall thinning [36]. Finally, the target moduli usually identified for scaffold for cardiac tissue engineering are set between tens of kPa and 1 MPa. We can conclude that mechanical properties are of great importance for cardiac tissue engineering. The material chosen for the scaffold should thus be mechanically performant. Natural polymers like proteins or polysaccharides, with low mechanical properties, should not be selected. The focus should be done on synthetic elastomers.

It has also been mentioned earlier that the degradation rate of the scaffold should be adapted in order to provide support until the new tissue is sufficiently regenerated. In the myocardium case, the scaffold should not degrade in the first weeks, while most of the geometric changes of the muscle are operated. The scaffold should keep its integrity during at least 6 weeks [37], and degrade gradually later. From this perspective, materials such as polyurethanes are not adapted.

A feature specific to cardiac engineering that was not mentioned in the above general presentation of tissue engineering is the conductivity of the material. Indeed, in a healthy heart, the cardiomyocytes beat in a synchronized fashion thanks to an electrical signal transported in the tissue. The literature confirms that conductive scaffolds based on conductive polymers like polypyrrole [38] or polyaniline [39] or containing carbon nanotubes [25] or gold nanowires [40] can improve the differentiation and the alignment of cardiomyocytes and the interaction between them. With such scaffolds, it is possible to improve even more the differentiation and the synchronization of the beating of the cells by applying an electrical stimulation to the culture [39–41]. It is here interesting to notice that beside an electrical stimulation, a mechanical stimulus can also improve the cardiac tissue culture: MSCs seeded on a stretched substrate are better aligned and differentiated [42]. But these last considerations are related to the cell culture and not to the scaffold preparation; they will thus not be developed in this work.

To conclude this section, in this work we want to fabricate a scaffold able to insure two functions: deliver healthy cardiomyocytes onto the infarct region and provide a mechanical support to the ventricle. The design of this device will take into account two main characteristics: the nature of the material and the structure of the scaffold. Furthermore, the material should be biocompatible, bioresorbable, degrade in more than a few weeks and have a modulus comprised

between tens of kPa and 1 MPa. The material should be processed into a porous and fibrous scaffold including anisotropy. The next sections will present the material and process method chosen in accordance with these target properties.

2. An elastomer tuned for cardiac tissue engineering: the poly(glycerol sebacate)

2.1. Preparation and properties of poly(glycerol sebacate)

Poly(glycerol sebacate) (PGS) was designed as a material intended for biomedical applications by Wang *et al.* in 2002 [43]. They proposed a synthesis by bulk polycondensation of glycerol and sebacic acid by simple blend and heating under vacuum. The final product is a transparent and almost colorless material, amorphous at 37°C and quite hydrophilic with a water-in-air contact angle of 32° [43]. The free –OH remaining from glycerol are responsible for its hydrophilicity [44]. PGS is a thermoset elastomer, but it is possible to stop the reaction after a first step to get independent oligomers or prepolymers (pPGS), that can be further processed by melting or dissolution (pPGS being soluble in 1,3-dioxolane, tetrahydrofuran, ethanol, isopropanol and *N,N*-dimethylformamide [43]). The shaped pPGS can then be cured under vacuum to achieve the crosslinking into the PGS elastomer. The final properties can be tuned by modifying the synthesis parameters: ratio of reagents, type of heating, time and temperature of curing.

Glycerol is found in the body as the building block of lipids. Sebacic acid is a natural metabolic product of the oxidation of fatty acids. Both monomers are thus nontoxic and PGS can be naturally metabolized in the body. Moreover, the use of their copolymers for medical application was approved by the US Food and Drug Administration (FDA) [43]. As PGS can be synthesized without the addition of any other additives (no catalyst, no solvent …), it seems adapted for *in vivo* applications [44]. Its biocompatibility was confirmed early *in vitro* as well as *in vivo* [43,45]. Compared to poly(lactide-*co*-glycolide) (PLGA), a well-known biopolymer, PGS allows similar or better attachment and proliferation of fibroblast [43] and Schwann cells [45]. *In vivo*, PGS triggers a lower inflammatory response and less fibrosis (*i.e.* avascular scar tissue) than PLGA [43,45]. However, a downside note can be emitted: it was established that the acidity of PGS can induce a higher inflammatory response. Indeed, the acidity is higher for a PGS with a low crosslinking density including more unreacted carboxylic acid groups. Additionally, the pH decreases during degradation because of the acids resulting from the aqueous hydrolysis of esters [46–48].

The degradation of PGS is driven by the cleavage of esters linkages through surface erosion. Thanks to this degradation mechanism, the geometry of a sub-cutaneous implant and the integrity at its surface are preserved during degradation, and the weight loss is linear until reaching 70% after 35 days of implantation. The water uptake stays quite low, preventing deformation and softening of the implant, and acceleration of the hydrolysis. Finally, the modulus decreases linearly and slowly during degradation: it reaches 50% of the initial modulus after 35 days [49]. While 60 days after implantation *in vivo*, PGS is totally absorbed, after the same period in PBS solution at 37°C, only 17% of the sample is degraded: this result shows that enzymatic digestion is also involved [43]. However, the degradation rate is correlated to the ratio of reactants according to Guo *et al.* [50] who found 20 to 40% of mass loss after 32 days of immersion in PBS at 37°C, depending on this ratio. Moreover, Pomerantseva *et al.* [51] showed that the degradation rate is not related to the curing time whereas it was proven that a longer curing time increases the crosslinking density of PGS.

Because a modification of the curing time affects the crosslinking density, it also alters the mechanical properties. Globally, PGS has a Young's modulus comprised between 0.025 to 1.2 MPa, which matches soft tissue's moduli, and a strain at break of up to 330% [44]. Wang *et al.* [43] observed that the modulus is not altered if PGS is hydrated. It shows a non-linear elasticity behavior and can be reversibly deformed at high strain [8,43,48]. PGS elasticity comes from the chemical crosslinking between the monomers and from the hydrogen-bonding interactions between the free –OH of glycerol [43]. As said above, mechanical properties can be tuned by the adjustment of the curing time: a longer reaction time leads to more crosslinked materials and thus to stiffer elastomers [52]. In the same way, increasing the curing temperature accelerates the kinetics of the reaction and thus increases the degree of crosslinking [8,53]. Interestingly, the modification of the ratio of reactants also affects the mechanical properties: a ratio closer to the stoichiometric proportions leads to a stiffer elastomer [52].

As it is necessary to cure PGS at high temperature, it is not possible to incorporate heat sensitive molecules or to polymerize the material *in vivo*, for example after injection. For these reasons, several teams chemically modified PGS by grafting acrylate functions allowing *in-situ* photopolymerization [54,55]. This method allows also a finer tuning of the mechanical properties, but it also has the drawback to introduce more toxic components.

2.2. Examples of applications and processing methods using PGS

PGS was used to fabricate scaffolds intended for tissue engineering in various fields such as vascular [56–60], cartilage [52,61,62], cardiac (see next subsection), retinal [63,64], nerve [45], tympanic [65] or skin [66] regeneration, but also for drug delivery [67–70].

Numerous processing methods where used to shape PGS in a suitable structure able to promote tissue regeneration. For example, for vascular engineering, networks of capillaries were fabricated by micromolding (see Figure 1.4.(A)) [56,57]. To get this result, pPGS is deposited on sucrose-coated micromolds. Sucrose is removed in water after PGS crosslinking to deliver a structured sheet. To get the final construct, PGS sheets are stacked. The same method was used by Bettinger *et al.* [71] to fabricate patterned surfaces able to control cell orientation and morphology. They found good alignment and elongation of endothelial cells seeded on smooth rounded lines (see Figure 1.4.(B)).

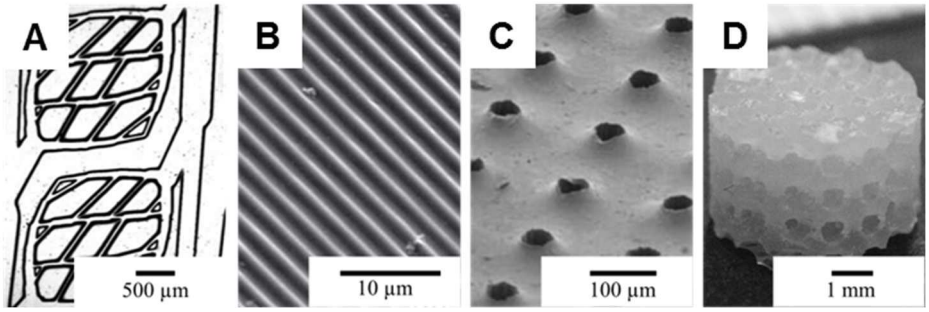

Figure 1.4. ***Examples of PGS constructs.*** **(A)** Network of capillaries [56]. **(B)** Smooth rounded lines [71]. **(C)** PGS sheet with holes pattern [63]. **(D)** 3D scaffold with large pores [52].

An approaching method was used by Neeley *et al.* [63] using a sucrose-coated PDMS negative mold to fabricate a PGS sheet patterned with holes (see Figure 1.4.(C)) able to deliver retinal cells. Molding method was also used by Kemppainen and Hollister [52] to fabricate porous 3D scaffolds (see Figure 1.4.(D)) with mechanical properties adapted to cartilage

regeneration. Here, a hydroxyapatite inversed mold is used to shape the PGS. After curing and decalcification of hydroxyapatite, the scaffold has pores 1 mm large and a porosity of 48%.

Other methods to prepare porous 3D scaffolds include particulate leaching. In this method, the prepolymer is mixed with NaCl particles. The blend is poured in a mold, cured, and the salt is dissolved to leave pores behind him. These porous scaffolds were designed for cartilage [61] and skin regeneration [66]. The porosity obtained by this method is finer than with the previous one (see Figure 1.5.(A)), pores diameter ranging from 50 to 250 µm [66], depending on the proportion of added salt. The porosity can then reach 80% [61]. This approach using salt can by slightly modified by the addition of a sintering step to prepare a salt template. Again, the prepolymer is poured on the salt, cured, and the template can then be dissolved. This salt fusion method was used to prepare tubular porous scaffolds (see Figure 1.5.(B)) adapted for vascular regeneration [59,72]. Vilariño-Feltrer *et al.* [73] showed that the microstructure of the final scaffold is not affected by the size of the particles sintered or the pressure used during sintering. However, low pPGS/salt ratio leads to higher porosity. In the same way, pouring pPGS solution instead of pure melted pPGS allows a better deposition and thus a higher porosity, which leads to a better cells colonization.

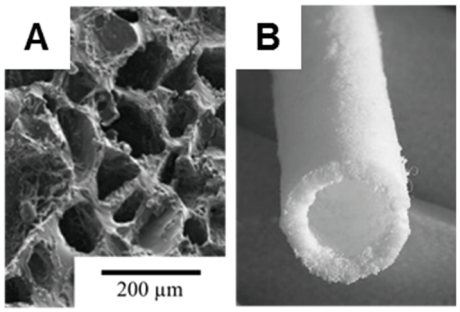

Figure 1.5. ***Porous PGS 3D scaffolds***. **(A)** Fine porosity obtained by salt leaching [66]. **(B)** Porous tubular scaffold obtained by salt fusion (inner diameter: 5 mm) [72].

All the above examples show that PGS was used for a large variety of tissue engineering applications using various processing methods. We have seen earlier that from a mechanical point of view, PGS is suitable for cardiac tissue engineering. The next subsection will thus focus on examples of PGS-based scaffolds designed for myocardium regeneration.

2.3. Application in cardiac tissue engineering

The interest of PGS relies on the versatility of its properties allowing finding the right properties for the targeted tissue. Chen *et al.* [8] tried for example to cure pPGS sheets at different temperatures to study the effects on the mechanical properties and the degradability. A higher temperature led to a higher stiffness. They found in all the cases a stiffness that could be suitable for cardiac applications, ranging between 0.056 MPa and 1.2 MPa. The degradability was very different according to the curing temperature. A sample cured at 110°C can totally resorb *in vitro* after about 15 days whereas a sample cured at 130°C loose almost no mass after 60 days. Marsano *et al.* [74] studied the influence of the mechanical properties on the tissue development. Here, they changed the curing time at 150°C to modulate the stiffness of porous PGS scaffolds obtained by salt leaching technic. Cardiomyocytes were seeded on the scaffolds that were perfused by culture media in a bioreactor. The authors found that the obtained tissue was more functional when cultured on the weaker scaffold having a compressive modulus of 2.35 kPa. The

tissue obtained on the stiffer scaffold having a compressive modulus of 5.99 kPa was not well developed.

The structure of PGS scaffolds was improved by microfabrication methods. Engelmayr *et al.* [75] used laser ablation to prepare scaffolds with accordion-like honeycomb pattern as pores (see Figure 1.6.(A)). To get this result, PGS sheets deposited on silicon wafers were exposed to a laser beam following a preprogrammed pattern. The thickness of the scaffold was increased by stacking two different layers resulting in 3D interconnected pores. When wet, these scaffolds have a modulus below 100 kPa, the value depending on the direction of solicitation because the mechanical properties are anisotropic. Cardiac cells culture on such scaffolds gave good cell alignment and contractibility. Park *et al.* [76] confirmed the importance of stacking two layers to have a scaffold thick enough (about 500 µm thick) fabricated by the same method. Here, they improved the cardiac cells culture by perfusion of culture medium through the 250 µm long and 150 µm wide accordion-like honeycomb pores. Neal *et al.* [77] studied influence of the pores geometry with PGS scaffolds quite similar to the previous one. They used micromolding to prepare 2-layers scaffolds with rectangular interconnected pores and observed the influence of the ratio length/width of the pores on the elongation and interconnectivity of myoblasts (muscle stem cells). Park *et al.* [78] tried then to improve cell culture on such scaffolds by adding growth factors and electrical stimulation during culture. The growth factor permits to decrease cell auto-destruction and to improve cell-to-cell connectivity and electrical activity. The electrical stimulation oriented the cells in the electrical field direction.

Guillemette *et al.* [79] also worked with PGS scaffolds including rectangular pores obtained by microablation, where they added parallel 10 µm high double-lines by micromolding (see Figure 1.6.(B)). This configuration allowed them to study the influence of the pore geometry and the surface topography, and they showed that the lines improved cells orientation. The modulus of these scaffolds ranges from 400 to 1200 kPa. The topography was also studied by Zhu *et al.* [4] who drew 3 µm-deep parallel channels with various width ranging from 10 µm to 50 µm (see Figure 1.6.(C)). They found that the best alignment of myocytes is achieved for 20 µm width channels separated by walls of 20 µm width. They investigated another way to improve cardiomyocytes culture: they covalently bonded to PGS a brain derived neurotrophic factor having beneficial effect on cardiomyocytes: N,N',N''-tris(2-hydroxyethyl)-1,3,5-benzenetricarboxamide. For this purpose, the molecule was added to glycerol and sebacic acid at the beginning of the polymerization at 130°C. After curing at 160°C, an elastomer that can deliver the molecule of interest during its degradation is obtained.

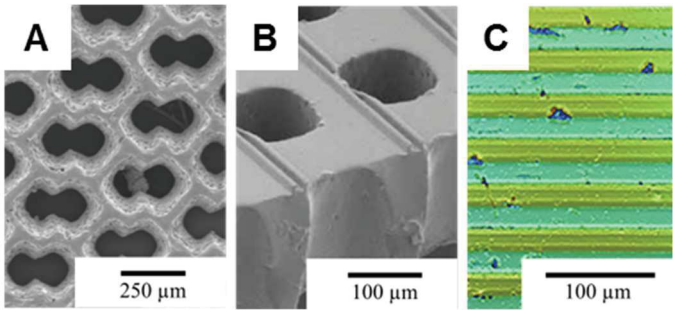

Figure 1.6. ***Different structures made of PGS experimented for cardiac tissue engineering.***
(A) Accordion-like honeycombs [81]. **(B)** Scaffold with rectangular pores and surface topography modified by parallel lines [79]. **(C)** Parallel channels 20 µm wide and 3 µm deep [4].

A similar approach was employed by Rai *et al.* [80]. Here, peptides were successfully covalently bonded to PGS sheets surface. Another way to improve PGS sheets properties consists of the addition of bioglass in the bulk [47]. The presence of this alkaline component does not affect significantly the mechanical properties of the composite but increases its biocompatibility by decreasing the acidity due to the degradation products of PGS.

Investigations were also conducted to enhance the development of cardiac tissue on PGS scaffolds by the optimization of the culture conditions. Radisic *et al.* [82] worked on porous scaffolds fabricated by salt leaching method with up to 91% of porosity, where parallel channels, cross-cutting the scaffolds, were cut by laser ablation. These channels permit the perfusion of culture medium. Cardiomyocytes and fibroblasts (cells involved in the extracellular matrix fabrication and representing about two thirds of the cardiac cells) were seeded and the oxygen supply was optimized to improve the cells phenotype. It has been also proven that pretreating PGS scaffolds by fibroblasts before cardiomyocytes seeding can improve the myocytes alignment and orientation [83]. Chen *et al.* [84] recommend to precondition PGS sheets by simple immersion in culture medium 6 days prior to cells seeding. In this work, the facilitation of cells detachment was also improved. Indeed, after implantation, healthy cardiomyocytes should detach from the scaffold to be integrated in the heart. It was shown here that this phenomenon is more efficient with non-gelatin coated PGS patches.

We can see from the above examples that PGS is promising for cardiac tissue engineering, and that it can be processed by various methods. The processes presented here allow the fabrication of structures with more (laser ablation, micromolding) or less (salt leaching) shape control at the microscopic level. In order to mimic the fibrous structure of the extracellular matrix and get functional materials, electrospinning is often employed. The next sections will show how electrospinning could provide such interesting structures.

3. Electrospinning for tissue engineering

3.1. Principle of electrospinning

Electrospinning is a process allowing the formation of a thin fiber by stretching of a polymer solution submitted to a high electric field. In practice, a polymer solution is injected to a metallic needle subjected to a high electrical potential (tens of kV). In front of the needle, a collector submitted to a negative voltage or connected to the ground is set up (Figure 1.7.(A)). Under the effect of the resulting high electric field (in the range of 1 kV/cm), a force due to the electric charges deforms the droplet of polymer solution at the tip of the needle. When the resulting electric pressure exceeds the pressure due to surface tension at the air-solution interface, the droplet form the so-called Taylor cone (Figure 1.7.(B)), and a thin jet of solution is ejected. The jet first follows a straight path, but then, under the effect of the viscoelasticity of the polymer, the Coulomb forces due to the charges and the surface forces due to the curvature, the jet undergoes whipping movements (Figure 1.7.(C)). These movements allow the stretching of the jet and evaporation of the solvent [85–88]. As a result, a continuous dry nanofiber is randomly deposited on the collector, forming a non-woven mat (Figure 1.7.(D)). The diameter of the fibers obtained by electrospinning is usually comprised between tens of nanometers and few microns. Because such mats have a high porosity and a large specific surface area they can be used as filters, sensors, catalyst support, or in biomedical applications (drug delivery, wound dressing, tissue engineering …).

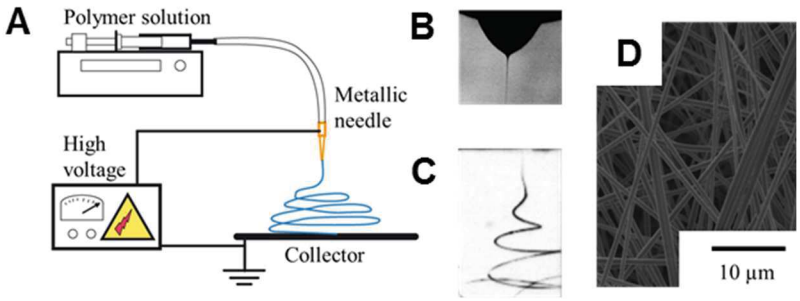

Figure 1.7. **(A)** Electrospinning set-up. **(B)** Taylor cone [89]. **(C)** Whipping movement [90]. **(D)** Electrospun non-woven mat.

In order to get the desired non-woven mat, the solution should be carefully designed. In particular, the fibers morphology depends on the solvent's conductivity and volatility and the solution surface tension. Moreover, the viscosity of the solution is important. Indeed, it was observed that for low concentration and thus little viscous solutions, no fibers but particles are fabricated. This phenomenon is caused by the Plateau-Rayleigh instability that tends to break the jet of liquid due to the effect of the surface tension. At higher concentration, beaded fibers are formed, but when the concentration and thus the viscosity are high enough, defect-free fibers can be fabricated [91]. Indeed, the result depends on the number of entanglements in the polymer solution, which is reflected by the viscosity. The measurement of the viscosity as a function of the concentration of a polymer with a given molar mass allows identifying four dilution regimes [92–94]. At low concentration C, more precisely when $C < C^*$ with C^* the critical chain overlap, the solution is in dilute regime and polymer chains do not interact. When $C^* < C < C_e$ with C_e the critical entanglement concentration, at the semi-diltue unentangled regime, polymer chain overlap. It is thus possible to electrospin continuous fibers, but because of the low number of entanglements, the jet does not resist to Plateau-Rayleigh intability and beads punctuate the fibers. Above C_e, the semi-dilute entangled regime is reached for polymers with high molar mass. The high number of entanglements allows then the formation of defect-free fibers [95–98]. However, for low molar mass, the third regime is a concentrated unentangled regime, which prevents the formation of continuous fibers. So, in order to favor the presence of entanglements, high molar mass polymers are preferably employed for electrospinning. Finally, a further increase of the concentration increases the fiber diameter until a too high viscosity is reached, when no electrospinning is possible. The four electrospinning regimes where for example studied by Lavielle *et al.* [97] for polycaprolactone fibers: Figure 1.8 represents the evolution of the morphology of the fibers as a function of the intrinsic viscosity multiplied by the concentration.

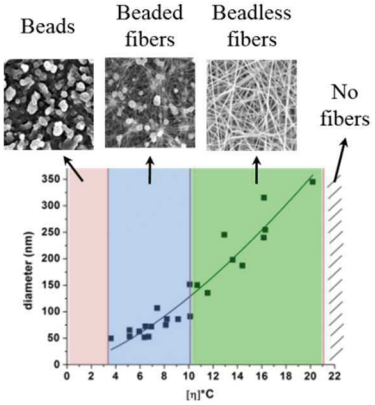

Figure 1.8. Representation of the four electrospinning regimes and of the evolution of the diameter as a function of $[\eta]C$ [97].

Besides, process parameters such as voltage, needle to collector distance or injection flow rate of the solution should be adjusted to get the desired result. Ambient parameters should also be taken into account as temperature, ambient humidity or nature of the surrounding gas are known to play a role in the process [86,88,99].

3.2. Electrospinning of composite fibers by blend or coaxial electrospinning

Electrospinning is a convenient method to prepare composites and functionalized nanofibrous structures. Indeed, it is easy to co-electrospin different components together to use the specific properties of each of them. The objective can be the addition of charges (conductive nano-charges for sensors, hydroxyapatite for bone tissue engineering (Figure 1.9.(B)), …), the fabrication of structured fibers (fibers with porous surface (Figure 1.9.(A)) or hollow fibers after selective dissolution of one component), or assistance to facilitate the process. To this end, two methods are available: blend electrospinning and coaxial electrospinning.

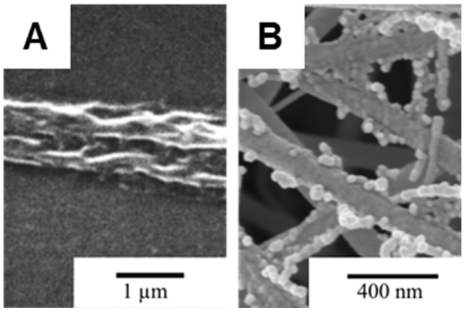

Figure 1.9. (A) Residual porous PLA fibers after removal of PVP from PVP/PLA blend fibers [100]. **(B)** Polyamide fibers decorated with hydroxyapatite nanoparticles [101].

3.2.1. Blend electrospinning

In blend electrospinning, the two components are simply blended and dissolved together, the resulting solution being eletrospun [102–104]. If the first component is electrospinable in the conditions of the prepared solution, it is possible to choose a second component more difficult to electrospin. The latter can be inorganic particles, polymeric particles insoluble in the selected solvent (in particular suspensions in water) or polymers with low molecular weight, unable to provide entanglements in the solution. The non-electrospinable material is carried by the first polymer – the carrier polymer – during the fiber formation. After electrospinning, the carrier polymer can be selectively solubilized to keep fibers composed of the non-electrospinable material only.

3.2.2. Coaxial electrospinning

Coaxial electrospinning is used to fabricate core-shell fibers (Figure 1.10.(B)). In this method, two concentrically aligned nozzles are used to inject a shell solution wrapping a core solution (Figure 1.10.(A)) [102,103,105–107]. The core solution is actually drawn by viscous forces resulting from ejection and stretching of the shell solution. Again, the objective can be the fabrication of fibers based on a material difficult to electrospin alone. In this case, the shell can be removed after electrospinning. In a similar way, it is possible to selectively remove the core to get hollow fibers (Figure 1.10.(C)). However, keeping both components can have an interest too, in particular to improve the biocompatibility of biopolymers [108–110].

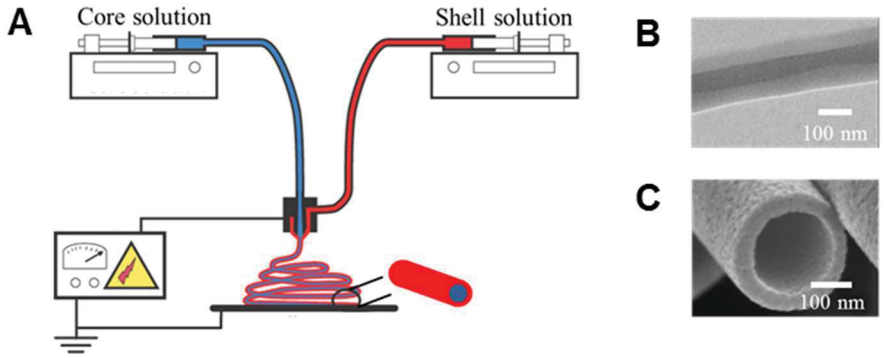

Figure 1.10. (A) Set-up for coaxial electrospinning. **(B)** Coaxial fibers with PCL as shell and PCL/PEG loaded with a model protein for the core [111]. **(C)** TiO2 hollow fibers obtained by electrospinning of PVP/TiO2 as shell material and mineral oil as the core, extraction of the core and calcination [112].

3.3. Advantages of electrospinning for tissue engineering

As explained in the above section describing tissue engineering approach, a well-designed scaffold should mimic the structure and the function of the extracellular matrix (ECM) [113]. Concerning electrospun scaffolds, the first outstanding aspect is their fibrous structure mimicking the hierarchical organization of the ECM. The diameter of electrospun fibers is similar to the diameters of the fibrils composing ECM (50 to 500 nm) [113]. Some results indicate that scaffolds composed of fibers with a diameter below the micron allow a better tissue response [113]. There is a link between fibers diameter and biocompatibility [114], but the best diameter depends on the cells seeded.

Low fiber diameters allow also a high surface to volume ratio. This property is beneficial to scaffolds because it offers more binding sites for cells receptors (and thus enhance cell attachment), more surface available to adsorb proteins, and larger surface exchange for drug delivery [113,115,116]. Furthermore, electrospun scaffolds have generally a porosity greater than 80%. Building an interconnected 3D porous system is of great importance for the transportation of the nutrient and the wastes. The pores should also help cell migration, and the ideal pore size should be adapted to the cells dimensions and depends thus on the cells nature. Unfortunately, electrospun scaffolds have an average pore size in the range of the micron, leading to poor cell infiltration. To face this issue, several methods were proposed, including fibers selective leaching [117], increase of the fibers diameter to increase the pore size [117], use of a porogen agent such as salt [118] or ice crystals [119], deposition of intercalated layers of biodegradable hydrogel [120], collection of the fibers in a liquid bath in order to decrease fibers bonding [121] or direct deposition of cells between fibers layers [122].

Besides their advantageous architectures, electrospun scaffolds are easy to functionalize. We have seen above that it is possible to electrospin composite fibers. Scaffolds properties can be adjusted by the mixing of different materials. For example, it is convenient to coelectrospin natural and synthetic polymers to combine the biofunctionality of the first and the mechanical properties of the second. This objective can be achieved either by blend or coaxial electrospinning. Notably, coaxial fibers – obtained by coaxial electrospinning, coating [123] or diping [124] – offer a real interest when the shell is composed of a natural polymer recognized by the living tissues. Furthermore, bioactive factors such as growth factors [125,126], differentiation factors [127], enzymes [128], chromophores [129], magnetic nanoparticles [130] or drugs

[107,131,132] can be loaded in the fibers by mixing or encapsulation. For this purpose, coaxial electrospinning is beneficial as the core can play the role of storage while the shell controls the release. Finally, fibers functionalization can also be achieved directly on their surface by grafting of peptides or proteins after the electrospinning step. The surface can also be structurally modified, in particular with pores that can help cells to attach and proliferate [114,115].

Other feasible modifications concern the geometry of the scaffolds. The topography of the collector or its movement can lead to not randomly deposited fibers. These aspects will be detailed in Chapter 5.

To conclude this part, it is noteworthy that in comparison to other methods to prepare nanofibers like phase separation [133] or self-assembly [134], electrospinning is versatile, easily scalable and unexpansive. All the reasons presented here justify the choice of this method to prepare our scaffolds.

4. Electrospinning of elastomers

The previous sections allowed us to identify the elastomers as materials of great interest for soft tissue engineering, in particular for cardiac applications. Moreover, electrospinning is a promising process to fabricate biomimetic structures useful for the regeneration of tissues. However, the elaboration of elastomeric nanofibrous scaffolds is tricky due to the 3D crosslinked structure of elastomers. Different strategies can be envisaged and will be discussed in the following sections.

4.1. Electrospinning of thermoplastic elastomers

Thermoplastic elastomers (TPE) combine elastomeric properties and the ability to be melted or dissolved thanks to physical bonds [135]. They are thus easy to process and no particular issues are identifiable for the electrospinning of such materials: the issues related to the preparation of the electrospinning solutions and the process itself are the same as for not crosslinked polymers.

4.1.1. Styrenic thermoplastic elastomers

Styrenic thermoplastics elastomers are block copolymers composed of rigid polystyrene blocks and soft blocks composed for example of polybutadiene [135].

In 1999, Fong and Reneker [136] fabricated a non-woven mat with regular fibers composed of the triblock copolymer styrene-butadiene-styrene (SBS) dissolved in THF and DMF. The mat is very stretchable and the authors studied the phase separation occurring during the solidification. Feng *et al.* [137] worked on the electrospinning of copolymer styrene-isoprene-styrene triblock. They obtained regular fibers from solutions concentrated from 8 to 15% in THF/DMF solvent mixture (Figure 1.11.(A)). A strain at break of 1711% and a modulus of 0.01 MPa were obtained. Van der Heijden *et al.* [138] aimed to avoid the use of carcinogenic solvents such as DMF for the electrospinning of styrene-butadiene-styrene by using butyl acetate. To form beadless fibers, they had to increase the conductivity by adding a salt (LiBr) and the number of entanglements by adding a small amount of triazolidione. After successful electrospinning of thinner fibers than conventional electrospun SBS fibers, the mat is immersed in a solution of triazolidione: SBS swells and reacts by its C=C bonds with the N=N bonds of triazolidione. This post-treatment increases the modulus of the mat and decreases its elongation at break.

Very stretchable non-woven mats can thus be easily fabricated by the electrospinning of styrene based thermoplastic elastomers. However, this kind of material is not appropriate for biomedical applications.

4.1.2. Thermoplastic polyurethanes

Thermoplastic polyurethanes (TPU) are very popular TPE materials used for electrospinning, especially in the biomedical field. Polyurethanes are synthesized from isocyanates, polyols and often a chain extender [11]. In TPU, hard segments are formed by the isocyanates that arrange themselves in semi-crystalline domains thanks to interactions like hydrogen bonding or π-stacking, while soft segments are formed by the polyols having a glass transition temperature below ambient temperature [139]. The increase of the temperature or the action of a solvent help to disassemble hard semi-crystalline domains, as for a thermoplastic polymer [11].

Stankus *et al.* [140] described the electrospinning of a TPU in 2004. The polymer is synthesized from poly(ε-caprolactone)-diol (PCL-diol) and 1,4-diisocyanatobutane and is electrospun in solution in 1,1,1,3,3,3-hexafluoro-propan-2-ol (HFIP), blended with collagen to biofunctionalized the material. Resulting membranes have a Young's modulus comprised between 2 and 8 MPa and a strain at break reaching 280%.

Other TPU synthesized from PCL-diol and other isocyantates were also electrospun. For example, Stylianopoulos *et al.* [141] made the reaction of PCL with hexamethylene diisocyanate (HDI) to fabricate membranes with a modulus lower than 1 MPa from solutions in HFIP. The same kind of results were obtained with the addition of 1,4-butandiol as hard segment and the control of the soft segments length (Figure 1.11.(B)) [142]. Han *et al.* [143] used L-lysine diisocyanate and L-lysine as chain extender to prepare membranes with ultimate tensile strength between 2 and 8 MPa.

Other diols were employed with various isocyanates, as a fluorated diol used to synthesized a TPU electrospun with a blend DMF/THF [144], but PCL is preferred for biomedical applications. Several commercial biocompatible TPU as Pellethane® [145], Artelon® [146] or Ellastolan® [147] are available and can be electrospun.

Even though they can form perfect fibers without the help of any additives, some authors like Stankus *et al.* [140] blended TPU with other materials in order to improve the properties of the membranes. A TPU synthesized from PCL-diol, HDI and butanediamine as chain extender was electrospun with gelatin in HFIP to increase the hydrophilicity of the material as well as the cell proliferation. A particularly stretchable membrane was prepared from a commercial TPU, Tecoflex™, blended with pPGS in various solvent like chloroform and DMF, HFIP, or 2,2,2-trifluoroethanol and acetic acid. The addition of pPGS allows an increase of the hydrophilicity and the biocompatibility of the material and a decrease of the modulus while improving the strain at break: the most interesting material has a Young's modulus of 0.83 MPa and can be stretched until 350% [148].

Finally, the diversity of the examples found in the literature shows that the use of TPU is very convenient to fabricate membranes with adequate properties for soft tissue engineering. However, we can notice than in most of these examples, HFIP, a toxic and expensive solvent, is used. Moreover, TPU cannot be used when the property of biodegradability is needed.

4.1.3. Copolyester-based thermoplastic elastomers

Apart from conventional thermoplastic elastomers like TPU or styrenic copolymers, it is possible to synthesize and process a large variety of TPE including polyesters-based polymers. For these latter, hard segments are composed of semi-crystalline polyesters blocks and the soft segments of polyesters or polyethers blocks [135].

Cao *et al.* [149] synthesized for example a copolymer where the hard segments are composed of poly(butylene terephthalate) and 1,4-cyclohexanedimethanol and the soft segments of poly(tetramethylene glycol). After successful electrospinning from solutions in dichloromethane/trifluoroacetic acid, the resulting membranes have a Young's modulus comprised between 2.81 MPa and 19.48 MPa and a strain at break up to 1280%. Wang *et al.* [150] fabricated regular fibers composed of a copolymer based on polyethylene terephtalte hard segments and polyethylene glycol soft segments, but the mats were not mechanically characterized.

A membrane stretchable up to 350% was fabricated for biomedical applications by Shah *et al.* [151]. They used a copolymer composed of soft segments based on poly(THF)-*co*-PCL and of hard segments based on PCL (Figure 1.11.(C)), the resulting mat being surprisingly less stretchable than the bulk material.

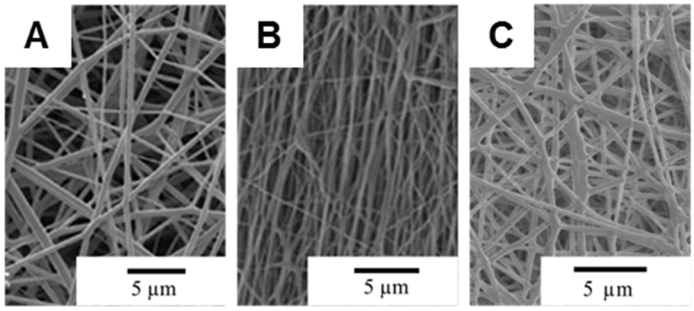

Figure 1.11. *Examples of TPE fibers.* **(A)** Styrene-isoprene-syrene-based fibers [137]. **(B)** TPU-based fibers [142]. **(C)** PCL-co-THF-based fibers [151].

4.2. Electrospinning of thermoset elastomers

In the case of thermoset elastomers, no solubilization is possible. Electrospinning solutions must be prepared before crosslinking. Then, the crosslinking reaction can be done during electrospinning – it should then be very fast because electrospinning is a very brief process [152] – or after, during a post-treatment step.

4.2.1. Simultaneous electrospinning and crosslinking of rubbers based on diene monomers

Because of their large elastic deformation, natural or synthetic rubbers are materials of great interest. Several teams tried to electrospin rubbers, but they had to face some difficulties. On the one hand, rubbers are composed of soluble macromer chains able to form entanglements. These macromers should by linked together by a vulcanization step. On the other hand, their T_g is much lower than ambient temperature and thus non-crosslinked fibers rapidly lose their shape by flowing [153].

To overcome this problem, Choi *et al.* [153] choose to crosslink polybutadiene *in situ*. For this purpose, they selected a fast-crosslinking system under UV light: thanks to a photoinitiator, a tri-thiol plays the role of a crosslinking agent and reacts with the double bonds of polybutadiene.

The fibers electrospun from a solution in THF are subjected to UV light during the rotation of the cylindrical collector. This system allows the fabrication of thick fibers with a diameter of several microns and slightly flat at the contact with the collector (see Figure 1.13.(A)) forming a mat stretchable up to 90%. Thiol-ene chemistry was also employed by Thielke *et al.* [154] to electrospin polybutadiene rubber crosslinked under UV light during electrospinning. They collected the fibers in a methanol bath to avoid the melting of the surface of the fibers touching the collector but fibers have the tendency to collapse together.

In the same way, Kerr-Phillips *et al.* [155] electrospun a butadiene-acrylonitrile copolymer blended with an acrylate crosslinking agent, a photoinitiator and a thermal initiator. An *in situ* crosslinking step under UV light during electrospinning was followed by a thermal crosslinking step at 80°C under vacuum. The crosslinking agent was chosen with low molar mass (poly(ethylene glycol) dimethacrylate of 550 g/mol) to avoid any modification of the viscosity of the electrospinning solution. The proportions of both initiators were chosen to slow down the reaction and avoid clogging at the needle. To verify the efficiency of the crosslinking, soluble fractions were extracted by Soxhlet method: the fibers morphology was not affected.

It is interesting to mention that in order to skip the *in situ* UV crosslinking step and settle for a thermal crosslinking, Liu *et al.* [156] used a carrier polymer able to keep the fibers structure. In this strategy, a solution containing ethylene-propylene-diene terpolymer blended with a thermal initiator in THF is injected as the core of coaxial fibers, where the shell is formed by polyvinylpyrrolidone (PVP). After a 2h curing step at 130°C, PVP is eliminated by dissolution in ethanol. Thanks to the PVP shell, coaxial fibers do not flow under heating and the fibers are still defined after the removal of the PVP sheath.

4.2.2. Other materials electrospun and crosslinked under UV light

Simultaneous electrospinning and UV crosslinking is a convenient way to electrospin elastomers, as it theoretically does not require post-treatments. Examples with various polymers comprising C=C insaturations can be found in the literature. For example, acrylates were used by Kim *et al.* [157] to fabricate elastomeric nanofibers. To reach this goal, they blended various acrylates (see Figure 1.12.(A)) with a photo- and a thermal initiator. Because the blend is initially liquid, it is heated to trigger the reaction. When the viscosity is high enough, the resulting oligomers blend is electrospun under UV exposure. This exposition is required otherwise the jet breaks into droplets. But when the fibers reach the collector the reaction is not over yet: the properties continue to evolve during time. The mechanical properties of the fibers were not measured at dry state, but a characterization with atomic force microscopy indicates that they have an elastomeric behavior at wet state.

The UV crosslinking method was optimized by Jeshvaghni *et al.* [158] for a biocompatible system containing a polyester bearing a fumarate group and a photoinitiator (see Figure 1.12.(B)). These two components, dissolved in a mixture of dichloromethane (DCM) and DMF with up to 30% of PCL, are electrospun and crosslinked in various conditions. In a first type of experience, the crosslinking takes place during electrospinning, with exposure of the jet to UV light. This method does not work well because UV crosslinking was not achieved before the landing of the solidified fiber. It can be improved by collection of the fibers in a liquid bath. Then, chains mobility is enough increased to achieve the crosslinking reaction. The fibers morphology remains good and the Young's modulus reaches 0.6 MPa, which is interesting for soft tissue engineering. Moreover, the strain at break reaches 115%. Two other methods were tested to increase chains

mobility during UV exposure after electrospinning: thermal treatment and solvent vapors exposure. It allowed to crosslink the material, but the morphology of the fibers was affected.

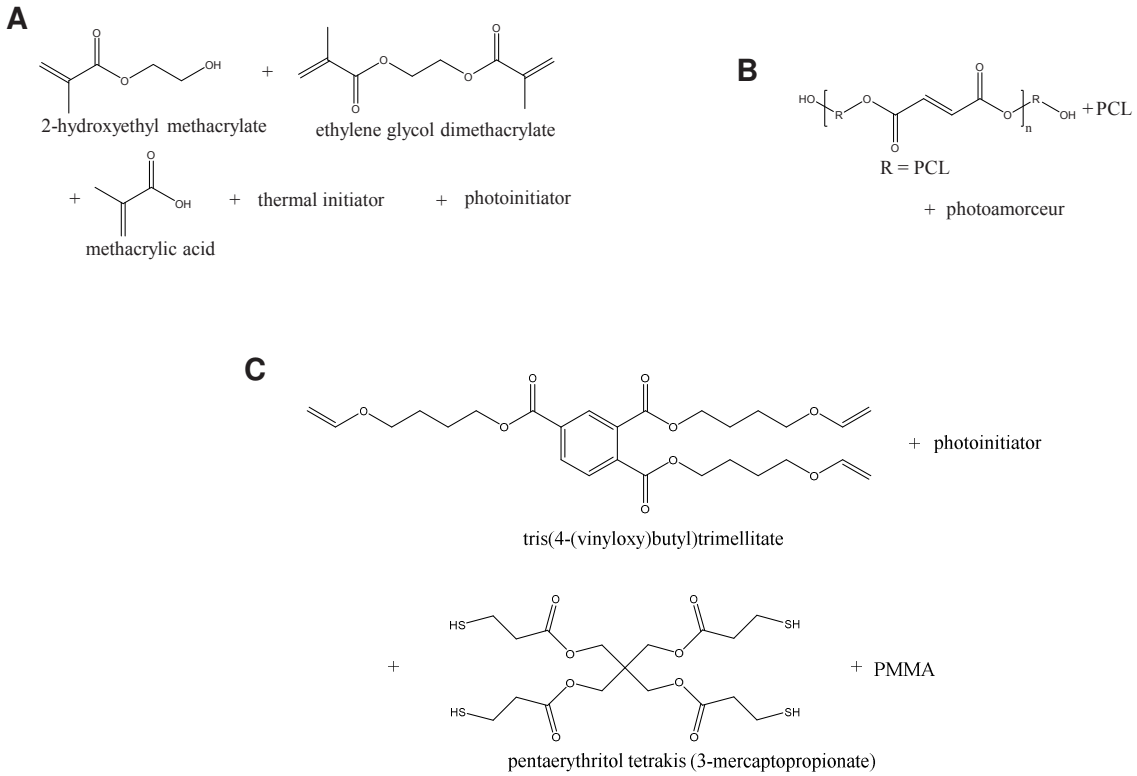

Figure 1.12. ***Examples of reactive mix electrospun and crosslinked under UV light.*** **(A)** Mix electrospun by Kim *et al.* [157]. **(B)** Mix electrospun by Jeshvaghani *et al.* [158]. **(C)** Mixture electrospun by Shanmuganathan *et al.* [159].

The thiol-ene chemistry used by Choi *et al.* [153] (see previous subsection) is advantageously reapplied by Shanmuganathan *et al.* [159] to electrospin under UV light the blend represented on Figure 1.12.(C). It contains a trifunctional vinyl ether and a tetrafunctional thiol with the addition of a photoinitiator and poly(methyl methacrylate) to bring a sufficient viscosity. The quantity of the latter is such that the reaction is fast enough to happen during electrospinning, that is to say in a few tens of milliseconds [156]: the resulting fibers are regular. The benefit of this method is that no solvent is needed as the vinyl ether acts as a solvent for the reactants. The mat reaches a maximal strain of 62% and has a good elastic recovery during stretch-release cyclic tests.

4.2.3. Electrospinning of silicones

The previous examples highlighted the benefits of *in situ* crosslinking. In particular, in the best cases, no post-treatment steps are needed. A post-electrospinning crosslinking step could also be avoided for systems that do not need external stimuli to trigger the reaction. We can find such system among silicones, when the reaction between the polymer and the crosslinking agent takes place at ambient temperature.

To prepare silicone-based fibers, Lu *et al.* [160] used the coaxial method. Indeed, the reactive mixture used to synthesize the silicone is initially not viscous enough: the employment of a carrier polymer is required. A PVP in ethanol solution and the mixture polymer/curing agent were thus coaxially injected. The experiment shows that the viscosity of the core increases very

fast due to the reaction. Consequently, the diameter of the fibers increases, until the clogging of the needle after four minutes of electrospinning. This method allows thus the fabrication of fibers containing the crosslinked elastomer without any post treatments, but with practical limitations. A post-electrospinning washing step is necessary to get the pure silicone fibers: they are here successfully obtained after removal of the PVP by immersion in water for fibers containing enough silicone in the core (see Figure 1.13.(B)).

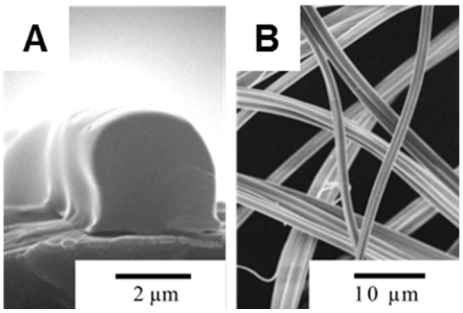

Figure 1.13. ***Examples of elastomer-based fibers***. **(A)** Crosslinked polybutadiene fibers slightly fused at the contact with the collector [153]. **(B)** Silicone fibers obtained after washing of crosslinked coaxial silicone/PVP fibers [160].

Guarino *et al.* [161] used the same coaxial method to prepare polydimethylsiloxane-based fibers. Here, the shell composed of a solution of PVP in DMF wraps the core containing the mixture polymer/curing agent diluted in THF to dilute the mixture and thus decrease the viscosity. The collector is heated to help the solvents evaporation. The PVP removal is done by washing in a water/ethanol mixture only 24h after electrospinning to ensure a complete crosslinking.

Another type of silicone was synthesized and electrospun by Pandini *et al.* [162]. The method is based here on a sol-gel reaction. The reaction between PCL chains with triethoxysilane groups at the end takes place in water in presence of HCl. It is triggered before electrospinning until having a sufficient molar mass. The process happens then under controlled humidity and should be followed by a thermal post-treatment at 50°C in the presence of HCl as a catalyst to ensure an efficient crosslinking. The resulting material has a low toxicity, but its mechanical properties were not characterized as the work focused on the shape memory properties.

4.2.4. Crosslinking by post-treatment of polyester-based elastomer fibers

In the field of soft tissue engineering, bioresorbable elastomers are getting interest. Among them, polyester elastomers seem promising thanks to their mechanical properties and their degradability by hydrolysis in non-toxic intermediates [163,164]. As these elastomers are insoluble, a two steps process is generally proposed. First, non-crosslinked prepolymers of low molar mass are processed by electrospinning. Then, a curing post-treatment leads to the crosslinking. This curing step allows the continuation of the polyesterification reaction at temperatures where the prepolymers are often liquids. Two challenges must therefore by faced. First, it is impossible to electrospin oligomers with a too low molar mass. Second, a way to avoid the flow of the prepolymer out of the fibers at the curing temperature should be found in order to keep the shape. The use of a carrier polymer solves these issues: it is selected to provide the entanglements during electrospinning and to keep the fibers shape at curing temperatures.

In this context, poly(lactic acid) (PLA) seems to be an attractive carrier polymer, PLA being often used for electrospinning for tissue engineering applications [165]. It was chosen by

Zhu *et al.* [166] to fabricate fibers composed of poly(1,8-octanediol citrate) (POC). This polyester was first prepolymerized by bulk polycondensation of citric acid and 1,8-octanediol. The prepolymer was electrospun in the presence of PLA in 2,2,2-trifluoroethanol. In order to achieve the crosslinking and get the elastomer, the fibers were heated 72h at 90°C. A mat composed of regular fibers is obtained with up to 50% of POC. Despite the presence of PLA, POC increases the hydrophilicity of the material: the water-in-air contact angle at the surface of the membrane reaches 106° against 130° for a pure PLA membrane. However, POC increases also the stiffness of the mat and the final properties do not really correspond to elastomeric properties.

Goins *et al.* [167] electrospun the same polyester using polyacrylic acid as carrier polymer. They fabricated fibers with up to 70% of POC from solutions in ethanol (see Figure 1.14.(A)) and cured them one or two days at 80 or 100°C. Again, the hydrophilicity is improved thanks to the POC, but no mechanical characterization was carried out.

Poly(xylitol sebacate) (PXS) is part, as PGS, of the poly(polyol sebacate) family. Its prepolymer was synthesized by Li and Chen [168] by polycondensation of a molar ratio xylitol/sebacic acid 2/5, before being electrospun by the coaxial method. Here, the prepolymer is dissolved in DMF and injected as core solution. The shell solution is composed of polyvinyl alcohol (PVA) in water/DMF. The crosslinking of PXS was achieved by a curing step at 130°C for 3 days. Then, the shell is removed by dissolution of PVA in water. A thick enough shell allows to keep the fibrous structure during the curing and a mat, still fibrous, is obtained after washing (see Figure 1.14.(B)). The removal, even partial, of the carrier polymer improves the mechanical properties. Indeed, the Young's modulus increases from 32 MPa for a pure PVA mat to 59 MPa for the cured but not purified PVA/PXS mat and decreases to 20 MPa after washing. After the same processing steps, the strain at break increases from 14% to 22% and finally 47%. After hydration of the cured and washed PVA/PXS mat, the strain at break increases up to 77% with a Young's modulus of 1.1 MPa showing thus interesting stretchable properties.

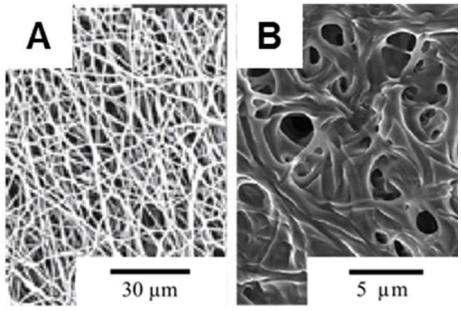

Figure 1.14. ***Examples of polyester elastomer-based fibers***. **(A)** POC/PAA fibers [167]. **(B)** PXS/PVA cured and washed fibers [168].

To conclude, polyester elastomers are not the easiest elastomers to electrospin, as they require a carrier polymer and several post-treatment steps. Thermoplastic elastomers, especially TPU are much easier to process, but polyesters have a more interesting structure to be used for biomedical application. They are biodegradable thanks to their ester linkages and there are fewer concerns about the toxicity of their degradation products. Morevover, their free –OH groups can be beneficial for the hydrophilicity and thus the biocompatibility, or for any functionalization. However, most of the previous examples show us that electrospinning of polyesters elastomers or of other elastomers requires the use of toxic solvents such as DMF, THF or HFIP.

5. Electrospinning of poly(glycerol sebacate)

As discussed above, the elastomer chosen for the present work is poly(glycerol sebacate). PGS being a thermoset polyester elastomer, its process raises the same challenges as the ones presented in the previous section. It must be electrospun at its prepolymer form and then be crosslinked during a thermal curing step. Because the prepolymer has a low molar mass, is soft and has a very low viscosity at curing temperature, its electrospinning requires the use of a carrier polymer essential for the formation of the fibers [169] and their retention during solidification and curing. Numerous examples of carrier polymers used to electrospin PGS by various methods can be found in the literature and are presented in the following subsections.

5.1. Use of proteins as carrier polymer

Proteins are natural biodegradable and biocompatible polymers, which are easily recognized by the cells [170]. Moreover, some of them can be crosslinked in elastomeric materials [11]. They constitute thus a logical choice as carrier polymer for PGS electrospinning.

Collagen, which is the most present protein in the body, is constitutive of the extra-cellular matrix and brings tensile strength [11]. It can be extracted from skin, for example. It has been used in coaxial electrospinning to fabricate fibers with pPGS in the core and collagen in the shell (see Figure 1.15.(A)) using HFIP [171]. The mechanical stability of the material was ensured by post-electrospinning crosslinking of collagen with glutaraldehyde vapors. Compared to pure collagen mats, pPGS/collagen mat is less rigid: pPGS decreases the Young's modulus from 30 to 4 MPa and increases the strain at break to 84%. Cell culture shows that pPGS/collagen blend also helps the differentiation of stem cells in cardiac cells.

Gelatin is a proteins mixture obtained from collagen. It is also popular to prepare electrospun scaffolds for tissue engineering. More specifically, pPGS/gelatin fibers were prepared by blend [172] (see Figure 1.15.(B)) or coaxial [173] electrospinning. In both cases, gelatin is crosslinked. The most interesting properties were measured for coaxial fibers, with a Young's modulus of 6 MPa and a strain at break of 50% [173].

Zein is a protein extracted from corn. Zein and pPGS were blended in acetic acid or ethanol [174,175]. As for the previous examples, pPGS is here not crosslinked after electrospinning because proteins cannot stand high temperatures. Vogt *et al.* [175] tried to improve the mechanical properties of their materials based on zein and pPGS by continuing the esterification before electrospinning until getting a still soluble highly branched pPGS. They obtained continuous fibers with up to 50% of pPGS (see Figure 1.15.(C)). The resulting materials are however not very stretchable with a strain at break that do not exceed 10% and a Young's modulus higher than 7 MPa.

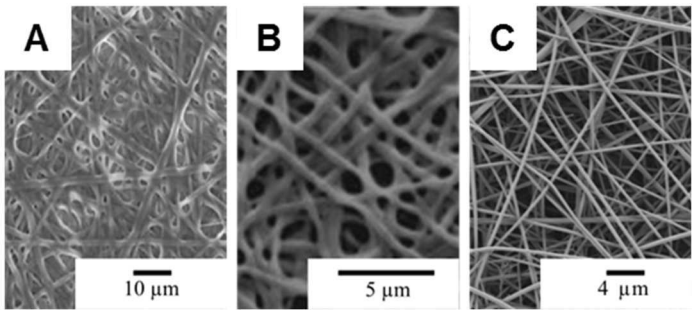

Figure 1.15. ***Examples of fibers composed of pPGS and a protein***. **(A)** Coaxial collagene/pPGS fibers [171]. **(B)** Gelatin/pPGS fibers [172]. **(C)** Zein/pPGS fibers [175].

5.2. Use of synthetic polymers as carrier polymer

Despite their advantages, proteins have drawbacks: immune rejection, variability of the properties depending on the extraction source and low mechanical properties [13]. Conversely, synthetic biopolymers such as polyesters or TPU, even if they do not bear natural recognizable sites for cells, have tunable and reproducible properties (mechanical and biodegradation). Their use as carrier polymer with PGS can thus be advantageous.

5.2.1. Use of polyesters as carrier polymers

Numerous reports of electrospinning of PGS with a polyester as carrier polymer can be found in the literature. Some typical examples are presented in the following sections.

Poly(lactic-co-glycolic acid)

Poly(lactic-*co*-glycolic acid) (PLGA) is a copolymer popular for biomedical applications because of its degradation by hydrolysis in non-toxic products [176]. However, it is not very hydrophilic and its high modulus (20 MPa to 2 GPa [177]) makes it not suitable for soft tissue engineering. For these reasons, Sfakis *et al.* [177] electrospun PLGA with pPGS by coaxial method from solutions in HFIP. Coaxial pPGS/PLGA fibers have a water-in-air contact angle of 66° instead of 122° for pure PLGA fibers, and a Young's modulus of 1.3 MPa instead of 4.8 MPa.

Poly(ε-caprolactone)

A very popular synthetic polyester for electrospinning in tissue engineering is poly(ε-caprolactone) (PCL) [116,178]. This popularity is justified by its biocompatibility, bioresorbability and convenient processability. More specifically, it is often used for electrospinning for tissue engineering. However, PCL is a hydrophobic semi-crystalline polymer and has a low degradation rate [178]. It is thus not adapted to soft tissues, but its drawbacks could by compensate by the association with another material such as PGS.

The first article reporting the preparation of PCL/pPGS nanofibers is Sant's article in 2011 [179]. In this work, fibers with up to 83% of pPGS were obtained by blend electrospinning using dichloromethane/ethanol as solvent mixture. Surprisingly, while a 3/1 pPGS/PCL ratio leads to a decrease of the Young's modulus and strain at break, a 5/1 ratio increases the modulus while keeping a strain at break of 600%, similar to pure PCL fibers. The authors justify this result by differences in the fibers morphology. But the addition of pPGS increases the hydrophilicity of the materials that can absorb water whereas the water-in-air contact angle on pure PCL membranes reaches 130°.

Numerous similar works were then published. We focus here on the studies where the objective is the preparation of scaffolds for cardiac tissue engineering. Rai *et al.* [180] fabricated cardiac patches from a ratio PCL/pPGS 1/1 dissolved in dichloromethane/methanol. The presence of pPGS increases the strain at break from 116±30% to 142±29% and the ultimate tensile strength (UTS) from 2 to 3 MPa with Young's modulus increasing from 6 to 8 MPa. Despite a modulus higher than myocardium's one, Rai *et al.* cite previous work to justify that their material is potentially adapted to cardiac regeneration. Indeed, cardiac patches that are stiffer than myocardium could decrease ventricle remodeling by decreasing wall stress, leading to higher functions recovery [36,181,182]. The characterizations show also that the addition of PCL allows

to reduce the degradation rate of PGS *in vivo* and to limit the acidification due to PGS degradation products. In addition, to improve their biomaterial, they grafted a growth factor at the fiber surface to enhance the adhesion, proliferation and morphology of myoblasts, cells known to enhance cardiac regeneration.

In another study, Tallawi *et al.* [183] chose another strategy to improve the therapeutic properties of the same kind of membranes. Indeed, the electrospinning process is done onto structured collectors with parallel 10 µm-deep grooves or squares. These grooves create anisotropy in the membrane (see Figure 1.16.(A)), which is positive for cardiomyocytes development. In particular, squares or parallel lines give a good alignment and a good communication between cells, what is essential for the regeneration of a healthy cardiac tissue.

In these examples, pPGS is blended with PCL before electrospinning, but the coaxial method was also employed. Hou *et al.* [184] compared the properties of blend and coaxial PCL/pPGS fibers, using 2,2,2-trifluoroethanol as solvent. Regular fibers are obtained after collection in a water bath and freeze-drying (see Figure 1.16.(B)). Blend fibers are composed of 0 to 50% of pPGS, these concentrations corresponding to the ratios resulting from the concentration and flow rates of solutions used for the coaxial process. Core-shell fibers are thicker but also more stretchable as a strain of 900% is reached against only 300% for blend fibers.

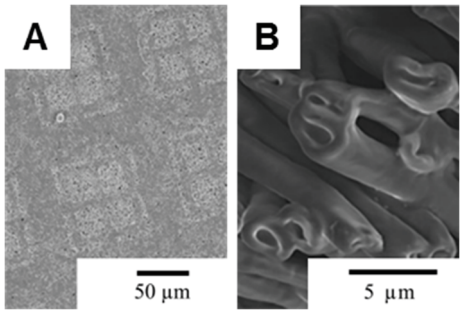

Figure 1.16. ***Examples of pPGS/PCL fibers***. **(A)** Deposit organized in squares [183]. **(B)** Coaxial fibers [184].

Polylactic acid

In the previous examples, the final material contains pPGS prepolymer and not PGS elastomer, because PCL has a low melting temperature which does not allow the PGS crosslinking during a curing step. A synthetic polyester commonly used for biomedical applications and that do not melt below 120°C – the mean curing temperature required for PGS – is poly(lactic acid) (PLA). PLA is biocompatible, degradable, and it is a semi-crystalline polymer with a melting point close to 180°C [185]. Its properties will be reviewed more deeply in Chapter 3. However, PLA is rigid and hydrophobic: PGS should compensate these drawbacks.

The first authors reporting the preparation of fibers composed of PGS and PLA were Yi and LaVan's in 2008 [169] who produced coaxial pPGS/PLA core/shell fibers. PGS was then crosslinked during 24h at 130°C and PLA was finally removed by washing in dichloromethane. The authors claim that they got fibers without PLA and having a good biocompatibility.

This strategy was enhanced by You *et al.* [186]. They improved the removal of the carrier polymer by adding polyethylene glycol in the shell, the core being composed of only PGS. Because PEG melts at the curing temperature (120°C), it is removed by dissolution in water before the crosslinking step, leaving pores at the surface of the fibers. After a one or two days-

long curing step, PGS is crosslinked and PLA can be removed by washing in chloroform. Infrared and DSC analysis suggest the elimination of PEG and PLA. Continuous fibers are obtained when a 70% concentrated PGS core solution is used (see Figure 1.17.(A)). At lower PGS content (core solution concentrated at 30%), the membrane fell apart. The use of PEG in the shell in addition to the PLA allows decreasing the Young's modulus to 1 MPa and increasing the strain at break to about 150%. This can be explained by the lower PLA amount required and by the pores left by the removed PEG at the surface of the fibers before crosslinking: they enhance the evaporation of the water produced by the polycondensation [186]. The same strategy was employed by the authors in the case of aligned fibers obtained thanks to the fast rotation of the collector [187].

More specifically, examples of PLA/PGS fibers fabricated for cardiac tissue engineering can be found in the literature. Ravichandran *et al.* [188] electrospun pPGS/PLA core/shell fibers using HFIP as solvent. After PGS crosslinking 24h at 130°C, PLA was removed by washing in a mixture of dichloromethane and hexane. This step results in short fibers about 4 µm long (see Figure 1.17.(B)). Here, the therapeutic approach is different: instead of seeding the cardiomyocytes on a scaffold, the objective was to inject the cells and the short nanofibers at the same time. The presence of the fibers allowed a better cells retention [188].

A patch composed of coaxial fibers with a PGS core and a PLA shell was prepared by Xu *et al.* [189] (Figure 1.17.(C)). In this approach, final fibers contain both crosslinked PGS and PLA, but it has the benefit to avoid any washing step using toxic solvents such as chloroform [186] or dichloromethane and hexane [188]. This type of strategy will be developed in Chapter 3.

Less frequently, PGS/PLA fibers were obtained by blend electrospinning. For example, Yan *et al.* [190] used a PLA/pPGS solution in DMF/DCM to fabricate continuous fibers with up to 25% of pPGS. These fibers are clearly hydrophilic after PGS crosslinking without any further purification. This work will also be described more precisely in Chapter 3.

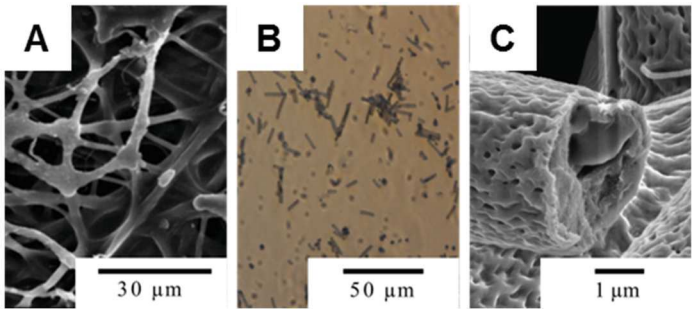

Figure 1.17. ***Examples of fibers obtained from PLA and PGS.*** **(A)** From a PLA/PEG shell and PGS core [186]. **(B)** Suspension of short fibers obtained after curing and washing of PGS/PLA core/shell fibers [188]. **(C)** Coaxial fibers with a PLA shell and PGS core [189].

5.2.2. Use of other synthetic polymers

Even if the majority of the examples found in the literature for PGS electrospinning involves PCL or PLA, other synthetic polymers were used as carrier polymers. We can cite the electrospinning of pPGS blended with a copolymer based on poly(butylene succinate) and poly(dilinoleic succinate) dissolved in dichloromethane/methanol [191]. The proportion of pPGS (30%) has here only a little influence on the mechanical properties. However, this type of material should be interesting for cardiac tissue engineering as this copolymer was already used for this kind of applications [192].

TPU stand as interesting carrier polymers thanks to their biocompatibility and elastomeric properties. We have seen above that pPGS has been electrospun blended with a TPU to get more stretchable membranes despite the absence of crosslinking: a maximal strain of 375% was obtained with 40% of pPGS whereas only 205% are reached for pure TPU [148].

However, in these examples, PGS is not crosslinked because of the low melting point of the carrier polymers. Other biocompatible polymers with high enough melting point were used to prepare PGS-based nanofibrous materials. A polysulfone was for example used as shell to wrap a pPGS core [193]. After a curing step of 48h at 130°C, a fluffy and deformable material is obtained. Its mechanical properties in elongation were however not characterized. Moreover, with TPU as with polysulfone, the scaffolds do not have the required biodegradability properties.

In the tissue engineering field, another very popular material is polyvinyl alcohol (PVA). This synthetic polymer is biocompatible, approved by the US Food and Drug Administration for biomedical applications and do not flow at the PGS curing temperature [194]. It was used with PGS in coaxial electrospinning [195] as well as in blend electrospinning [194,196]. In these examples, PGS is crosslinked thanks to PVA's appropriate thermal properties. Saudi *et al.* [196] synthesized a pPGS from a glycerol/sebacic acid ratio of 1/0.8 heated during 3h. It was electrospun blended with PVA in various proportions in a water/DMF solvent mixture. The resulting fibers were cured 24h at 120°C. The final membranes are hydrophilic: a maximal apparent contact angle of 30° was measured. The most stretchable material after hydration contains 40% of PGS and can be stretched up to 287%. Its Young's modulus reaches 0.04 MPa and its UTS 3.33 MPa. The biological characterization shows that the best cytocompatibility is obtained for the ratio PVA/PGS 50/50.

As PVA is water-soluble, it can be removed, at least partially, by washing in water [194,195]. It is thus possible, as for the method with PLA, to crosslink PGS and to remove the carrier polymer to tend towards fibers composed of only the crosslinked elastomer. The method with PVA has the benefit to need no toxic solvent during the washing step. However, PVA contains –OH groups able to react with PGS, making its removal difficult. These strategies will be developed in Chapter 4.

5.3. Crosslinking under UV light after chemical modifications of PGS

The fabrication of PGS-based nanofibrous scaffolds is hampered by the thermal crosslinking due to the low viscosity of pPGS at curing temperature. We can thus consider other crosslinking methods, like UV crosslinking. But to follow this idea, PGS should be chemically modified.

Acrylates groups were for example grafted on pPGS [197] (see Figure 1.18). The resulting macromers with 1 to 24% of acrylation and a number average molar mass of 3.74 kDa were processed by blend electrospinning in HFIP with the initiator and some gelatin to help the fibers formation. Continuous fibers with up to 70% of acrylated PGS were fabricated and post-treated under UV light to achieve the crosslinking. The mechanical properties were measured at dry and wet state for various degree of acrylation. The Young's modulus of these membranes is close to 10 MPa at dry state and decreases below 1 MPa at wet state. Poorly stretchable fibers were nevertheless obtained with strain at break ranging between 20 and 40%. Cell culture shows that cell adhesion and proliferation are satisfying. However, we can notice that gelatin is here important for cells development, acrylated PGS being not sufficient. The porosity of this kind of materials was improved by the alignment of acrylated PGS/gelatin fibers and sacrificial PEG

fibers removed by washing in water (Figure 1.18) [198]: in this way, cells development is better monitored.

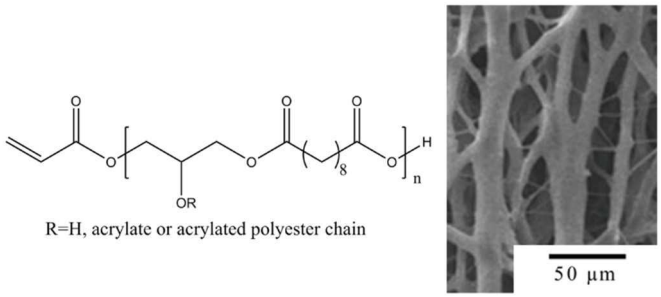

Figure 1.18. Chemical structure of acrylated PGS and acrylated PGS/gelatin fibers [198].

To conclude this part, numerous works focus on acrylated PGS-based scaffolds, but acrylated PGS has the drawback to introduce less biocompatible components. It should however be noticed that in most of the previous examples of pPGS electrospinning, toxic solvents such as DMF, HFIP, chloroform or dichloromethane were also used.

6. Summary of the objectives

This first chapter explained first why it is important to heal the cardiac muscle. For this purpose, tissue engineering is clearly a promising method. In order to help the tissue to regenerate, tissue engineering aims to create an environment mimicking host tissue's environment for cells. In particular, tissue engineers want to fabricate scaffolds with a structure and mechanical and physico-chemical properties similar to the extracellular matrix.

Here, we chose a polyester thermoset elastomer, poly(glycerol sebacate) as building material for its suitable properties, and electrospinning as the processing method to fabricate a fibrous scaffolds. As shown by the numerous examples summarized in the table below, PGS electrospinning is quite challenging. The first step presented in the following work focus on the synthesis and the characterization of the prepolymer and elastomer. Indeed, a good control of synthesis parameters and thus of the resulting properties is crucial. The synthesized prepolymer was then used in two different methods. In a first strategy, composite fibers were prepared, analyzed and tested *in vitro* and *in vivo*. A second strategy allowed the fabrication of a really elastomeric scaffold. And finally, diverse methods were tested to arrange the fibers deposition more precisely in order to improve the porosity and thus the possibility for the cells to infiltrate the scaffold.

Table 1.1. Examples of electrospinning of PGS and its application. The mechanical properties are given at dry state.

Carrier polymer	Method	Solvents	Post-treatments	E ε UTS	Target application	Tested cells
Collagen [171]	Coaxial	HFIP	Crosslinking of collagen	4 MPa 84% -	Cardiac	Mesenchymal stem cells
Gelatin [172]	Blend	Acetic acid	Crosslinking of gelatin	10 MPa 32% 1,5 MPa	Cardiac	Cardiac fibroblast Cardiomyocytes
Gelatin [173]	Coaxial	HFIP/TFE	Crosslinking of gelatin	6 MPa 50% 61 MPa	Cardiac	Cardiomyocytes
Zein [175]	Blend	Ethanol	None	≥ 7 MPa ≤ 10% -	Soft tissues	-
TPU [148]	Blend	CH_2Cl_2/DMF or HFIP or TFE/acetic acid	None	0.83 MPa 370% 10 MPa	Vocal folds	Fibroblasts
PBS-DLS [191]	Blend	CH_2Cl_2/ Methanol	None	4.7 MPa 132% 1.8 MPa	Soft tissues	-
PLGA [177]	Coaxial	HFIP	None	1.3MPa - -	Salivary glands	Salivary epithelial cells

PCL [179]	Blend	CH_2Cl_2/ Ethanol	None	35 MPa 600% 2.5 MPa	Aortic valve	Human umbilical vein endothelial cells
PCL [180]	Blend	CH_2Cl_2/ Methanol	None	8 MPa 142% 3 MPa	Cardiac	Cardiac progenitor cells Aortic endothelial cells
PCL [184]	Coaxial	TFE	None	16 MPa 900% 2.5 MPa	-	Human umbilical vein endothelial cells
PLA (+PEG) [186]	Coaxial	THF/DMF	Curing 24h or 48h at 120°C then washing in chloroform	1 MPa 160% 0.4 MPa	Soft tissues	Umbilical artery smooth muscles cells
PLA [189]	Coaxial	THF/$CHCl_3$/DMF	Curing 24h at 130°C	18 MPa 25% 1 MPa	Soft tissues	Fibroblasts
PLA [190]	Blend	CH_2Cl_2/DMF	Curing 48H at 120°C	7.2 MPa 67% 1 MPa	Nerves	Nerve cells
PVA [196]	Blend	Water/DMF	Curing 24h at 120°C	0.4 MPa 156% 2 MPa	Neurons	Pheochromocytoma cells
PVA [195]	Coaxial	THF/water	Curing 72h at 130°C then washing in water	35 MPa 130% 7 MPa	Soft tissues	Fibroblasts

References

1. Cannon, B. Cardiovascular disease: Biochemistry to behaviour. *Nature* **2013**, *493*, S2–S3.
2. Go Alan S.; Mozaffarian Dariush; Roger Véronique L.; Benjamin Emelia J.; Berry Jarett D.; Blaha Michael J.; Dai Shifan; Ford Earl S.; Fox Caroline S.; Franco Sheila; et al. Heart Disease and Stroke Statistics—2014 Update. *Circulation* **2014**, *129*, e28–e292.
3. Chen, Q.-Z.; Harding, S.E.; Ali, N.N.; Lyon, A.R.; Boccaccini, A.R. Biomaterials in cardiac tissue engineering: Ten years of research survey. *Materials Science and Engineering: R: Reports* **2008**, *59*, 1–37.
4. Zhu, C.; Rodda, A.E.; Truong, V.X.; Shi, Y.; Zhou, K.; Haynes, J.M.; Wang, B.; Cook, W.D.; Forsythe, J.S. Increased Cardiomyocyte Alignment and Intracellular Calcium Transients Using Micropatterned and Drug-Releasing Poly(Glycerol Sebacate) Elastomers. *ACS Biomater. Sci. Eng.* **2018**, *4*, 2494–2504.
5. Sabbah, H.N. The cardiac support device and the Myosplint: treating heart failure by targeting left ventricular size and shape. *The Annals of Thoracic Surgery* **2003**, *75*, S13–S19.
6. Naveed, M.; Mohammad, I.S.; Xue, L.; Khan, S.; Gang, W.; Cao, Y.; Cheng, Y.; Cui, X.; DingDing, C.; Feng, Y.; et al. The promising future of ventricular restraint therapy for the management of end-stage heart failure. *Biomedicine & Pharmacotherapy* **2018**, *99*, 25–32.
7. Kenar, H.; Kose, G.T.; Hasirci, V. Design of a 3D aligned myocardial tissue construct from biodegradable polyesters. *J Mater Sci: Mater Med* **2010**, *21*, 989–997.
8. Chen, Q.-Z.; Bismarck, A.; Hansen, U.; Junaid, S.; Tran, M.Q.; Harding, S.E.; Ali, N.N.; Boccaccini, A.R. Characterisation of a soft elastomer poly(glycerol sebacate) designed to match the mechanical properties of myocardial tissue. *Biomaterials* **2008**, *29*, 47–57.
9. Place, E.S.; George, J.H.; Williams, C.K.; Stevens, M.M. Synthetic polymer scaffolds for tissue engineering. *Chemical Society Reviews* **2009**, *38*, 1139–1151.
10. O'Brien, F.J. Biomaterials & scaffolds for tissue engineering. *Mater. Today* **2011**, *14*, 88–95.
11. Chen, Q.; Liang, S.; Thouas, G.A. Elastomeric biomaterials for tissue engineering. *Progr. Polym. Sci.* **2013**, *38*, 584–671.
12. Langer, R.; Vacanti, J.P. Tissue engineering. *Science* **1993**, *260*, 920–926.
13. Peña, B.; Laughter, M.; Jett, S.; Rowland, T.J.; Taylor, M.R.G.; Mestroni, L.; Park, D. Injectable Hydrogels for Cardiac Tissue Engineering. *Macromolecular Bioscience* **2018**, *18*.
14. Engler, A.J.; Sen, S.; Sweeney, H.L.; Discher, D.E. Matrix Elasticity Directs Stem Cell Lineage Specification. *Cell* **2006**, *126*, 677–689.
15. Macchiarelli, G.; Ohtani, O.; Nottola, S.; Stallone, T.; Camboni, A.; M Prado, I.; M Motta, P. A micro-anatomical model of the distribution of myocardial endomysial collagen. *Histol Histopathol* **2002**, *17*, 699–706.
16. Kitsara, M.; Agbulut, O.; Kontziampasis, D.; Chen, Y.; Menasché, P. Fibers for hearts: A critical review on electrospinning for cardiac tissue engineering. *Acta Biomaterialia* **2017**, *48*, 20–40.
17. Kai, D.; Prabhakaran, M.P.; Jin, G.; Ramakrishna, S. Guided orientation of cardiomyocytes on electrospun aligned nanofibers for cardiac tissue engineering. *Journal of Biomedical Materials Research Part B: Applied Biomaterials* **2011**, *98B*, 379–386.
18. Rockwood, D.N.; Akins, R.E.; Parrag, I.C.; Woodhouse, K.A.; Rabolt, J.F. Culture on electrospun polyurethane scaffolds decreases atrial natriuretic peptide expression by cardiomyocytes in vitro. *Biomaterials* **2008**, *29*, 4783–4791.
19. Kofidis, T.; Akhyari, P.; Boublik, J.; Theodorou, P.; Martin, U.; Ruhparwar, A.; Fischer, S.; Eschenhagen, T.; Kubis, H.P.; Kraft, T.; et al. In vitro engineering of heart muscle: Artificial myocardial tissue. *The Journal of Thoracic and Cardiovascular Surgery* **2002**, *124*, 63–69.
20. Tijore, A.; Irvine, S.A.; Sarig, U.; Mhaisalkar, P.; Baisane, V.; Venkatraman, S. Contact guidance for cardiac tissue engineering using 3D bioprinted gelatin patterned hydrogel. *Biofabrication* **2018**, *10*, 025003.
21. Shachar, M.; Tsur-Gang, O.; Dvir, T.; Leor, J.; Cohen, S. The effect of immobilized RGD peptide in alginate scaffolds on cardiac tissue engineering. *Acta Biomaterialia* **2011**, *7*, 152–162.

22. Ishii, O.; Shin, M.; Sueda, T.; Vacanti, J.P. In vitro tissue engineering of a cardiac graft using a degradable scaffold with an extracellular matrix–like topography. *J. Thorac. Cardiovasc. Surg.* **2005**, *130*, 1358–1363.
23. Shin, M.; Ishii, O.; Sueda, T.; Vacanti, J.P. Contractile cardiac grafts using a novel nanofibrous mesh. *Biomaterials* **2004**, *25*, 3717–3723.
24. Liu, Y.; Wang, S.; Zhang, R. Composite poly(lactic acid)/chitosan nanofibrous scaffolds for cardiac tissue engineering. *International Journal of Biological Macromolecules* **2017**, *103*, 1130–1137.
25. Stout, D.A.; Basu, B.; Webster, T.J. Poly(lactic–co-glycolic acid): Carbon nanofiber composites for myocardial tissue engineering applications. *Acta Biomaterialia* **2011**, *7*, 3101–3112.
26. Tay, C.Y.; Yu, H.; Pal, M.; Leong, W.S.; Tan, N.S.; Ng, K.W.; Leong, D.T.; Tan, L.P. Micropatterned matrix directs differentiation of human mesenchymal stem cells towards myocardial lineage. *Experimental Cell Research* **2010**, *316*, 1159–1168.
27. Yang, Y.; Lei, D.; Huang, S.; Yang, Q.; Song, B.; Guo, Y.; Shen, A.; Yuan, Z.; Li, S.; Qing, F.-L.; et al. Elastic 3D-Printed Hybrid Polymeric Scaffold Improves Cardiac Remodeling after Myocardial Infarction. *Advanced Healthcare Materials 0*, 1900065.
28. Hidalgo-Bastida, L.A.; Barry, J.J.A.; Everitt, N.M.; Rose, F.R.A.J.; Buttery, L.D.; Hall, I.P.; Claycomb, W.C.; Shakesheff, K.M. Cell adhesion and mechanical properties of a flexible scaffold for cardiac tissue engineering. *Acta Biomaterialia* **2007**, *3*, 457–462.
29. Fujimoto, K.L.; Guan, J.; Oshima, H.; Sakai, T.; Wagner, W.R. In Vivo Evaluation of a Porous, Elastic, Biodegradable Patch for Reconstructive Cardiac Procedures. *The Annals of Thoracic Surgery* **2007**, *83*, 648–654.
30. Fujimoto, K.L.; Tobita, K.; Merryman, W.D.; Guan, J.; Momoi, N.; Stolz, D.B.; Sacks, M.S.; Keller, B.B.; Wagner, W.R. An Elastic, Biodegradable Cardiac Patch Induces Contractile Smooth Muscle and Improves Cardiac Remodeling and Function in Subacute Myocardial Infarction. *Journal of the American College of Cardiology* **2007**, *49*, 2292–2300.
31. McDevitt, T.C.; Woodhouse, K.A.; Hauschka, S.D.; Murry, C.E.; Stayton, P.S. Spatially organized layers of cardiomyocytes on biodegradable polyurethane films for myocardial repair. *Journal of Biomedical Materials Research Part A* **2003**, *66A*, 586–595.
32. Boffito, M.; Sartori, S.; Ciardelli, G. Polymeric scaffolds for cardiac tissue engineering: requirements and fabrication technologies. *Polymer International* **2014**, *63*, 2–11.
33. Kaiser, N.J.; Coulombe, K.L.K. Physiologically inspired cardiac scaffolds for tailoredin vivofunction and heart regeneration. *Biomed. Mater.* **2015**, *10*, 034003.
34. Engler, A.J.; Carag-Krieger, C.; Johnson, C.P.; Raab, M.; Tang, H.-Y.; Speicher, D.W.; Sanger, J.W.; Sanger, J.M.; Discher, D.E. Embryonic cardiomyocytes beat best on a matrix with heart-like elasticity: scar-like rigidity inhibits beating. *Journal of Cell Science* **2008**, *121*, 3794–3802.
35. Bhana, B.; Iyer, R.K.; Chen, W.L.K.; Zhao, R.; Sider, K.L.; Likhitpanichkul, M.; Simmons, C.A.; Radisic, M. Influence of substrate stiffness on the phenotype of heart cells Available online: http://onlinelibrary.wiley.com/doi/abs/10.1002/bit.22647 (accessed on Jun 26, 2019).
36. Wall, S.T.; Walker, J.C.; Healy, K.E.; Ratcliff, M.B.; Guccione, J.M. Theoretical Impact of the Injection of Material Into the Myocardium. *Circulation* **2006**, *114*, 2627–2635.
37. Stuckey, D.J.; Ishii, H.; Chen, Q.-Z.; Boccaccini, A.R.; Hansen, U.; Carr, C.A.; Roether, J.A.; Jawad, H.; Tyler, D.J.; Ali, N.N.; et al. Magnetic Resonance Imaging Evaluation of Remodeling by Cardiac Elastomeric Tissue Scaffold Biomaterials in a Rat Model of Myocardial Infarction. *Tissue Engineering Part A* **2010**, *16*, 3395–3402.
38. Kai, D.; Prabhakaran, M.P.; Jin, G.; Ramakrishna, S. Polypyrrole-contained electrospun conductive nanofibrous membranes for cardiac tissue engineering. *Journal of Biomedical Materials Research Part A* **2011**, *99A*, 376–385.
39. Fernandes, E.G.R.; Zucolotto, V.; Queiroz, A.A.A.D. Electrospinning of Hyperbranched Poly-L-Lysine/Polyaniline Nanofibers for Application in Cardiac Tissue Engineering. *Journal of Macromolecular Science, Part A* **2010**, *47*, 1203–1207.

40. Dvir, T.; Timko, B.P.; Brigham, M.D.; Naik, S.R.; Karajanagi, S.S.; Levy, O.; Jin, H.; Parker, K.K.; Langer, R.; Kohane, D.S. Nanowired three-dimensional cardiac patches. *Nature Nanotechnology* **2011**, *6*, 720–725.
41. Tandon, N.; Cannizzaro, C.; Chao, P.-H.G.; Maidhof, R.; Marsano, A.; Au, H.T.H.; Radisic, M.; Vunjak-Novakovic, G. Electrical stimulation systems for cardiac tissue engineering. *Nature Protocols* **2009**, *4*, 155–173.
42. Guan, J.; Wang, F.; Li, Z.; Chen, J.; Guo, X.; Liao, J.; Moldovan, N.I. The stimulation of the cardiac differentiation of mesenchymal stem cells in tissue constructs that mimic myocardium structure and biomechanics. *Biomaterials* **2011**, *32*, 5568–5580.
43. Wang, Y.; Ameer, G.A.; Sheppard, B.J.; Langer, R. A tough biodegradable elastomer. *Nat Biotech* **2002**, *20*, 602–606.
44. Rai, R.; Tallawi, M.; Grigore, A.; Boccaccini, A.R. Synthesis, properties and biomedical applications of poly(glycerol sebacate) (PGS): A review. *Progress in Polymer Science* **2012**, *37*, 1051–1078.
45. Sundback, C.A.; Shyu, J.Y.; Wang, Y.; Faquin, W.C.; Langer, R.S.; Vacanti, J.P.; Hadlock, T.A. Biocompatibility analysis of poly(glycerol sebacate) as a nerve guide material. *Biomaterials* **2005**, *26*, 5454–5464.
46. Li, Y.; Cook, W.D.; Moorhoff, C.; Huang, W.-C.; Chen, Q.-Z. Synthesis, characterization and properties of biocompatible poly(glycerol sebacate) pre-polymer and gel. *Polym. Int.* **2012**, *62*, 534–547.
47. Chen, Q.; Jin, L.; Cook, W.D.; Mohn, D.; Lagerqvist, E.L.; Elliott, D.A.; Haynes, J.M.; Boyd, N.; Stark, W.J.; Pouton, C.W.; et al. Elastomeric nanocomposites as cell delivery vehicles and cardiac support devices. *Soft Matter* **2010**, *6*, 4715–4726.
48. Liang, S.-L.; Cook, W.D.; Thouas, G.A.; Chen, Q.-Z. The mechanical characteristics and in vitro biocompatibility of poly(glycerol sebacate)-Bioglass® elastomeric composites. *Biomaterials* **2010**, *31*, 8516–8529.
49. Wang, Y.; Kim, Y.M.; Langer, R. In vivo degradation characteristics of poly(glycerol sebacate). *Journal of Biomedical Materials Research Part A* **2003**, *66A*, 192–197.
50. Guo, X.-L.; Lu, X.-L.; Dong, D.-L.; Sun, Z.-J. Characterization and optimization of glycerol/sebacate ratio in poly(glycerol-sebacate) elastomer for cell culture application. *Journal of Biomedical Materials Research Part A* **2014**, *102*, 3903–3907.
51. Pomerantseva, I.; Krebs, N.; Hart, A.; Neville, C.M.; Huang, A.Y.; Sundback, C.A. Degradation behavior of poly(glycerol sebacate). *Journal of Biomedical Materials Research Part A* **2009**, *91A*, 1038–1047.
52. Kemppainen, J.M.; Hollister, S.J. Tailoring the mechanical properties of 3D-designed poly(glycerol sebacate) scaffolds for cartilage applications. *Journal of Biomedical Materials Research Part A* **2010**, *94A*, 9–18.
53. Li, X.; Hong, A.T.-L.; Naskar, N.; Chung, H.-J. Criteria for Quick and Consistent Synthesis of Poly(glycerol sebacate) for Tailored Mechanical Properties. *Biomacromolecules* **2015**, *16*, 1525–1533.
54. Nijst, C.L.E.; Bruggeman, J.P.; Karp, J.M.; Ferreira, L.; Zumbuehl, A.; Bettinger, C.J.; Langer, R. Synthesis and Characterization of Photocurable Elastomers from Poly(glycerol-co-sebacate). *Biomacromolecules* **2007**, *8*, 3067–3073.
55. Yeh, Y.-C.; Highley, C.B.; Ouyang, L.; Burdick, J.A. 3D printing of photocurable poly(glycerol sebacate) elastomers. *Biofabrication* **2016**, *8*, 045004.
56. Fidkowski, C.; Kaazempur-Mofrad, M.R.; Borenstein, J.; Vacanti, J.P.; Langer, R.; Wang, Y. Endothelialized Microvasculature Based on a Biodegradable Elastomer. *Tissue Engineering* **2005**, *11*, 302–309.
57. Bettinger, C.J.; Weinberg, E.J.; Kulig, K.M.; Vacanti, J.P.; Wang, Y.; Borenstein, J.T.; Langer, R. Three-Dimensional Microfluidic Tissue-Engineering Scaffolds Using a Flexible Biodegradable Polymer. *Advanced Materials* **2006**, *18*, 165–169.
58. Motlagh, D.; Yang, J.; Lui, K.Y.; Webb, A.R.; Ameer, G.A. Hemocompatibility evaluation of poly(glycerol-sebacate) in vitro for vascular tissue engineering. *Biomaterials* **2006**, *27*, 4315–4324.

59. Crapo, P.M.; Gao, J.; Wang, Y. Seamless tubular poly(glycerol sebacate) scaffolds: High-yield fabrication and potential applications. *Journal of Biomedical Materials Research Part A* **2008**, *86A*, 354–363.
60. Yang, X.; Gao, Z.; Liu, H.; Wu, W. Biodegrading highly porous elastomeric graft regenerates muscular and innervated carotid artery—Comparative study with vein graft. *Journal of Tissue Engineering and Regenerative Medicine* **2019**, *0*.
61. Theerathanagorn, T.; Klangjorhor, J.; Sakulsombat, M.; Pothacharoen, P.; Pruksakorn, D.; Kongtawelert, P.; Janvikul, W. In vitro human chondrocyte culture on plasma-treated poly(glycerol sebacate) scaffolds. *Journal of Biomaterials Science, Polymer Edition* **2015**, *26*, 1386–1401.
62. Liu, Y.; Tian, K.; Hao, J.; Yang, T.; Geng, X.; Zhang, W. Biomimetic poly(glycerol sebacate)/polycaprolactone blend scaffolds for cartilage tissue engineering. *J Mater Sci: Mater Med* **2019**, *30*, 53.
63. Neeley, W.L.; Redenti, S.; Klassen, H.; Tao, S.; Desai, T.; Young, M.J.; Langer, R. A microfabricated scaffold for retinal progenitor cell grafting. *Biomaterials* **2008**, *29*, 418–426.
64. Pritchard, C.D.; Arnér, K.M.; Langer, R.S.; Ghosh, F.K. Retinal transplantation using surface modified poly(glycerol-co-sebacic acid) membranes. *Biomaterials* **2010**, *31*, 7978–7984.
65. Wieland, A.M.; Sundback, C.A.; Hart, A.; Kulig, K.; Masiakos, P.T.; Hartnick, C.J. Poly(glycerol sebacate)-engineered plugs to repair chronic tympanic membrane perforations in a chinchilla model. *Otolaryngol Head Neck Surg* **2010**, *143*, 127–133.
66. Zhang, X.; Jia, C.; Qiao, X.; Liu, T.; Sun, K. Porous poly(glycerol sebacate) (PGS) elastomer scaffolds for skin tissue engineering. *Polymer Testing* **2016**, *54*, 118–125.
67. Sun, Z.-J.; Chen, C.; Sun, M.-Z.; Ai, C.-H.; Lu, X.-L.; Zheng, Y.-F.; Yang, B.-F.; Dong, D.-L. The application of poly (glycerol–sebacate) as biodegradable drug carrier. *Biomaterials* **2009**, *30*, 5209–5214.
68. Tobias, I.S.; Lee, H.; Engelmayr, G.C.; Macaya, D.; Bettinger, C.J.; Cima, M.J. Zero-order controlled release of ciprofloxacin-HCl from a reservoir-based, bioresorbable and elastomeric device. *Journal of Controlled Release* **2010**, *146*, 356–362.
69. Yang, B.; Lv, W.; Deng, Y. Drug loaded poly(glycerol sebacate) as a local drug delivery system for the treatment of periodontal disease. *RSC Advances* **2017**, *7*, 37426–37435.
70. Hsieh, Y.-K.; Chang, C.-T.; Jen, I.-H.; Pu, F.-C.; Shen, S.-H.; Wan, D.; Wang, J. Use of Gold Nanoparticles to Investigate the Drug Embedding and Releasing Performance in Biodegradable Poly(glycerol sebacate). *ACS Appl. Nano Mater.* **2018**, *1*, 4474–4482.
71. Bettinger, C.J.; Orrick, B.; Misra, A.; Langer, R.; Borenstein, J.T. Microfabrication of poly (glycerol–sebacate) for contact guidance applications. *Biomaterials* **2006**, *27*, 2558–2565.
72. Gao, J.; Crapo, P.M.; Wang, Y. Macroporous Elastomeric Scaffolds with Extensive Micropores for Soft Tissue Engineering. *Tissue Engineering* **2006**, *12*, 917–925.
73. Vilariño-Feltrer, G.; Muñoz-Santa, A.; Conejero-García, Á.; Vallés-Lluch, A. The effect of salt fusion processing variables on structural, physicochemical and biological properties of poly(glycerol sebacate) scaffolds. *International Journal of Polymeric Materials and Polymeric Biomaterials* **2019**.
74. Marsano, A.; Maidhof, R.; Wan, L.Q.; Wang, Y.; Gao, J.; Tandon, N.; Vunjak-Novakovic, G. Scaffold stiffness affects the contractile function of three-dimensional engineered cardiac constructs. *Biotechnology Progress* **2010**, *26*, 1382–1390.
75. Engelmayr Jr, G.C.; Cheng, M.; Bettinger, C.J.; Borenstein, J.T.; Langer, R.; Freed, L.E. Accordion-like honeycombs for tissue engineering of cardiac anisotropy. *Nature Materials* **2008**, *7*, 1003–1010.
76. Park, H.; Larson, B.L.; Guillemette, M.D.; Jain, S.R.; Hua, C.; Engelmayr, G.C.; Freed, L.E. The significance of pore microarchitecture in a multi-layered elastomeric scaffold for contractile cardiac muscle constructs. *Biomaterials* **2011**, *32*, 1856–1864.
77. Neal, R.A.; Jean, A.; Park, H.; Wu, P.B.; Hsiao, J.; Engelmayr, G.C.; Langer, R.; Freed, L.E. Three-Dimensional Elastomeric Scaffolds Designed with Cardiac-Mimetic Structural and Mechanical Features. *Tissue Engineering Part A* **2013**, *19*, 793–807.

78. Park, H.; Larson, B.L.; Kolewe, M.E.; Vunjak-Novakovic, G.; Freed, L.E. Biomimetic scaffold combined with electrical stimulation and growth factor promotes tissue engineered cardiac development. *Experimental Cell Research* **2014**, *321*, 297–306.
79. Guillemette, M.D.; Park, H.; Hsiao, J.C.; Jain, S.R.; Larson, B.L.; Langer, R.; Freed, L.E. Combined Technologies for Microfabricating Elastomeric Cardiac Tissue Engineering Scaffolds. *Macromolecular Bioscience* **2010**, *10*, 1330–1337.
80. Rai, R.; Tallawi, M.; Barbani, N.; Frati, C.; Madeddu, D.; Cavalli, S.; Graiani, G.; Quaini, F.; Roether, J.A.; Schubert, D.W.; et al. Biomimetic poly(glycerol sebacate) (PGS) membranes for cardiac patch application. *Materials Science and Engineering: C* **2013**, *33*, 3677–3687.
81. Jean, A.; Engelmayr, G.C. Finite element analysis of an accordion-like honeycomb scaffold for cardiac tissue engineering. *Journal of Biomechanics* **2010**, *43*, 3035–3043.
82. Radisic, M.; Park, H.; Chen, F.; Salazar-Lazzaro, J.E.; Wang, Y.; Dennis, R.; Langer, R.; Freed, L.E.; Vunjak-Novakovic, G. Biomimetic Approach to Cardiac Tissue Engineering: Oxygen Carriers and Channeled Scaffolds. *Tissue Engineering* **2006**, *12*, 2077–2091.
83. Radisic, M.; Park, H.; Martens, T.P.; Salazar-Lazaro, J.E.; Geng, W.; Wang, Y.; Langer, R.; Freed, L.E.; Vunjak-Novakovic, G. Pre-treatment of synthetic elastomeric scaffolds by cardiac fibroblasts improves engineered heart tissue. *Journal of Biomedical Materials Research Part A* **2008**, *86A*, 713–724.
84. Chen, Q.-Z.; Ishii, H.; Thouas, G.A.; Lyon, A.R.; Wright, J.S.; Blaker, J.J.; Chrzanowski, W.; Boccaccini, A.R.; Ali, N.N.; Knowles, J.C.; et al. An elastomeric patch derived from poly(glycerol sebacate) for delivery of embryonic stem cells to the heart. *Biomaterials* **2010**, *31*, 3885–3893.
85. Doshi, J.; Reneker, D.H. Electrospinning process and applications of electrospun fibers. *Journal of Electrostatics* **1995**, *35*, 151–160.
86. Subbiah, T.; Bhat, G.S.; Tock, R.W.; Parameswaran, S.; Ramkumar, S.S. Electrospinning of nanofibers. *Journal of Applied Polymer Science* **2005**, *96*, 557–569.
87. Li, D.; Xia, Y. Electrospinning of Nanofibers: Reinventing the Wheel? *Advanced Materials* **2004**, *16*, 1151–1170.
88. Bhardwaj, N.; Kundu, S.C. Electrospinning: A fascinating fiber fabrication technique. *Biotechnology Advances* **2010**, *28*, 325–347.
89. Reneker, D.H.; Yarin, A.L. Electrospinning jets and polymer nanofibers. *Polymer* **2008**, *49*, 2387–2425.
90. Yarin, A.L.; Koombhongse, S.; Reneker, D.H. Bending instability in electrospinning of nanofibers. *Journal of Applied Physics* **2001**, *89*, 3018–3026.
91. Fong, H.; Chun, I.; Reneker, D.H. Beaded nanofibers formed during electrospinning. *Polymer* **1999**, *40*, 4585–4592.
92. Heo, Y.; Larson, R.G. The scaling of zero-shear viscosities of semidilute polymer solutions with concentration. *Journal of Rheology* **2005**, *49*, 1117.
93. Graessley, W.W. Polymer chain dimensions and the dependence of viscoelastic properties on concentration, molecular weight and solvent power. *Polymer* **1980**, *21*, 258–262.
94. Allais, M.; Mailley, D.; Hébraud, P.; Ihiawakrim, D.; Ball, V.; Meyer, F.; Hébraud, A.; Schlatter, G. Polymer-free electrospinning of tannic acid and cross-linking in water for hybrid supramolecular nanofibres. *Nanoscale* **2018**, *10*, 9164–9173.
95. Shenoy, S.L.; Bates, W.D.; Frisch, H.L.; Wnek, G.E. Role of chain entanglements on fiber formation during electrospinning of polymer solutions: good solvent, non-specific polymer–polymer interaction limit. *Polymer* **2005**, *46*, 3372–3384.
96. McKee, M.G.; Wilkes, G.L.; Colby, Ralph.H.; Long, T.E. Correlations of Solution Rheology with Electrospun Fiber Formation of Linear and Branched Polyesters. *Macromolecules* **2004**, *37*, 1760–1767.
97. Lavielle, N.; Popa, A.-M.; de Geus, M.; Hébraud, A.; Schlatter, G.; Thöny-Meyer, L.; Rossi, R.M. Controlled formation of poly(ε-caprolactone) ultrathin electrospun nanofibers in a hydrolytic degradation-assisted process. *European Polymer Journal* **2013**, *49*, 1331–1336.

98. Gupta, P.; Elkins, C.; Long, T.E.; Wilkes, G.L. Electrospinning of linear homopolymers of poly(methyl methacrylate): exploring relationships between fiber formation, viscosity, molecular weight and concentration in a good solvent. *Polymer* **2005**, *46*, 4799–4810.
99. Huang, Z.-M.; Zhang, Y.-Z.; Kotaki, M.; Ramakrishna, S. A review on polymer nanofibers by electrospinning and their applications in nanocomposites. *Composites Science and Technology* **2003**, *63*, 2223–2253.
100. Bognitzki, M.; Frese, T.; Steinhart, M.; Greiner, A.; Wendorff, J.H.; Schaper, A.; Hellwig, M. Preparation of fibers with nanoscaled morphologies: Electrospinning of polymer blends. *Polymer Engineering & Science* **2001**, *41*, 982–989.
101. Esfahani, H.; Prabhakaran, M.P.; Salahi, E.; Tayebifard, A.; Rahimipour, M.R.; Keyanpour-Rad, M.; Ramakrishna, S. Electrospun nylon 6/zinc doped hydroxyapatite membrane for protein separation: Mechanism of fouling and blocking model. *Materials Science and Engineering: C* **2016**, *59*, 420–428.
102. Greiner, A.; Wendorff, J.H. Electrospinning: A Fascinating Method for the Preparation of Ultrathin Fibers. *Angewandte Chemie International Edition* **2007**, *46*, 5670–5703.
103. Zhang, Y.; Su, B.; Venugopal, J.; Ramakrishna, S.; Lim, C. Biomimetic and bioactive nanofibrous scaffolds from electrospun composite nanofibers. *Int J Nanomedicine* **2007**, *2*, 623–638.
104. Nagam Hanumantharao, S.; Rao, S. Multi-Functional Electrospun Nanofibers from Polymer Blends for Scaffold Tissue Engineering. *Fibers* **2019**, *7*, 66.
105. Sun, Z.; Zussman, E.; Yarin, A.L.; Wendorff, J.H.; Greiner, A. Compound Core–Shell Polymer Nanofibers by Co-Electrospinning. *Advanced Materials* **2003**, *15*, 1929–1932.
106. Yarin, A.L. Coaxial electrospinning and emulsion electrospinning of core–shell fibers. *Polymers for Advanced Technologies* **2011**, *22*, 310–317.
107. Lu, Y.; Huang, J.; Yu, G.; Cardenas, R.; Wei, S.; Wujcik, E.K.; Guo, Z. Coaxial electrospun fibers: applications in drug delivery and tissue engineering. *WIREs Nanomed Nanobiotechnol* **2016**, *8*, 654–677.
108. Zhang, Y.Z.; Venugopal, J.; Huang, Z.-M.; Lim, C.T.; Ramakrishna, S. Characterization of the Surface Biocompatibility of the Electrospun PCL-Collagen Nanofibers Using Fibroblasts. *Biomacromolecules* **2005**, *6*, 2583–2589.
109. Guarino, V.; Cirillo, V.; Ambrosio, L. Bicomponent electrospun scaffolds to design extracellular matrix tissue analogs. *Expert Review of Medical Devices* **2016**, *13*, 83–102.
110. Nadim, A.; Khorasani, S.N.; Kharaziha, M.; Davoodi, S.M. Design and characterization of dexamethasone-loaded poly (glycerol sebacate)-poly caprolactone/gelatin scaffold by coaxial electro spinning for soft tissue engineering. *Materials Science and Engineering: C* **2017**, *78*, 47–58.
111. Zhang, Y.Z.; Wang, X.; Feng, Y.; Li, J.; Lim, C.T.; Ramakrishna, S. Coaxial Electrospinning of (Fluorescein Isothiocyanate-Conjugated Bovine Serum Albumin)-Encapsulated Poly(ε-caprolactone) Nanofibers for Sustained Release. *Biomacromolecules* **2006**, *7*, 1049–1057.
112. Li, D.; Xia, Y. Direct Fabrication of Composite and Ceramic Hollow Nanofibers by Electrospinning. *Nano Lett.* **2004**, *4*, 933–938.
113. Sell, S.; Barnes, C.; Smith, M.; McClure, M.; Madurantakam, P.; Grant, J.; McManus, M.; Bowlin, G. Extracellular matrix regenerated: tissue engineering via electrospun biomimetic nanofibers. *Polym. Int.* **2007**, *56*, 1349–1360.
114. Boudriot, U.; Dersch, R.; Greiner, A.; Wendorff, J.H. Electrospinning Approaches Toward Scaffold Engineering—A Brief Overview. *Artif. Organs* **2006**, *30*, 785–792.
115. Agarwal, S.; Wendorff, J.H.; Greiner, A. Progress in the Field of Electrospinning for Tissue Engineering Applications. *Adv. Mater.* **2009**, *21*, 3343–3351.
116. Cipitria, A.; Skelton, A.; R. Dargaville, T.; D. Dalton, P.; W. Hutmacher, D. Design, fabrication and characterization of PCL electrospun scaffolds—a review. *J. Mater. Chem.* **2011**, *21*, 9419–9453.
117. Ekaputra, A.K.; Prestwich, G.D.; Cool, S.M.; Hutmacher, D.W. Combining Electrospun Scaffolds with Electrosprayed Hydrogels Leads to Three-Dimensional Cellularization of Hybrid Constructs. *Biomacromolecules* **2008**, *9*, 2097–2103.

118. Nam, J.; Huang, Y.; Agarwal, S.; Lannutti, J. Improved Cellular Infiltration in Electrospun Fiber via Engineered Porosity. *Tissue Engineering* **2007**, *13*, 2249–2257.
119. Leong, M.F.; Rasheed, M.Z.; Lim, T.C.; Chian, K.S. In vitro cell infiltration and in vivo cell infiltration and vascularization in a fibrous, highly porous poly(D,L-lactide) scaffold fabricated by cryogenic electrospinning technique. *Journal of Biomedical Materials Research Part A* **2009**, *91A*, 231–240.
120. Hong, Y.; Huber, A.; Takanari, K.; Amoroso, N.J.; Hashizume, R.; Badylak, S.F.; Wagner, W.R. Mechanical properties and in vivo behavior of a biodegradable synthetic polymer microfiber–extracellular matrix hydrogel biohybrid scaffold. *Biomaterials* **2011**, *32*, 3387–3394.
121. Ki, C.S.; Park, S.Y.; Kim, H.J.; Jung, H.-M.; Woo, K.M.; Lee, J.W.; Park, Y.H. Development of 3-D nanofibrous fibroin scaffold with high porosity by electrospinning: implications for bone regeneration. *Biotechnol Lett* **2008**, *30*, 405–410.
122. Yang, X.; Shah, J.D.; Wang, H. Nanofiber Enabled Layer-by-Layer Approach Toward Three-Dimensional Tissue Formation. *Tissue Engineering Part A* **2008**, *15*, 945–956.
123. Erdem, R.; İlhan, M.; Sancak, E. Analysis of EMSE and mechanical properties of sputter coated electrospun nanofibers. *Applied Surface Science* **2016**, *380*, 326–330.
124. Fan, Z.-Z.; He, H.-W.; Yuan, D.; Pang, L.-L.; Huang, Y.-Z.; Long, Y.-Z.; Ning, X. Fabrication of epoxy resin reinforced polyimide (PI) nanofibrous membrane. *Materials Letters* **2019**, *252*, 138–141.
125. Sahoo, S.; Ang, L.T.; Goh, J.C.-H.; Toh, S.-L. Growth factor delivery through electrospun nanofibers in scaffolds for tissue engineering applications. *Journal of Biomedical Materials Research Part A* **2010**, *93A*, 1539–1550.
126. Jia, X.; Zhao, C.; Li, P.; Zhang, H.; Huang, Y.; Li, H.; Fan, J.; Feng, W.; Yuan, X.; Fan, Y. Sustained Release of VEGF by Coaxial Electrospun Dextran/PLGA Fibrous Membranes in Vascular Tissue Engineering. *Journal of Biomaterials Science, Polymer Edition* **2011**, *22*, 1811–1827.
127. Nasehi, F.; Karshenas, M.; Nadri, S.; Barati, G.; Salim, A. Core-shell fibrous scaffold as a vehicle for sustained release of retinal pigmented epithelium-derived factor (PEDF) for photoreceptor differentiation of conjunctiva mesenchymal stem cells. *Journal of Biomedical Materials Research Part A* **2017**, *105*, 3514–3519.
128. Ji, X.; Su, Z.; Liu, C.; Wang, P.; Zhang, S. Regulation of enzyme activity and stability through positional interaction with polyurethane nanofibers. *Biochemical Engineering Journal* **2017**, *121*, 147–155.
129. Kwak, G.; Lee, G.H.; Shim, S.; Yoon, K.-B. Fabrication of Light-Guiding Core/Sheath Fibers by Coaxial Electrospinning. *Macromolecular Rapid Communications* **2008**, *29*, 815–820.
130. Korina, E.; Stoilova, O.; Manolova, N.; Rashkov, I. Polymer fibers with magnetic core decorated with titanium dioxide prospective for photocatalytic water treatment. *Journal of Environmental Chemical Engineering* **2018**, *6*, 2075–2084.
131. Pant, B.; Park, M.; Park, S.-J. Drug Delivery Applications of Core-Sheath Nanofibers Prepared by Coaxial Electrospinning: A Review. *Pharmaceutics* **2019**, *11*, 305.
132. Huang, H.-H.; He, C.-L.; Wang, H.-S.; Mo, X.-M. Preparation of core-shell biodegradable microfibers for long-term drug delivery. *Journal of Biomedical Materials Research Part A* **2009**, *90A*, 1243–1251.
133. Ma, P.X.; Zhang, R. Synthetic nano-scale fibrous extracellular matrix. *J. Biomed. Mater. Res.* **1999**, *46*, 60–72.
134. Hartgerink, J.D.; Beniash, E.; Stupp, S.I. Self-Assembly and Mineralization of Peptide-Amphiphile Nanofibers. *Science* **2001**, *294*, 1684–1688.
135. Biron, M. Élastomères thermoplastiques (TPE). *Techniques de l'ingénieur* **2000**, *AM 3 400*, AM 3 400-1 à AM 3 400-34.
136. Fong, H.; Reneker, D.H. Elastomeric nanofibers of styrene–butadiene–styrene triblock copolymer. *Journal of Polymer Science Part B: Polymer Physics* **1999**, *37*, 3488–3493.
137. Feng, S.-Q.; Shen, X.-Y.; Fu, Z.-Y.; Ji, Y.-L. Studies on the electrospun submicron fibers of SIS and its mechanical properties. *Journal of Applied Polymer Science* **2009**, *114*, 1580–1586.

138. van der Heijden, S.; De Bruycker, K.; Simal, R.; Du Prez, F.; De Clerck, K. Use of Triazolinedione Click Chemistry for Tuning the Mechanical Properties of Electrospun SBS-Fibers. *Macromolecules* **2015**, *48*, 6474–6481.
139. Guelcher, S.A. Biodegradable Polyurethanes: Synthesis and Applications in Regenerative Medicine. *Tissue Engineering Part B: Reviews* **2008**, *14*, 3–17.
140. Stankus, J.J.; Guan, J.; Wagner, W.R. Fabrication of biodegradable elastomeric scaffolds with sub-micron morphologies. *Journal of Biomedical Materials Research Part A* **2004**, *70A*, 603–614.
141. Stylianopoulos, T.; Bashur, C.A.; Goldstein, A.S.; Guelcher, S.A.; Barocas, V.H. Computational predictions of the tensile properties of electrospun fibre meshes: Effect of fibre diameter and fibre orientation. *Journal of the Mechanical Behavior of Biomedical Materials* **2008**, *1*, 326–335.
142. Shababdoust, A.; Ehsani, M.; Shokrollahi, P.; Zandi, M. Fabrication of curcumin-loaded electrospun nanofiberous polyurethanes with anti-bacterial activity. *Prog Biomater* **2018**, *7*, 23–33.
143. Han, J.; Cao, R.-W.; Chen, B.; Ye, L.; Zhang, A.-Y.; Zhang, J.; Feng, Z.-G. Electrospinning and biocompatibility evaluation of biodegradable polyurethanes based on L-lysine diisocyanate and L-lysine chain extender. *Journal of Biomedical Materials Research Part A* **2011**, *96A*, 705–714.
144. Wu, W.; Yuan, G.; He, A.; Han, C.C. Surface Depletion of the Fluorine Content of Electrospun Fibers of Fluorinated Polyurethane. *Langmuir* **2009**, *25*, 3178–3183.
145. Lee, K.; Lee, B.; Kim, C.; Kim, H.; Kim, K.; Nah, C. Stress-strain behavior of the electrospun thermoplastic polyurethane elastomer fiber mats. *Macromol. Res.* **2005**, *13*, 441–445.
146. Borg, E.; Frenot, A.; Walkenström, P.; Gisselfält, K.; Gretzer, C.; Gatenholm, P. Electrospinning of degradable elastomeric nanofibers with various morphology and their interaction with human fibroblasts. *Journal of Applied Polymer Science* **2008**, *108*, 491–497.
147. Hunley, M.T.; Pötschke, P.; Long, T.E. Melt Dispersion and Electrospinning of Non-Functionalized Multiwalled Carbon Nanotubes in Thermoplastic Polyurethane. *Macromolecular Rapid Communications* **2009**, *30*, 2102–2106.
148. Jiang, L.; Jiang, Y.; Stiadle, J.; Wang, X.; Wang, L.; Li, Q.; Shen, C.; Thibeault, S.L.; Turng, L.-S. Electrospun nanofibrous thermoplastic polyurethane/poly(glycerol sebacate) hybrid scaffolds for vocal fold tissue engineering applications. *Materials Science and Engineering: C* **2019**, *94*, 740–749.
149. Cao, D.; Fu, Z.; Li, C. Electrospun fiber membranes of novel thermoplastic polyester elastomers: Preparation and characterization. *Journal of Applied Polymer Science* **2011**, *122*, 1698–1706.
150. Wang, J.-N.; Jia, B.-B.; Li, C.-J. Preparation of Petaloid TPEE@AlOOH Nanofibers with Cr (VI)-Removal Capacity. *NANO* **2014**, *10*, 1550029.
151. Shah, M.I.; Yang, Z.; Li, Y.; Jiang, L.; Ling, J. Properties of Electrospun Nanofibers of Multi-Block Copolymers of [Poly-epsilon-caprolactone-b-poly(tetrahydrofuran-co-epsilon-caprolactone)]m Synthesized by Janus Polymerization. *Polymers* **2017**, *9*, 559.
152. Reneker, D.H.; Yarin, A.L. Electrospinning jets and polymer nanofibers. *Polymer* **2008**, *49*, 2387–2425.
153. Choi, S.-S.; Hong, J.-P.; Seo, Y.S.; Chung, S.M.; Nah, C. Fabrication and characterization of electrospun polybutadiene fibers crosslinked by UV irradiation. *Journal of Applied Polymer Science* **2006**, *101*, 2333–2337.
154. Thielke, M.W.; Bruckner, E.P.; Wong, D.L.; Theato, P. Thiol-ene modification of electrospun polybutadiene fibers crosslinked by UV irradiation. *Polymer* **2014**, *55*, 5596–5599.
155. Kerr-Phillips, T.E.; Woehling, V.; Agniel, R.; Nguyen, G.T.M.; Vidal, F.; Kilmartin, P.; Plesse, C.; Travas-Sejdic, J. Electrospun rubber fibre mats with electrochemically controllable pore sizes. *J. Mater. Chem. B* **2015**, *3*, 4249–4258.
156. Liu, L.; Zhang, F.; Hu, S.; Zhang, L.; Wen, S. Preparation of Ultrafine Ethylene/Propylene/Diene Terpolymer Rubber Fibers by Coaxial Electrospinning. *Macromolecular Materials and Engineering* **2012**, *297*, 298–302.
157. Kim, S.H.; Kim, S.-H.; Nair, S.; Moore, E. Reactive Electrospinning of Cross-Linked Poly(2-hydroxyethyl methacrylate) Nanofibers and Elastic Properties of Individual Hydrogel Nanofibers in Aqueous Solutions. *Macromolecules* **2005**, *38*, 3719–3723.

158. Jeshvaghani, E.S.; Ghasemi-Mobarakeh, L.; Mansurnezhad, R.; Ajalloueian, F.; Kharaziha, M.; Dinari, M.; Jokandan, M.S.; Chronakis, I.S. Fabrication, characterization, and biocompatibility assessment of a novel elastomeric nanofibrous scaffold: A potential scaffold for soft tissue engineering. *Journal of Biomedical Materials Research Part B: Applied Biomaterials* **2018**, *106*, 2371–2383.
159. Shanmuganathan, K.; Elliot, S.M.; Lane, A.P.; Ellison, C.J. Highly Stretchable Thermoset Fibers and Nonwovens Using Thiol–ene Photopolymerization. *ACS Appl. Mater. Interfaces* **2014**, *6*, 14259–14265.
160. Lu, S.; Duan, X.; Han, Y.; Huang, H. Silicone rubber/polyvinylpyrrolidone microfibers produced by coaxial electrospinning. *Journal of Applied Polymer Science* **2013**, *128*, 2273–2276.
161. Guarino, V.; Branda, F.; Ausanio, G.; Iannotti, V.; Lanotte, L.; Ambrosio, L. Elastomagnetic NI-PDMS nanofibers via coaxial electrospinning. *Mater. Res. Express* **2018**, *5*, 085029.
162. Pandini, S.; Agnelli, S.; Merlettini, A.; Chiellini, F.; Gualandi, C.; Paderni, K.; Focarete, M.L.; Messori, M.; Toselli, M. Multifunctional Electrospun Nonwoven Mats with Two-Way Shape Memory Behavior Prepared from Sol–Gel Crosslinked Poly(epsilon-Caprolactone). *Macromolecular Materials and Engineering* **2017**, *302*, 1600519.
163. Bruggeman, J.P.; de Bruin, B.-J.; Bettinger, C.J.; Langer, R. Biodegradable poly(polyol sebacate) polymers. *Biomaterials* **2008**, *29*, 4726–4735.
164. Dong, W.; Li, T.; Xiang, S.; Ma, P.; Chen, M. Influence of Glutamic Acid on the Properties of Poly(xylitol glutamate sebacate) Bioelastomer. *Polymers* **2013**, *5*, 1339–1351.
165. Jin, G.; He, R.; Sha, B.; Li, W.; Qing, H.; Teng, R.; Xu, F. Electrospun three-dimensional aligned nanofibrous scaffolds for tissue engineering. *Materials Science and Engineering: C* **2018**, *92*, 995–1005.
166. Zhu, L.; Zhang, Y.; Ji, Y. Fabricating poly(1,8-octanediol citrate) elastomer based fibrous mats via electrospinning for soft tissue engineering scaffold. *J Mater Sci: Mater Med* **2017**, *28*, 93.
167. Goins, A.; Ramaswamy, V.; Dirr, E.; Dulany, K.; Irby, S.; Webb, A.; Allen, J. Development of poly (1,8 octanediol-co-citrate) and poly (acrylic acid) nanofibrous scaffolds for wound healing applications. *Biomed. Mater.* **2017**, *13*, 015002.
168. Li, Y.; Chen, Q.-Z. Fabrication of Mechanically Tissue-Like Fibrous Poly(xylitol sebacate) Using Core/Shell Electrospinning Technique. *Advanced Engineering Materials* **2015**, *17*, 324–329.
169. Yi, F.; LaVan, D.A. Poly(glycerol sebacate) Nanofiber Scaffolds by Core/Shell Electrospinning. *Macromol. Biosci.* **2008**, *8*, 803–806.
170. Saludas, L.; Pascual-Gil, S.; Prósper, F.; Garbayo, E.; Blanco-Prieto, M. Hydrogel based approaches for cardiac tissue engineering. *International Journal of Pharmaceutics* **2017**, *523*, 454–475.
171. Ravichandran, R.; Venugopal, J.R.; Sundarrajan, S.; Mukherjee, S.; Ramakrishna, S. Cardiogenic differentiation of mesenchymal stem cells on elastomeric poly (glycerol sebacate)/collagen core/shell fibers. *World Journal of Cardiology* **2013**, *5*, 28–41.
172. Kharaziha, M.; Nikkhah, M.; Shin, S.-R.; Annabi, N.; Masoumi, N.; Gaharwar, A.K.; Camci-Unal, G.; Khademhosseini, A. PGS:Gelatin nanofibrous scaffolds with tunable mechanical and structural properties for engineering cardiac tissues. *Biomaterials* **2013**, *34*, 6355–6366.
173. Ravichandran, R.; Venugopal, J.R.; Sundarrajan, S.; Mukherjee, S.; Ramakrishna, S. Poly(Glycerol Sebacate)/Gelatin Core/Shell Fibrous Structure for Regeneration of Myocardial Infarction. *Tissue Engineering Part A* **2011**, *17*, 1363–1373.
174. Dippold, D.; Tallawi, M.; Tansaz, S.; Roether, J.A.; Boccaccini, A.R. Novel electrospun poly(glycerol sebacate)–zein fiber mats as candidate materials for cardiac tissue engineering. *European Polymer Journal* **2016**, *75*, 504–513.
175. Vogt, L.; Liverani, L.; Roether, J.A.; Boccaccini, A.R. Electrospun Zein Fibers Incorporating Poly(glycerol sebacate) for Soft Tissue Engineering. *Nanomaterials* **2018**, *8*, 150.
176. Gentile, P.; Chiono, V.; Carmagnola, I.; Hatton, P.V. An Overview of Poly(lactic-co-glycolic) Acid (PLGA)-Based Biomaterials for Bone Tissue Engineering. *Int J Mol Sci* **2014**, *15*, 3640–3659.
177. Sfakis, L.; Kamaldinov, T.; Khmaladze, A.; Hosseini, Z.F.; Nelson, D.A.; Larsen, M.; Castracane, J. Mesenchymal Cells Affect Salivary Epithelial Cell Morphology on PGS/PLGA Core/Shell Nanofibers. *International Journal of Molecular Sciences* **2018**, *19*, 1031.

178. Woodruff, M.A.; Hutmacher, D.W. The return of a forgotten polymer—Polycaprolactone in the 21st century. *Progress in Polymer Science* **2010**, *35*, 1217–1256.
179. Sant, S.; Hwang, C.M.; Lee, S.-H.; Khademhosseini, A. Hybrid PGS–PCL microfibrous scaffolds with improved mechanical and biological properties. *J Tissue Eng Regen Med* **2011**, *5*, 283–291.
180. Rai, R.; Tallawi, M.; Frati, C.; Falco, A.; Gervasi, A.; Quaini, F.; Roether, J.A.; Hochburger, T.; Schubert, D.W.; Seik, L.; et al. Bioactive Electrospun Fibers of Poly(glycerol sebacate) and Poly(epsilon-caprolactone) for Cardiac Patch Application. *Advanced Healthcare Materials* **2015**, *4*, 2012–2025.
181. Wenk, J.F.; Eslami, P.; Zhang, Z.; Xu, C.; Kuhl, E.; Gorman, J.H.; Robb, J.D.; Ratcliffe, M.B.; Gorman, R.C.; Guccione, J.M. A Novel Method for Quantifying the In-Vivo Mechanical Effect of Material Injected Into a Myocardial Infarction. *The Annals of Thoracic Surgery* **2011**, *92*, 935–941.
182. Morita, M.; Eckert, C.E.; Matsuzaki, K.; Noma, M.; Ryan, L.P.; Burdick, J.A.; Jackson, B.M.; Gorman, J.H.; Sacks, M.S.; Gorman, R.C. Modification of infarct material properties limits adverse ventricular remodeling. *Ann. Thorac. Surg.* **2011**, *92*, 617–624.
183. Tallawi, M.; Dippold, D.; Rai, R.; D'Atri, D.; Roether, J.A.; Schubert, D.W.; Rosellini, E.; Engel, F.B.; Boccaccini, A.R. Novel PGS/PCL electrospun fiber mats with patterned topographical features for cardiac patch applications. *Materials Science and Engineering: C* **2016**, *69*, 569–576.
184. Hou, L.; Zhang, X.; Mikael, P.E.; Lin, L.; Dong, W.; Zheng, Y.; Simmons, T.J.; Zhang, F.; Linhardt, R.J. Biodegradable and Bioactive PCL–PGS Core–Shell Fibers for Tissue Engineering. *ACS Omega* **2017**, *2*, 6321–6328.
185. Lasprilla, A.J.R.; Martinez, G.A.R.; Lunelli, B.H.; Jardini, A.L.; Filho, R.M. Poly-lactic acid synthesis for application in biomedical devices — A review. *Biotechnology Advances* **2012**, *30*, 321–328.
186. You, Z.-R.; Hu, M.-H.; Tuan-Mu, H.-Y.; Hu, J.-J. Fabrication of poly(glycerol sebacate) fibrous membranes by coaxial electrospinning: Influence of shell and core solutions. *Journal of the Mechanical Behavior of Biomedical Materials* **2016**, *63*, 220–231.
187. Wu, H.-J.; Hu, M.-H.; Tuan-Mu, H.-Y.; Hu, J.-J. Preparation of aligned poly(glycerol sebacate) fibrous membranes for anisotropic tissue engineering. *Materials Science and Engineering: C* **2019**, *100*, 30–37.
188. Ravichandran, R.; Venugopal, J.R.; Sundarrajan, S.; Shayanti Mukherjee; Sridhar, R.; Ramakrishna, S. Minimally invasive injectable short nanofibers of poly(glycerol sebacate) for cardiac tissue engineering. *Nanotechnology* **2012**, *23*, 385102.
189. Xu, B.; Li, Y.; Fang, X.; Thouas, G.A.; Cook, W.D.; Newgreen, D.F.; Chen, Q. Mechanically tissue-like elastomeric polymers and their potential as a vehicle to deliver functional cardiomyocytes. *J. Mech. Behav. Biomed. Mater.* **2013**, *28*, 354–365.
190. Yan, Y.; Sencadas, V.; Jin, T.; Huang, X.; Chen, J.; Wei, D.; Jiang, Z. Tailoring the wettability and mechanical properties of electrospun poly(l-lactic acid)-poly(glycerol sebacate) core-shell membranes for biomedical applications. *J. Colloid Interface Sci.* **2017**, *508*, 87–94.
191. Liverani, L.; Piegat, A.; Niemczyk, A.; El Fray, M.; Boccaccini, A.R. Electrospun fibers of poly(butylene succinate–co–dilinoleic succinate) and its blend with poly(glycerol sebacate) for soft tissue engineering applications. *European Polymer Journal* **2016**, *81*, 295–306.
192. Tallawi, M.; Zebrowski, D.C.; Rai, R.; Roether, J.A.; Schubert, D.W.; El Fray, M.; Engel, F.B.; Aifantis, K.E.; Boccaccini, A.R. Poly(Glycerol Sebacate)/Poly(Butylene Succinate-Butylene Dilinoleate) Fibrous Scaffolds for Cardiac Tissue Engineering. *Tissue Engineering Part C: Methods* **2014**, *21*, 585–596.
193. Lee, S.; Kim, B.; Kim, S.-H.; Kim, E.; Jang, J.-H. Superhydrophobic, Reversibly Elastic, Moldable, and Electrospun (SupREME) Fibers with Multimodal Functions: From Oil Absorbents to Local Drug Delivery Adjuvants. *Advanced Functional Materials* **2017**, *27*.
194. Jeffries, E.M.; Allen, R.A.; Gao, J.; Pesce, M.; Wang, Y. Highly elastic and suturable electrospun poly(glycerol sebacate) fibrous scaffolds. *Acta Biomaterialia* **2015**, *18*, 30–39.

195. Xu, B.; Li, Y.; Zhu, C.; Cook, W.D.; Forsythe, J.; Chen, Q. Fabrication, mechanical properties and cytocompatibility of elastomeric nanofibrous mats of poly(glycerol sebacate). *European Polymer Journal* **2015**, *64*, 79–92.
196. Saudi, A.; Rafienia, M.; Kharazi, A.Z.; Salehi, H.; Zarrabi, A.; Karevan, M. Design and fabrication of poly (glycerol sebacate)-based fibers for neural tissue engineering: Synthesis, electrospinning, and characterization. *Polymers for Advanced Technologies* **2019**.
197. Ifkovits, J.L.; Devlin, J.J.; Eng, G.; Martens, T.P.; Vunjak-Novakovic, G.; Burdick, J.A. Biodegradable Fibrous Scaffolds with Tunable Properties Formed from Photo-Cross-Linkable Poly(glycerol sebacate). *ACS Appl. Mater. Interfaces* **2009**, *1*, 1878–1886.
198. Ifkovits, J.L.; Wu, K.; Mauck, R.L.; Burdick, J.A. The Influence of Fibrous Elastomer Structure and Porosity on Matrix Organization. *PLOS ONE* **2010**, *5*, e15717.

CHAPTER 2

Synthesis and characterization of poly(glycerol sebacate)

This chapter aims to describe the synthesis of poly(glycerol sebacate) and to determine the effect of various conditions. Indeed, many examples of the synthesis are found in the literature, but because many parameters should be taken into account, it is difficult to anticipate the final properties of the material.

The synthesis is divided in two steps: the prepolymerization and the crosslinking. Various parameters such as heating method (conventional or under microwave irradiations), temperature and ratio of reactants will be studied. The prepolymer will be characterized by its degree of esterification. The degree of crosslinking and the mechanical properties of the elastomer will be compared for different synthesis conditions.

Synthesis and characterization of poly(glycerol sebacate)

1. State of the art and objectives

1.1. Principle of poly(glycerol sebacate) synthesis

Poly(glycerol sebacate) is usually synthesized in two steps: prepolymerization and crosslinking. The prepolymerization leads to soluble oligomers, the prepolymer (pPGS), by polycondensation of glycerol and sebacic acid (Figure 2.1). Because it is an esterification, it is important to shift the equilibrium toward the polymer by elimination of the water. To characterize the pPGS, the degree of esterification (DE) can be measured. It is defined as:

$$DE\ (\%) = \frac{n_{esters}^{fin}}{n_{acids}^{init}} \times 100$$

for conditions where carboxylic acids are not in excess. Several parameters have an influence on the DE and on the properties of the synthesized prepolymer. They are discussed in the literature as detailed below. Among them, there is the temperature, the type of heating, or the ratio of glycerol to sebacic acid introduced (G/SA). The stoichiometric ratio corresponds to G/SA equal to 2/3 i.e. when the number of –OH groups is equal to the number of –COOH groups (Figure 2.1). Glycerol contains two primary alcohols for one secondary alcohol which is less reactive than primary alcohols. So, at the beginning of the reaction, secondary alcohols might not react and linear segments will be synthesized. To create branching units, secondary alcohols must be forced to react, when few primary alcohols left. Stoichiometric ratio, with a higher proportion of secondary alcohols, leads thus to more branched prepolymers.

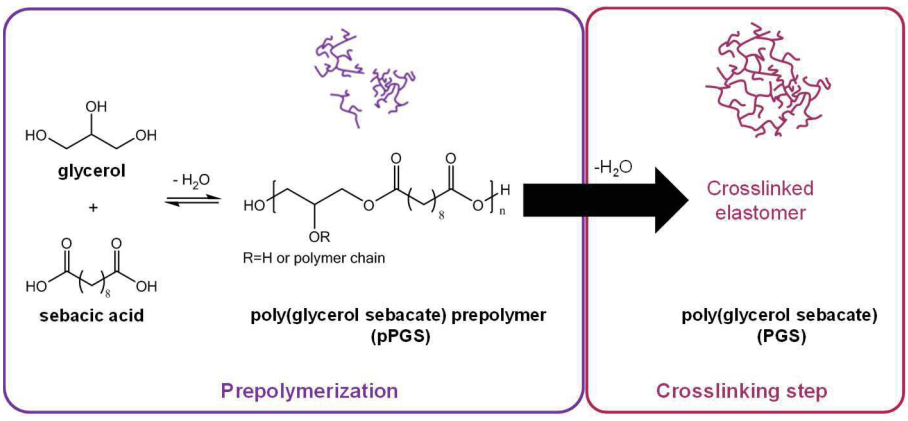

Figure 2.1. Scheme describing PGS synthesis.

The second step is the crosslinking step, where the branched prepolymers are bonded together in an insoluble 3D network (Figure 2.1). To achieve this goal, crosslinking is done by heating under vacuum, in order to extract water from the reactive medium and force the esterification. Vacuum is employed only when glycerol, a relatively volatile molecule, is already largely bonded in pPGS to avoid its evaporation.

1.2. Influence of synthesis parameters on the structure of PGS and its mechanical properties

Wang *et al.* [1] proposed the synthesis of PGS elastomer in 2002 with a G/SA ratio equal to 1/1. They divided the prepolymerization in two sub-stages: they started the reaction at 120°C under argon atmosphere during 24h and then under reduced pressure (40 mTorr) during 48h. These conditions drive the equilibrium toward the polyester while they limit the evaporation of the glycerol. The elastomer was obtained by curing a film of prepolymer in a vacuum oven during 24h at 120°C under 120 mTorr.

Since this first report, several teams published works aiming to study the effect of various parameters on PGS synthesis and its mechanical properties. Indeed, it was found that pPGS and PGS properties depend strongly on parameters like temperature or time of reaction, as illustrated in Figure 2.2.

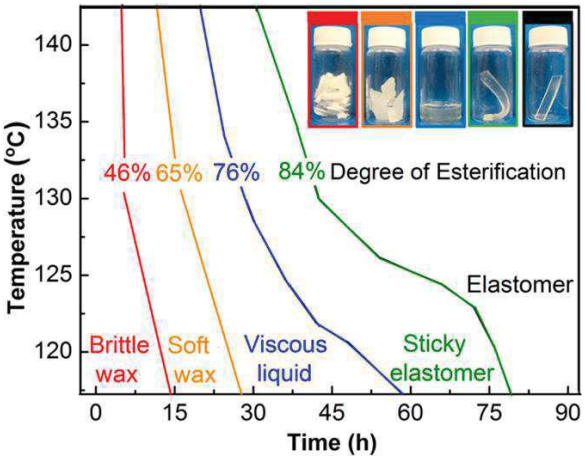

Figure 2.2. Map describing the evolution of the DE and the state of pPGS and PGS as a function of the reaction time and temperature (adapted from Li *et al.* [2]).

Influence of the reaction temperature

Chen *et al.* [3] investigated the influence of the reaction temperature. They carried out the reaction in two steps (under argon atmosphere and then under reduced pressure) with an equimolar mixture of glycerol and sebacic acid placed in a mold. The two steps were conducted at 110°C, 120°C or 130°C. The resulting elastomers had moduli between 0.056 and 1.2 MPa and ultimate strains between 41 and 448%, the temperature increase leading to a crosslinking density increase and thus to stiffening.

Influence of the ratio glycerol/sebacic acid

As discussed above, another important parameter for PGS synthesis is the ratio G/SA. Kafouris *et al.* [4] divided the synthesis in three steps in order to analyze the effect of G/SA on the branched prepolymers and then on the elastomers. The tested G/SA ratios correspond to a percentage of glycerol comprised between 29 and 66%. The first step takes place under argon

atmosphere and is followed by the second step under vacuum. These two first steps were enough to make crosslinked networks starting from proportions close to stoichiometric ones (G/SA 2/3 or 2/4). For ratio further from stoichiometry (2/2 and 2/5), a third step – additional heating under vacuum – was required for full crosslinking. However, these three steps could not lead to crosslinking of ratio 2/1, too far from stoichiometry with three alcohols for one carboxylic acid. SEC and mass spectroscopy analyses revealed that the branched prepolymers were composed of short oligomers of 2 to 9 units. According to Dynamic Mechanical Thermal Analysis (DMTA), the stiffest elastomer is fabricated with the stoichiometric ratio 2/3. This material also has the lowest sol fraction (< 20%) after extraction during one week in THF and the lowest degree of swelling in various solvents. On the contrary, G/SA equal to 2/5 led to a soft and easy to swell elastomer, indicating that the material's properties can be tailored by the choice of G/SA.

In summary, a G/SA ratio close to stoichiometry allows a faster crosslinking and leads to stiffer elastomers.

Influence of a catalyst

Other paths are tested to enhance PGS synthesis. In particular, it would be interesting to decrease the time of reaction, reaching in the former examples several days. Indeed, the kinetics could be improved if the reaction was catalyzed. However, as PGS is intended for biomedical applications, toxic additives should not be incorporated in the reactive mixture. Godinho *et al.* [5] catalyzed thus the reaction using enzymes. They dissolved glycerol and sebacic acid in ratio 1/1 in t-butanol with lipase B free or immobilized, and conducted the reaction at 60°C during 24h in close vessel. In this configuration, the water resulting from esterification cannot escape from the reactor. For this reason, zeolite molecular sieves were added in the blend as a desiccant. This method presents the benefit to allow the reaction in mild conditions, but it requires post-synthesis purifications to remove the enzyme, the desiccant and the solvent. It can be noticed that after 24h of prepolymerization, the degree of conversion reaches about 70% [5], whereas for a synthesis at 120°C with same total reaction time and ratio of reactants, Kafouris *et al.* reached only 59% [4]. Additionally, according to mass spectroscopy analysis, enzymatic catalyst favors the formation of linear oligomers, with mostly four to six units.

Influence of the type of heating

Aydin *et al.* [6] found another way to accelerate the synthesis. They exploited the benefits of microwave irradiation that allows a rapid and direct distribution of heat to the reactive medium, especially for polar molecules [7]. In this way, they fabricated a crosslinked elastomer after three minutes of prepolymerization and 16h of curing. The prepolymerization was conducted in a domestic microwave oven where a Petri dish containing glycerol and sebacic acid was placed. The reactants were heated during 1 minute at 650 W before a break of 10 s to let the water vapor go out. This procedure was repeated three times and the dish was then placed in a vacuum oven heated at 150°C to achieve the crosslinking. The resulting elastomer has a Young's modulus of 0.5 MPa and an ultimate strain of 180%. DSC revealed a T_g at -36°C and two melting points at -16°C and 62°C. However, NMR analyses showed that the ratio G/SA decreased after synthesis, indicating that some glycerol evaporated. The authors explain this phenomenon by high temperatures reached in the microwave [6].

The benefit of microwave heating in comparison to standard heating was more deeply studied by Li *et al.* [2]. They compared the kinetic for a reaction carried out under conventional

heating under nitrogen atmosphere during 90 h and under heating in a domestic microwave oven set at 600 W during 30 minutes. In the latter case, the oven was open every minute to control the temperature and let the water vapor to escape. After both prepolymerization methods, the material was casted into films and cured at 1 mTorr. To follow the reaction, the degree of esterification was calculated after titration of samples dissolved or swollen in ethanol/toluene. Titration was done by KOH solution using bromothymol blue as colorimetric indicator. So, the prepolymer synthesized after 30 minutes in the microwave oven reaches a DE of 52%, whereas standard prepolymerization requires 12h to reach 56% of esterification. However, 30 minutes-microwave reaction also leads to up to 60% of evaporation of glycerol, due to high temperatures reaches in the oven. The authors underlined that this glycerol loss is even worsen during curing under vacuum if the employed prepolymer has a low DE, because fewer glycerol units are bonded. The large modification of the ratio G/SA during microwave synthesis leads to changes in PGS properties and makes a stiffer material. For example, a PGS prepared from microwave heating followed by curing and having a DE of 74% has a Young's modulus of 0.8 MPa and a maximal strain close to 150%. A PGS prepared from conventional heating followed by curing having a DE of 80% has a Young's modulus of 0.3 MPa and a maximal strain above to 200%. Yet, Li *et al.* confirmed that for a same type of heating, the higher the time or temperature of reaction are, the higher the DE is and thus the stiffer the material is.

Finally, microwave heating brings some benefits in terms of kinetic but the method has the drawback to decrease the reproducibility of the synthesis by allowing one reactant – glycerol – to evaporate during synthesis. In order to limit this phenomenon and have a better control on the synthesis, it is possible to use a laboratory microwave reactor that allows an efficient stirring of the reactive mixture and a good monitoring of the temperature and the power. Coativy *et al.* [8] blended for example glycerol, sebacic acid, but also stearic acid in a closed beaker heated in a laboratory microwave. This procedure allowed them to fix the reaction temperature at 180°C and the maximal power at 400 W, with continuous stirring of the mixture. They identified that the resulting mass loss at the end of the reaction corresponds only to the water evaporation. Lau *et al.* [9] studied the effect of the multimode microwave method (domestic oven kind) versus the single mode laboratory reactor. The same procedure was used for both type of microwave reactor, consisting of the repetition of 3 minutes-lasting cycles of heating with a power of 150 W. While single-mode allowed fixing the temperature at 130°C, no control was possible with multimode. DE was calculated from the amount of water collected. The prepolymerization step was followed by a curing step under vacuum. Comparison of the evolution of DE during prepolymerization and of the modulus after crosslinking showed that single mode microwave heating allows a faster reaction. Thus, a stiffer elastomer is synthesized after a similar reaction time. Single mode, a technic that can be provided by laboratory microwave reactors, should thus be preferred. This result can be explained by the fact that single mode systems can provide a more homogenous microwave distribution and higher power densities [7]. This method was also compared to conventional heating by Lau and colleagues They found that the reaction rate is increased by six fold thanks to single mode microwave.

However, the structure of the synthesized PGS is different. Indeed, Li *et al.* underlined in their work that during prepolymerization, almost only primary alcohols react; secondary alcohols react only when the reaction is efficiently shifted to the polymer thanks to vacuum during curing [2]. Nevertheless, Lau *et al.* [9] determined that glycerol is well activated by microwaves. In particular, secondary alcohols react more easily than with conventional heating. Hence, microwave heating leads to more branched prepolymers, as it was confirmed by IR, NMR and

mass spectroscopy analyses. The resulting elastomers are thus also stiffer. The Young's moduli and strains at break are in the range of 0.55 MPa and 55% and 3.5 MPa and 15% depending on the curing time, a longer curing time leading again to a stiffer and less stretchable elastomer.

In summary, microwave irradiation has a large effect on PGS properties, because it allows accelerating considerably the reaction, especially for secondary alcohols. It is however important to use a single-mode reactor in order to ensure a good control of the reaction.

All these examples illustrate how the synthesis parameters have a great influence on PGS properties. The properties found by the different teams are highly variable because they also depend on parameters such as the kind of reactor, the value of the reduced pressure or the glycerol loss. These reasons justify the usefulness of the present study about PGS synthesis: it allows assessing the properties obtained in the conditions employed in our lab.

1.3. Synthesis of PGS derivatives and copolymers

So, by changing synthesis parameters, PGS properties can be modulated, but a finer modulation as well as a facilitated process could also be achieved by making copolymerization and preparing PGS derivatives.

Photopolymerizable PGS

For example, PGS was acrylated to make it curable under UV light [10,11]. Here, acrylic groups are grafted on pPGS during a step using solvent and several toxic reactants. With the same ideas, methacrylates were grafted on pPGS to form macromers that can be electrospun without the help of any carrier polymer [12].

Copolymerization with carboxylic acids

Monomers found in classical polymers for biomedical applications were also used to tune PGS. Sun *et al.* [13] copolymerized glycerol, sebacic acid and lactic acid (LA) in several molar ratios without any other additives to make polyesters with improved degradation rate and mechanical properties. PGS-*co*-LA was also synthesized as surgical sealant by Chen *et al.* [14]. The objective was here a gel sufficiently liquid at ambient temperature to be injected but able to solidify at 37°C in the body at the contact of the tissue. In order to get a polyester with this property, they copolymerized pPGS with LA, again without the help of any solvent, catalyst or other reactant.

Glycolic acid was also used as comonomer in a similar procedure [15]. Again, it allows another degree of control on the polyester properties. However, the addition of glycolic or lactic moieties makes the material stiffer. The strength of the elastomer was also increased by adding citric acid to pPGS prepolymer as a crosslinker [16]. The less crosslinked elastomer prepared here has a modulus of about 1 MPa and a strain at break of about 100%.

Copolymerization with amines

Instead of using diacids to change PGS chemical structure, diamines can be incorporated. Cheng *et al.* [17] synthesized for examples polyesteramides that involve strong hydrogen bonds and have good strength and good stretching abilities. Amide bonding can also be formed

between pPGS and gelatin: pH responsive elastomers with water swelling capacities can be prepared in this way [18]. With a water-in-air contact angle situated between 85 and 45°, depending on the proportion of gelatin, they are more hydrophilic than pure PGS. Moreover, they are soft elastomers as their Young's modulus in the hydrated state stays below 1 MPa, for a strain at break potentially higher than 250%.

Copolymerization with alcohols, in particular with PEG

Beside the utilization of different acids to modify PGS, it is possible to use other alcohols. In particular, diols can be used to increase the distance between two crosslinking points. For example, many works were published reporting the synthesis of PGS-*co*-PEG. Liu and Cai [19] first modified PGS synthesis by adding a first step where sebacic acid reacts with glycol to form linear chains. Then glycerol is added to start the crosslinking which is achieved during a final curing step. The resulting material shows a shape memory behavior.

Longer linear chains were obtained by using PEG polymers with a molar mass of 1000 g/mol. Patel *et al.* [20] synthesized block copolymers in three steps: the bulk polycondensation of sebacic acid with PEG followed by the addition of glycerol and a final curing step. The prepolymer resulting from the second step has a molecular weight between 4000 and 5000 Da depending on the ratio of reactant. Thanks to the PEG, the final elastomer is more hydrophilic with a contact angle of 65° when 60% of PEG is incorporated. Moreover, PEG makes it less stiff, the copolymer with 60% of PEG having a Young's modulus of 40 kPa.

Wang *et al.* [21] modified the synthesis procedure: after the first step of polycondensation between PEG and sebacic acid, they added both glycerol and sebacic acid before crosslinking. They studied the effect of the proportion of PEG and of the ratio between the number of carboxylic acids and of alcohols. They found that the presence of the flexible PEG chains decreases the tensile strength of the elastomers and increases the strain at break. However, these materials cannot be stretched at more than 50%. The less stiff material, synthesized from 40% of PEG and a –COOH/–OH ratio equal to 1/1, has a Young's modulus of 183 kPa. The hydrophilicity was also evaluated by contact angles measurements: the more hydrophilic elastomer is composed of 20% of PEG and a –COOH/–OH ratio equal to 2/3 and has a contact angle value close to 40°. These block copolymers support cells proliferation [20,21].

In addition, PGS-*co*-PEG was modified to facilitate its crosslinking. It was for example methacrylated for UV crosslinking [22]. Tyramine was grafted as side chain to unable enzyme-catalyzed crosslinking [23] and HDI for room temperature crosslinking [24,25]. Final properties were improved by addition of aniline pentamer as side chains to fabricate conductive elastomers [26] or by incorporation of lactic acid to increase the strength of the material [27]. But in these last examples, not biocompatible reactants were often used as catalysts.

Finally, many parameters are available for tuning of PGS properties. In the present work, the objective is to synthesize a prepolymer with low molar mass that can be used for electrospinning. So, this chapter is devoted to the analysis of the effect on PGS of some parameters, namely the type of heating, the curing temperature and time, and the ratio of reactants used.

The improvement of the electrospinning process by using PGS derivatives has also been considered. It was hypothesized that electrospinning could be facilitate if long poorly-branched prepolymers were used instead of pure pPGS. Indeed, as explained in the first chapter, pPGS

molar mass is too low for the molecules to entangle. The molar mass of pPGS can be increased by continuing the reaction. However, an insoluble gel is obtained before long enough chains are synthesized. So, the idea was here to decrease the crosslinking points density by using a long diol. PGS-*co*-PEG prepolymers were thus synthesized with different PEG size and ratio PEG/sebacic acid and electrospun. However, the degrees of polymerization of the prepolymer remained quite low and they required thus the use of a carrier polymer. With a PEG with 400 g/mol, it was possible to reduce the amount of carrier polymer. However, the fibers did not resist to curing, certainly because of the low melting point of PEG. No further work dedicated to PGS-*co*-PEG was thus carried out. Details are given in appendix 1.

2. Materials and methods

PGS synthesis was done in two steps. The first prepolymerization step was conducted by microwave and standard heating for comparison. Resulting pPGS were characterized by their degree of esterification and by DSC. Curing step was then carried out in order to characterize the PGS elastomer.

2.1. Materials

Glycerol (>99.96%, Fisher Chemicals), sebacic acid (98%, ACROS Organics) were used without purification as reactants. Absolute anhydrous ethanol (>99.9%, Carlo Erba), toluene (99.8%, Sigma-Aldrich), tetrahydrofurane (THF, 99%, Sigma-Aldrich) and d-DMSO (99.8%D, Eurisotop) were used as received for the characterizations.

2.2. Prepolymer synthesis by conventional heating

Glycerol and sebacic acid were weighted to reach the desired molar ratio (in this work, 1/1 or 2/3) with a total weight close to 50 g. The mixture was placed with a stirrer bar in a three-neck round-bottomed flask surmounted by a Vigreux condenser and a lateral water condenser connected to a flask to collect the produced water. The reaction mixture is stirred under argon at 130 or 150°C. Samples are taken at different time step to follow the kinetic. Final prepolymer is a yellow to orange paste.

2.3. Prepolymer synthesis by microwave heating

Glycerol and sebacic acid were weighted to reach the desired molar ratio (in this work, 1/1 or 2/3) with a total weight between 15 and 20 g. The mixture was placed with a stirrer bar in a round-bottomed flask with a narrow neck surmounted by a glass tube extender finished by an opened glass stopcock to allow the vapor to escape. The flask was placed in the microwave reactor (Discover SP, CEM). The latter was programmed to provide continuously an adequate power in order to reach and hold the desired temperature. The power fluctuated between 20 W and 80 W but its maximal value was fixed at 200 W. The resulting prepolymer appears like a wax, a paste or a viscous liquid depending on the extend of reaction. Its color varies from white to yellow (Figure 2.3). It is often transparent at the end of the heating, but its turbidity and its viscosity increases during cooling and time; the turbidity appears sometimes after several days, revealing the crystallization.

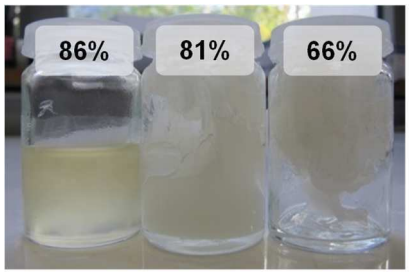

Figure 2.3. Example of pPGS with G/SA 1/1 with decreasing DE from left to right..

2.4. Curing step

PGS was crosslinked in a vacuum oven (Vacutherm VT6025, Fisher Scientific) under reduced pressure (between 5 and $10x10^{-3}$ mbars). The temperature was controlled by a thermocouple placed close to the sample. The pPGS films were prepared by solvent casting in THF or by melting of pPGS. Specific molds were used to prepare samples for tensile tests. Before curing starts, samples were degassed at ambient temperature during 30 minutes under vacuum. Films were then heated at 150°C during various period of time.

The achieved PGS is then a transparent yellow elastomer (Figure 2.4) that turns cloudy during time when the resulting crosslinking rate stays low, illustrating again crystallization. In addition, the less crosslinked it is, the more sticky it is.

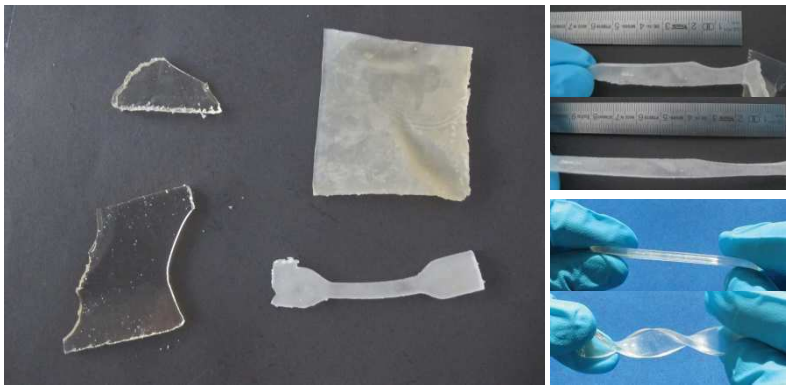

Figure 2.4. Examples of PGS elastomers.

2.5. Characterization of the (pre)polymer by DE calculation

The degree of esterification (DE) of PGS, which corresponds in our case to the conversion rate of sebacic acid, was determined by two methods. Soluble samples were dissolved in d-DMSO and analyzed by ^{1}H NMR (300 MHz Ultrashield, Bruker). The integration of the peaks corresponding to the protons in alpha position relatively to the carbonyl was evaluated and DE was calculated as follow (see Figure 2.5):

$$DE\ (\%) = \frac{I_E}{I_E + I_A} \times 100$$

With I_A and I_E the integration of the peaks on the spectra obtained by ^{1}H NMR, respectively at 2.18 ppm for the carboxylic acids (–C**H**$_2$–COOH) and 2.28 ppm for the esters (–C**H**$_2$–COOR).

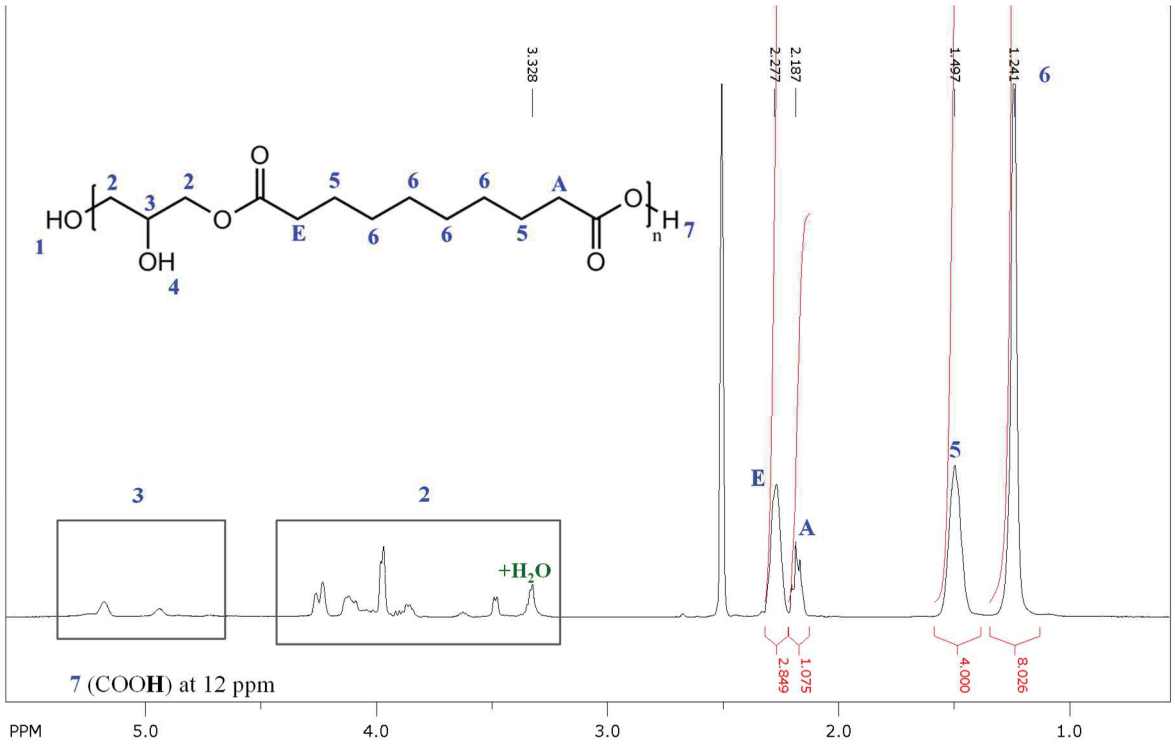

Figure 2.5. ^{1}H NMR spectra in d-DMSO for a pPGS with a DE of 73%.

This method is however not possible for high conversion rates, when PGS is crosslinked enough to be insoluble. But the titration method is suitable for the prepolymer and the elastomer. In this method, remaining –COOH are titrated by a 0.025 g/mol KOH solution in ethanol, using bromothymol blue as colorimetric indicator. Before titration, the elastomer swells during 2h. As the –COOH are difficult to access in the elastomer, the equivalence point was considered reached when the color change in green was hold during at least 1h. DE can then be calculated as:

$$DE\ (\%) = 1 - \frac{V_{eq} C_{KOH} (M_{SA} + M_G\ (n_G/n_{SA}))}{2m_{PGS}} \times 100$$

Where M_{SA} and M_G are the molar mass of sebacic acid and glycerol, n_G/n_{SA} the molar ratio of glycerol and sebacic acid used for the synthesis and m_{PGS} the mass of PGS analyzed. All titrations were repeated three times.

In order to evaluate the size of the polymer chains fabricated, a theoretical number-average degree of polymerization was calculated thanks to Carother's equation adapted to the functionality of the molecules [28]:

$$\overline{DP_n} = \frac{2}{2 - \frac{DE}{100}\bar{f}}$$

where $\bar{f}$ corresponds to the average functionality of the monomer blend. For a stoichiometric ratio, we have:

$$\bar{f} = \frac{\sum N_i f_i}{\sum N_i}$$

where N_i is the number of molecules introduced with a functionality f_i. $\bar{f}$ is thus equal to 2.4 for the ratio G/SA 2/3. However, for a non-stoichiometric ratio, functional groups in excess bring

nothing in term of functionality. $\bar{f}$ is then equal to twice the total number of functional groups in default divided by the total number of molecules. It is equal to 2 for G/SA 1/1.

It is here important to notice that this simple model does not consider the different reactivity of primary and secondary alcohols of glycerol. More accurate models based on statistic exist [29] but were not chosen here in order to simplify the explanations. Two PGS prepared with a different G/SA but with a same DE are thus composed of molecules with different $\overline{DP_n}$ in the selected model. Indeed, the size of the prepolymer evolves differently according to G/SA, and the gel point is reached for different conversion rate, as shown on Figure 2.6: the theoretical gel point (asymptote) is reached for DE equal to 83% for G/SA 2/3 and 100% for 1/1.

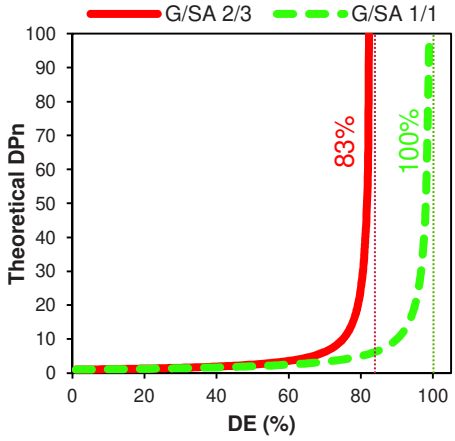

Figure 2.6. Evolution of $\overline{DP_n}$ according to DE and G/SA

^{13}C NMR analyses (400 MHz, Bruker) were also carried out in d-DMSO. ^{13}C NMR could also allow the calculation of the degree of esterification. However, the method employed here does not allow a quantitative spectrum.

2.6. Other characterizations (in particular for the elastomer)

2.6.1. Extraction of soluble parts

The sol fraction was determined after extraction of the soluble part by the Soxhlet method. 1 g of elastomer was placed in a Soxhlet extractor placed atop a flask containing 250 mL of THF. The solvent is heated to reflux at 96°C during 24h. The remaining gel part was dried at 40°C under vacuum during 24h. Sol part was weighted after evaporation of the THF. Sol fraction is given as:

$$sol\ frac\ (\%) = \frac{m_{sol}}{m_{elast}} \times 100$$

2.6.2. Swelling degree

PGS swelling capacity in water was estimated by immersion of 2 g of polymer in 8 mL of distilled water during one week. Swelling degree is defined as:

$$swelling\ degree\ (\%) = \frac{m_{elast}^{swollen}}{m_{elast}^{dry}} \times 100$$

2.6.3. Differential scanning calorimetry

Thermal transitions in the prepolymer and the elastomer were determined by DSC. Samples of approximately 2 mg were introduced in the calorimeter (Q200, TA Instruments), heated and

cooled at 2°C/min under a nitrogen atmosphere between -50°C and 70°C. The melting point (T_m) and crystallization temperature (T_c) were defined as the temperature at the maximum of the peak, respectively endothermic and exothermic. These temperatures, the corresponding enthalpies and the glass transition temperature were calculated with the software TA Universal Analysis.

2.6.4. Mechanical characterization

We have seen that the mechanical properties of the material is one the key parameters for the target application. However, in the present work, it is not PGS films that should be exploited but fibers made of PGS. Actually, mechanical properties evolve very differently depending on whether PGS is cured as a film or blended with another polymer in nanofibers. Thus, they will be deeply characterized in the Chapters 3 and 4. Besides, it is not trivial to fabricate homogenous samples for tensile test. Thus, the current chapter tries only to roughly identify how the curing or the ratio G/SA can affect the elastomer. Mechanical tests were here conducted on an Anton-Paar rheometer at 25 mm/min on rectangular samples.

3. Synthesis and characterization of the prepolymer: results[1]

The objective of this study was to understand how the synthesis conditions affect the properties of PGS. A good comprehension of the effect of the parameters allows preparing prepolymers well adapted for the application. Depending on the utilization, the goal was a more stretchable and hydrophilic pPGS (Chapter 3) or a prepolymer close to the gel point (Chapter 4). In order to find the best conditions to reach these objectives, different types of heating, reaction temperatures and ratios of reactant were tested.

3.1. Advantage and drawback of microwave heating

During synthesis, samples were collected to follow the evolution of the esterification degree calculated from NMR data. The kinetic was then compared for the two heating types with a same reaction temperature (150°C) and ratio of reactants (1/1). The result is shown on Figure 2.7.

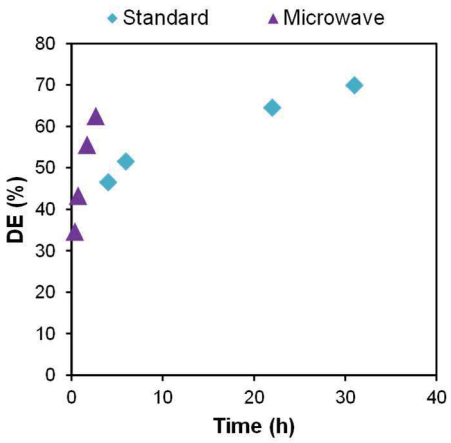

Figure 2.7. Comparison of the evolution of DE with standard and microwave heating at 150°C for G/SA = 1/1.

[1] A few data of this part were obtained by Özgün Uyumaz, master student under my supervision.

Clearly, the reaction is accelerated by the microwave heating. For example, after 240 min of conventional heating, DE is at 47%, whereas it already reaches 43% after only 40 minutes of microwave heating. This result is in accordance with Lau's work where a six-fold acceleration of the reaction was identified [9].

Moreover, microwave synthesis is known to allow a good reproducibility [9]. This feature was verified by repeating three times the reaction in the exact same conditions: same mass of reactants, same ratio G/SA (1/1), same temperature (180°C) and same time (210 min). NMR gave DEs of 85%, 83% and 85%. Considering the accuracy of DE measurement by NMR, we can confirm that the reaction is reproducible.

However, we have seen that microwave irradiation can induce the evaporation of glycerol out of the reactor. It was thus important to quantify the possible glycerol loss (GL). GL can be estimated from the mass remaining in the reactor at the end of the synthesis, taking in account the evaporation of the water. The expression is the following:

$$GL\ (\%) = \frac{m_{tot}^{init} - m_{tot}^{fin} - \frac{DE}{100} \times M_{H2O} \times \frac{2m_{SA}^{init}}{M_{SA}}}{m_{G}^{init}}$$

With m_{tot}^{init} the total mass introduced in the reactor, m_{tot}^{fin} the total mass in the flask at the end of reaction after evaporation of remaining water, m_{SA}^{init} and m_{G}^{init} the mass of sebacic acid and glycerol introduced in the reactor. This calculation gave negative values, certainly because m_{tot}^{fin} was overestimated. Indeed, it is difficult to efficiently remove water from the prepolymer post-synthesis without evaporating more glycerol. Nevertheless, it is possible to estimate the maximal GL if we consider that all the produced water remains in the reactor:

$$GL_{max}\ (\%) = \frac{m_{tot}^{init} - m_{tot}^{fin}}{m_{G}^{init}}$$

In this way, for a synthesis with G/SA 1/1 during 210 minutes, we find a maximal glycerol loss of 12% when the reaction is conducted at 150°C and 27% at 180°C. This stays far below Li's value who found 60% of glycerol loss after 30 min of reaction. In the procedure described here, GL is well limited thanks to the narrow opening of the flask and to the microwave reactor that allows a more homogenous distribution of power than a domestic microwave oven. This homogeneity avoids the apparition of local "hot points" in the reactive medium, where the temperature could reach glycerol evaporation temperature. Another factor can explain the loss of glycerol that was noticed here: glycerol can also leave the reactive medium carried by water steam.

3.2. Influence of the reaction temperature

The influence of the temperature on the kinetic was studied for 1/1 reactants ratio and both heating method. The results are shown on Figure 2.8.

For both heating mode, it is clear that a higher temperature allows an acceleration of the reaction. No synthesis at 130°C was finally conducted to prepare pPGS intended for electrospinning, because the reaction was too slow. However, we have seen that a higher heating temperature also increases glycerol loss. So, for same G/SA and DE, two pPGS prepared at two different temperatures can have slightly different structure.

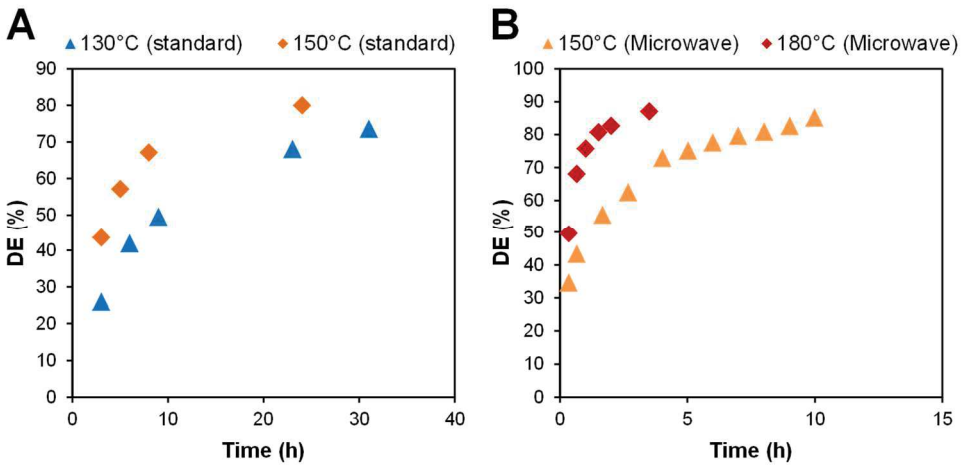

Figure 2.8. Comparison of the kinetic according to the temperature and starting from G/SA = 1/1. **(A)** at 130°C and 150°C with standard heating. **(B)** at 150°C and 180°C for microwave heating.

3.3. Influence of the ratio of reactants

The influence of the ratio of reactants G/SA on the kinetic was studied for reactions conducted at 150°C with both heating modes. Two ratios were tested. The G/SA ratio 2/3 corresponds to a stoichiometric ratio as the same number of –OH and –COOH groups are introduced. With the ratio 1/1, –OH groups are introduced in excess. From Figure 2.9, it can be seen that regardless of the heating mode, DE increases faster in the 1/1 case. Indeed, DE is related to the conversion of carboxylic groups. In the 1/1 case, an excess of –OH group is present, with the same number of carboxylic acids and primary alcohols. So, in theory DE could reach 100% without involving secondary alcohols. In reality, some secondary alcohols react otherwise no 3D network could be formed. But in the 2/3 case, DE can only reach 66% with primary alcohols and then, secondary alcohols have to react. As secondary alcohols are less reactive than primary alcohols, the conversion rate increases more slowly in the 2/3 case. This is particularly the case for the conventional heating. With microwave heating, the difference is attenuated because this mode of heating increases secondary alcohols reactivity, as mentioned above [9].

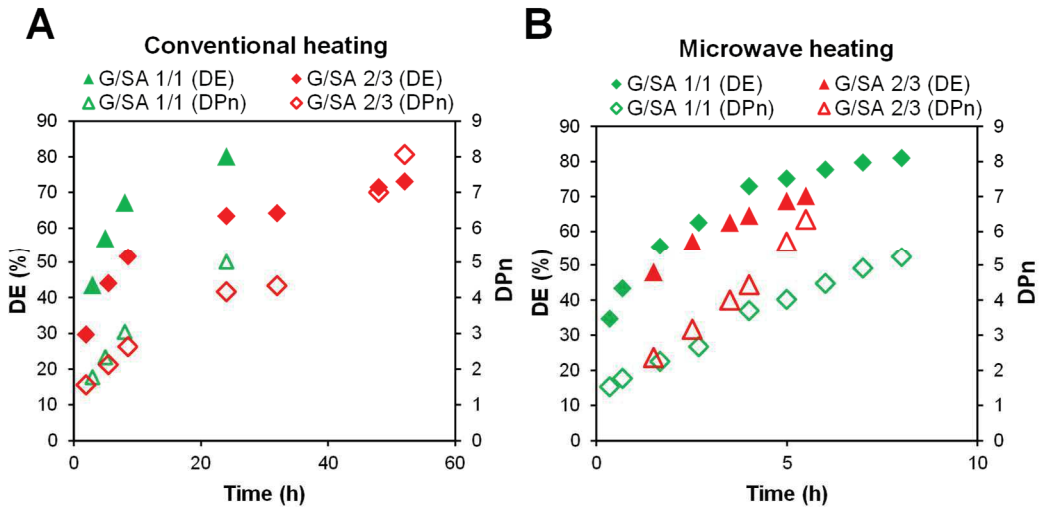

Figure 2.9. Comparison of the kinetic at 150°C according to the ratio G/SA. **(A)** with standard heating. **(B)** with microwave heating.

Nevertheless, as mentioned above (see Figure 2.6), the same DE corresponds to different $\overline{DP_n}$ for a G/SA ratio of 1/1 or 2/3. In particular, $\overline{DP_n}$ increases more rapidly when the stoichiometric ratio (2/3) is used. This is visible for microwave heating on Figure 2.9.(B). In practice, after 300 minutes of microwave heating, the 1/1 ratio has a DE of 75% but a theoretical $\overline{DP_n}$ of only 4, whereas the ratio 2/3 reaches a DE of only 69%, corresponding to a $\overline{DP_n}$ of 7.

The structures of pPGS prepared with different G/SA are thus different. DSC measurements were done on pPGS samples synthesized by microwave irradiations in order to get more information about it. No glass transition was detected. However, several melting points could be identified, corresponding to different crystalline domains. Temperatures and heat of fusion (ΔH_f) are given in Table 2.1. It can be noticed that for a quite similar $\overline{DP_n}$, the melting point and the heat of fusion are lower for the ratio 2/3. This result indicates that pPGS 2/3 has a more branched structure than the 1/1 one: branching units decrease the free space in the elastomer, making crystallization more difficult. This is in agreement with the fact that more secondary –OH of glycerol react in the case of a 2/3 ratio.

Table 2.1. Melting points and heats of fusion for pPGS synthesized by microwave heating with different G/SA.

G/SA	DE	$\overline{DP_n}$	Melting point(s)	ΔH_f
1/1	80%	5	15°C, 25°C, 36°C	69 J/g
2/3	62%	4	6°C (other peaks not clear)	57 J/g

3.4. Characterization of the prepolymer by ^{13}C NMR

Typical ^{13}C NMR spectrum is given in Figure 2.11. Two areas are of interest. The first one, on the left (170-175 ppm), corresponds to **C**=O from carboxylic acids and esters.

The second area of interest is situated between 58 and 75 ppm. The peaks correspond to the carbons labelled A to N of the following substituted glycerol units (Figure 2.10):

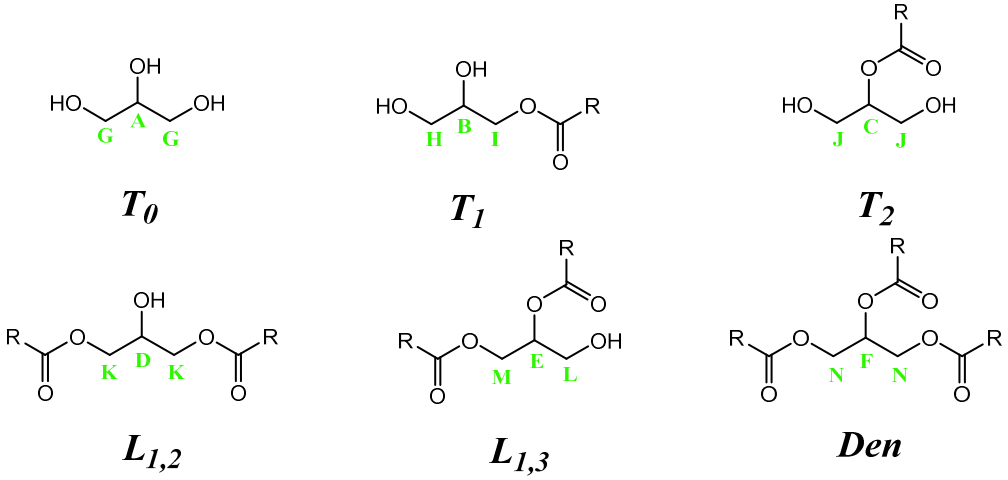

Figure 2.10. Substituted glycerol units and identification of the carbons (*T* is for terminal, *L* for linear and *Den* for dendritic).

The identification of the peaks was done according to Li *et al.* [30] and Moorhoff *et al.*[31]. The integration of these peaks could allow the calculation of the degree of esterification by a new method and the estimation of the degree of substitution of glycerol, what could be interesting to

compare the structure of different pPGS. However, despite coherent values of DE found by this method, the ^{13}C NMR method employed here does not allow a quantitative spectrum.

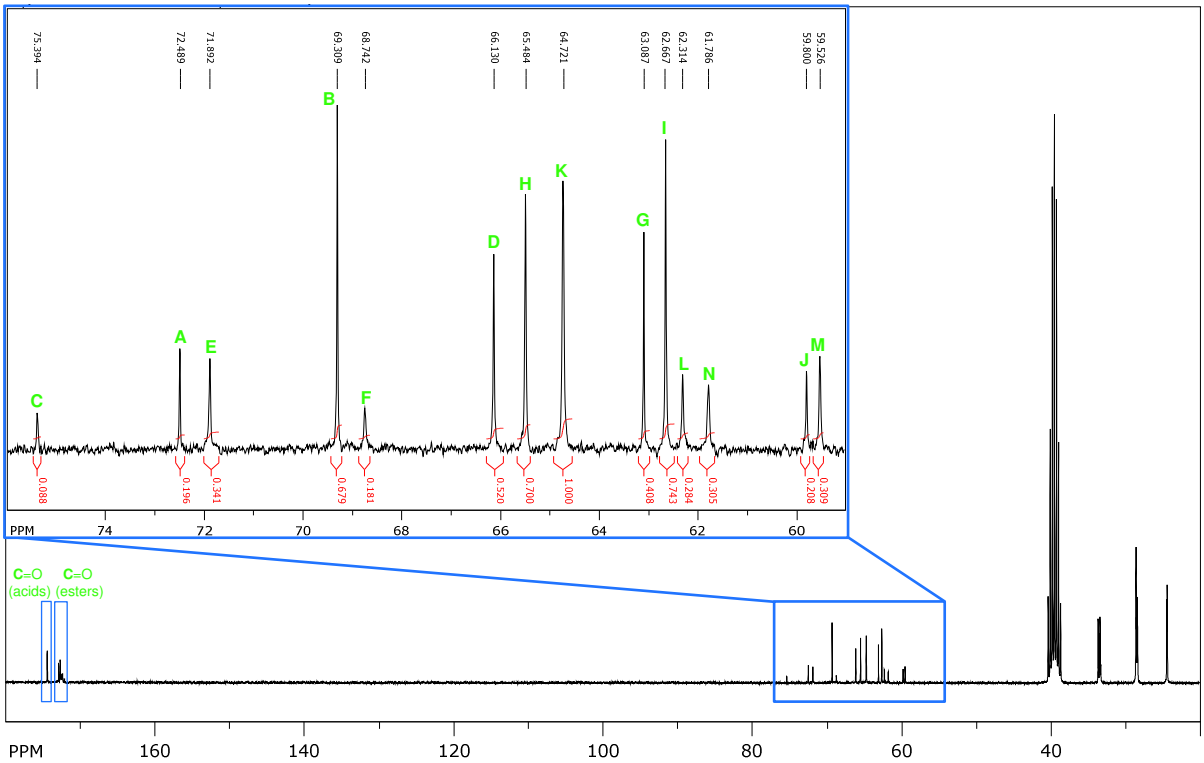

Figure 2.11. ^{13}C NMR spectrum of pPGS made from G/SA 1/1 with DE=76%.

To conclude this part about pPGS synthesis, the parameters to prepare the prepolymers were chosen according to the objectives of the electrospinning experiments. For time saving and reproducibility questions, the final pPGS were all synthesized under microwave irradiations.

Two prepolymers were mainly further used for electrospinning. In Chapter 3, PGS was chosen to decrease the stiffness and the hydrophobicity of PLA-based scaffolds. The prepolymer employed was thus synthesized from a G/SA ratio equal to 1/1 to decrease its degree of branchment and increase the number of free –OH. Its DE was 85%. In Chapter 4, it was crucial to use a pPGS close to its gel point in order to crosslinking the fibers quickly, before their melting. The pPGS used was thus synthesized with a ratio 2/3 and had a DE of 72%.

While this first part allowed to understand how all these parameters affect the prepolymer, the next section presents their effect on the properties of the elastomer.

4. Synthesis and characterization of the elastomer: results

Some of the prepolymers synthesized above were cured under reduced pressure to prepare elastomer-based films that were characterized.

4.1. Comment about the method for DE determination

The degree of esterification of prepolymers was determined by ^{1}H NMR analysis as it is a convenient method. However, because of the insolubility of the elastomers, the DE of crosslinked PGS was measured by titration. Both methods are compared for prepolymers on Figure 2.12. It can be noticed that the DE is underestimated by the titration method. The

difference decreases when DE increases. The underestimation can be explained by a side reaction between KOH and CO_2 forming potassium carbonate.

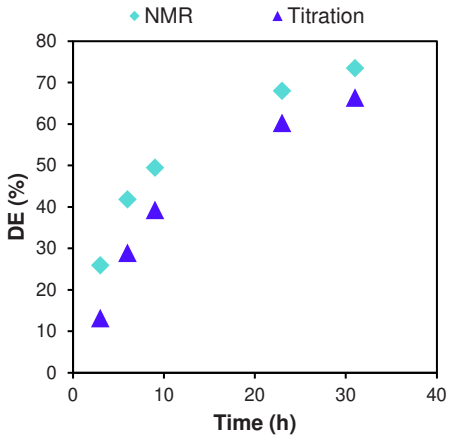

Figure 2.12. Comparison of DE determination method for a reaction at 130°C under conventional heating with G/SA 1/1.

The esterification degree measured for crosslinked PGS by titration and for pPGS by NMR should thus not be compared without precautions.

4.2. Results after crosslinking

4.2.1. Sol fraction

The fraction in soluble parts was determined for two different solid crosslinked PGS. They were prepared by curing of pPGS films at 150°C under vacuum during 50h. The films were prepared by solvent casting using THF. The pPGS used differ by the G/SA ratio; they were both synthesized by microwave irradiations at 180°C. Their DE are different according to titration, but they have the same theoretical $\overline{DP_n}$ (see Table 2.2.). It can be noticed that titration gives DE values indicating that the material is below the theoretical gel point (83% for 2/3 ratio, 100% for 1/1), which confirms that titration method underestimate the DE value. This early gel point could also be explained by evaporation of a part of the glycerol. Nevertheless, the $\overline{DP_n}$ values remain low, indicating an heterogeneous crosslinking leading to a high oligomers content.

This is confirmed by the quite high sol fraction values. However, there are less soluble parts in the 2/3 PGS, indicating that it has a higher degree of crosslinking. This result is in agreement with the result found after prepolymerization: pPGS 2/3 are more branched.

4.2.2. Swelling degree

The same crosslinked PGS were used to measure the swelling capacity in water. The values are given in Table 2.2. Here, a lower degree of swelling is registered for PGS 2/3, confirming again a higher degree of crosslinking.

Table 2.2. Sol fraction and swelling degree for two crosslinked PGS.

G/SA	DE	$\overline{DP_n}$	Sol fraction (%)	Swelling degree
1/1	91%	11	64%	1.8
2/3	76%	11	42%	1.1

4.2.3. DSC analysis

The thermal behavior of the elastomer was characterized by DSC. Typical thermogram is given in Figure 2.13 (sol+gel). A glass transition close to -20°C and two melting points can be seen during heating phase, and one crystallization peaks during cooling. Sebacic acid units are responsible for crystalline domains. However, at the temperature of use (37°C), PGS is amorphous.

On Figure 2.13, the thermograms of a PGS before (sol+gel) and after (gel) Soxhlet extraction are compared. It can be seen that the second melting peak disappeared after extraction, because short molecules were removed. Only one melting peak remains, in addition to a slightly visible T_g.

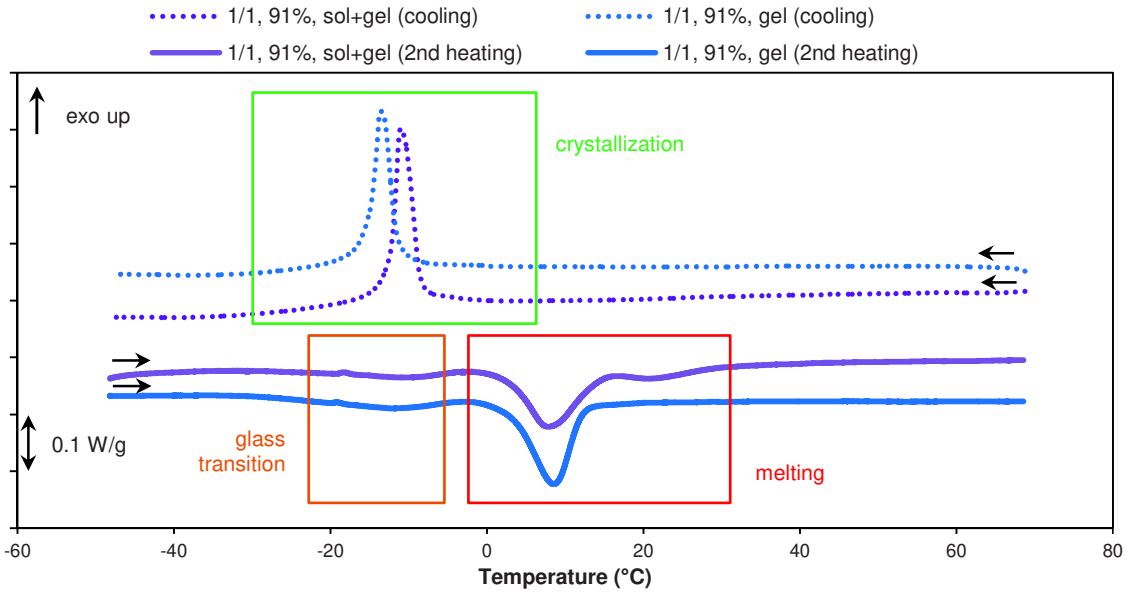

Figure 2.13. Typical DSC cooling and heating curves obtained for washed PGS (gel) and unwashed one (sol+gel).

Table 2.3 gives T_g, T_m and T_c values for purified gel parts of the PGS characterized above (synthesized from different G/SA but with the same $\overline{DP_n}$). T_m and T_c are lower for the ratio 2/3, indicating again that the stoichiometric proportions allow a higher degree of crosslinking.

Table 2.3. Thermal properties of different extracted crosslinked PGS (gel part); influence of G/SA

G/SA	DE	Theoretical $\overline{DP_n}$	T_g	T_m	T_c
1/1	91%	11	-17°C	9°C	-11°C
2/3	76%	11	-17°C	0°C	-17°C

Table 2.4 refers to two PGS synthesized from a 2/3 ratio. The same prepolymer was cured during different times, leading to different degrees of esterification. It can be seen that the longer the curing step is, the lower crystallization temperature is. This result confirms results found by Jeffries [32] and Jaafar [33] who explain that when the elastomer is more branched or more crosslinked, polymer chains have less mobility to crystallize.

Table 2.4. Thermal properties of different raw crosslinked PGS; influence of the curing time

G/SA	Curing time	DE	Theoretical $\overline{DP_n}$	T_g	T_m	T_c
2/3	26h	81%	36	-27°C	-7 and 14°C	-21 and 2°C
2/3	50h	89%	> theoretical gel point	-26°C	-5 and 13°C	-23 and 5°C

4.2.4. Mechanical properties

Samples for tensile tests were prepared by curing pPGS in PTFE molds with the desired geometry (1x8x55 mm). PTFE was used to ensure a good unmolding without defect. However, the surface tension between the PTFE and the hot liquid pPGS is high; it is thus difficult to obtain a flat surface and samples with constant cross section. Results given here are thus only estimations, but they can give an overview of how synthesis and curing parameters can affect the elastomer properties.

Globally, Young's moduli were found between 0.3 and 1.5 MPa, and strains at break are higher than 35% and can exceed 100%. The softer materials prepared here are thus adapted for cardiac applications. Tensile tests were done on samples after different curing time of a same pPGS (Figure 2.14.(A)) and for PGS synthesized with different G/SA (Figure 2.14.(B)). For the latter, pPGS from different G/SA but with a same theoretical $\overline{DP_n}$ (approximately 7) were cured at the same temperature (150°C) during the same time (48h). Typical curves are shown on Figure 2.14. The modulus and ultimate strength are higher and the strain at break is lower for more cured samples and samples prepared from 2/3 ratio, indicating again that these samples are more crosslinked.

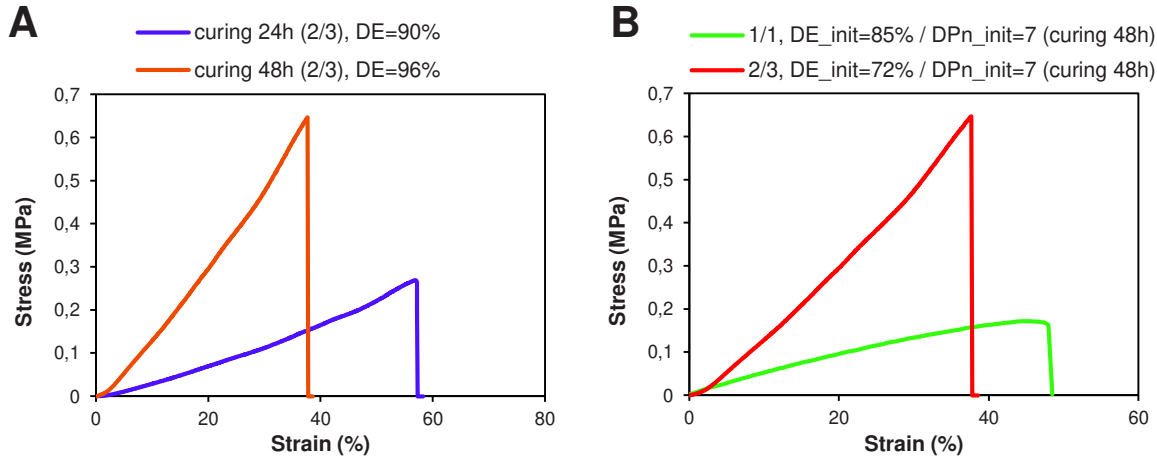

Figure 2.14. Typical curves for tensile tests. **(A)** Comparison according the curing time. **(B)** Comparison according to G/SA.

Additional tensile tests could be desirable in order to determine modulus and ultimate strain values for various synthesis parameters. Moreover, cyclic tests could help to determine how elastic PGS elastomers are.

5. Conclusion

To conclude this chapter, PGS properties, in particular mechanical properties, can be easily tuned by changing the reaction temperature, the prepolymerization or curing time and the ratio of reactants G/SA. To summarize, increasing time or temperature increases the conversion rate in esters, and thus increases the crosslinking rate and the stiffness of the material. Moreover, starting the reaction with the stoichiometric ratio (G/SA equal to 2/3) leads to more branched polymers and to stiffer materials too. All these results allow us to choose the right conditions to prepare a suitable pPGS for a given application. In particular, a 1/1 ratio with a low DE would give a soft elastomer with a lot of –OH available interesting to improve a stiff and hydrophobic polymer, while a 2/3 ratio with a high DE would be easier to crosslink and gives a better thermomechanical behavior during curing.

References:

1. Wang, Y.; Ameer, G.A.; Sheppard, B.J.; Langer, R. A tough biodegradable elastomer. *Nat Biotech* **2002**, *20*, 602–606.
2. Li, X.; Hong, A.T.-L.; Naskar, N.; Chung, H.-J. Criteria for Quick and Consistent Synthesis of Poly(glycerol sebacate) for Tailored Mechanical Properties. *Biomacromolecules* **2015**, *16*, 1525–1533.
3. Chen, Q.-Z.; Bismarck, A.; Hansen, U.; Junaid, S.; Tran, M.Q.; Harding, S.E.; Ali, N.N.; Boccaccini, A.R. Characterisation of a soft elastomer poly(glycerol sebacate) designed to match the mechanical properties of myocardial tissue. *Biomaterials* **2008**, *29*, 47–57.
4. Kafouris, D.; Kossivas, F.; Constantinides, C.; Nguyen, N.Q.; Wesdemiotis, C.; Patrickios, C.S. Biosourced Amphiphilic Degradable Elastomers of Poly(glycerol sebacate): Synthesis and Network and Oligomer Characterization. *Macromolecules* **2013**, *46*, 622–630.
5. Godinho, B.; Gama, N.; Barros-Timmons, A.; Ferreira, A. Enzymatic synthesis of poly(glycerol sebacate) pre-polymer with crude glycerol, by-product from biodiesel prodution. *AIP Conference Proceedings* **2018**, *1981*, 020031.
6. Aydin, H.M.; Salimi, K.; Rzayev, Z.M.O.; Pişkin, E. Microwave-assisted rapid synthesis of poly(glycerol-sebacate) elastomers. *Biomaterials Science* **2013**, *1*, 503.
7. Barlow, S.; Marder, S.R. Single-Mode Microwave Synthesis in Organic Materials Chemistry. *Advanced Functional Materials* **2003**, *13*, 517–518.
8. Coativy, G.; Misra, M.; Mohanty, A.K. Microwave Synthesis and Melt Blending of Glycerol Based Toughening Agent with Poly(lactic acid). *ACS Sustainable Chem. Eng.* **2016**, *4*, 2142–2149.
9. Lau, C.C.; Bayazit, M.; Knowles, J.; Tang, J. Tailoring Degree of Esterification and Branching of Poly(glycerol sebacate) by Energy Efficient Microwave Irradiation. *Polym. Chem.* **2017**.
10. Nijst, C.L.E.; Bruggeman, J.P.; Karp, J.M.; Ferreira, L.; Zumbuehl, A.; Bettinger, C.J.; Langer, R. Synthesis and Characterization of Photocurable Elastomers from Poly(glycerol-co-sebacate). *Biomacromolecules* **2007**, *8*, 3067–3073.
11. Yeh, Y.-C.; Highley, C.B.; Ouyang, L.; Burdick, J.A. 3D printing of photocurable poly(glycerol sebacate) elastomers. *Biofabrication* **2016**, *8*, 045004.
12. Hu, J.; Kai, D.; Ye, H.; Tian, L.; Ding, X.; Ramakrishna, S.; Loh, X.J. Electrospinning of poly(glycerol sebacate)-based nanofibers for nerve tissue engineering. *Materials Science and Engineering: C* **2017**, *70, Part 2*, 1089–1094.
13. Sun, Z.-J.; Wu, L.; Huang, W.; Zhang, X.-L.; Lu, X.-L.; Zheng, Y.-F.; Yang, B.-F.; Dong, D.-L. The influence of lactic on the properties of Poly (glycerol–sebacate–lactic acid). *Materials Science and Engineering: C* **2009**, *29*, 178–182.
14. Chen, Q.; Liang, S.; Thouas, G.A. Synthesis and characterisation of poly(glycerol sebacate)-co-lactic acid as surgical sealants. *Soft Matter* **2011**, *7*, 6484–6492.
15. Sun, Z.-J.; Wu, L.; Huang, W.; Chen, C.; Chen, Y.; Lu, X.-L.; Zhang, X.-L.; Yang, B.-F.; Dong, D.-L. Glycolic acid modulates the mechanical property and degradation of poly(glycerol, sebacate, glycolic acid). *J. Biomed. Mater. Res.* **2010**, *92A*, 332–339.
16. Liu, Q.-Y.; Wu, S.-Z.; Tan, T.-W.; Weng, J.-Y.; Zhang, L.-Q.; Liu, L.; Tian, W.; Chen, D.-F. Preparation and Properties of a Novel Biodegradable Polyester Elastomer with Functional Groups. *Journal of Biomaterials Science, Polymer Edition* **2009**, *20*, 1567–1578.
17. Cheng, H.; Hill, P.S.; Siegwart, D.J.; Vacanti, N.; Lytton-Jean, A.K.R.; Cho, S.-W.; Ye, A.; Langer, R.; Anderson, D.G. A Novel Family of Biodegradable Poly(ester amide) Elastomers. *Adv. Mater.* **2011**, *23*, H95–H100.
18. Yoon, S.; Chen, B. Elastomeric and pH-responsive hydrogels based on direct crosslinking of the poly(glycerol sebacate) pre-polymer and gelatin. *Polymer Chemistry* **2018**, *9*, 3727–3740.
19. Liu, L.; Cai, W. Novel copolyester for a shape-memory biodegradable material in vivo. *Materials Letters* **2009**, *63*, 1656–1658.
20. Patel, A.; Gaharwar, A.K.; Iviglia, G.; Zhang, H.; Mukundan, S.; Mihaila, S.M.; Demarchi, D.; Khademhosseini, A. Highly elastomeric poly(glycerol sebacate)-co-poly(ethylene glycol) amphiphilic block copolymers. *Biomaterials* **2013**, *34*, 3970–3983.
21. Wang, Y.; Wu, H.; Wang, Z.; Zhang, J.; Zhu, J.; Ma, Y.; Yang, Z.; Yuan, Y. Optimized Synthesis of Biodegradable Elastomer PEGylated Poly(glycerol sebacate) and Their Biomedical Application. *Polymers* **2019**, *11*, 965.

22. Wu, Y.; Wang, L.; Guo, B.; Ma, P.X. Injectable biodegradable hydrogels and microgels based on methacrylated poly(ethylene glycol)-co-poly(glycerol sebacate) multi-block copolymers: synthesis, characterization, and cell encapsulation. *J. Mater. Chem. B* **2014**, *2*, 3674–3685.
23. Choi, S.M.; Lee, Y.; Son, J.Y.; Bae, J.W.; Park, K.M.; Park, K.D. Synthesis and characterization of in situ gellable poly(glycerol sebacate)-co-poly(ethylene glycol) polymers. *Macromol. Res.* **2017**, 1–7.
24. Wang, Z.; Ma, Y.; Wang, Y.; Liu, Y.; Chen, K.; Wu, Z.; Yu, S.; Yuan, Y.; Liu, C. Urethane-based low-temperature curing, highly-customized and multifunctional poly(glycerol sebacate)-co-poly(ethylene glycol) copolymers. *Acta Biomaterialia* **2018**.
25. Yu, S.; Shi, J.; Liu, Y.; Si, J.; Yuan, Y.; Liu, C. A mechanically robust and flexible PEGylated poly(glycerol sebacate)/β-TCP nanoparticle composite membrane for guided bone regeneration. *J. Mater. Chem. B* **2019**.
26. Dong, R.; Zhao, X.; Guo, B.; Ma, P.X. Biocompatible Elastic Conductive Films Significantly Enhanced Myogenic Differentiation of Myoblast for Skeletal Muscle Regeneration. *Biomacromolecules* **2017**.
27. Jia, Y.; Wang, W.; Zhou, X.; Nie, W.; Chen, L.; He, C. Synthesis and characterization of poly(glycerol sebacate)-based elastomeric copolyesters for tissue engineering applications. *Polym. Chem.* **2016**, *7*, 2553–2564.
28. Odian, G. Step Polymerization. In *Principles of Polymerization*; John Wiley & Sons, Ltd, 2004; pp. 39–197 ISBN 978-0-471-47875-1.
29. Kuchanov, S.I.; Pis'men, L.M. Calculation of the polycondensation kinetics of monomers containing reaction centres of variable activity. *Polymer Science U.S.S.R.* **1972**, *14*, 985–993.
30. Li, Y.; Cook, W.D.; Moorhoff, C.; Huang, W.-C.; Chen, Q.-Z. Synthesis, characterization and properties of biocompatible poly(glycerol sebacate) pre-polymer and gel. *Polym. Int.* **2012**, *62*, 534–547.
31. Moorhoff, C.; Li, Y.; Cook, W.D.; Braybrook, C.; Chen, Q.-Z. Characterization of the prepolymer and gel of biocompatible poly(xylitol sebacate) in comparison with poly(glycerol sebacate) using a combination of mass spectrometry and nuclear magnetic resonance. *Polymer International* **2015**, *64*, 668–688.
32. Jeffries, E.M.; Allen, R.A.; Gao, J.; Pesce, M.; Wang, Y. Highly elastic and suturable electrospun poly(glycerol sebacate) fibrous scaffolds. *Acta Biomaterialia* **2015**, *18*, 30–39.
33. Jaafar, I.H.; Ammar, M.M.; Jedlicka, S.S.; Pearson, R.A.; Coulter, J.P. Spectroscopic evaluation, thermal, and thermomechanical characterization of poly(glycerol-sebacate) with variations in curing temperatures and durations. *J. Mater. Sci.* **2010**, *45*, 2525–2529.

CHAPTER 3

Elaboration of composite PLA/PGS fibers

The prepolymers that were synthesized in the previous chapter cannot be directly used for electrospinning. They should first be mixed with a carrier polymer. In the present chapter, polylactic acid (PLA) was chosen to play this role. This polymer is commonly used for tissue engineering but it suffers from a lack of hydrophilicity and stretchability. Its blend with a soft and hydrophilic PGS to form composite fibers can thus be advantageous.

In this chapter, PLA/PGS fibers with various diameters and PGS contents will be electrospun and cured at different temperature. The influence of the diameters and the curing temperature on physico-chemical properties will be investigated. Then, *in vitro* and *in vivo* characterizations will be carried out to identify the best candidate for cardiac tissue engineering. Finally, arguments will be given in order to explain the biological results by the properties of the scaffolds.

Elaboration of composite PLA/PGS fibers

1. Context and objectives

It was concluded from Chapter 1 that to get nanofibers composed of crosslinked PGS, it is essential to use a carrier polymer able to provide entanglements necessary for electrospinning and to keep the fibrous structure during thermal crosslinking of the elastomer. To this end, the carrier polymer should have a sufficient molar mass and should not lose its mechanical strength when heated. Examples from literature introduced in Chapter 1 show that the use of biocompatible polyesters is promising. Here, we choose a common biocompatible polyester that resists to temperature: polylactic acid.

PLA is a polymer synthesized from lactic acid extracted from biomass. Because the monomer is chiral, several isomers of the polymer can be found: poly-L-lactic acid (PLLA), poly-D-lactic acid (PDLA) and poly- L,D-lactic acid (PDLLA) when both isomers are included. PLA is semi-crystalline when it contains enough of one of the isomers (for example with more than 90% of L-lactic acid). The heat of fusion of a 100% crystalline PLA is generally estimated at 93 J/g [1]. It is biocompatible and approved by the FDA and by European authority for biomedical applications. It degrades slowly by hydrolysis to form oligomers that can be naturally metabolized by the body. With a glass transition temperature between 40°C and 80°C and a melting point between 120°C and 180°C depending on the isomers proportions, PLA is an easy-to-process thermoplastic. Its properties make him a candidate of choice for the fabrication of medical devices [2]. However, PLA is hydrophobic, biologically inert and difficult to functionalize. Moreover, with a Young's modulus higher than 1 GPa, it is too stiff for myocardial application. Thus, functionalizing PLA by blending it with a material – here PGS – that is more suitable for the targeted application could be beneficial [3].

In the strategy presented in this part, pPGS is mixed with PLA in the same solution. The electrospinning of this solution allows fabricating composite fibers with pPGS and PLA that can then be cured. After crosslinking, fibers containing PLA blended with crosslinked PGS are finally obtained. Because PLA is not soluble in benign solvents like water or ethanol, it is kept inside the fibers to avoid any additional toxicity brought during the removing of the carrier polymer. The presence of PLA causes of course no troubles regarding the biocompatibility of the material.

Papers reporting the coelectrospinning of pPGS and PLA were already described in Chapter 1. Here, focus is done on studies where cells were seeded on membranes containing both PGS and PLA. The only example of blend electrospinning of pPGS and PLA followed by a crosslinking step is reported by Yan *et al.* [4,5]. They used pPGS with G/SA 1/1 synthesized by

conventional heating at 120°C during 24h. pPGS and PLA were mixed together in DMF and DCM for electrospinning. After electrospinning, membranes with 0%, 25%, 40% or 50% of pPGS were put in the vacuum oven at 120°C during 48h. With 40% and 50% of PGS, fibers are then surrounded by melted parts. The authors interpret one SEM picture of a 25% PGS fiber to claim that PGS and PLA phases segregated to form a PGS shell and a PLA core. They justify this statement by IR, DSC and water-in-air contact angles analyses. They found indeed no emergence or disappearance of peaks on the IR spectra and no shift of PLA's T_g and conclude that both PGS and PLA phases are totally separated. However, these phases can be distinct but blended. Nevertheless, the authors noticed a high increase of the hydrophilicity of the mat: a water droplet forms an angle of 125° on a PLA mat, whereas it is totally absorbed by the PGS/PLA membrane. Moreover, the addition of 25% of PGS decreases the Young's modulus from 35.9±7.1 MPa to 7.2±1.4 MPa while the strain at break increases from 29±6% to 66±8% for a maximal stress of 1.1±0.2 MPa. Lastly, neurons cells were seeded on these membranes. The proliferation is the same on PLA and on PLA/PGS scaffolds, showing the biocompatibility of the latter ones. Cells adhesion is also good and intercellular contacts are established. Cells differentiation seems improved by PLA/PGS formulation.

Other studies about the use of PLA/PGS fibers in tissue engineering were published by Qizhi Chen and Bing Xu's team [6–8], but with core/shell fibers. In these three articles, pPGS is synthesized from G/SA 1/1 with conventional heating at 130°C during 24h and solubilized in THF to form the core solution. The shell solution is composed of PLA solubilized in DMF/chloroform. Fibers were then cured at 130°C during 24h. The authors point out that PLA and PGS can react together during this step. Mechanical characterization shows that with a higher proportion of PGS core, the modulus decreases while the strain at break increases. The mats with the highest content of PGS reach a strain at break of 25±3% and an UTS of 1±0.2 MPa. They show a non-linear elasticity behavior. Cytotoxicity tests with fibroblasts confirmed the good biocompatibility of PLA/PGS membranes. Furthermore, the ability of these materials to deliver cells for intestinal regeneration [6] or to support the activity of cardiomyocytes beating clusters was proved [7]. Finally, the same process was used to prepare PGS/PLA core/shell aligned fibers by high speed rotation of the collector but without biological characterization [8].

In this part, we focus on blended PLA/PGS scaffolds for cardiac tissue regeneration. For this purpose, PLA was mixed with pPGS and electrospun using various parameters in order to fabricate PLA/pPGS continuous fibers with 30% of pPGS. Two categories of fibers were produced, with diameters of 500 and 1500 nm. The resulting fibers were cured at 90°C or 120°C in order to achieve two different crosslinking densities. Here, it is expected that the presence of PGS not only allows elastomeric properties at the surface of the fibers, but its hydrophilic surface and the presence of –OH groups can favor the surface functionalization. To increase the cellular attachment, the surface of the fibers was also functionalized by Matrigel. The effect of fiber diameter, crosslinking condition and surface functionalization on the physico-chemical and mechanical behavior of the scaffolds was investigated. The influence of PGS proportion was also tested but it was concluded that this parameter was here not relevant, and is not part of the main study (see part 3.6). Then, rat neonatal cardiomyocytes cultured on PLA/PGS scaffolds were studied as a function of the different scaffold's characteristics. Furthermore, the *in vivo* biocompatibility of the PLA/PGS scaffolds was studied in a cardiac environment, after implantation of acellular mats on the surface of the heart of healthy Swiss mice. Vascularization and low inflammation provide arguments for a potential cardiac application.

2. Materials and methods[1]

2.1. Materials

Glycerol (>99.96%, Fisher Chemicals), sebacic acid (98%, ACROS Organics), d-DMSO (99.8%D, Euriso-top), poly(D-lactic acid) (PLA, Ingeo 7000D, 180000 g/mol, 95% L-lactic acid / 5% D-lactic acid, NatureWorks), dimethylformamide (DMF, >99.8%, Sigma-Aldrich) and dichloromethane (DCM, >99.8%, Carlo Erba) were used as received.

2.2. Synthesis and characterization of the prepolymer (pPGS)

The synthesis was done under microwave irradiation following the procedure presented in Chapter 2. 6.259 g of glycerol and 13.741 g of sebacic acid were introduced in a round-bottomed flask to reach a 1:1 molar ratio. A stirrer bar was added and the flask was surmounted by a glass extender tube and an opened glass stopcock. The flask was put inside the microwave oven (Discover SP, CEM) and heated from room temperature to 180°C at a maximal power of 200 W under a low stirring. The temperature was hold during 220 minutes. After this time, a transparent pale yellow slightly viscous liquid was obtained. Its viscosity and turbidity increased upon cooling and time. Sample was taken for ^{1}H NMR analysis in d-DMSO. To ensure a reliable reproducibility, the degree of esterification (DE) of pPGS was calculated.

2.3. Preparation of PLA and PLA/PGS fibrous mats

Solvent and concentrations were chosen after an optimization process and trials with various formulations. The selected parameters gave the more stable electrospinning process thanks to appropriate viscosity and solvent evaporation rates. PLA pellets were dissolved in DCM while pPGS was dissolved in DMF. Both solutions were stirred with a magnetic stirrer overnight and mixed together at least one hour before electrospinning. They were prepared and blended together in order to reach the desired PLA/pPGS and solvent ratios. To investigate the influence of the fibers diameter, solutions with 7 wt% of PLA and 3 wt% of pPGS in different solvent were prepared. DCM:DMF 6:4 (wt:wt) was used to make thin fibers and DCM:DMF 7:3 (wt:wt) for thick fibers. To investigate the influence of the presence or absence of PGS, solutions with 10 wt% of PLA in DCM:DMF 6:4 (wt:wt) were also prepared.

Electrospinning was performed using a home-made vertical set-up with two metallic 18-gauge needles and a cylindrical collector 16 cm away from the tip of the needles. Homogeneity of the mat was improved by rotation of the collector at 125 rpm and translation of the needles. The needles and the collector were connected to high-voltage power supplies (SL10, Spellman). For each membrane, the corresponding solution was introduced in two different 10 mL plastic syringes. The solutions were injected to the tip of the needles at a constant rate by a syringe pump (Fisher Scientific) through silicone pipes. The fibers were collected on an aluminum foil at 22°C with a dew point between 7 and 8°C. The experiments were performed during the time necessary to inject overall 5 mL of solution in accordance with the flow rate.

PLA/PGS_{thin} sample was prepared from 7 wt% of PLA and 3 wt% of pPGS in DCM:DMF 6:4 solution injected at 2.5 mL/h at each needle with 18 kV applied at the needles and -2 kV at the collector. PLA/PGS_{thick} was prepared from 7 wt% of PLA and 3 wt% of pPGS

[1] All biological experiments, data analysis and corresponding interpretations were carried out by Pr. Onnik Agbulut's team "Cellules souches et biotherapies" at the Institut de Biologie Paris-Seine with my collaboration.

in DCM:DMF 7:3 solution injected at 4 mL/h at each needle with 18 kV applied at the needles and -2 kV at the collector. PLA_{thin} was prepared from 10 wt% of PLA in DCM:DMF 6:4 solution injected at 2.8 mL/h at each needle with 16 kV applied at the needles and -5 kV at the collector.

The mats were peeled off from the aluminum, cut in the desired shape and fixed between two Teflon frames tight together by screws in order to limit membrane shrinkage during curing. They were put in the vacuum oven (Vacutherm VT6025, Fisher Scientific) at room temperature with a pressure bellow 10^{-2} mbar during 30 minutes to let all the volatile compounds to evaporate. They were then heated at the desired temperature (90°C or 120°C) for 48h to achieve the crosslinking process of the pPGS into the elastomeric PGS. The crosslinked membranes were then kept in a desiccator before use.

2.4. Physico-chemical and mechanical characterization of PLA and PLA/PGS mats

The surface of the membranes was characterized by scanning electron microscopy (SEM) before and after the curing process. Prior to observation, the surfaces were coated by a thin layer of gold with a sputter coater (Q150RS, Quorum). The SEM (Vega 3, Tescan) was used in high vacuum mode with a voltage of 5 kV. The mean diameter of the fibers was calculated over 100 diameters measurements on each surface using ImageJ software (National Institutes of Health [NIH], Bethesda, MD, USA). Images after sterilization and after Matrigel coating were also taken to characterize potential surface modifications.

Differential scanning calorimetry (DSC) analyses were made to characterize the influence of formulation, curing or sterilization on the crystallinity of PLA in the fibers. Samples of approximately 2 mg were introduced in the calorimeter (Q200, TA Instruments), heated at 3°C/min under a nitrogen atmosphere between -20°C and 180°C. The melting point (T_m) and crystallization temperature (T_c) were defined as the temperature at the maximum of the peak, respectively endothermic and exothermic. These temperatures, the corresponding enthalpies and the glass transition temperature were calculated with the software TA Universal Analysis.

Uniaxial tensile tests were performed on hydrated membranes to study the influence of formulation and curing on the mechanical properties. The samples were cut in a rectangular shape of 5 mm width and about 20 mm long. They were immersed in deionized water 24h before measurement. Their thickness was then measured using a rheometer (Discovery HR-3, TA Instruments) with a compression procedure between Peltier plates at 0.5 μm/s: the thickness was evaluated as the gap between the plates when the variation of the axial force was higher than 0.05 N/μm. The same rheometer was used for tensile tests with the Linear Tension Geometry. The specimens were fixed in the clamps with an initial gap of 10 mm and rehydrated before the beginning of the test. The tests were conducted at 100 μm/s until breaking. Five measurements were performed for each type of samples. Young's modulus (E) was calculated as the slope of the stress-strain curve in the initial linear region, and the Ultimate Tensile Strength (UTS) and the strain at break (ε_{break}) were read on the curves.

The hydrophilicity of the membranes was characterized by the sessile drop method. The apparent water contact angle (aCA) was measured using a goniometer (DSA25, Krüss). The volume of the deposited droplet was 4μL, and the mean angle was calculated from 10 droplet depositions for the most hydrophobic samples which did not absorb the water droplet. These values are given with the standard error of the mean. For more hydrophilic samples which absorbed water, the evolution of the apparent contact angle was recorded upon time.

2.5. Isolation of neonatal cardiomyocytes and cell culture

Newborn rat cardiomyocytes were obtained from 1-day-old Wistar RjHan rat (Janvier Labs, Le Genest-Saint-Isle, France). Once the ventricles were isolated, the cardiomyocytes were isolated using a neonatal heart dissociation kit (Miltenyi Biotec, Paris, France) according to the manufacturer's instructions. Before the seeding, all PLA and PLA/PGS mats were sterilized by autoclave. Subsequently, to increase the cellular attachment, mats were functionalized through pre-incubation with a Matrigel solution (Corning Life Sciences, Amsterdam, The Netherlands) diluted in DMEM/F12 (Thermo Fisher Scientific, Saint-Herblain, France) medium for 2h at room temperature, and washed twice with phosphate-buffered saline (PBS) and then with culture medium. $8x10^5$ cells were seeded on the PLA and PLA/PGS mats maintained with a CellCrown™ (Scaffdex, Tampere, Finland) in a 48-well plate, and cultured with DMEM medium (with 4.5g/L D-Glucose and without Na Pyruvate) supplemented with L-glutamine, penicillin-streptomycin, 10% horse serum and 5% fetal bovine serum (FBS) at 37°C and 5% CO_2 for 3 or 6 days.

2.6. Cell morphology analysis: immunostaining and SEM

Immunostaining was used to assess cell morphology of cardiomyocytes on PLA and PLA/PGS mats. Briefly, samples were fixed in 4% paraformaldehyde (PFA) for 10 min at room temperature (RT). Cells were permeabilized with 0.2% Tween (Sigma-Aldrich, France) and treated with 5% bovine serum albumin (BSA) blocking solution for 1 hour at RT. Mouse anti-α Actinin (clone EA-53, 1:200, Sigma-Aldrich, France) and Alexa Fluor-488 goat-anti-mouse (1:1000, Thermo-Fisher Scientific, France) secondary antibodies were incubated for 1h30 and 45 min at RT, respectively. Slides were mounted with mowiol containing 5 μg/ml Hoescht 33342 (Thermo Fisher Scientific, Saint-Herblain, France). Images were captured using a motorized confocal laser scanning microscope (Leica TCS SP5). All the measurements were performed blinded for experimental conditions using ImageJ software.

For the SEM observation, cells were fixed in 2% glutaraldehyde in phosphate buffer (0.1 M) for 30 min at RT and washed again in the phosphate buffer. Then a post-fixation step took place using 1% osmium in sodium cacodylate (0.1 M) for 15 min at RT. After, cell dehydration was performed in a series of increasing ethanol concentrations (50, 70, 95 and 100%) for 10 min each. Finally, the samples were dried using critical point dryer for 2.5 hours. The samples were sputtered with a thin platinum layer prior to SEM observation using the (ACE600, Leica), and then analyzed using the Gemini SEM 500, from Zeiss. The images were performed by applying beam voltage of 1 kV and using the SE2 detector.

2.7. Cardiac surgery

Fifty-four Swiss mice were used for the *in vivo* assessment. All procedures were performed in accordance with national and European legislations, in conformity with the Public Health Service Policy on Human Care and Use of Laboratory Animals under the license A751320. All animal studies were approved by our institutional Ethics Committee "Charles Darwin" (Permit number: 4370) and conducted according to the French and European laws, directives, and regulations on animal care (European Commission Directive 86/609/EEC). All animals underwent a left lateral thoracotomy after intraperitoneal ketamine (100 mg/kg; Merial, France)-xylazin (10 mg/kg; Bayer, France) anesthesia and tracheal ventilation. Analgesia was performed for 2 days after

surgery with a 2 mg/kg intraperitoneal injection of profenid® (Merial). Acellular PLA and PLA/PGS mats were sutured (approximative surface 100 mm^2) on the surface of the ventricle of the mice. The animals were sacrificed 7 and 28 days after implantation to assess the biocompatibility of PLA and PLA/PGS mats by cervical dislocation. After sacrifice, hearts were removed and weighted. For histological and molecular analysis, ventricles separated in two halves by a short-axis section through the mid-portion of the heart. Upper part was immediately fixed in 4% of formaldehyde for 24h, dehydrated, and embedded in paraffin and lower part were snap frozen in liquid nitrogen immediately after dissection.

2.8. Histology

Ten μm heart sections were made using a microtome (Leica Microsystems, Nanterre, France), stained with hematoxylin and eosin, mounted in Eukitt (CML, France) and examined by light microscopy. Images were taken with a microscope (Leica Microsystems, Nanterre, France) equipped with a digital camera. At least five animals were used for each experimental point.

2.9. Statistical Analysis

Analyses were performed using the Prism 6 software. Normality was check using Shapiro-Wilk normality test and equal variance was checked with the test of Bartlett. If normality of distributions and/or equal variance were not assumed, the non-parametric Kruskal-Wallis test was used instead of ANOVA. If a significant difference was found, then multiple comparison tests were performed to compare the different groups analyzed (Dunn's or Bonferroni's multiple comparison test following Kruskal-Wallis or ANOVA, respectively). The level of significance was set to 0.05. Values are given as means ± standard error of the mean.

3. Results

3.1. Synthesis of pPGS

In this work, samples were prepared with 30% of PGS and 70% of PLA. The use of PLA as a biomaterial is very common but has some drawbacks for cardiac applications: PLA is hydrophobic and rigid. Here, the addition of PGS in the scaffolds aims to make it more elastomeric and hydrophilic. Yet, Kafouris *et al.* [9] demonstrated that a PGS elastomer prepared from a glycerol/sebacic acid 1/1 molar ratio is more stretchable and elastic than the one prepared from a 2:3 ratio, with the latter being more crosslinked. Moreover, the 1/1 ratio introduces more initial –OH groups than –COOH groups, inducing more free –OH in the final elastomer (Figure 3.1). Because –OH groups are responsible for the hydrophilicity of the material, the 1/1 ratio was chosen here to prepare the PGS-based scaffolds.

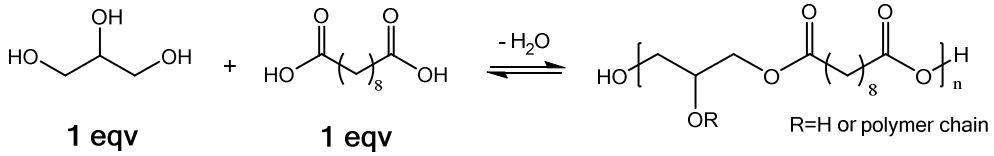

Figure 3.1. Chemical scheme describing the preparation path for poly(glycerol sebacate) (PGS).

The pPGS prepolymer was synthesized under microwave irradiation. This method ensures a fast and reliable polycondensation of PGS [10]. To verify the reproducibility of the experiment, the extend of reaction of the prepolymer was controlled by NMR. The degree of

esterification (DE) was calculated as explained in Chapter 1. The pPGS used for these experiments has a calculated DE of 85%. It was deducted from preliminary experiments that this DE gives a pPGS still soluble but close to its gel point, which can accelerate the crosslinking step.

3.2. Control of the fibers morphology of PLA and PLA/PGS mats

Here, the fibrous scaffolds were prepared by blend electrospinning with solutions containing 30% of pPGS because preliminary experiments showed that higher percentages of pPGS reduce process stability and give less regular fibers (see part 3.6). In the present work, different fibers diameters and annealing parameters are compared.

Three different PLA or PLA/PGS solutions were electrospun giving three kinds of fibers, with two categories of diameters, depending on the used solvent. Fibers diameters were measured on the bottom surface of the membranes which was in contact with the collector and corresponding to the first produced fibers as well as on the top surface of the membranes corresponding to the last produced fibers. Actually, PLA fiber diameters' distribution is broader with a larger average diameter on the top surface of the membranes compared to the bottom of the membranes (Figure 3.2). Another behavior is observed for PLA/PGS fibers, the average fibers diameter being similar on both sides. This phenomenon could be explained by the evolution of the electric field during electrospinning. Indeed, it is known that electrospun fibers diameter increases when the electric field decreased [11] because a lower charge density reduces electrospinning whipping movements and elongation of the fiber. Thus, after a certain time of PLA electrospinning, the collector is covered by an insulating layer of non-entirely discharged fibers: the electric field between the needle and the collector decreases consequently during electrospinning. But PLA/pPGS fibers are more conductive, as it will be proven in Chapter 5; the layer of the fibers does thus not reduce the electric field during electrospinning. Because of this difference observed in the two sides, in the following work, membranes surfaces are compared on the bottom surface and surface characterization and cells seeding were done on the bottom surface for all samples.

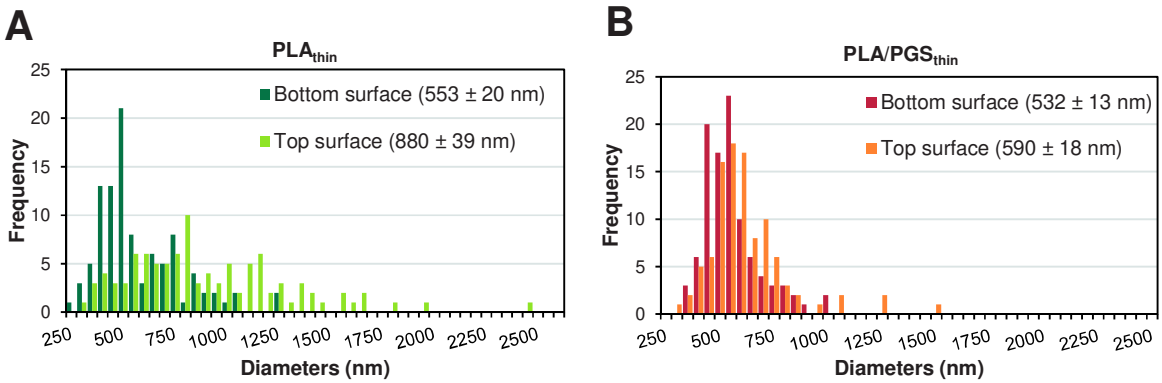

Figure 3.2. Diameters distribution on bottom and top surfaces of the membranes with mean diameters ± standard error of the mean **(A)** for PLA_{thin} and **(B)** for PLA/PGS_{thin}.

PLA_{thin} and PLA/PGS_{thin} were prepared in DCM:DMF 6:4 and led to the fabrication of scaffolds with fiber diameter in the range of 500 nm whereas PLA/PGS_{thick} were prepared in DCM:DMF 7:3 resulting in thicker fibers with average diameter in the order of 1500 nm (see Figure 3.3 and Table 3.1). While PLA and PLA/pPGS fibers prepared in DCM:DMF 6:4 have comparable diameters, fibers prepared in DCM:DMF 7:3 are significantly thicker because of the

higher volatility of the solvent used for the latter. Indeed, as DCM has a higher vapor pressure than DMF, the DCM:DMF 7:3 solvent mixture evaporates faster during electrospinning than the DCM:DMF 6:4, giving less time to the electrospun jet to be stretched before getting dry.

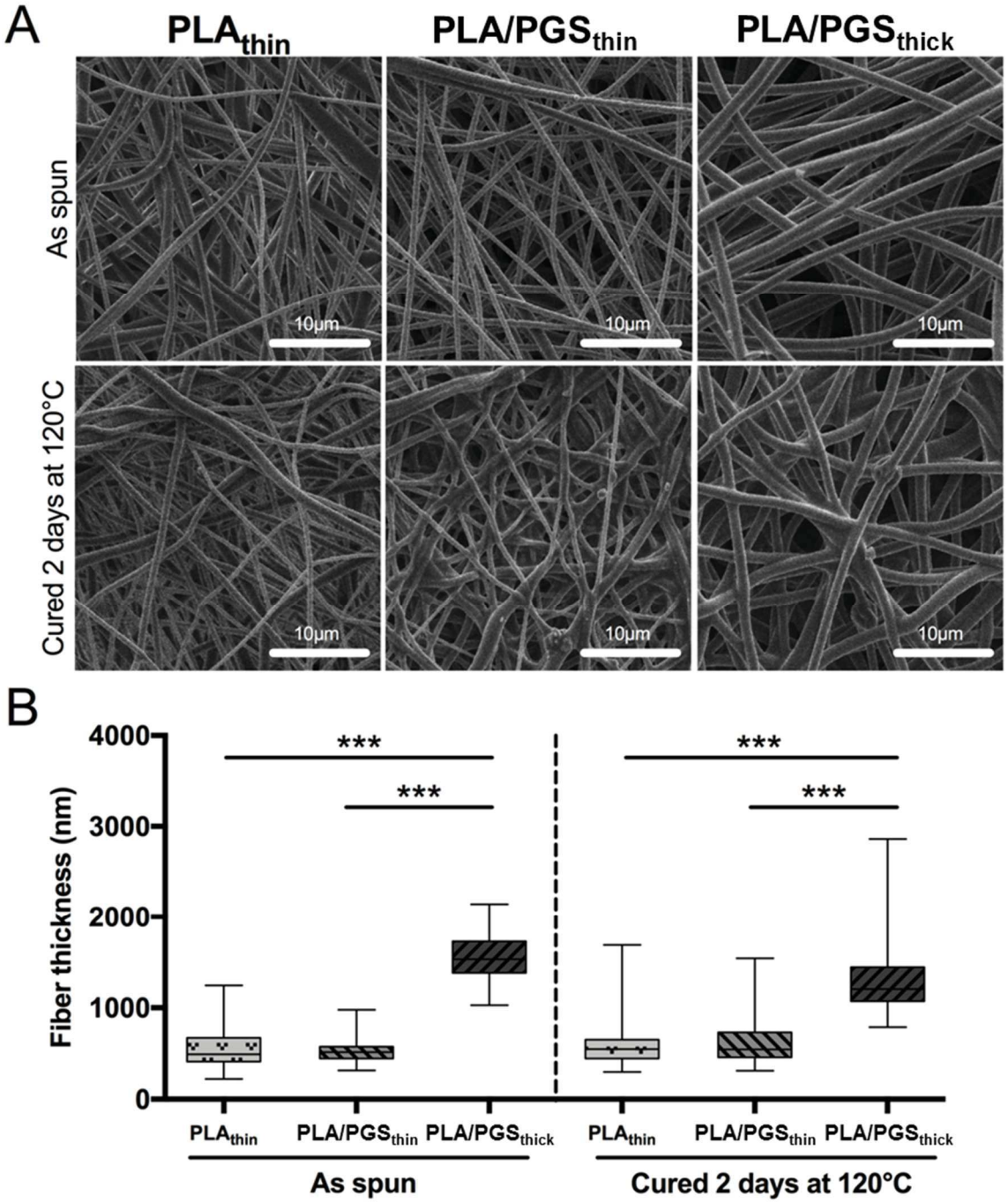

Figure 3.3. ***Morphology of the PLA and PLA/PGS electrospun fibers.*** **(A)** SEM pictures and **(B)** fibers diameters of PLA and PLA/PGS mats before and after crosslinking with 2 days of curing at 120°C. The lower and upper borders of the box are the quartiles, the line in the box is the median and the end of whiskers represent the minimum and the maximum of the data. ***p-value < 0.001.

After crosslinking at 90°C or 120°C, PLA/PGS fibers are slightly fused together at the contact points, but the mats are still fibrous. This effect is due to pPGS which can flow during curing at these temperatures because of its low viscosity before the crosslinking. This

phenomenon spread the diameters distribution to higher values without changing significantly the mean values, as shown in Figure 3.3. The PLA fibers are not melted at all. Again, the crosslinking step does not modify significantly the mean fibers diameters.

Table 3.1. Fiber diameters of PLA and PLA/PGS mats. Values were calculated from bottom side and are given as means ± standard error of the mean.

	As spun	Cured at 90°C	Cured at 120°C
PLA_{thin}	553 ± 20 nm	-	605 ± 27 nm
PLA/PGS_{thin}	532 ± 13 nm	578 ± 20 nm	621 ± 24 nm
PLA/PGS_{thick}	1544 ± 25 nm	1145 ± 38 nm	1343 ± 41 nm

Besides, the morphology of cured fibers is not modified by sterilization by autoclave, as shown in Figure 3.4.(A). Moreover, the sterilization does not degrade PLA polymer. Indeed, size exclusion chromatography analyses gave the same number-average molar mass (M_n) and mass-average molar mass (M_w) of PLA in the as spun fibers, sterilized fibers and cured and sterilized fibers (Figure 3.4.(B)).

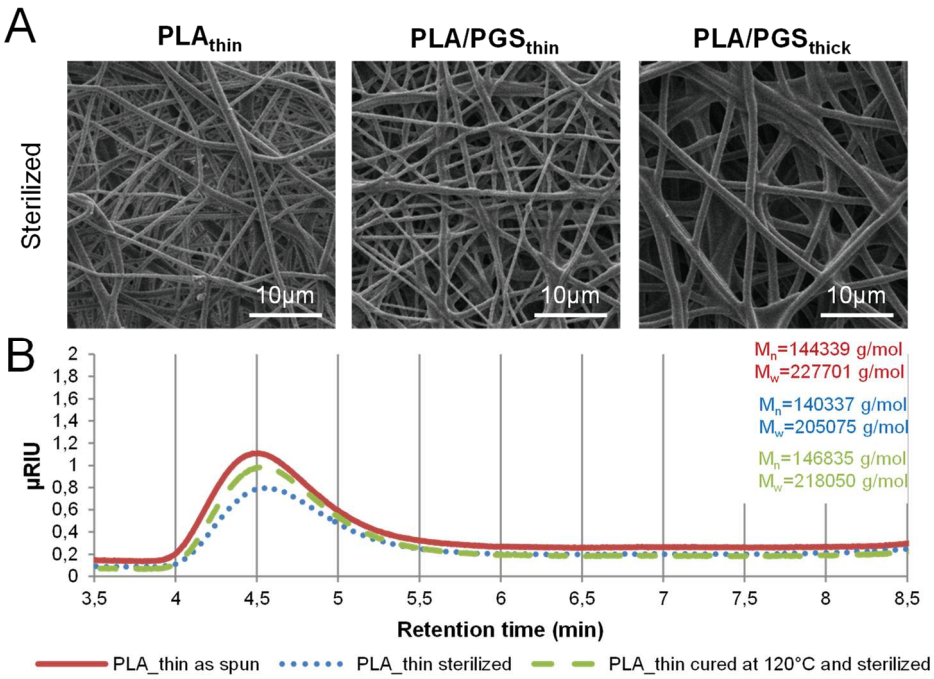

Figure 3.4. ***Results after sterilization by autoclave.*** **(A)** SEM pictures and **(B)** SEC curves.

3.3. Crystallinity of the PLA and PLA/PGS mats

Although the PLA used in this study is made from 95% L-lactic acid and 5% D-lactic acid, it is capable to crystallize. In particular, it was observed that PLA-containing membranes undergo shrinkage during annealing or sterilization, possibly showing crystallization. DSC measurements were thus carried out to understand the phenomenon.

Fibers were first analyzed as spun, for thick and thin fibers, with or without pPGS. The thermograms of the first heating run show several phenomena (Figure 3.5.(A)).

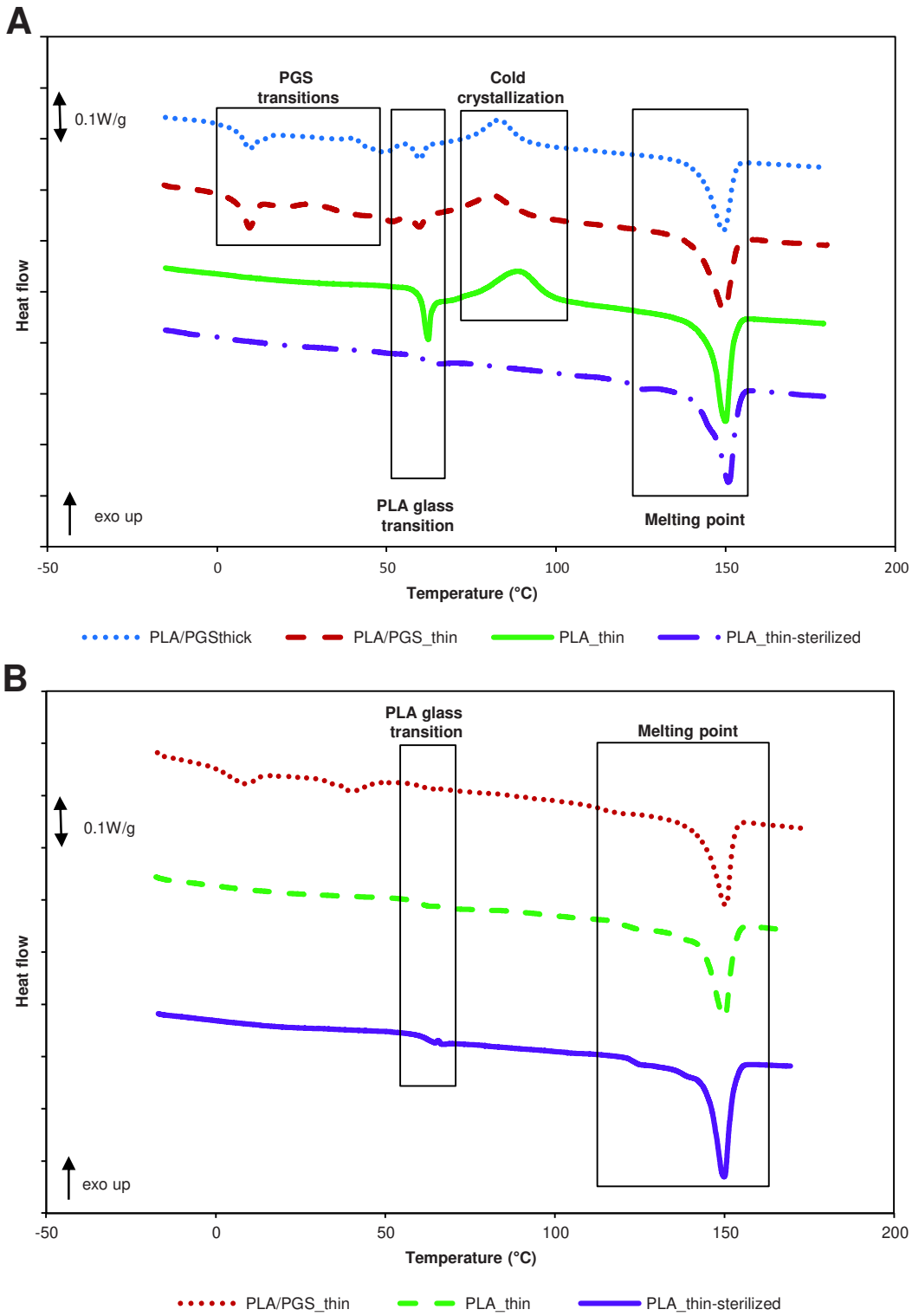

Figure 3.5. ***Heating curves from DSC analysis*** for **(A)** as spun samples and **(B)** samples cured at 120°C.

Between 0°C and 50°C, several endothermic peaks due to PGS moieties melting transitions are observed, in accordance with literature [12]. The thermal transitions at higher temperature are only due to PLA. The glass transition temperature (T_g) is observed around 60°C for pure PLA fibers and for PLA/PGS fibers. A relaxation enthalpy is observable at T_g, showing that PLA is in a nonequilibrium state in the electrospun fibers. The absence of significant shift of

PLA's T_g points out that PGS and PLA coexist in separated domains. PLA's melting point (T_m) is visible close to 150°C for each sample. All these temperatures are reported in Table 3.2. It can be noticed that for some samples, the melting peak is visibly divided in two peaks: the intense one at 150°C and a smaller one at lower temperature. This second peak can correspond to another crystal structure or to imperfect crystals [13].

Table 3.2. Glass transition temperature (T_g), cold crystallization temperature (T_c), melting temperature (T_m) and crystallinity (χ_c) of PLA in the fibers, before and after curing at 120°C, sterilized or not.

		T_g (°C)	T_c (°C)	T_m (°C)	$\chi_c^{before\ cc}$	$\chi_c^{after\ cc}$
As spun	PLA/PGS_{thin}	59	81	149	0.20	0.36
	PLA/PGS_{thick}	59	83	149	0.14	0.31
	PLA_{thin}	61	89	150	0.16	0.31
	PLA_{thin} sterilized	61	-	151	0.32	0.32
Cured at 120°C	PLA/PGS_{thin}	61	-	150	0.34	0.34
	PLA_{thin}	60	-	150	0.34	0.34
	PLA_{thin} sterilized	62	-	150	0.35	0.35

Between T_g and T_m, an exothermic peak is noticed. According to the literature, this peak is due to cold crystallization [14]. During the electrospinning process, solidification occurs too fast to let PLA crystallize completely. A metastable sate is thus observed for PLA after electrospinning. As PLA's T_g is above room temperature, this state is maintained. But during the heating process of DSC, molecular chains of PLA get enough thermal energy to organize in crystallites. Morel *et al.* [15] showed that the cold crystallization temperature T_{cc} is lower for thinner PLA fibers because the molecular orientation is higher: the crystallinity is thus higher in thin fibers. These results were confirmed by our measurements on PLA/PGS thin and thick fibers. In addition, it is interesting to compare the crystallinity of PLA just after electrospinning, namely before cold crystallization ($\chi_c^{\text{before cc}}$), and after cold crystallization occurring during DSC heating run ($\chi_c^{\text{after cc}}$). The values are reported in Table 3.2 after calculation using the following equations:

$$\chi_c^{before\ cc} = \frac{\Delta H_m - \Delta H_c}{\Delta H_m^{100\%}} \times \frac{100}{\%PLA}$$

$$\chi_c^{after\ cc} = \frac{\Delta H_m}{\Delta H_m^{100\%}} \times \frac{100}{\%PLA}$$

with ΔH_m the melting enthalpy, ΔH_c the enthalpy of cold crystallization and $\Delta H_m^{100\%}$ the melting enthalpy of 100% crystalline PLA equal to 93 J/g [1].

Furthermore, the comparison of χ_c before and after cold crystallization shows that PLA is twice as crystalline after cold crystallization as before: χ_c starting between 15% to 20% before cold crystallization and reaching 30% to 40% after. However, after sterilization, the same fibers do not show a cold crystallization anymore. During autoclave sterilization, the fibers are indeed heated at 110°C, a temperature higher than cold crystallization temperature (80-90°C) leading to PLA crystallization and thus shrinkage of the scaffolds during their sterilization.

Moreover, the same phenomenon is observed after the crosslinking step. The results after curing at 120°C are given in Figure 3.5 and Table 3.2 but the same tendency was observed after curing at 90°C. All the samples melt at 150°C without any prior cold crystallization during the DSC heating ramp, confirming that crystallization occurred during annealing. This is the reason why the membranes are shrunk and more rigid after the curing step. The crystallization of PLA fibers during an annealing process was already studied by Ribeiro *et al.* [16]. No significant changes are observed after additional sterilization, because PLA was already crystallized. So, it can be concluded that after curing, membranes are more stable and easier to sterilize.

3.4. Mechanical properties of the PLA and PLA/PGS mats

For the desired application, the scaffold's mechanical strength should be sufficient to facilitate the handling and the suture process for cardiac applications. Moreover, as already mentioned, the scaffold's therapeutic properties can be enhanced by its mechanical properties if they match myocardium properties, namely a Young's modulus comprised between 200 and 500 kPa at the end of diastole [17]. Thus, it is necessary to characterize the membranes' mechanical behavior. Uniaxial tensile tests experiments were conducted on the fibrous mats and stress-strain curves were drawn. Typical evolution of the stress upon strain after different crosslinking steps on PLA/PGS_{thin} fibers are represented on Figure 3.6.(A). This figure shows clearly that annealing increases the stiffness of PLA/PGS_{thin} membranes. To make a more quantitative comparison, the Young's modulus (E) (Figure 3.6.(B)) and the Ultimate Tensile Strength (UTS) (Figure 3.6.(C)) were determined for different formulation and crosslinking parameters. The strains at break (ε_{break}) (Figure 3.6.(D)) are also given as an indication, but most of the cured samples broke at the clamps. Despite many trials, it was almost impossible to prevent this break, certainly because of the thinness of the membranes after shrinkage during annealing. The values are consequently only reliable for not cured samples.

It can be noticed that crosslinking results in higher E and UTS value. Moreover, annealing at higher temperature increases E and UTS too. This stiffening upon curing can be explained by three causes. Firstly, PLA crystallizes during annealing as demonstrated by the DSC analyses, a phenomenon leading to the stiffening of PLA [18]. This reason is sufficient to explain the stiffening of the pure PLA scaffolds. Secondly, the annealing step aims to crosslink pPGS in a stiffer PGS elastomer, even stiffer if it is crosslinked at higher temperature [10]. And thirdly, because of the heat during the curing step, melted pPGS flows out of the fibers and creates fixed contact points between fibers as observed on the SEM pictures. During the tensile test with a fibrous mat, fibers move along each other to align before getting really stretched. Yet, when fibers are not fused together as for not cured fibers or pure PLA fibers, the material can undergo a higher elongation with a lower strength due to low fiber-fiber friction interaction. In the case of the cured PLA/PGS fibers, the fused contact points increase the resistance to the stretching. Thus, the crosslinking of PGS and the fusion of the fiber-fiber contact points during annealing explain why E and UTS increase more significantly during curing for PLA/PGS fibers than for PLA fibers.

Because of the thinness of the membranes, they broke early at the clamps and no clear influence of curing on ultimate strains is noticeable. Surprisingly, PLA/PGS_{thick} fibers show here a lower ε_{break} after curing at 90°C than before curing or after curing at 120°C. Because the five tested samples came from the same membrane, we can consider that this is due to defects in this precise membrane.

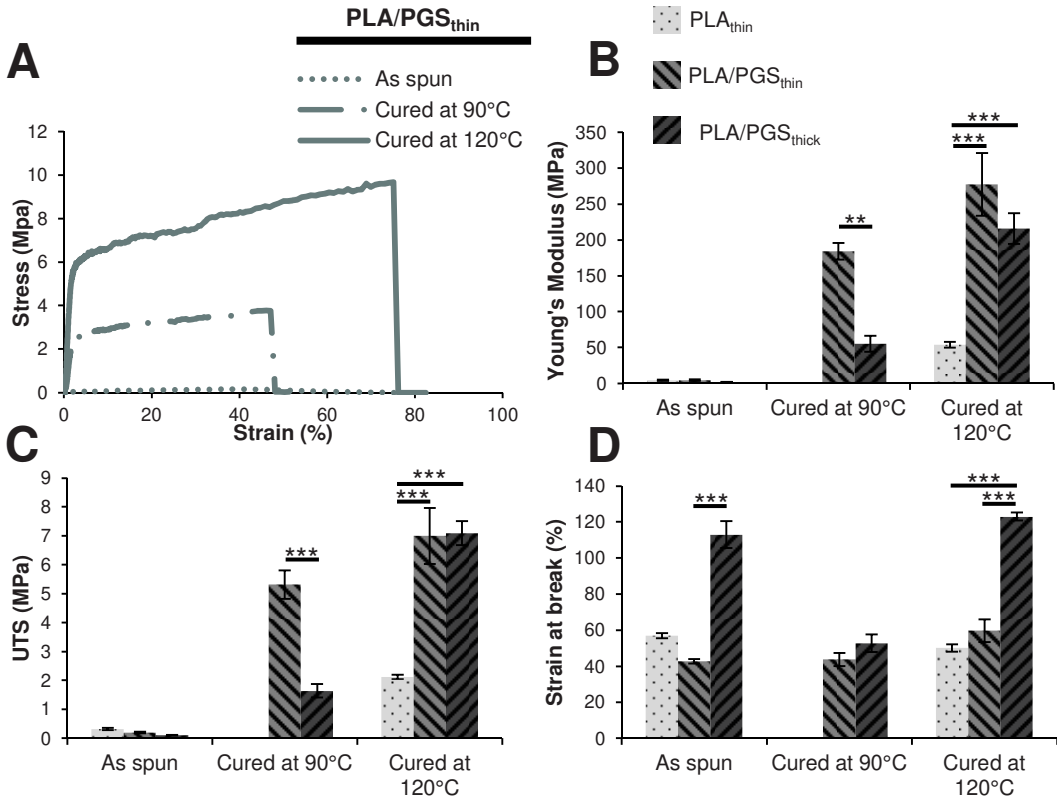

Figure 3.6. ***Mechanical properties of the PLA and PLA/PGS mats at wet state***. **(A)** Representative evolution of stress-strain curves upon curing for PLA/PGS$_{thin}$ fibers. Evolution of **(B)** Young's modulus; **(C)** Ultimate tensile strength and **(D)** strain at break upon curing of PLA$_{thin}$, PLA/PGS$_{thin}$ and PLA/PGS$_{thick}$ fibers. **p<0,01, ***p<0,001.

Young's moduli and UTS of PLA/PGS$_{thick}$ fibers tend to be globally lower than for PLA/PGS$_{thin}$ fibers, whereas the maximal strains tend to be larger. This result can be linked to DSC results. Indeed, Morel *et al.* [15] highlighted a relation between the higher crystallinity and molecular orientation in thin PLA fibers and their higher modulus. We can thus explain the higher rigidity of PLA/PGS$_{thin}$ mats by our DSC measurements: they justify the higher modulus of thin individual fibers. Moreover, the lower strains at break for thin fibers could be explained by the higher density of contact points with thinner fibers, the contact points making cohesion of the material.

Finally, tensile tests indicate that PLA/PGS mats, and in particular PLA/PGS$_{thin}$ mats are stiffer than pure PLA ones, but this method measures the macroscopic mechanical properties of the fibrous mats, which depends also on the behavior of the fibers along each other, as discussed above.

3.5. Evaluation of the hydrophilicity of PLA and PLA/PGS mats

Cell adhesion, a feature of great importance for tissue engineering applications, can be enhanced by the scaffold's hydrophilicity [19,20]. However, PLA, a hydrophobic polymer, was used in the present study. The addition of PGS, a more hydrophilic polymer [4], was expected to improve the hydrophilicity of the scaffolds. Sessile drop method was thus used to characterize the wettability of the membranes.

Different surface's behaviors were noticed. The apparent water contact angle (aCA) was static on pure PLA membranes or on PLA/PGS membranes cured at 120°C. The mean values are shown in Figure 3.7.(A). The annealing step does not modify the hydrophilicity of pure PLA mats, which showed an aCA of 128±6° before curing and 127±4° after. For thin fibers, the presence of PGS leads to a slight decrease in the aCA value. However, all these mats show a strong hydrophobic behavior which is justified by the roughness induced by the fibrous structure [21]. This roughness is increased and thus the aCA value is increased for the larger fibers, even if they contain PGS: cured PLA/PGS_{thick} fibers have an aCA close to PLA fibers' aCA. The hydrophobicity of the PLA/PGS membranes is not conform to Yan *et al.*'s results, where a superhydrophilic behavior was found for such membranes cured 2 days at 120°C [4]. However, it is difficult to compare Yan's materials to the mats prepared in the present work, as PGS was prepared with other synthesis parameters (heating mode and reaction time). The use of a pPGS with a lower DE would lead to a less crosslinked PGS and could explain a higher hydrophilicity, as explained further in this section.

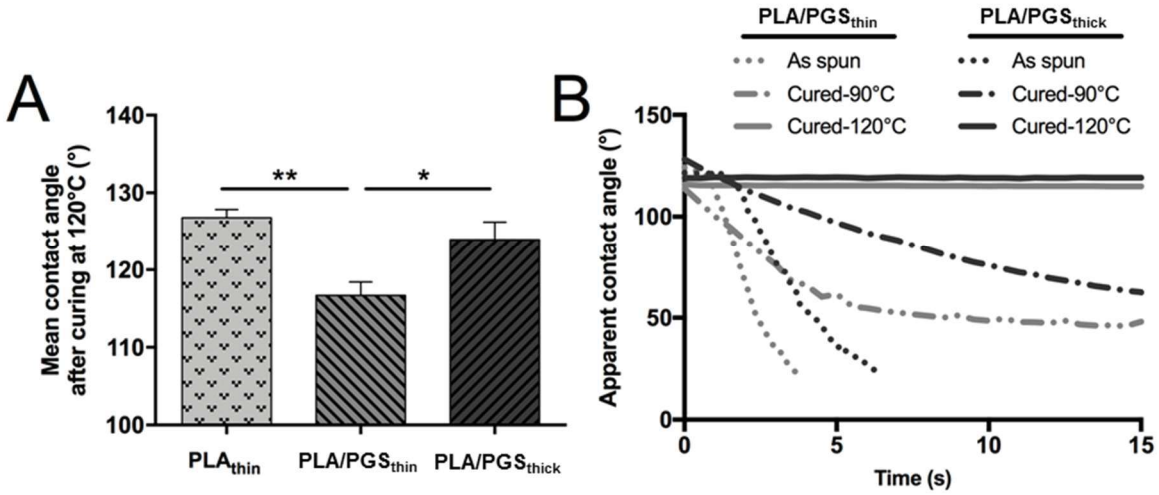

Figure 3.7. Hydrophilicity of the PLA and PLA/PGS mats. **(A)** Mean apparent water contact angle (aCA) of PLA_{thin}, PLA/PGS_{thin} and PLA/PGS_{thick} mats after curing at 120°C. **(B)** Typical evolution of the aCA during time on PLA/PGS_{thin} and PLA/PGS_{thick} mats for different curing steps. *p<0,05, **p<0,01.

Yet, PLA/PGS scaffolds not cured or cured at 90°C absorb the water droplet, what is illustrated by the decrease of the aCA during time. This behavior reveals their sufficient hydrophilicity which permits water imbibition thanks to their porosity. Nevertheless, because the aCA is continuously evolving upon time, it is not possible to define a reliable aCA value to compare the hydrophilicity of the different mats. The decrease in aCA was thus recorded upon time, as shown in Figure 3.7.(B). The initial value was not selected as a comparable value because it was strongly dependent on the strength applied during the droplet deposition. Furthermore, the end of the curve and the potential plateau value is influenced by the volume available for the water in the mat, namely its surface and thickness.

It can be noticed from Figure 3.7.(B) that the curves present up to three domains, this evolution corresponding to transition from an air-pocket regime to a penetration regime. The air-pocket regime depends strongly on the impact force applied during droplet deposition and the surface roughness of the mat. If the force is too weak and the membrane is very fluffy, which may be the case for as spun fibers, the droplet visibly remains at the top of the fibers during a few seconds, confining air pockets in the mat. It results in a constant aCA. The droplet starts

then to spread at the surface of the mat while imbibing it thanks to capillarity forces [22]. aCA decreases quite fast under the effect of these two phenomena. At a certain point, the droplet's spreading stops and only penetration occurs: aCA decreases more slowly. This last stage with only penetration is confirmed by the constant value of droplets' diameters as shown on the example given in Figure 3.8.

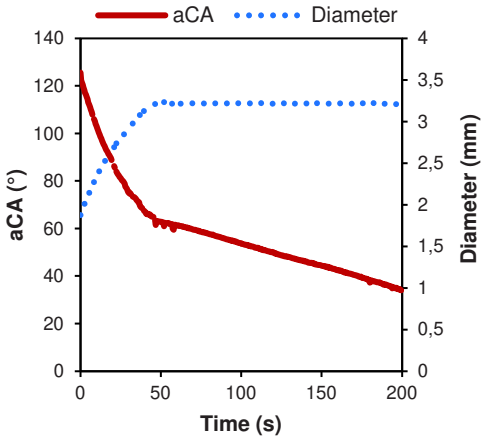

Figure 3.8. Compared evolution of aCA and diameter of the water droplet on PLA/PGS$_{thin}$ cured at 90°C.

Figure 3.7.(B) shows that non-cured PLA/PGS mats absorb water faster than cured samples. Furthermore, it seems that increasing the crosslinking temperature leads to a slower absorption, until no absorption after annealing at 120°C. This can be easily explained as the crosslinking reaction consists in the reaction between alcohols and carboxylic acids. So, not crosslinked PGS includes more free –OH groups explaining the highest hydrophilicity. In the same way, increasing the synthesis temperature increases the kinetic of PGS crosslinking reaction [10]. PGS cured during the same time at higher temperature is thus necessarily less hydrophilic. Finally, harsh annealing conditions (2 days at 120°C) decrease hydrophilicity differences between PLA and PLA/PGS materials. Thus, from the hydrophilicity point of view, the most interesting scaffolds are the less crosslinked. But it is necessary to find a good balance between hydrophilicity and a sufficient PGS crosslinking rate that ensures insolubility of the material and good mechanical properties. Moreover, a too high hydrophilicity could also be unfavorable to cell adhesion, and other surface properties such as rugosity, local mechanical properties or surface charge play a role too.

3.6. Effect of PGS content

The previous results focus on samples that could be easily produced, namely with no more than 30% of PGS. However, it was hypothesized that the properties (elastomeric and hydrophilic properties) of the scaffolds could be improved by the increase of the PGS content. Efforts were thus done in order to prepare samples with 40% of PGS. It was not possible to electrospin solution with 4% of pPGS and 6% of PLA solubilized in DCM:DMF 7:3, the process being not stable at all. Thick fibers could thus not be prepared, but thin PLA/PGS fibers could be electrospun from solutions with 4% of pPGS and 6% of PLA solubilized in DCM:DMF 6:4. The process parameters was similar to the one detailed above. Electrospinning could hardly be conducted during the time necessary to get an exploitable membrane. The mat fabricated with this method comprised some areas with droplets that were not used further. The process is

certainly less stable because of the lower amount of carrier polymer in the solution and of the resulting lower quantity of entanglements.

3.6.1. Fibers morphology

The surface of the membranes with 40% of PGS was characterized on the bottom surface as spun and after curing at 90°C and 120°C. After electrospinning, fibers comprise few beads, as surrounded on Figure 3.9. Globally, they are quite similar to PLA/PGS_{thin}, except that after curing, larger areas of melted pPGS are visible on samples with 40% of PGS. The porosity is thus more noticeably reduced. The mean diameters are given on Figure 3.9.

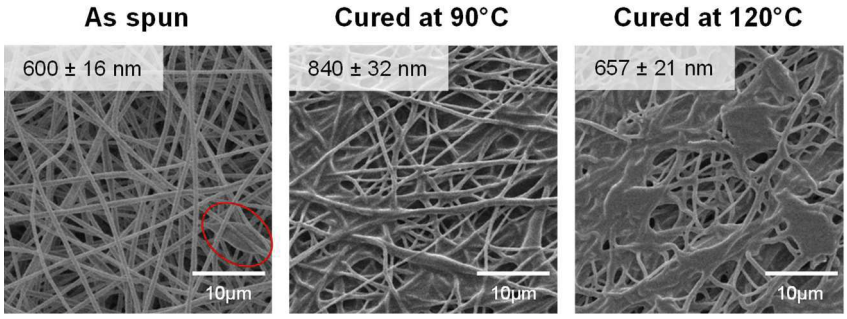

Figure 3.9. SEM pictures showing the morphology of PLA/PGS thin electrospun fibers with 40% of PGS with the mean diameters given ± standard error of the mean.

3.6.2. DSC measurements

Samples with 40% of PGS were analyzed by DSC. The thermal behavior is similar to PLA/PGS_{thin}'s behavior with T_g, T_c and T_m having comparable values (Table 3.3). Crystallinity before and after cold crystallization and before and after curing at 120°C is however slightly lower, pPGS acting as an impurity for PLA crystallites.

Table 3.3. DSC results for PLA/PGS thin electrospun fibers with 40% of PGS.

	T_g (°C)	T_c (°C)	T_m (°C)	$\chi_c^{before\ cc}$	$\chi_c^{after\ cc}$
As spun	Not visible	81	149	0.13	0.30
Cured at 120°C	Not visible	-	150	0.31	0.31

3.6.3. Mechanical properties

With higher PGS content, these membranes were expected to be softer. In order to verify this hypothesis, tensile tests were conducted on the samples as spun, cured at 90°C and cured at 120°C. As spun membranes having a PGS content of 40% present a mechanical behavior different from samples with 30%. As shown on Figure 3.10.(A), in both cases, the stress-strain curves are divided in three parts. First, a linear behavior characterized by a high Young's modulus is observed. Then, the membranes are subjected to irreversible deformations mainly due to fiber-fiber friction and plastic deformations until progressive rupture and dissociation of the fibrous membranes. Regarding the first linear mode, the Young's modulus reaches 13.1±0.3 MPa with a PGS content of 40% whereas a value of 4.4±1 MPa was measured in the case of a PGS content of 30%. This result is quite surprising, because it was expected that adding more PGS makes the material softer. This result could be explained by the difference in the fibrous morphology of the

tested materials. On Figure 3.11, it can be seen the membrane with 40% of PGS comprises more fixed contact points (because of the pasty pPGS) that contribute to the Young's modulus. Indeed, the linear deformations observed at small strains correspond to the elastic bending and stretching of the fiber strands located between consecutive contact points: a higher density of contact points increases the Young's modulus.

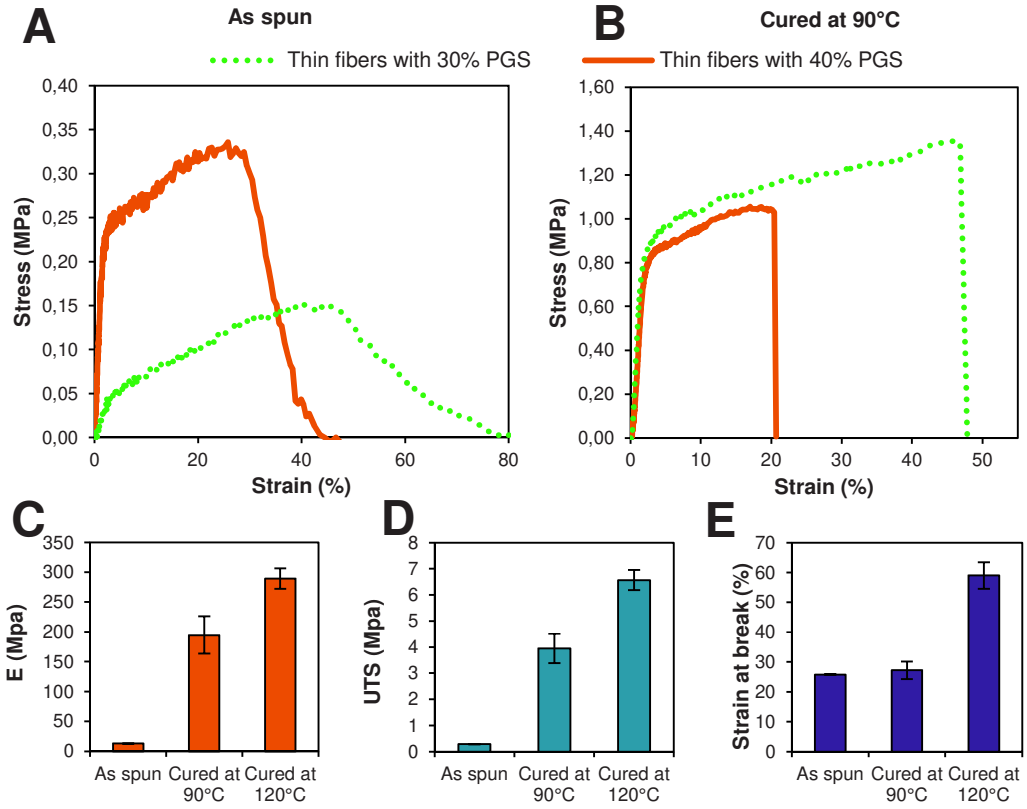

Figure 3.10. ***Mechanical properties of PLA/PGS membranes at wet state.*** Comparison of typical stress-strain curves for PLA/PGS thin fibers with 30% and 40% of PGS **(A)** as spun and **(B)** after curing at 90°C. Evolution of **(C)** Young's modulus; **(D)** Ultimate tensile strength and **(E)** strain at break upon curing of mats with 40% of PGS. Mean values are given ± standard error of the mean.

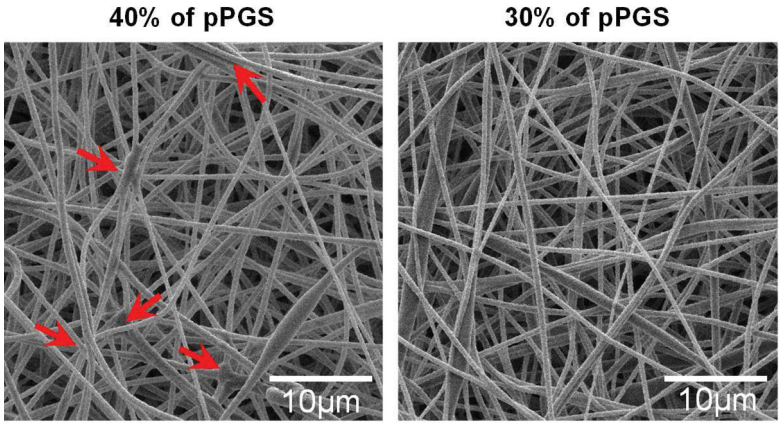

Figure 3.11. Comparison of the density of contact points PLA/pPGS thin fibers as spun with 40% and 30% of pPGS.

Such results resulting from the addition of an elastomer to a thermoplastic was already found by Lee *et al.* [23]. This hypothesis is also validated by the lower UTS and the more progressive rupture of the samples for the case of a PGS content of 30%.

After curing at 90°C, the mechanical behavior is the same with 40% and 30% of PGS (Figure 3.10.(B)), because in both cases a lot of fixed contact points appear. Concretely, the modulus increases as well as the UTS and the strain at break, exactly as for samples with 30% of PGS. The values are similar to samples with less PGS at each step (Figure 3.10.(C)-(E)). The modulus is thus higher than the one expected for cardiac tissue engineering.

3.6.4. Characterization of the hydrophilicity

PGS content was also increased in order to increase the hydrophilicity of the mats. Water-in-air contact angle measurements were thus done. As spun samples absorbed the water droplet, so again no angle value can be given. However, records of the evolution of aCA during time show that the absorption is faster when there is more PGS in the material (Figure 3.12.(A)). In order to quantify this difference, the slope of the first part of the curve was measured for 10 droplets on each sample to give a mean value with the standard deviation. The slope is –102±10°/s with 40% of PGS and –52±7°/s with 30% of PGS, attesting for a more hydrophilic behavior with more PGS. This difference disappears after curing at 90°C, as shown on Figure 3.12.(B). The droplet is again absorbed more slowly than on as spun samples. But the mean value of the slope of the first part of the curve is not significantly different according to the PGS content. It reaches –6±1°/s with 40% of PGS and –7±3°/s with 30% of PGS. Finally, for samples cured at 120°C, it was possible to measure a mean aCA. The value was 114±5° with 40% of PGS, what is very close to 117±7° found for PLA/PGS$_{thin}$ cured at 120°C. It can be again concluded that curing delete differences in hydrophilicity. Consequently, the increase in PGS content allows here no clear improvement of the hydrophilicity for samples useable for biological application (namely cured samples).

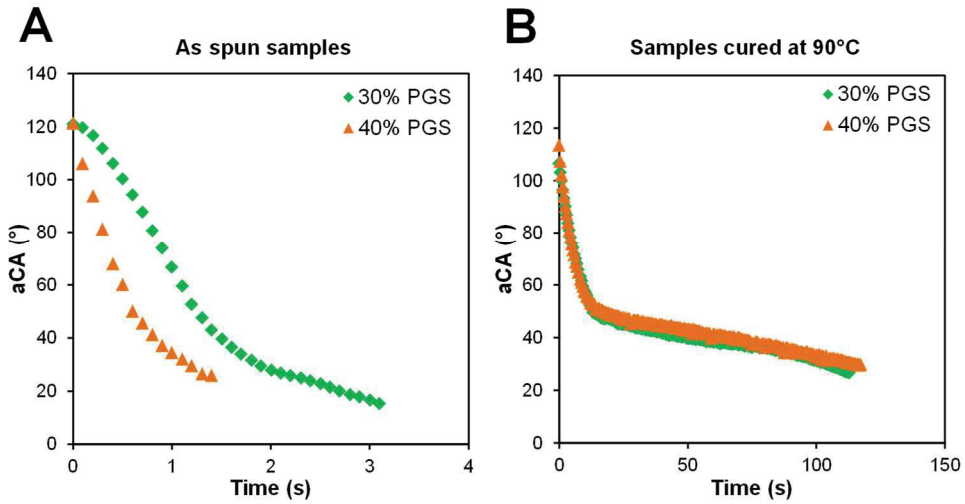

Figure 3.12. Typical evolution of the aCA during time on PLA/PGS thin fibers with 30% and 40% of PGS. **(A)** For as spun samples. **(B)** For samples cured at 90°C.

To conclude this aside dedicated to the effect of an increase of the PGS content, we can say that these materials are not of great interest. They are indeed difficult to produce because of the instabilities of the electrospinning jet. Moreover, the morphology of the fibers is worse than with less

PGS, especially after the curing step that let arise numerous melted areas. Finally, despite slightly different properties of as spun samples, especially a higher hydrophilicity, mats with 40% of PGS become very similar to materials with 30% of PGS after curing. Their mechanical properties and hydrophilicity do not justify the use of a difficult process. Moreover, preliminary biological tests, in particular cell culture suggested that these materials are not more relevant for cardiac tissue engineering than their counterpart (data not shown). For all these reasons, the complete study presented here does not take into account mats with 40% of PGS.

3.7. Cellularization of PLA and PLA/PGS mats and influence of Matrigel coating

To assess the cytocompatibility of the PLA and PLA/PGS mats for the biological application, neonatal rat cardiomyocytes were seeded on nude or Matrigel-coated PLA_{thin} or PLA/PGS_{thin} mats. Immunostaining of α-actinin, a surrogate marker of functional cardiomyocytes [24], was used to evaluate the cell attachment and the growth after 3 days of culture on these mats. As demonstrated in Figure 3.13, in the absence of Matrigel coating, neonatal cardiomyocytes were able to adhere on the PLA_{thin} or PLA/PGS_{thin} mats. However, the round morphology of the cardiomyocytes showed the difficulty of the cells to spread on nude-fibers as shown by Figure 3.13.(A), (B) and (D). In contrast, cardiomyocytes seeded on Matrigel coated-mats exhibited physiological shape with a well-organized sarcomeric structure as observed by α-actinin immunostaining (Figure 3.13.(A) and (B)) and by SEM images (Figure 3.13.(D) and (E)). The effect of the coating was similar between PLA_{thin} and PLA/PGS_{thin} mats. As Matrigel may form a continuous film at the surface of the samples, samples without cells were also analyzed by SEM to evaluate the porosity of the mats after functionalization (Figure 3.13.(A) and (B)). SEM images highlighted that some film parts remain on PLA fibers, but not on PLA/PGS fibers, where Matrigel certainly wrap the fibers. This could indicate a better interaction of Matrigel with PGS than with PLA.

Cell attachment after coating could be enhanced by a higher hydrophilicity. The hydrophilicity of Matrigel-coated patches was thus characterized (Figure 3.13.(C)). As the membranes absorb water, aCA was registered upon time; (Figure 3.13.(C)) shows that hydrophilicity of PLA_{thin} and PLA/PGS_{thin} fibers crosslinked at 120°C is dramatically improved after coating as the aCA decreases significantly upon time. This demonstrates that Matrigel is present, coating each fiber individually.

Finally, to determine the capacity of neonatal cardiomyocytes to grow and to infiltrate in the Matrigel coated PLA_{thin}, PLA/PGS_{thin} and PLA/PGS_{thick} scaffolds, we measured the size of the cardiomyocytes and the maximum Z position of the cardiomyocytes after 6 days of culture (Figure 3.14.(B) and (C)). As demonstrated in Figure 3.14.(B), we noticed an increase in the cardiomyocyte size on the PLA/PGS_{thin} mats in comparison to PLA_{thin} and PLA/PGS_{thick} after 6 days of culture independently of the curing temperature. Furthermore, the cell colonization into the mats was increased by 2-fold in PLA/PGS_{thin} cured at 120°C than PLA_{thin} (Figure 3.14.(C)). These findings suggest a higher capacity of the PLA/PGS_{thin} mats, especially cured at 120°C, to support the spreading of the cardiomyocytes *in vitro*.

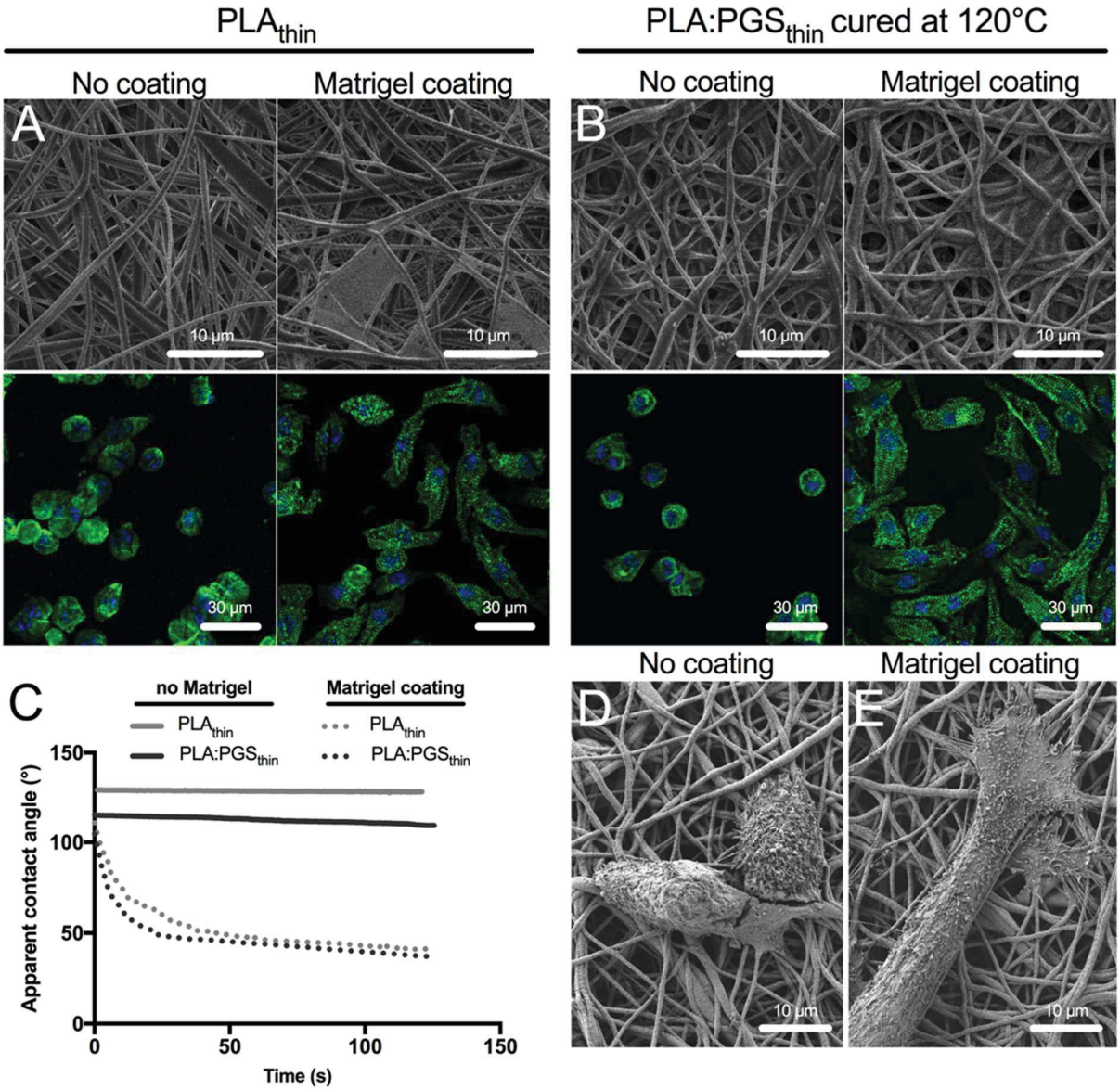

Figure 3.13. ***Influence of Matrigel on the hydrophilicity and cellularization of the PLA and PLA/PGS mats.*** SEM images of nude or Matrigel-coated **(A, upper panel)** PLA_{thin} and **(B, upper panel)** PLA/PGS_{thin} mats. Three days after cardiomyocytes seeding on **(A, lower panel)** PLA_{thin} or **(B, lower panel)** PLA/PGS_{thin} mats, cardiomyocytes were immunolabeled with the antibody against α-actinin (green). Nuclei appear blue due to Hoescht 33342 staining. **(C)** Typical evolution of the aCA during time of nude or Matrigel-coated PLA_{thin} and PLA/PGS_{thin} mats. SEM images of the cellularized **(D)** PLA_{thin} and **(E)** PLA/PGS_{thin} mats.

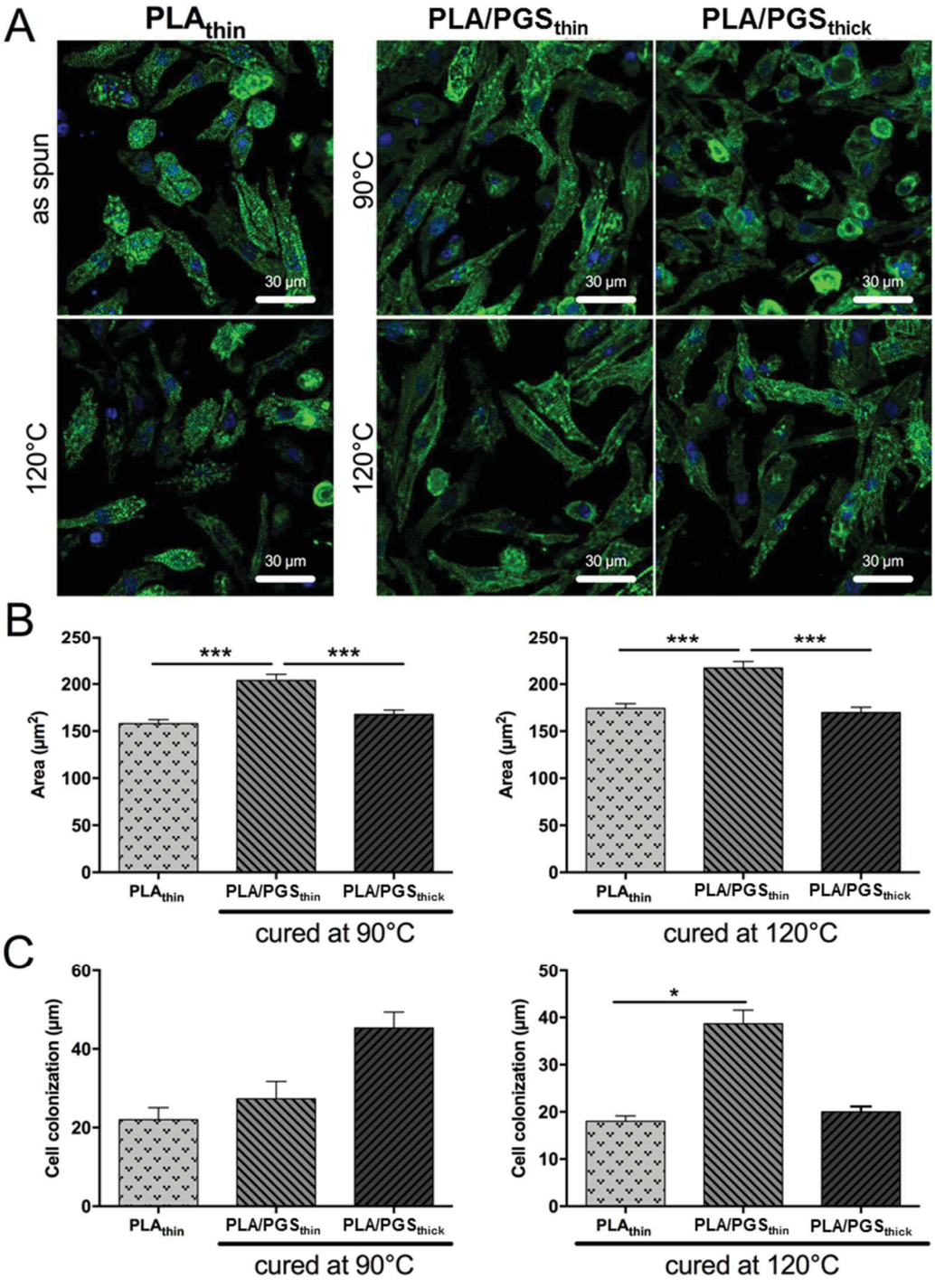

Figure 3.14. ***Cellularization of the PLA and PLA/PGS mats with neonatal rat cardiomyocytes.*** **(A)** Six days after cardiomyocytes seeding on Matrigel-coated PLA_{thin}, PLA/PGS_{thin} and PLA/PGS_{thick} cured at 90°C or 120°C, cardiomyocytes were immunolabeled with the antibody against α-actinin (green). Nuclei appear blue due to Hoescht 33342 staining. **(B)** Mean of the cardiomyocyte surfaces on the mats (n=2, n>125-200 cells) and **(C)** the maximum Z position of the cardiomyocytes into the mats (n=3) were measured 6 days after cell culture. Values are given as means ± standard error of the mean. *p<0,05 ***p<0,001.

3.8. Biocompatibility of the PLA and PLA/PGS mats

The biocompatibility of the PLA_{thin}, PLA/PGS_{thin} and PLA/PGS_{thick} mats was studied in a cardiac environment, after implantation of acellular mats on the surface of the heart of healthy Swiss mice. Previous studies demonstrated that PGS has a good biocompatibility [25,26]. However, grafted PGS were completely absorbed in 1 to 2 months [26]. It should be noted that the ideal scaffold should degrade at a similar rate to the healing of the tissue or organ [27].

In this study, acellular PLA_{thin}, PLA/PGS_{thin} and PLA/PGS_{thick} mats were sutured on the surface of the heart of healthy swiss mice for 7 days and 28 days. We first evaluated the ratio of heart weight to body weight because this ratio increases during cardiac remodeling and hypertrophy. As demonstrated in Figure 3.15, seven days after implantation, PLA_{thin} and PLA/PGS_{thin} cured at 120°C showed lower heart weight to body weight ratio in comparison to the other groups, indicating that these scaffolds are less invasive scaffolds after implantation. Following this, we focused on PLA_{thin} and PLA/PGS_{thin} cured at 120°C for further analysis.

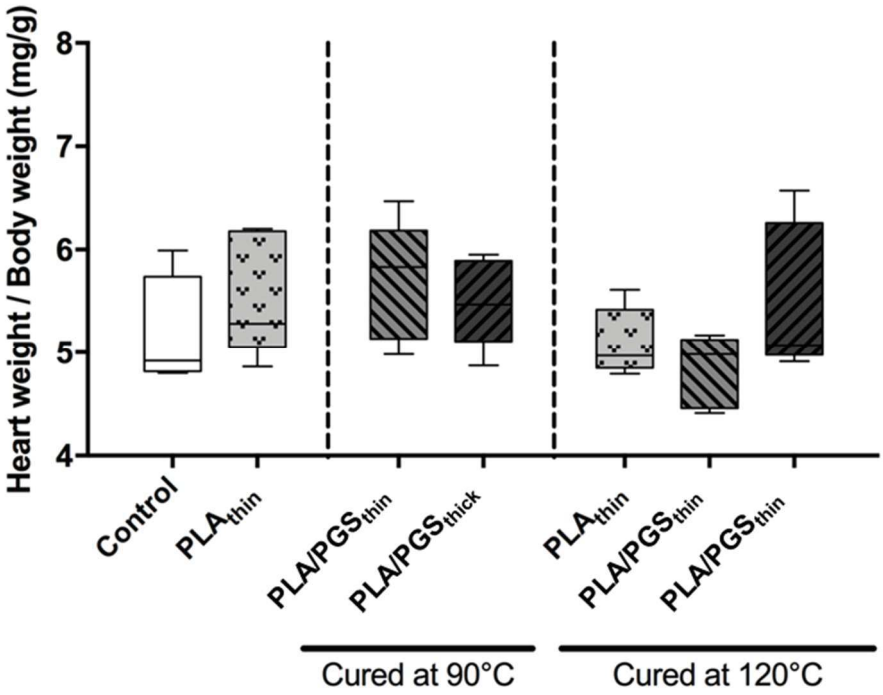

Figure 3.15. ***Evaluation of heart weight to body weight ratio at 7th day after implantation of acellular mats on the surface of the heart of healthy mice.*** Seven days after implantation of acellular mats, the mice were sacrificed and then the hearts were removed and weighted. Heart weight at mg was divided to body weight at g to obtain heart weight to body weight ratio.

The integrity of the mats was visualized by polarized microscopy and hematoxylin-eosin staining after 7 (Figure 3.16) and 28 (Figure 3.17) days of implantation. Moreover, hematoxylin-eosin staining allows the analysis of the foreign body response with respect to inflammation, granulomatous reaction, and epicardial fibrosis. As demonstrated in Figure 3.16, after 7 days, both PLA_{thin} and PLA/PGS_{thin} scaffolds were visible and well-integrated on the ventricle. In contrast to PLA/PGS_{thin}, PLA_{thin} scaffolds have a more diffuse structure after implantation (Figure 3.16.(A) and (D)). The diffuse structure of the PLA_{thin} mat fibers was also accompanied by cell infiltration composed predominantly of mononuclear cells with the accumulation of multinucleated giant cells at the grafted area (see arrows in Figure 3.16.(C)) demonstrating the

presence of moderate foreign body reaction. The situation remains similar 28 days after implantation (Figure 3.17), foreign body reaction persists with PLA_{thin} mats whereas PLA/PGS_{thin} mats were perfectly integrated on the surface of the ventricle and only a few mononucleated cells are visualized in the mats demonstrating a perfect biocompatibility of this scaffold. The more intense inflammatory response with PLA samples could indicate that the acid degradation products from PLA [28] induce a higher acidity than PGS degradation products. As demonstrated in Figure 3.17.(D), PLA/PGS_{thin} mats also induce the formation of the capillaries at the grafted area (see arrowheads in Figure 3.17.(D)). Taken together, with a good integrity after 28 days and a low inflammatory response, PLA/PGS_{thin} mats cured at 120°C present all characteristics to be a potential scaffold for cardiac tissue engineering.

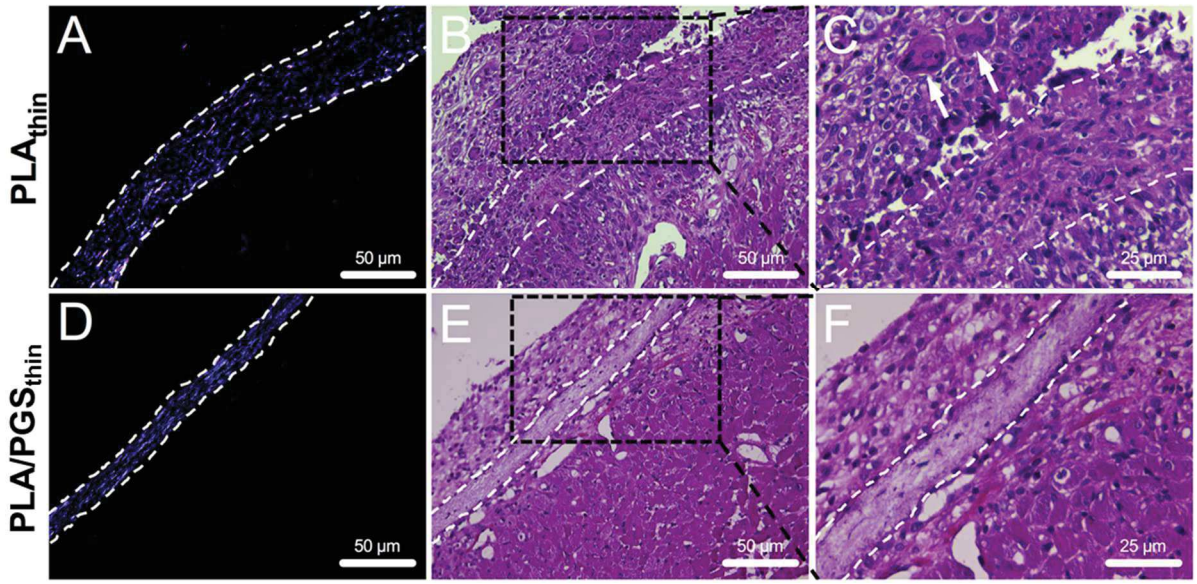

Figure 3.16. ***Biocompatibility of the PLA and PLA/PGS mats after implantation on the surface of the heart of healthy mice.*** The integrity of the mats was visualized by **(A and D)** polarized microscopy and **(B-C and E-F)** hematoxylin-eosin staining after 7 days of implantation of acellular **(A-C)** PLA_{thin} and **(D-F)** PLA/PGS_{thin} cured at 120°C mats. Arrows indicate the accumulation of multinucleated giant cells. White dot lines represent grafted mats. Black dot lines in **B** and **E** show higher magnification area in **C** and **F**, respectively.

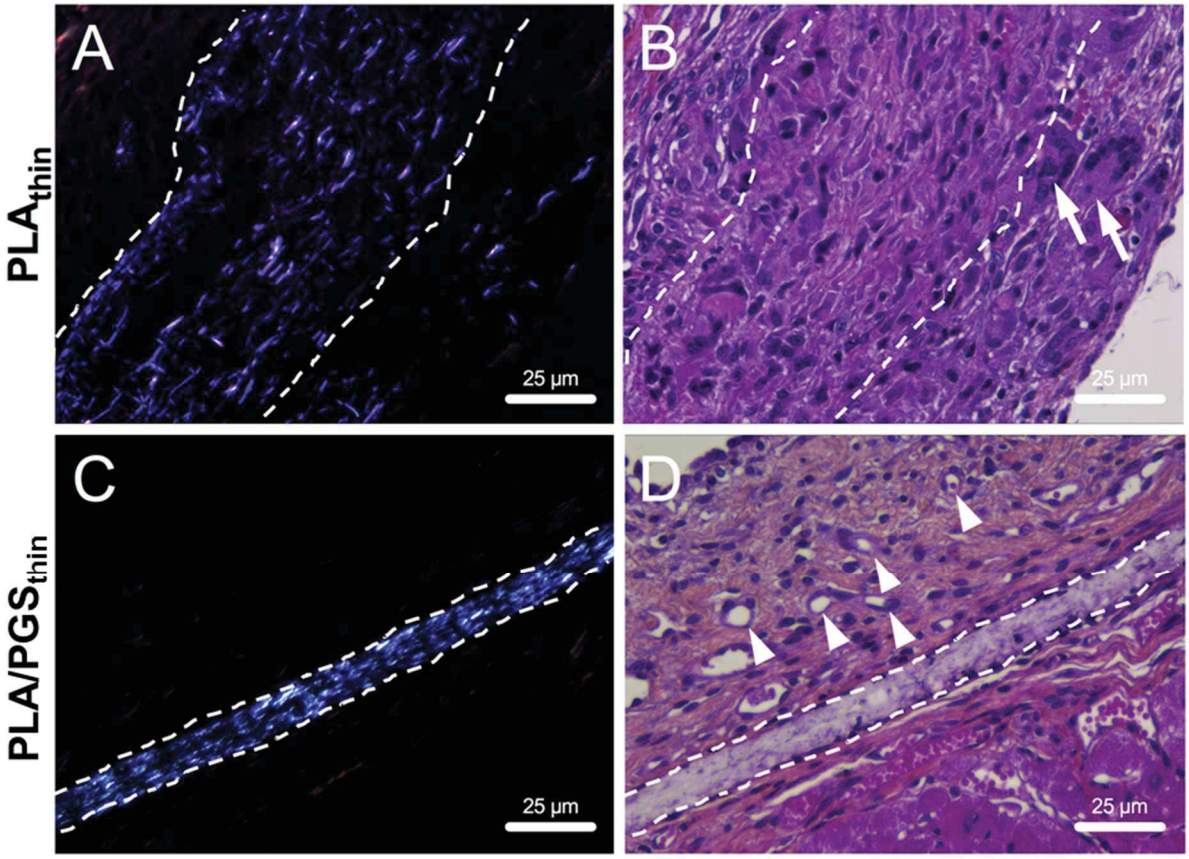

Figure 3.17. ***Biocompatibility of the PLA and PLA/PGS mats after implantation on the surface of the heart of healthy mice***. The integrity of the mats was visualized by **(A and C)** polarized microscopy and **(B and D)** hematoxylin-eosin staining after 28 days of implantation of acellular **(A-B)** PLA_{thin} and **(C-D)** PLA/PGS_{thin} cured at 120°C mats. Arrows indicate the accumulation of multinucleated giant cells and arrowheads indicate capillaries. White dot lines represent grafted mats.

4. Discussion

PGS is an attractive biopolymer for biological applications, especially for the cardiac bioengineering due to its Young's modulus matching heart's stiffness and its *in vitro* and i*n vivo* compatibility [29]. However, PGS processing remains quite challenging by its thermoset elastomer properties. In the current study, PLA/PGS blend electrospun nanofibers were fabricated with varying parameters to evaluate the effect of fiber diameter and annealing temperature on the *in vitro* and *in vivo* cardiac response for bioengineering applications.

Thus, it was shown that PLA/PGS_{thin}, especially cured at 120°C, support the spreading and the infiltration of the cardiomyocytes after 6 days of culture. This result is in accordance with the hydrophilicity of the membranes, PLA/PGS_{thin} materials being slightly more hydrophilic. This allows a better interaction with Matrigel, which is confirmed by the absence of visible Matrigel film between PLA/PGS fibers, whereas such film is visible at the surface of PLA fibers. Matrigel is a protein mixture of laminin, collagen IV, entactin, collagen and heparin sulfate proteoglycan and some growth factors, which has been shown to improve the cardiac markers and the properties of neonatal rat cardiomyocytes on a scaffold [30]. Consequently, the improved Matrigel coating and penetration in the PLA/PGS_{thin} mats allow a better material-cells interaction and promote cells infiltration by contrast to PLA fibers.

The curing condition at 90°C does not improve the cells spreading on the mats in comparison to curing at 120°C despite a higher hydrophilicity matching with Matrigel-coated mats. This result can be due to a less complete crosslinking reaction, meaning more unreacted carboxylic acids. Yet, these acids are identified as responsible for PGS cytotoxicity [31]. Surprisingly, PLA/PGS_{thick} scaffolds allow less cardiomyocytes spreading, whereas chemical composition is similar to PLA/PGS_{thin} mats. The slightly higher aCA measured for the thick fibers would not explain this difference, because we think that this increase is explained by the roughness of the materials rather than the hydrophilicity of the material in the fibers. Beside, tensile tests revealed a higher stiffness for PLA/PGS_{thin} mats whereas lower substrate stiffness should be better for cardiac cells culture [32]. Despite the fact that the moduli measured here correspond to the deformation of the whole fibrous mats, and not to the stiffness perceived by the cells, the crystallinity measurements confirm that the thin fibers themselves are certainly more rigid. The differences in the mechanical properties should thus not explain the different behavior of cells. The result should actually be also explained by thinner size of the fibers which enhance cardiomyocytes spreading.

The application of a scaffold in cardiac tissue engineering requires a biocompatibility including low immune response associated to increased vascularization to support the loss of tissue. Furthermore, cardiac remodeling after myocardial infarction is a dynamic process, but most of the geometric changes of left ventricle occur within the first weeks. Certainly, the integrity of the scaffold is necessary during this remodeling period, but after that, it should gradually degrade.

In this study, experiments show that pure PLA fibers have diffuse structure with cell infiltration. This phenomenon can be easily understood thanks to the SEM observation (Figure 3.3.(A)). Indeed, fibers are visibly less attached together in comparison to PLA/PGS fibers, were some melted pPGS connect fibers together. However, the tissue formed inside the scaffold is few vascularize and comprise inflammatory cells. The presence of mononuclear cells with the accumulation of multinucleated giant cells at the grafted area after 28 days indicates also a chronic immune response against the mats. By contrast, the inflammatory response is weaker for PLA/PGS_{thin} cured at 120°C mats, despite a very low cell infiltration. Its better biocompatibility can again be explained by its higher hydrophilicity, parameter known to have a better tolerance to the organ host [33]. No *in vitro* or *in vivo* degradation studies were conducted in this work. It has been shown previously that the degradability rate of PGS were too fast for the cardiac remodeling process with complete absorption in 1 to 2 months [26]. However, we demonstrate that, even with PGS as one of the component, the scaffold kept a good integrity during 28 days, indicating its suitability for cardiac tissue engineering.

5. Conclusion

In this work, potential scaffolds for cardiac tissue engineering were prepared by blend electrospinning of PLA/pPGS. A sufficient curing of the mats (2 days at 120°C) leads to a low cytotoxicity of the scaffolds. It is regrettable that no investigation was done in order to determine whether transesterification happens between PGS and PLA during curing, conducting to another polyester structure. No literature about this subject was found. Curing also induces the crystallization of the PLA and thus the stiffening of the material, but this allows a good resistance to sterilization by autoclave. This feature is very interesting as it can render easier the implementation of such devices. The presence of PGS increases the hydrophilicity and contributes to a better functionalization by Matrigel. However, the addition of 40% of PGS does not increase significantly the hydrophilicity of the mats in comparison to mats with only 30% of PGS. PLA/PGS Matrigel-coated scaffolds allow better cardiomyocytes spreading and penetration. Results are better for thin fibers (500 nm in average diameter) than for thick fibers (diameter of 1500 nm). Additionally, PLA/PGS_{thin} grafted scaffolds give a lower inflammatory response associated with an increased capillarization in comparison to pure PLA scaffolds, pointing out that the first is the best candidate for cardiac tissue engineering. All these biological results were difficult to justify by the mechanical properties of the materials, as the global properties of the fibrous mats were measured here, and not the surface properties perceived by the cells. Local mechanical tests at the surface of the fibers, for example with AFM technic, could thus be of great interest. Actually, with the process strategy chosen here, the scaffold shows no elastomeric behavior. However, the surface of the scaffold could be elastomeric thanks to PGS. Finally, the ability of PLA/PGS_{thin} membranes cured at 120°C to help the regeneration of a defective heart should be tested in future experiments.

References

1. Migliaresi, C.; Cohn, D.; Lollis, A.D.; Fambri, L. Dynamic mechanical and calorimetric analysis of compression-molded PLLA of different molecular weights: Effect of thermal treatments. *J. Appl. Polym. Sci.* **1991**, *43*, 83–95.
2. Lasprilla, A.J.R.; Martinez, G.A.R.; Lunelli, B.H.; Jardini, A.L.; Filho, R.M. Poly-lactic acid synthesis for application in biomedical devices — A review. *Biotechnology Advances* **2012**, *30*, 321–328.
3. Saini, P.; Arora, M.; Kumar, M.N.V.R. Poly(lactic acid) blends in biomedical applications. *Advanced Drug Delivery Reviews* **2016**, *107*, 47–59.
4. Yan, Y.; Sencadas, V.; Jin, T.; Huang, X.; Chen, J.; Wei, D.; Jiang, Z. Tailoring the wettability and mechanical properties of electrospun poly(l-lactic acid)-poly(glycerol sebacate) core-shell membranes for biomedical applications. *J. Colloid Interface Sci.* **2017**, *508*, 87–94.
5. Yan, Y.; Sencadas, V.; Zhang, J.; Wei, D.; Jiang, Z. Superomniphilic Poly(glycerol sebacate)–Poly(l-lactic acid) Electrospun Membranes for Oil Spill Remediation. *Adv. Mater. Interfaces* **2017**, *4*, 1700484.
6. Xu, B.; Rollo, B.; Stamp, L.A.; Zhang, D.; Fang, X.; Newgreen, D.F.; Chen, Q. Non-linear elasticity of core/shell spun PGS/PLLA fibres and their effect on cell proliferation. *Biomaterials* **2013**, *34*, 6306–6317.
7. Xu, B.; Li, Y.; Fang, X.; Thouas, G.A.; Cook, W.D.; Newgreen, D.F.; Chen, Q. Mechanically tissue-like elastomeric polymers and their potential as a vehicle to deliver functional cardiomyocytes. *J. Mech. Behav. Biomed. Mater.* **2013**, *28*, 354–365.
8. Xu, B.; Cook, W.D.; Zhu, C.; Chen, Q. Aligned core/shell electrospinning of poly(glycerol sebacate)/poly(l-lactic acid) with tuneable structural and mechanical properties. *Polym. Int.* **2016**, *65*, 423–429.
9. Kafouris, D.; Kossivas, F.; Constantinides, C.; Nguyen, N.Q.; Wesdemiotis, C.; Patrickios, C.S. Biosourced Amphiphilic Degradable Elastomers of Poly(glycerol sebacate): Synthesis and Network and Oligomer Characterization. *Macromolecules* **2013**, *46*, 622–630.
10. Li, X.; Hong, A.T.-L.; Naskar, N.; Chung, H.-J. Criteria for Quick and Consistent Synthesis of Poly(glycerol sebacate) for Tailored Mechanical Properties. *Biomacromolecules* **2015**, *16*, 1525–1533.
11. Herrero-Herrero, M.; Gómez-Tejedor, J.A.; Vallés-Lluch, A. PLA/PCL electrospun membranes of tailored fibres diameter as drug delivery systems. *European Polymer Journal* **2018**, *99*, 445–455.
12. Jaafar, I.H.; Ammar, M.M.; Jedlicka, S.S.; Pearson, R.A.; Coulter, J.P. Spectroscopic evaluation, thermal, and thermomechanical characterization of poly(glycerol-sebacate) with variations in curing temperatures and durations. *J. Mater. Sci.* **2010**, *45*, 2525–2529.
13. Zhou, H.; Green, T.B.; Joo, Y.L. The thermal effects on electrospinning of polylactic acid melts. *Polymer* **2006**, *47*, 7497–7505.
14. Inai, R.; Kotaki, M.; Ramakrishna, S. Deformation behavior of electrospun poly(L-lactide-co-ε-caprolactone) nonwoven membranes under uniaxial tensile loading. *J. Polym. Sci. B* **2005**, *43*, 3205–3212.
15. Morel, A.; Domaschke, S.; Urundolil Kumaran, V.; Alexeev, D.; Sadeghpour, A.; Ramakrishna, S.N.; Ferguson, S.J.; Rossi, R.M.; Mazza, E.; Ehret, A.E.; et al. Correlating diameter, mechanical and structural properties of poly(l-lactide) fibres from needleless electrospinning. *Acta Biomaterialia* **2018**, *81*, 169–183.
16. Ribeiro, C.; Sencadas, V.; Costa, C.M.; Gómez Ribelles, J.L.; Lanceros-Méndez, S. Tailoring the morphology and crystallinity of poly(L-lactide acid) electrospun membranes. *Sci. Technol. Adv. Mater.* **2011**, *12*.
17. Chen, Q.; Liang, S.; Thouas, G.A. Elastomeric biomaterials for tissue engineering. *Progr. Polym. Sci.* **2013**, *38*, 584–671.
18. Tsuji, H.; Ikada, Y. Properties and morphologies of poly(l-lactide): 1. Annealing condition effects on properties and morphologies of poly(l-lactide). *Polymer* **1995**, *36*, 2709–2716.
19. D'Sa, R.A.; Raj, J.; Dickinson, P.J.; McCabe, F.; Meenan, B.J. Human Fetal Osteoblast Response on Poly(Methyl Methacrylate)/Polystyrene Demixed Thin Film Blends: Surface Chemistry Vs Topography Effects. *ACS Appl. Mater. Interfaces* **2016**, *8*, 14920–14931.
20. Kitsara, M.; Blanquer, A.; Murillo, G.; Humblot, V.; Vieira, S.D.B.; Nogués, C.; Ibáñez, E.; Esteve, J.; Barrios, L. Permanently hydrophilic, piezoelectric PVDF nanofibrous scaffolds promoting unaided electromechanical stimulation on osteoblasts. *Nanoscale* **2019**, *11*, 8906–8917.

21. Szewczyk, P.K.; Ura, D.P.; Metwally, S.; Knapczyk-Korczak, J.; Gajek, M.; Marzec, M.M.; Bernasik, A.; Stachewicz, U. Roughness and Fiber Fraction Dominated Wetting of Electrospun Fiber-Based Porous Meshes. *Polymers* **2019**, *11*, 34.
22. Kurusu, R.S.; Demarquette, N.R. Wetting of Hydrophilic Electrospun Mats Produced by Blending SEBS with PEO–PPO–PEO Copolymers of Different Molecular Weight. *Langmuir* **2016**, *32*, 1846–1853.
23. Lee, K.H.; Kim, H.Y.; Ryu, Y.J.; Kim, K.W.; Choi, S.W. Mechanical behavior of electrospun fiber mats of poly(vinyl chloride)/polyurethane polyblends. *Journal of Polymer Science Part B: Polymer Physics* **2003**, *41*, 1256–1262.
24. Tandon, V.; Zhang, B.; Radisic, M.; Murthy, S.K. Generation of tissue constructs for cardiovascular regenerative medicine: from cell procurement to scaffold design. *Biotechnol. Adv.* **2013**, *31*, 722–735.
25. Chen, Q.-Z.; Bismarck, A.; Hansen, U.; Junaid, S.; Tran, M.Q.; Harding, S.E.; Ali, N.N.; Boccaccini, A.R. Characterisation of a soft elastomer poly(glycerol sebacate) designed to match the mechanical properties of myocardial tissue. *Biomaterials* **2008**, *29*, 47–57.
26. Stuckey, D.J.; Ishii, H.; Chen, Q.-Z.; Boccaccini, A.R.; Hansen, U.; Carr, C.A.; Roether, J.A.; Jawad, H.; Tyler, D.J.; Ali, N.N.; et al. Magnetic Resonance Imaging Evaluation of Remodeling by Cardiac Elastomeric Tissue Scaffold Biomaterials in a Rat Model of Myocardial Infarction. *Tissue Engineering Part A* **2010**, *16*, 3395–3402.
27. Langer, R.; Vacanti, J.P. Tissue engineering. *Science* **1993**, *260*, 920–926.
28. Tajbakhsh, S.; Hajiali, F. A comprehensive study on the fabrication and properties of biocomposites of poly(lactic acid)/ceramics for bone tissue engineering. *Materials Science and Engineering: C* **2017**, *70*, 897–912.
29. Chen, Q.-Z.; Ishii, H.; Thouas, G.A.; Lyon, A.R.; Wright, J.S.; Blaker, J.J.; Chrzanowski, W.; Boccaccini, A.R.; Ali, N.N.; Knowles, J.C.; et al. An elastomeric patch derived from poly(glycerol sebacate) for delivery of embryonic stem cells to the heart. *Biomaterials* **2010**, *31*, 3885–3893.
30. Park, H.; Radisic, M.; Lim, J.O.; Chang, B.H.; Vunjak-Novakovic, G. A novel composite scaffold for cardiac tissue engineering. *In Vitro Cell. Dev. Biol. Anim.* **2005**, *41*, 188–196.
31. Li, Y.; Cook, W.D.; Moorhoff, C.; Huang, W.-C.; Chen, Q.-Z. Synthesis, characterization and properties of biocompatible poly(glycerol sebacate) pre-polymer and gel. *Polym. Int.* **2012**, *62*, 534–547.
32. Bhana, B.; Iyer, R.K.; Chen, W.L.K.; Zhao, R.; Sider, K.L.; Likhitpanichkul, M.; Simmons, C.A.; Radisic, M. Influence of substrate stiffness on the phenotype of heart cells Available online: http://onlinelibrary.wiley.com/doi/abs/10.1002/bit.22647 (accessed on Jun 26, 2019).
33. Franz, S.; Rammelt, S.; Scharnweber, D.; Simon, J.C. Immune responses to implants – A review of the implications for the design of immunomodulatory biomaterials. *Biomaterials* **2011**, *32*, 6692–6709.

CHAPTER 4

Elaboration of elastomeric fibers

Despite promising results found with the composite fibers presented in the previous chapter, we can infer that our scaffolds intended for cardiac tissue engineering could be improved if they had elastomeric properties. To reach this goal, it is essential to eliminate the carrier polymer after crosslinking in order to keep pure PGS fibers.

In the present chapter, polyvinylpyrrolidone and hydroxypropyl-β-cyclodextrin are used as carrier material. Diverse strategies will be tested. The composition of the final membranes will be analyzed and their mechanical properties will be tested at dry and wet state. These fibers will be compared to PGS fibers prepared by a similar method found in the literature using polyvinylalcohol as carrier polymer, to highlight the interest of our new strategy.

Elaboration of elastomeric fibers[1]

In the previous chapters, it was shown that to obtain nanofibers composed of crosslinked PGS, it is essential to use a carrier polymer able to provide entanglements in electrospinning solution and to keep the fibrous structure during thermal crosslinking of the elastomer. The method presented in Chapter 3 gives interesting results; however, it does not allow fabricating materials with mechanical properties close to myocardium's ones. Interesting PGS properties can indeed not be expressed if PGS is mixed with a rigid carrier polymer. In order to get an elastomeric nanofibrous membrane, the carrier polymer should be removed. The latter is sacrificial and is only employed for the formation and support of the fibrous structure. In Chapter 1, an example was described where PLA/PGS fibers were fabricated and cured and PLA was removed to get fibers composed of only PGS [1]. Chloroform, a toxic solvent, was however used to dissolve PLA. In order to get more satisfying results, it is thus necessary to use a carrier polymer soluble in solvents with low toxicity, such as water or ethanol.

In the present chapter, the strategy is the following: first, pPGS is electrospun with a carrier material soluble in water. Then the fibers can be cured while the fibers shape is kept thanks to the carrier material. And finally, the fibers containing crosslinked PGS are purified by washing in water.

1. State of the art and objectives

Several examples of similar strategies can be found in the literature. A few teams chose polyvinyl alcohol (PVA) as carrier polymer, a water-soluble and biocompatible polymer having a high melting temperature (between 160 and 200°C depending on the degree of saponification). Xu *et al.* [2] used PVA with coaxial electrospinning with a PGS core and a PVA shell. After electrospinning, the fibers were cured and the shell was dissolved in hot water. The result is still a fibrous material, but fibers are surrounded by a discontinuous film (Figure 4.1.(A)). To confirm the PVA removal, infra-red and DSC analysis were done. Analysis showed that PVA was only partially removed, but quantification remains tricky, especially on infra-red spectrum where characteristic peaks of both components overlap. However, the mechanical behavior evolves after washing, the membrane becoming less rigid. This result confirms the removal of a part of the PVA, the latter being a rigid thermoplastic [3]. Moreover, the purified membrane becomes softer when hydrated, the Young's modulus decreasing from 35 MPa to 2 MPa. The authors

[1] This chapter was achieved with the participation of Özgün Uyumaz, master student under my supervision. In particular, he fixed some parameters identified as key parameters for electrospinning of pPGS/PVP/HPβCD blends.

explain this result by the plasticization of remaining PVA and lubrication of the fibers by water. The resilience was calculated from the stress-strain curve as the following ratio:

$$Resilience = \frac{area\ under\ unloading\ curve}{area\ under\ loading\ curve}$$

It corresponds to the proportion of energy recovered by the material after stretching: a perfectly elastic material has a resilience of 100%. Results show here that energy is better restored when the material is hydrated (resilience higher than 95% on average). It can also be noticed that resilience is lower during the first cycle stretching-releasing than for the following cycles. It indicates an irreversible modification of the structure of the material, for example the rupture of the remaining PVA areas. Lastly, the authors confirmed the low cytotoxicity of these PGS membranes where some PVA remains.

These first results are interesting, but coaxial process raises some drawbacks: it is difficult to scale-up and the proportion of both polymers are not totally controlled. Blend electrospinning is easier to implement. This method was used by Jeffries *et al.* [4] who mixed pPGS and PVA. After electrospinning, the fibers were cured at various temperatures and during various periods of time. They were then purified by washing in water to remove the PVA, then in ethanol to remove remaining monomers and pPGS oligomers. Several formulations were tested but best results were obtained for a PGS/PVA ratio of 55/45. Indeed, it is essential to have enough PGS to keep a fibrous structure after washing. A sufficient quantity of PVA is also crucial to hinder the fusion of the fibers during curing. The crosslinking step plays also an important role as the more crosslinked PGS is, the better fibers' morphology is preserved. After optimization, this method allows the fabrication of continuous fibers (Figure 4.1.(B)). However, more than 55% of the initial mass remains after washing, showing that some PVA remains. This was confirmed, but not quantified, by infra-red and DSC analyses. It can be explained by several factors, such as an "entanglement" of PVA in the PGS network or the possible reaction between the –OH groups of PVA and the –COOH groups of PGS. By the way, more PVA remains when the crosslinking reaction is pushed further. Crosslinking has also an effect on mechanical properties, measured here at wet state. The Young's modulus, strain at break and UTS increase from 100 kPa, 800%, and 0.8 MPa for the less crosslinked material to 800 kPa, 200% and 1.4 MPa for the most crosslinked. Despite the remaining rigid PVA, the membranes have an elastomeric behavior adequate for soft tissue applications. Moreover, cytocompatibility tests show that the remaining traces of PVA do not alter biocompatibility of these materials. Finally, these materials totally resorb after 14 days of subcutaneous implantation demonstrating their potential for biomedical application.

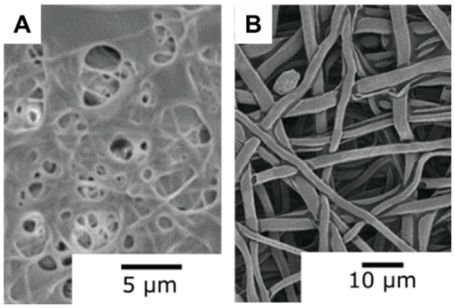

Figure 4.1. PGS fibers obtain with the help of PVA **(A)** by coaxial electrospinning [2] and **(B)** by blend electrospinning [4].

In summary, on one hand, coaxial method allowed to fabricate a material based on PGS but containing traces of PVA and poorly fibrous. The process is difficult to implement. On the

other hand, blend method is easier and gives better results in term of morphology, but it is difficult to find a common solvent for PGS and PVA. In the example described above, HFIP is used, which is an expensive and toxic solvent. About this point, Saudi *et al.* [5] proposed a method where PGS and PVA are solubilized together in DMF and water, but they did not purified their fibers after curing (see Chapter 1). In addition, the drawback of all these methods is the presence of alcohol groups on PVA which can be covalently bonded to PGS during the curing step. Thus, PVA removal is difficult and the final properties of the material could be altered. A carrier polymer that may not react with PGS would be preferable.

In the present study, polyvinylpyrrolidone (PVP) was chosen as carrier polymer because it has a T_g of 180°C, it is water soluble and presents no reactive sites for PGS. Moreover, it is approved by the FDA for biomedical applications. PVP was already used with pPGS in blend electrospinning by Keirouz *et al.* [6] to prepare fibers with up to 40% of pPGS. But in this work, the authors did not try to fully crosslink PGS. Our work dealt with the elaboration of crosslinked PGS fibers. Thus, different strategies using PVP as a carrier polymer were explored such as coaxial and blend electrospinning. The addition of hydroxypropyl-β-cyclodextrin (HPβCD), a biocompatible oligosaccharide having a high temperature of degradation (278°C) was also studied. Indeed, HPβCD is known to have the ability to stabilize the electrospinning process [7–9]. Cyclodextrins can form fibers by electrospinning thanks to the formation of aggregates replacing entanglements. Besides, their cavity can be exploited to encapsulate drugs by host-guest inclusion complexes [10]. The effect of the curing step on the final fiber morphology and mechanical properties of the resulting membranes was carefully studied in dry and wet states in order to establish their suitability for soft tissue engineering. The properties were also compared to mats made from a blend PVA/pPGS.

2. Materials and methods

2.1. Materials

Polyvinylpyrrolidone (PVP, 1300000g/mol, Aldrich), hydroxypropyl-β-cyclodextrin (HPβCD (degree of substitution: 2 to 6), 97%, Acros Organics), dimethylformamide (DMF, >99.8%, Sigma-Aldrich), absolute anhydrous ethanol (>=99,9%, Carlo Erba), tetrahydrofuran (THF, 99%, Sigma-Aldrich) and 1,1,1,3,3,3-hexafluoro-2-propanol (HFIP, >99.0%, TCI Chemicals) were used as received. Poly(vinylalcohol) (PVA, Gohsenol® EG-05PW, saponification value 86.5-89.0 %mol) was generously donate by Nippon Gohsei™ and used as received. Glycerol (>99.96%, Fisher Chemicals) and sebacic acid (98%, ACROS Organics) were employed to synthesized pPGS in various conditions according to the microwave procedure presented in Chapter 2. Details are given for the synthesis of the pPGS employed for the final materials.

2.2. Method for blend electrospinning

2.2.1. Optimization of the formulation of pPGS/HPBCD/PVP electrospinning solutions

Preliminary experiments were necessary to identify the optimal electrospinning conditions. A first experiment of blend electrospinning (BlendP) was carried out by mixing pPGS with only PVP. For this experiment, a pPGS 2/3 with a DE of 73% was used. It was dissolved in a solvent mixture DMF/ethanol 3/7 (w/w) with PVP. The final concentrations were 3 wt% for pPGS and 7 wt% for PVP. Solvents and concentrations were selected after optimization of the formulation.

A vertical home-made electrospinning set-up with a cylindrical rotating collector covered by an aluminum foil was used. A 18 gauge needle 15 cm away from the collector was fed by the solution at 0.4 mL/h by a syringe pump (PHD 2000, Hardvard Apparatus). High voltage was applied to the needle (10 kV) by a power supply (SL10, Spellman). The membrane was produced after 1h45 of electrospinning.

Next experiments were carried out using PVP and HPβCD as carrier materials. Several experiments detailed in Appendix 2 allowed identifying the best type of pPGS: a pPGS synthesized from a G/SA ratio equal to 2/3 and a DE of 72%.

Experiments were then conducted with this kind of pPGS, PVP, and various proportions of HPβCD. The compositions of the solutions are summarized in the Table 4.1. Samples are named CDX with X the percentage of HPβCD in the solid expressed in percentage of weight by total weight of solid. For each case, the total concentration of solid in the solutions was 13 wt% and the PGS content in the solid was fixed at 50%. PVP and HPβCD represent thus 50% of the solid too. Here, only the ratio PVP/HPβCD was changed, by testing different HPβCD content in the solid (X). The solvent was kept the same as for PVP/pPGS fibers: DMF/ethanol 3/7.

Table 4.1. Composition of electrospinning solutions in DMF/ethanol 3/7 (w/w). All percentages are expressed as weight of solid over total weight of solution.

	CD0	**CD5**	**CD10**	**CD15**	**CD20**	**CD25**
%pPGS in solution	6.5%	6.5%	6.5%	6.5%	6.5%	6.5%
%HPβCD in solution	0%	0.65%	1.3%	1.95%	2.6%	3.25%
%PVP in solution	6.5%	5.85%	5.2%	4.55%	3.9%	3.25%

In order to verify the electrospinnability of the blends a home-made horizontal electrospinning set-up was used. One metallic 18 gauge needle was fed with the solution at 1.2 mL/h. The collector was placed 16 cm from the tip of the needle and rotated at 150 rpm. High voltage was applied to the collector (-2 kV) and to the needles (10-11 kV). Samples were electrospun during 10 minutes. If the process was stable and allowed the formation of continuous fibers, samples were produced during 1h30 to get thick enough membranes detachable from the collector covered by backing paper.

2.2.2. Preparation of elastomeric mats

Synthesis and characterization of the prepolymer (pPGS)

PGS was synthesized from a ratio G/SA 2/3 by microwave heating. Briefly, 6.987 g (75.9 mmol, 2 equivalents) of glycerol, 23.013 g (113.9 mmol, 3 equivalents) of sebacic acid and a stirrer bar were introduced in a 100 mL round-bottomed flask. A glass extender tube finished by an open glass stopcock was connected to the flask's opening to let the water vapors to quite the reactor. The flask was placed in a microwave oven (Discover SP, CEM) and heated at 150°C with a maximal power of 200 W. After 400 minutes at 150°C, a pale-yellow liquid is obtained. After cooling to room temperature, pPGS was pasty. The flask was placed under vacuum less than 1 hour to evaporate excess of water without important loss of potential remaining glycerol. Sample was taken for ^{1}H NMR (400 MHz, Bruker) analysis in d-DMSO: DE value was measured at 72%. This pPGS was used for the preparation of the elastomeric mats that were characterized in this study.

Electrospinning of pPGS/PVP/ HPβCD blends (CD25)

The formulation with 25% of HPβCD gave the most fibrous final result. It was thus chosen to prepare large membranes, suitable for characterization. In order to prepare homogenous samples, a home-made vertical electrospinning set-up including a cylindrical rotating collector and translating needles was used. Two metallic 18 gauge needles were fed with the solution at 2.4 mL/h. The collector was placed 15 cm above the tip of the needles and rotated at 150 rpm. High voltage was applied to the collector (-5 kV) and to the needles (14 kV). Samples were electrospun during 5h. The collector was covered by backing paper to facilitate the detachment of the mat.

Electrospinning of pPGS/PVA blends (PVA50)

This study aims to compare samples prepared from a pPGS/HPβCD/PVP blend with samples prepared from a pPGS/PVA blend. Fibrous mats with 50 wt% of pPGS and 50 wt% of PVA were thus electrospun, with a procedure adapted from Bellani *et al.* [11]. This method, given in appendix 3, was developed in our team with my collaboration for the synthetic aspects. It was used to fabricate tubular scaffolds for vascularization of 3D engineered tissues.

PVA is soluble in water but not in most organic solvents. As pPGS is poorly soluble in water, HFIP was chosen as common solvent for pPGS/PVA blend. Solutions were prepared with 3.2 wt% of pPGS and 3.2 wt% of PVA in HFIP.

The same electrospinning set-up was used as for pPGS/HPβCD/PVP samples. The distance between the needles and the collector was fixed at 18 cm and the applied voltage at 25 kV at the needles and -1 kV at the collector. The solution was infused at 2.0 mL/h at each syringe. Because of its low stability, the process was stopped after 1h but it was enough to obtain detachable and easy to handle samples. All other parameters were kept the same as for pPGS/HPβCD/PVP. These samples containing 50% of PVA were named PVA50.

2.3. Method for coaxial electrospinning

For coaxial process, pPGS was solubilized in a good solvent (THF or ethanol) to reach high concentrations of about 50 wt% for the core. Shell solutions were prepared by dissolution of PVP and optionally HPβCD in DMF/ethanol 3/7. Samples were electrospun using a home-made vertical electrospinning set-up equipped with a coaxial needle 20 cm away from a flat collector covered by an aluminum foil. The inner channel of the coaxial needle is an 18 gauge needle and is fed by the pPGS solution at about 0.5 mL/h by a syringe pump (PHD 2000, Hardvard Apparatus). The outer channel has an inner diameter of 2 mm and an outer diameter of 4 mm and is fed by the shell solution at about 2.5 mL/h. High voltage was applied to the needle (10-12 kV) by a power supply (SL10, Spellman). Experiments were conducted during 2 hours. Thick, stretchable and sticky samples were obtained. Parts of them could be peel-off and post-treated.

In the coaxial process, the relative proportion in percentage of the core component and the shell component depends on the concentration of the corresponding solutions and on the injection flow rates. For each experiment condition, the following ratio can be calculated:

$$R_{core}(\%) = \frac{Q_c C_c}{Q_s C_s + Q_c C_c} \times 100$$

with Q_c, C_c and Q_s, C_s the flow rates in mL/h and % of pPGS in the core solution (c) and of PVP in the shell solution (s).

The results given in the following sections are for two experiments named CoaxP and CoaxCD. CoaxP corresponds to a pure PVP shell; CoaxP for a PVP/HPβCD shell. The conditions used for the process are given in Table 4.2.

Table 4.2. Electrospinning parameters used to prepare coaxial fibers.

	CoaxP	**CoaxCD**
Core solution	50% of pPGS in ethanol injected at 0.4 mL/h	56% of pPGS in THF injected at 0.5 mL/h
Shell solution	15% of PVP in DMF/ethanol injected at 2.4 mL/h	7% of PVP / 7% of HPβCD in DMF/ethanol injected at 2.5 mL/h
R_{core}	35%	44%

2.4. Crosslinking of the PGS and purification of the fibers

In this work, the objective was pure crosslinked PGS fibers. For this purpose, it was necessary to cure the membranes after electrospinning. They were peeled and cut in the appropriate shape to be placed between two frames tight together before being placed in a vacuum oven. This preparation aims to limit membrane shrinkage during curing. Without the frames, fibers are free to get closer and they tend to merge together. The hold membranes were put in a pre-heated vacuum oven (Vacutherm VT6025, Fisher Scientific). The curing step was then conducted under a pressure bellow 10^{-2} mbar with different curing conditions. Parameters of each experiment are given in the results part. Globally, incremental curing schemes were preferred. Curing starts usually at 120°C. At this temperature, pPGS viscosity is very low. It would flow out of the fibers if the carrier material could not give a sufficient support. But this temperature triggers the crosslinking reaction. After a first step at 120°C, PGS is partially crosslinked and its viscosity is higher. It is then possible to increase the temperature in order to accelerate the reaction until getting a fully crosslinked elastomer.

Different curing schemes were tested for preliminary experiments. Two schemes were selected for final elastomeric membranes: a short one with a maximal reached temperature of 140°C named C_{short} (24h at 120°C followed by 48h at 140°C) and a long one with a maximal temperature of 170°C named C_{long} (24h at 120°C followed by 48h at 140°C and 24h at 170°C). The effect of each was compared.

When the crosslinking is achieved, fibers can be purified by removal of the carrier material. For this, samples were immersed in gently stirred osmosed water. After 1h, 2h30 and 19h of immersion, the water was changed and the membranes were rinsed. After 24h of washing, they were dried overnight under vacuum.

2.5. Characterization of PGS-based mats

The surface of the as spun, cured, and cured and washed mats was observed by scanning electron microscopy (SEM) after coating by a thin layer of gold. The SEM (Vega 3, Tescan) was used in high vacuum mode with a voltage of 5 kV. Mean diameter of the as spun fibers on CD25 and PVA50 samples was calculated over 100 diameters measurements using ImageJ software. The mean values are given with the standard deviation.

The efficiency of the purification was first evaluated by measuring the mass loss after washing. Attenuated Total Reflectance-Fourier Transform Infrared (ATR-FTIR) spectroscopic analyses were also performed (Nicolet 380, Thermo Fisher) before and after washing to characterize the evolution of the composition. Results were compared to raw materials' spectra.

The mechanical properties of not cured, cured, and purified (after crosslinking and washing in water) mats were characterized at dry state by uniaxial tensile tests using the Linear Tension Geometry of a rheometer (Discovery HR3, TA Instruments). Rectangular samples were cut with 5 mm width and about 20 mm long. Washed samples were also characterized at wet state after two days of immersion in osmosed water. Width and thickness were then measured after hydration. The samples were fixed in the clamps with an initial gap of 10 mm and then pre-loaded with an axial force of about 0.01 N. The gap after preloading was set as the initial length. The tensile tests were conducted at 150 μm/s until breaking. 5 measurements were performed for each type of samples except for some hydrated samples that were too difficult to handle to make measurements. Young's modulus was calculated as the slope of the curve in the initial (between 0 and 1% of deformation) linear part.

Cyclic tests were conducted on cured and washed samples at dry and wet state to evaluate elastic recovery. Specimens were cut and their dimensions measured in the same way than for tensile tests. After pre-loading, they were stretched at 150 μm/s until a strain of 15%, to be consistent with earlier works [2,12], 15% elongation being a typical value for cardiac muscle [13]. After stretching, samples were released at the same rate until 0% elongation to conclude one cycle, and a new cycle was started. The loading-release cycle was repeated 10 times.

Experiments were necessary to prove that some cyclodextrins remain in CD25 after washing and that their cavity can be used to encapsulate molecules of therapeutic interest. We chose here to test the ability of the membrane to remove methylene blue (MB) from a dye solution. Methylene blue is known to form host-guest inclusion complex with cyclodextrins [14–17]. 3 mg of membrane were immersed in 3 mL of a gently stirred MB solution concentrated at 10 mg/L. After 24h of soaking, the solution was analyzed by UV-vis spectroscopy (UV-2600, Shimadzu) and the spectrum was compared to the initial solution's one. Moreover, it was necessary to verify that the dye removal is not only due to adsorption on PGS. The spectrum from the solution obtained from soaking of CD25-C_{long} washed was thus compared to the result after soaking of PVA50-C_{long} washed.

Limited cell culture experiments were done on CD25-C. Patches cut in the membranes were sterilized by autoclave and pre-incubated by Matrigel. Newborn rat cardiomyocytes were seeded on the patches fixed in CellCrown™ with culture medium. After 3 days of culture, cells were observed by confocal laser scanning microscope. The cell culture and observation procedures were similar to the procedures used for PLA/PGS samples in Chapter 3[2].

[2] All biological characterizations were done by Pr. Agbulut's team in Institut de Biologie Paris-Seine.

3. Results and discussion

3.1. Towards the use of cyclodextrin for thermomechanical and potential drug-encapsulation properties

PVP was chosen as carrier polymer because of its high T_g (180°C). pPGS/PVP fibers were thus prepared by blend electrospinning (BlendP). It was possible to fabricate regular fibers with 70% of PVP and 30% of pPGS (Figure 4.2). The obtained mat was cured during 24h at 150°C. But even with such a low pPGS content, fibers do not resist to curing and merge together, closing the pores of the mat.

Coaxial fibers were then prepared (CoaxP) with a theoretical PGS amount R_{core} of 35%, indicating the presence of a theoretical quite thick shell. Large and slightly flat fibers were obtained (Figure 4.2). Despite the shell, after curing at 130°C, the fibers are merged together again, as shown on Figure 4.2.

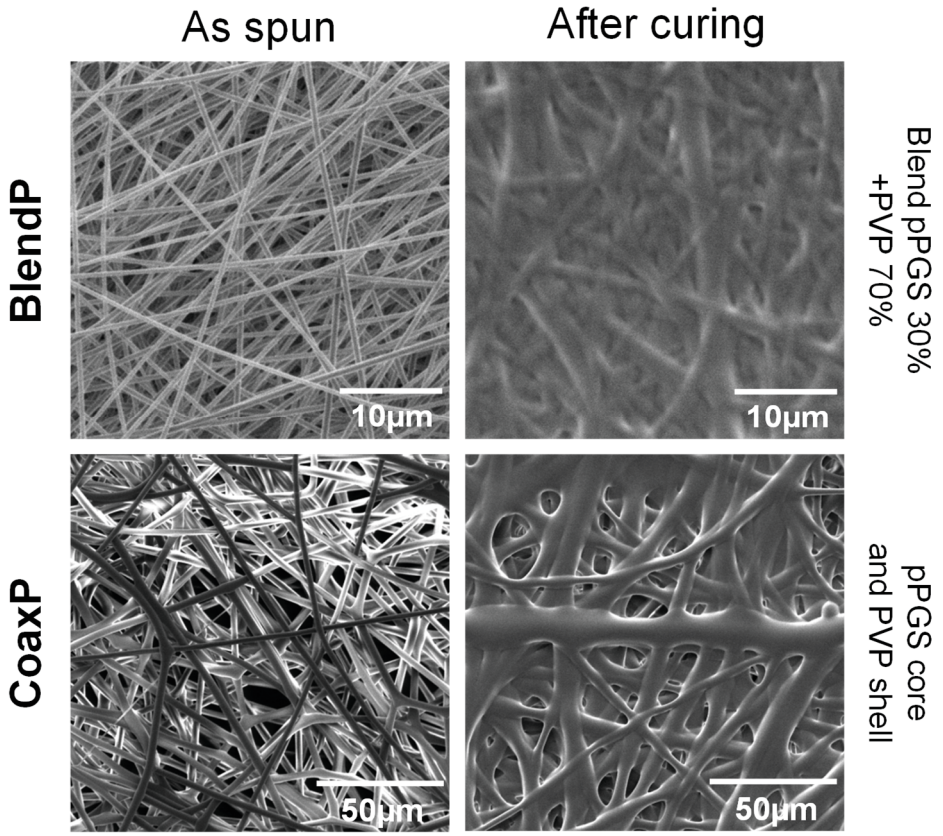

Figure 4.2. Illustration of the melting of pPGS/PVP fibers prepared by blend and coaxial electrospinning.

From these results, it was hypothesized that pPGS have the ability to plasticize PVP. This assumption was confirmed by DSC (3°C/min from -20 to 200°C) carried out on blend fibers containing 30% of pPGS. Indeed, a glass transition of 83°C was measured (Figure 4.3) whereas a T_g of 180°C was measured in the case of pure PVP. Thus, pPGS may increase the free volume of PVP leading to a glass transition of the pPGS/PVP composite lower than the curing temperature. PVP can thus not play its role of template polymer. Moreover, from coaxial results, it can be deducted that PVP and pPGS phases are not totally separated as the latter is able to

plasticize PVP. It was thus important to find another compound able to provide the support during the curing step.

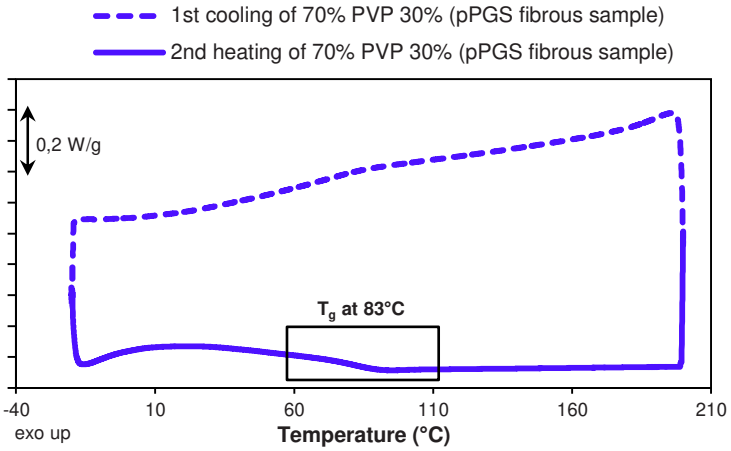

Figure 4.3. First cooling and second heating ramp for a fibrous sample with 70% of PVP and 30% of pPGS (3°C/min). It can be noticed that with this low prepolymer amount, signals corresponding to pPGS are not visible.

Consequently, it was proposed to select hydroxypropyl-β-cyclodextrin (HPβCD) as an interesting compound allowing the enhancement of the thermomechanical properties of pPGS/PVP fibers. Indeed, HPβCD is an FDA approved biocompatible molecule having a high degradation point of 278°C. Furthermore, HPβCD is known to have the ability to stabilize the electrospinning process [7–9]. Finally, HPβCD is a cyclic oligosaccharide made of 7 glucose units (see Figure 4.4) having a hydrophobic cavity which can be exploited to encapsulate drugs by host-guest inclusion complexes [10].

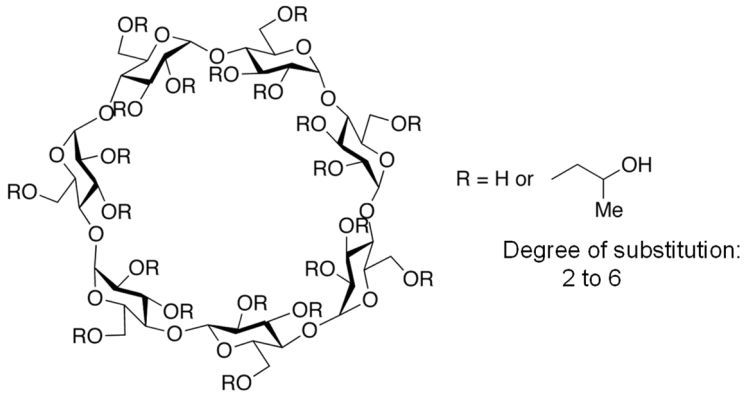

Figure 4.4. Chemical structure of hydroxypropyl-β-cyclodextrin.

3.2. Coaxial electrospinning with PVP/HPβCD as shell

Coaxial electrospinning was firstly studied to prepare PGS-based fibers. Shell composition was studied by adding various amounts of HPβCD in PVP solutions. Fibers were prepared with a PGS R_{core} value of 44%, the dry shell containing 50 wt% of PVP and 50 wt% of HPβCD. The electrospinning process was difficult because of the clogging of the needle that required a break to clean the tip every 20 to 25 minutes. After two hours of electrospinning, a thick and sticky membrane is fabricated. The as spun fibers are large (diameters between 1.5 µm and 3 µm were measured) and slightly flat. After curing (24h at 140°C and 72h at 170°C), melted pPGS does not close the pores (Figure 4.5). The fibers are however slightly fused together at the contact points.

Finally, after purification by washing in water to remove the carrier material, the membrane is still fibrous despite the presence of some closed pores (Figure 4.5).

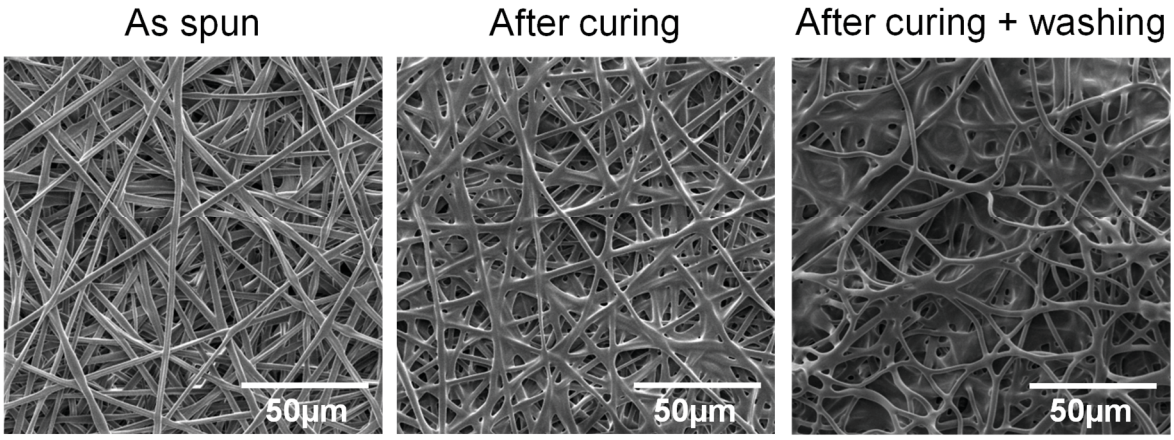

Figure 4.5. PGS-based membrane made from coaxial fibers with PVP and HPβCD in the shell (CoaxCD): as spun, after curing and after washing.

In these experiments, the presence of the carrier material in the shell could bring one advantage: it is more accessible and less closely mixed with PGS. Its removal by washing should be easy. The efficiency of the washing was evaluated by ATR-FTIR. The spectra obtained from the coaxial fibers just after electrospinning, after curing, and after washing were compared to pPGS, PVP and HPβCD spectra (Figure 4.6). Two areas of interest are considered. The first one corresponds to the elongation of C=O bonds (1650-1730 cm^{-1}): pPGS spectrum show characteristic peaks for acids at 1710 cm^{-1} and for esters at 1730 cm^{-1}. The same signal is visible for the as spun fibers, with a less clear acids peak. After curing, the peak is shifted to the left, confirming the esterification. These PGS peaks partially overlap PVP peak from amide C=O bond (1650 cm^{-1}) (Figure 4.6.(B)), making quantification impossible. The second interesting area includes the peaks for C–O in esters bonds (1160 cm^{-1}), C–O in HPβCD (1027 cm^{-1}), C–N in PVP (1287 cm^{-1}). Because of the overlapping of the peaks, it was difficult to quantify the presence of each component; however, evolution of intensities can be followed. The intensity of the peak at 1027 cm^{-1} clearly decreases relatively to PGS peak after washing (Figure 4.6.(C), showing that cyclodextrin was partially lost during the washing step. However, PVP peak at 1287 cm^{-1} did not clearly decrease relatively to PGS peak. Surprisingly, it seems that HPβCD was easier to wash away, despite the fact that cyclodextrin can be covalently bonded with PGS.

These experiments prove that coaxial electrospinning can be a solution for the preparation of elastomeric PGS-based fibers. However, its implementation is complicated because of the regular interruptions required during this process of coaxial electrospinning. Moreover, it is difficult to scale-up as a specific needle is required: no large-scale process like needless electrospinning can be intended. Finally, no clear benefits regarding the purification of the material could be identified. Efforts were thus focused in the following on blend electrospinning of pPGS, PVP and HPβCD.

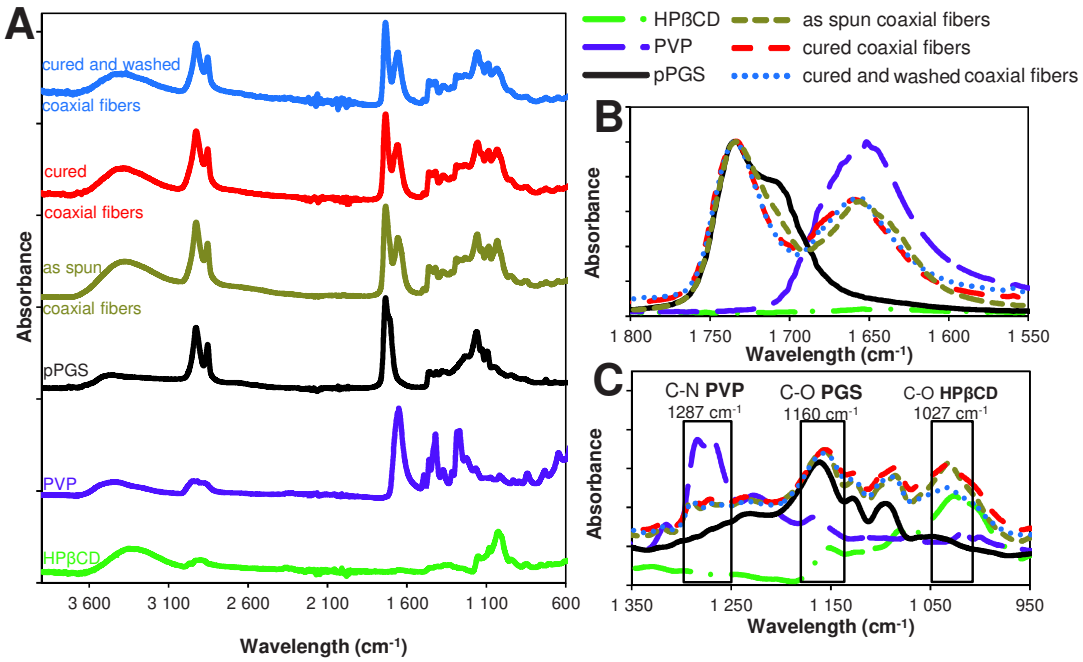

Figure 4.6. ***FTIR spectra of coaxial fibers just after electrospinning, after curing and after washing compared to HPβCD, PVP, and corresponding pPGS spectra.*** **(A)** Full spectra. **(B)** C=O peaks. **(C)** C–O and C–N peaks.

3.3. Optimization of blend electrospinning of pPGS/PVP/HPβCD

In order to prepare regular pPGS/PVP/HPβCD fibers able to withstand the curing step, the formulation of the solution had to be carefully adjusted. In particular, experiments were necessary to determine what type of pPGS should be used. These results are presented in appendix 2. They show that a pPGS synthesized from a G/SA ratio equal to 2/3 and a DE of 72%, corresponding to a $\overline{DP_n}$ of 7, allows the best result after curing. Indeed, this pPGS is close to the gel point; in this way, its viscosity increases fast and it does not flow out of the fibers during curing. The shape of the fibers is thus well preserved.

The proportion of each component (pPGS, PVP and HPβCD) in the fibers is also a crucial parameter. Indeed, it is interesting to increase the pPGS content as much as possible in order to improve the productivity in regard to PGS. Moreover, it was hypothesized that a sufficient proportion of PGS is required to create a continuous PGS network in the fibers able to resist after curing and washing.

On the other hand, a sufficient amount of carrier polymer is needed to keep the fibers shape during thermal treatment. Finally, electrospinning solutions parameters come into play at different levels: formation of the fibers during electrospinning, conservation of the fibrous structure during curing and persistence of the fibers after washing. With three components in the solutions, a lot of parameters must be taken into account: % of pPGS, % of PVP, % of HPβCD, total solid content and solvents mix.

For these reasons and according to other works [4], it was decided to fix the PGS content in the dry fibers at 50% and to work with solutions with 13% of solid dissolved in DMF/ethanol 3/7. The last parameter to be fixed was the proportion of PVP and HPβCD, the total of both being logically fixed at 50% of the solid part.

3.3.1. Effect of cyclodextrin and PVP contents on the fiber morphology

The objective is to find a formulation able to allow the formation of fibers with at least 50% of pPGS with the help of PVP and HPβCD as carrier materials. The electrospinning of solutions with less than 15% of HPβCD in the solid was not stable due to periodic breaking of the jet (several times a minute) leading to solution projections on the collector. It did not permit the formation of continuous regular fibers, as shown on Figure 4.7.(A). Without cyclodextrin, the deposit is an almost continuous film.

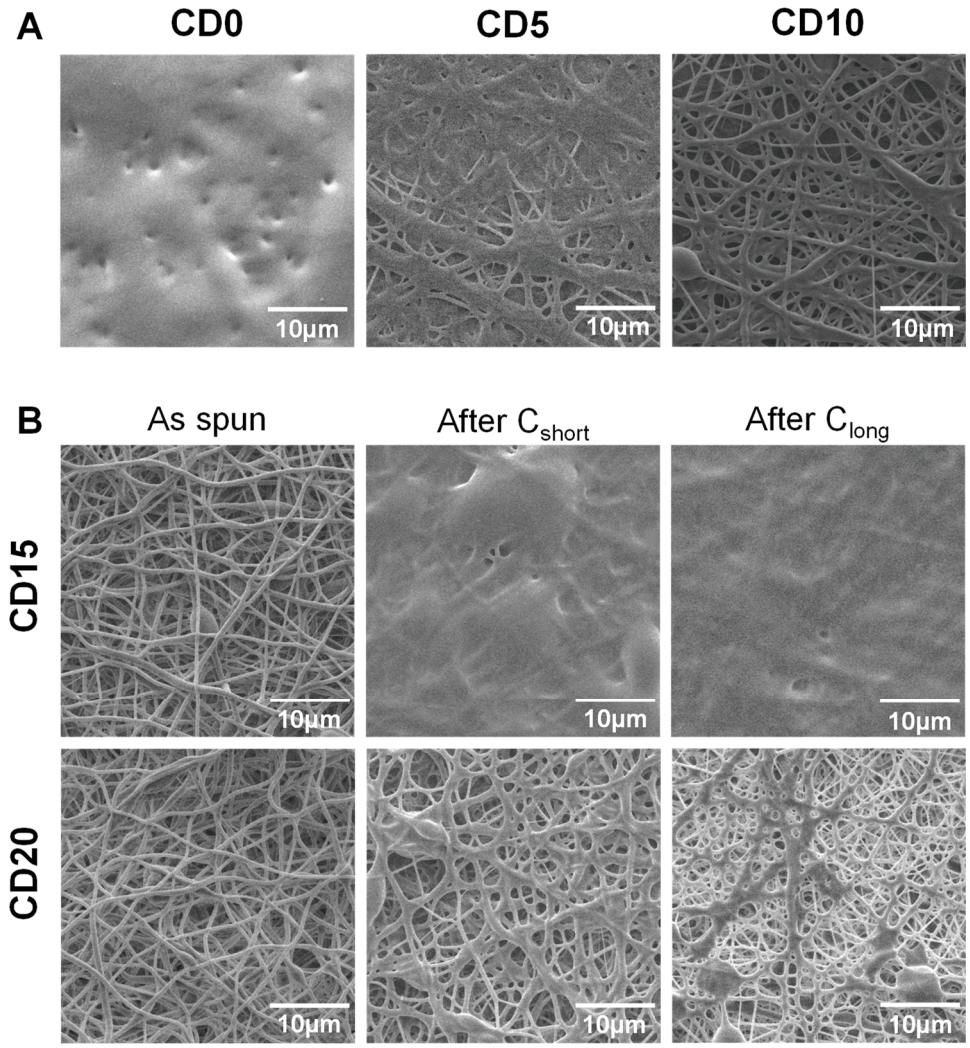

Figure 4.7. ***Morphology of pPGS/HPBCD/PVP fibers for various formulations.*** **(A)** Samples with low HPβCD content giving poorly-formed fibers that were not cured. **(B)** Samples with enough HPβCD to form fibers and result after curing.

When the amount of cyclodextrin is increased, fibers appear, but they are fused and merged together: PVP is not sufficient to hold such a high proportion of pPGS in the fibers. With 15% of HPβCD and more, it was possible to fabricate membranes made of continuous fibers comprising beads.

These materials were cured to verify that it is possible to crosslinking the PGS without the loss of the fibers shape. Figure 4.7.(B) shows that 15% of HPβCD was not enough to avoid the melting of the fibers after C_{short} and consequently after C_{long} curing conditions: PVP may be plasticized by pPGS again. HPβCD, with a high degradation temperature (278°C), is thus

required to keep the fibrous structure. Finally, with at least 20% of HPβCD, it was possible to get fibers with crosslinked PGS and only few melted areas, mostly at the contact points between fibers and around the beads (Figure 4.7.(B)).

3.4. Fabrication of elastomeric mats

3.4.1. Morphology of the fibers

In this work, the mechanical properties of the mats prepared from pPGS/HPβCD/PVP and pPGS/PVA blends are compared with an identical pPGS weight amount of 50%. For the strategy based on the use of HPβCD and PVP, contents of 25 wt% of HPβCD and 25 wt% of PVP were taken. These conditions with a total concentration of pPGS/HPβCD/PVP of 13 wt% led to the fabrication of thin fibers (CD25 having a mean diameter of 318 ± 143 nm) comprising some beads (Figure 4.8). In the case of 50/50 pPGS/PVA fibers, regular fibers were only obtained for a total concentration of solid of 6.4 wt%, leading to regular fibers but thicker diameters (PVA50 having a mean diameter of 1402 ± 503 nm) (Figure 4.8). CD25 fibers are less regular, but in any case, fibers morphology is more or less modified by the curing step. In addition, the preparation of PVA50 fibers requires the use of a costly and toxic solvent, HFIP. Electrospinning of CD25 requires also a toxic solvent, DMF, but as it is mixed with ethanol, lower quantities are necessary. The strategy with PVP and HPβCD seems thus advantageous in this point of view.

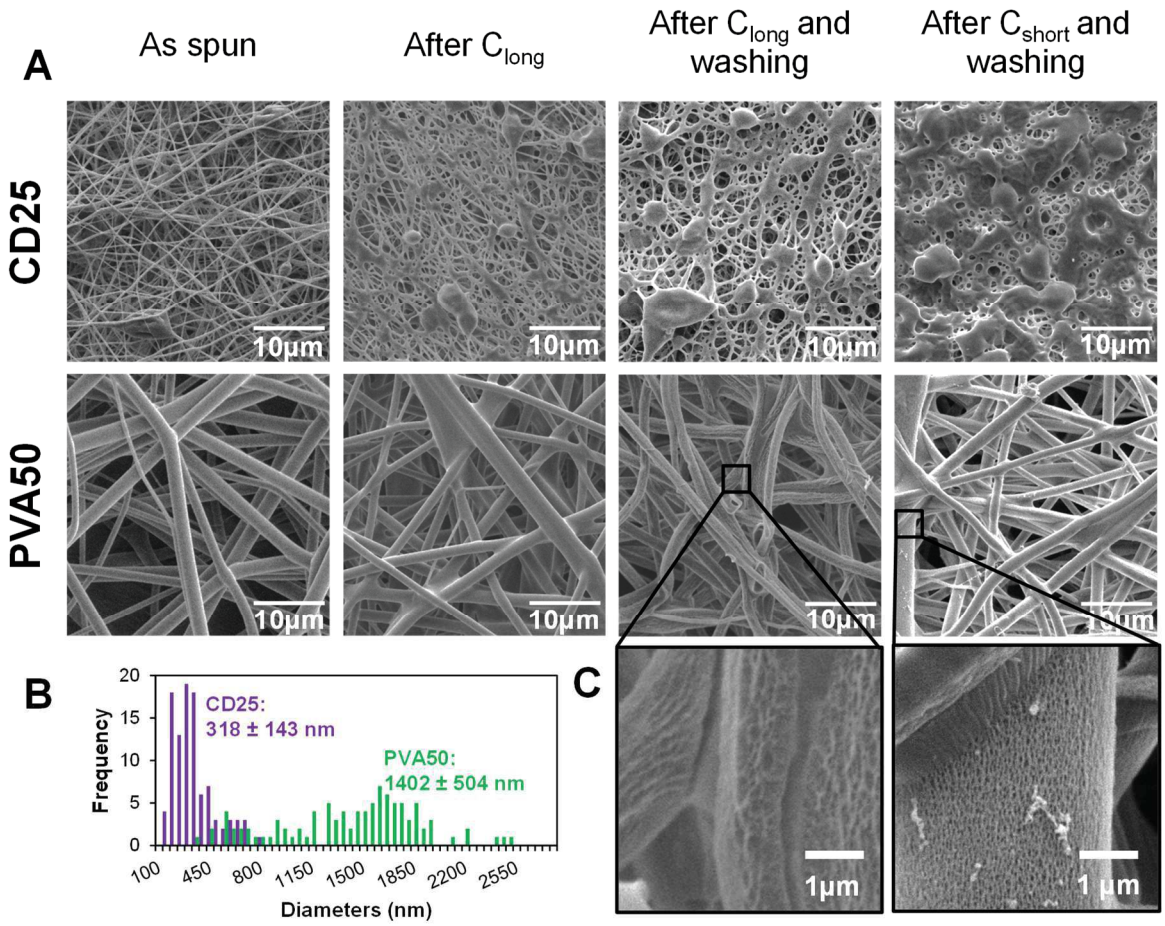

Figure 4.8. ***Morphology of the fibers as spun and after post-treatments.*** **(A)** Low magnification SEM pictures, **(B)** Diameter distribution of diameters of as spun fibers and **(C)** high magnification pictures of PVA50-C-washed fibers.

After curing, crosslinked PGS/HPβCD/PVP fibers (CD25-C) are fused together at the contact points and some melted spots are also visible. Figure 4.8 show the result after C_{long}, but the same observations can be done after C_{short} curing conditions. The integrity of PVA/PGS fibers is better preserved after curing, however, fibers also merged at contact points.

After the steps of washing in water, CD25-C partially loss their fibrous morphology. Especially, numerous continuous areas are observed on CD25-C crosslinked with C_{short} conditions, leading to a high density of less porous areas. In the case of C_{long} crosslinking conditions, a higher porosity is observed. From these results, it can be concluded that if PGS is not enough crosslinked, some of the material can be dissolved or swell out of the fibers and deposit around them. However, the fibrous structure is well preserved in the case of washed crosslinked PVA50-C fibers. They are still attached together by melted material. Besides, it can be observed that PVA left a remarkable roughness or even small pores at the surface of the fibers after its removal (Figure 4.8.(C)). These better results in term of morphology obtained for PVA50, can be justified by strong interactions between PGS and PVA as –OH groups of PVA can react with –COOH groups of PGS.

3.4.2. Composition of the fibers

In order to verify the efficiency of the purification step, the weights of the membranes before and after washing and drying were compared. In all cases, 65% to 80% of the initial mass remains after washing showing that pure PGS membranes are not obtained. However, the removal seems to be more efficient after the C_{short} curing than after C_{long}: 68% of CD25-C_{short} remains after washing versus 72% for CD25-C_{long}.The same tendency is observed in the case of PVA50: 75% of the initial weight remains after washing for PVA50-C_{short} whereas a percentage of 78% is measured for PVA50-C_{long}. Thus, the C_{long} procedure leads to a higher crosslinking density due to the "entrapment" of the carrier material in the fiber matrix. This "entrapment" can be the effect of covalent bonding, especially between PVA or HPβCD and PGS, or the effect of an entanglement of the carrier polymer (PVA for PVA50 or PVP for CD25) in the PGS network. However, it can be noticed that the removal is more efficient for CD25 than for PVA50.

In order to get more insight into the efficiency of the fiber washing step, ATR-FTIR characterization was carried out. Thus, the spectra of CD25-C and PVA50-C before and after washing were compared to pPGS, PVP, HPβCD (Figure 4.9.(A)-(C)) and PVA spectra (Figure 4.9.(D)-(F)).

Same areas as the ones studied for coaxial fibers are of interest. pPGS spectrum shows characteristic peaks of acids at 1710 cm^{-1} and of esters at 1730 cm^{-1}. In the fibers after curing, the peak at 1710 cm^{-1} is not visible anymore (Figure 4.9.(B)), confirming the esterification. The PGS characteristic peaks partially overlap the PVP peak arising from amide C=O bond (1650 cm^{-1}) in CD25 sample (Figure 4.9.(B)). In the same way, C=O bonds of residual acetate groups of PVA (1724 cm^{-1}) are overlapped by the C=O peaks of PGS in PVA50 (Figure 4.9.(E)).

The second interesting area includes the C–O peaks of esters bonds (1160 cm^{-1}), C–O in HPβCD (1027 cm^{-1}), C–N in PVP (1287 cm^{-1}) and C–C in PVA (845 cm^{-1}). It was again difficult to quantify each component because of the overlapping of the peaks. The comparison of the relative intensities led to the same conclusion than for coaxial fibers: cyclodextrin was partially lost during the washing step while PVP reduction is not clear.

On one hand, HPβCD molecules can be covalently bonded to PGS. However, all HPβCD molecules are not bonded to PGS, because there are more –OH groups from

cyclodextrin than –COOH groups from PGS. To evaluate the difference, we can find the number of free –COOH (n_{COOH}) from the DE of the pPGS. The number of –OH from HPβCD ($n_{OH}^{HP\beta CD}$) can be evaluated knowing that the molecule comprises 7 glucose units having each 3 –OH. The molar mass ($M_{HP\beta CD}$) of HPβCD was evaluated knowing that its degree of substitution by hydroxypropyl units is between 2 and 6, giving a maximal (1482 g/mol) and a minimal (1250 g/mol) value. We can write:

$$\frac{n_{COOH}}{n_{OH}^{H\beta CD}} = \frac{2\frac{(1-DE)}{M_{SA}} \times x_{PGS} \times \frac{\frac{M_{SA}}{G/SA}}{\frac{M_{SA}}{G/SA} + M_G}}{\frac{x_{H\beta CD}}{M_{H\beta CD}} \times 21}$$

with M_{SA} and M_G the molar mass of sebacic acid and glycerol, x_{PGS} the proportion of PGS in the fibers (here 0.5) and $x_{HP\beta CD}$ the proportion of HPβCD (here 0.25). Finally, we find that there are 3 to 4 times more –OH groups from cyclodextrin than –COOH groups from PGS. More than two thirds of them are secondary alcohols. And in addition to these alcohols, some –OH of PGS remain unreacted. Logically, some cyclodextrins remain free after curing and can thus be washed away.

On the other hand, no reaction between PVP and PGS was forestalled. PVP should thus be easily removed in water. According to the results, we can assume that the high molar mass PVP macromolecules are actually trapped in the PGS network. Another explanation could be the reaction between PGS –OH groups and the PVP amides leading to the opening of the lactames of PVP.

In PVA50, the peak at 845 cm^{-1} decreased relatively to PGS peak after washing (Figure 4.9.(F)), demonstrating the partial removal of PVA. The remaining PVA is certainly bonded to the PGS or trapped in the network through entanglements.

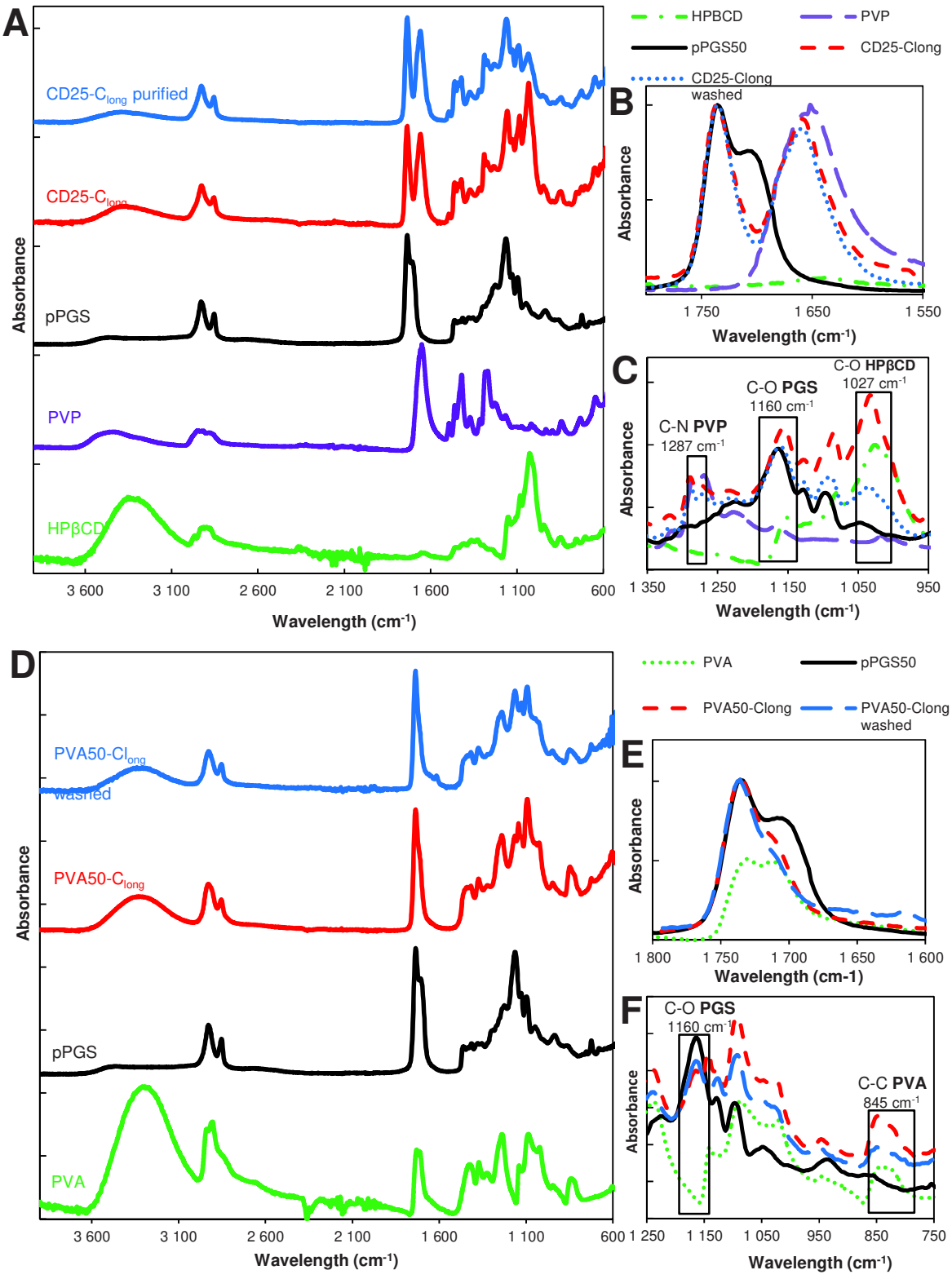

Figure 4.9. ***FTIR spectra of CD25 and PVA50 after curing and after washing compared to HPβCD, PVP, PVA and corresponding pPGS spectra.*** **(A)** Full spectra. **(B)** C=O peaks. **(C)** C–O and C–N peaks.

3.4.3. Mechanical properties

Tensile tests at dry state

The objective of this work was to prepare a scaffold with mechanical properties matching soft tissues properties, especially myocardium's one. As a reminder, left ventricular stiffness is about 10-20 kPa at the beginning of diastole and in the range 200-500 kPa at the end of diastole [18]. Tensile tests were thus conducted to determine if the PGS-based membranes are suitable regarding such specifications. The effect of the curing and of the washing was evaluated, as well as the nature of the carrier material. Typical stress-strain curves are drawn on Figure 4.10.(A), and the mean Young's moduli (E), strain at break (ε_{break}) and ultimate tensile strength (UTS) are given on Figure 4.10.(B) with the standard deviations.

Comparison of the results of as spun and cured samples clearly shows that the curing step increases the modulus and the stress at break. Two explanations can be given about this observation. First, the curing step leads to the crosslinked elastomer network which is a material with a higher strength. However, the maximal strain is not significantly improved by crosslinking because the heating leads to the fusion of the fibers at the contact points and therefore to strong bonding between them. The movement of the fibers along each other is thus inhibited, which is a reason for the increase of the modulus and UTS.

The washing step decreases the Young's modulus and increases the strain at break. This result highlights the fact that the rigid carrier materials were at least partially removed, allowing the elastomer to have more influence on the mechanical properties. After washing, it can be seen that the longest curing step leads to higher modulus and UTS and lower strain at break. Indeed, C_{long} pushes further the reaction to a higher crosslinking density. Moreover, it has been shown by weighing that the rigid carrier materials are less efficiently washed away after C_{long} than after C_{short} curing step, what explains the modulus increase too.

In addition, it should be noticed that cured and washed PVA50 and CD25 have different mechanical behaviors. PVA50 stress-strain curves show a clear first elastic domain with high modulus, before a plastic or elastomeric region with lower modulus until breaking at higher strains. For cured and washed CD25, the first high modulus-domain is drastically reduced, and almost invisible. This difference can be explained by the structure and composition of the mats. PVA50 and CD25 can be compared to point-bonded PVC/TPU-based structures described by Lee *et al.* [19]. PVA50 still contains a large amount of rigid PVA but the density of bonding between its fibers is low; this case corresponds to fibers with high PVC/TPU ratio. When the mat is stretched, these bonds hinder the slipping of the fibers, while PVA phase endures the load until a critical stress is reached. Then, the elastomeric PGS phase governs the behavior. CD25 samples are more similar to PVC/TPU fibers with high TPU content, the density of bonding points being very high. Moreover, we can consider that the carrier polymer content is lower. Indeed, it was shown that the mass loss after washing is higher for CD25 than for PVA50. In addition to that, a fraction of the remaining carrier material is cyclodextrin, which is included in the elastomeric network as crosslinking points and takes thus part to the elastomeric behavior. So, the mat is a quasi-continuous elastomeric phase, and behaves almost as such.

The values given in Figure 4.10.(B) indicate that PVA50 has a higher modulus and UTS than CD25 regardless of the post-treatments. After curing and washing, PVA50 has a modulus higher than 50 MPa for a strain at break close to 150% and an UTS close to 5 MPa. CD25-C_{short} and C_{long} washed have Young's moduli of 2 and 6 MPa respectively and UTS below 2 MPa. The average strain at break reached after washing 390% for C_{short} and 111% for C_{long}. In summary, the

use of PVA as carrier polymer leads to stiffer materials than in the case of the use of HPβCD and PVP.

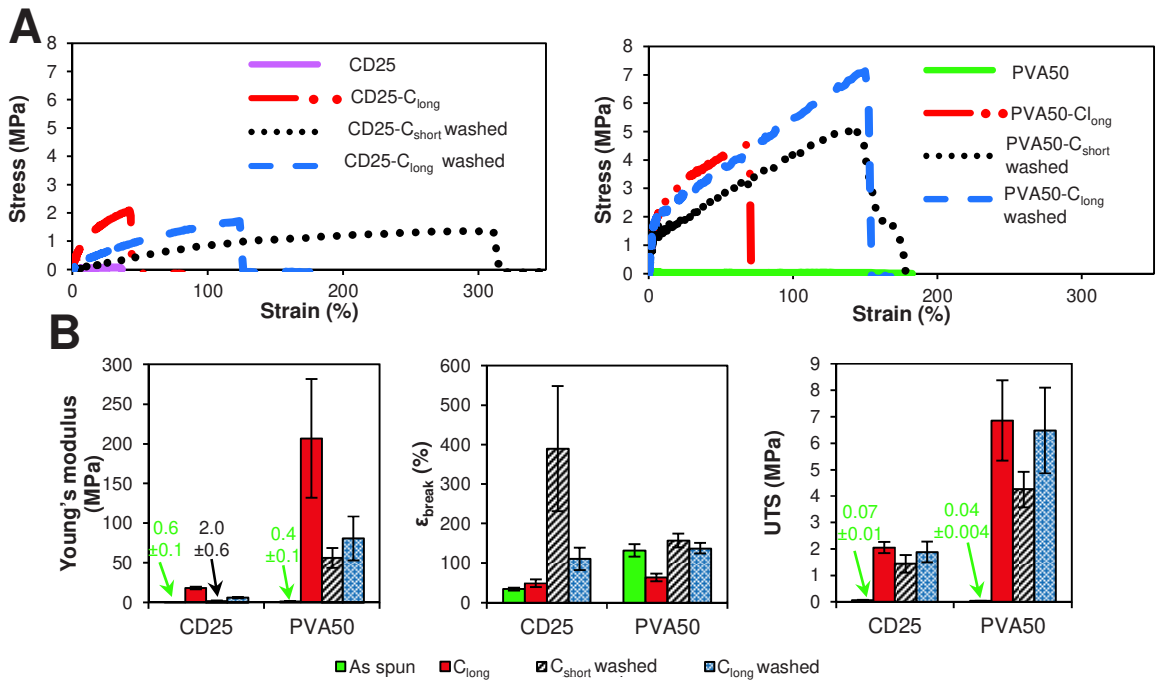

Figure 4.10. ***Mechanical properties for dry samples.*** **(A)** Typical stress-strain curves. **(B)** Evolution of modulus, strain at break and UTS along curing and washing.

Tensile tests at wet state

CD25 sample shows lower modulus and thus is more suitable for soft tissue application, but in all the cases, the obtained moduli obtained are close to 2 MPa, which is far beyond heart's modulus. Nevertheless, the mats were characterized at dry state whereas they are dedicated to be used in a wet medium. Tensile tests were thus also performed with hydrated samples.

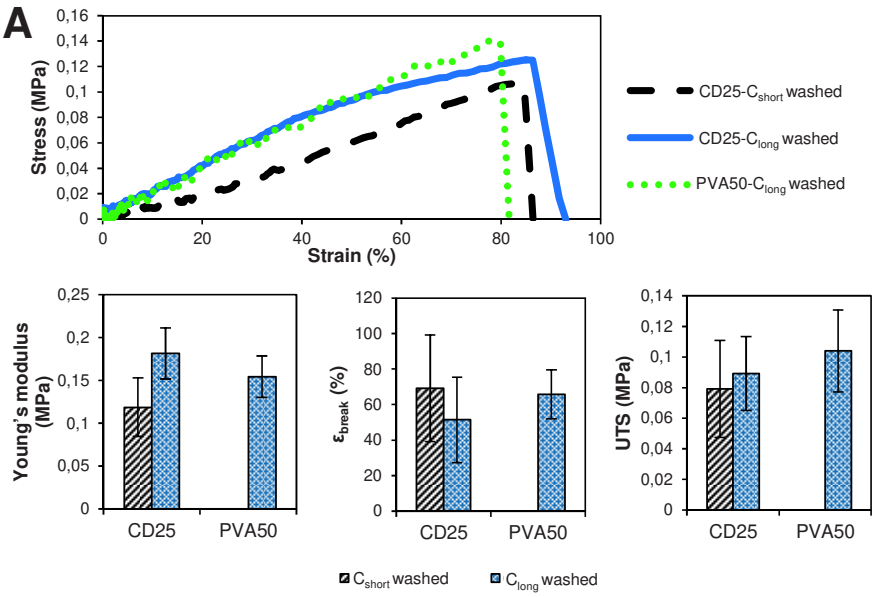

Figure 4.11. ***Mechanical properties for wet samples.*** **(A)** Typical smoothed stress-strain curves. **(B)** Modulus, strain at break and UTS for washed samples after C_{short} and C_{long}.

For wet samples, the axial force measured by the apparatus was very low giving stress-strain curves with a lot of noise. For this reason, the curves were smoothed using the moving window average method with 5 points. Some typical smoothed curves are shown on Figure 4.11.(A).

The results show a clear decrease in modulus, UTS and strain at break for all samples after hydration. Indeed, the material swells in water and behaves like a hydrogel. The water inside can plasticize the polymers and enhance the dissipation of the friction energy; the deformation is thus easier. It results in a wider elastic domain, the linear part reaching strains of several tens of %. The values do not significantly change according to the sample. The moduli are close to 100-200 kPa (see Figure 4.11), what is more suitable for soft tissue than the same dry samples. The maximal strains are quite low but still high enough as the typical strain underwent by the heart tissue is 15% [12]. The main drawback is the low UTS value, making these wet samples easy to break.

Dynamic tensile testing

From Figure 4.10, it can be noticed that most of the dry samples do not show a linear elastic behavior for strains higher than 3%. Cyclic mechanical tests were thus conducted to study how the materials recover after several cycles of deformation. Figure 4.12 represents some typical stress-strain curves obtained with dry samples over 3 cycles of deformation to 15%. The maximal strain value was chosen to mimic the strain underwent by the heart tissue.

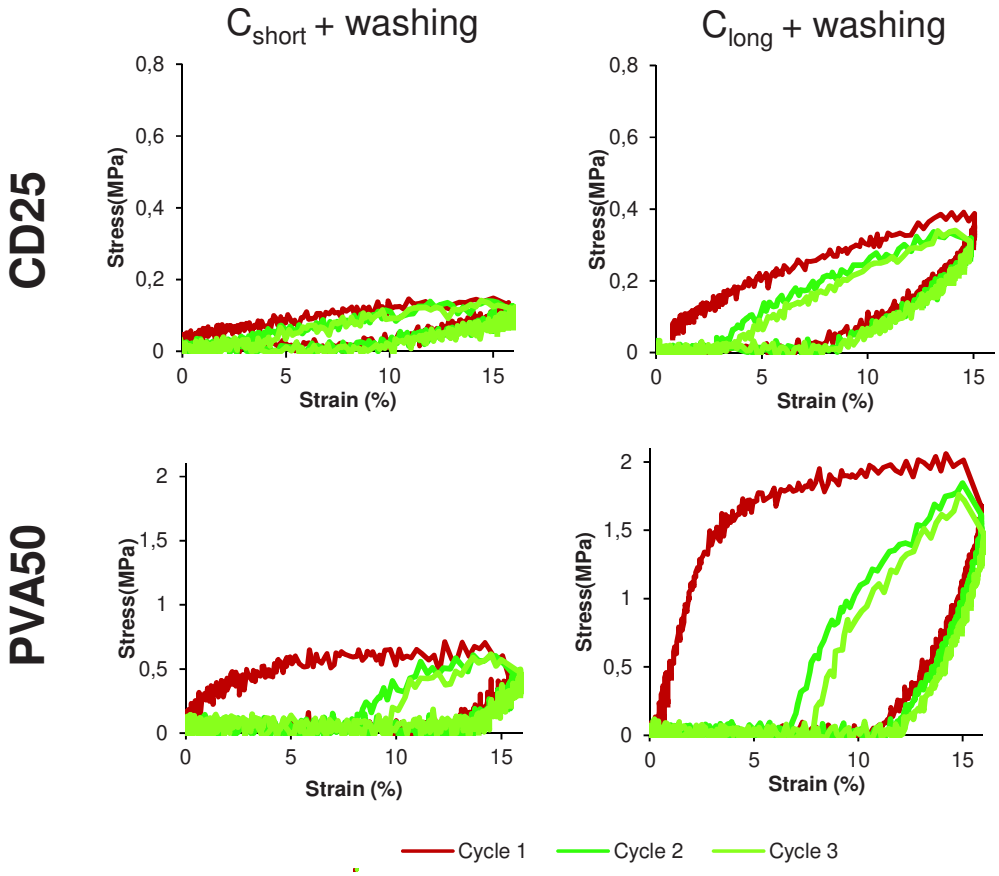

Figure 4.12. Stress-strain curve obtained for dry CD25-C washed and PVA50-C washed between 0 and 15% of strain for 3 cycles.

For each sample, during the first cycle, the stretching part of the curve is very different from the releasing part of the curve. But after the first deformation and release, all the following cycles overlap, with lower loss of energy. This result suggests that the membranes underwent an irreversible deformation during the first cycle. This can be justified be the movement of the fibers along each other.

The resilience was calculated for 10 cycles. The calculated values confirm the poor recovery during the first cycle (Figure 4.13 in grey). PVA50 recovery is close to 10% after C_{short} and C_{long}. CD25 recovery is slightly higher with values above 20%. An average value was calculated for cycle 2 to 10 as they are similar. The recovery reaches then nearly 40% for CD25 and 50% for PVA50 for samples after C_{short}. After C_{long}, the recovery is worse for PVA50 with 33% but stable for CD25.

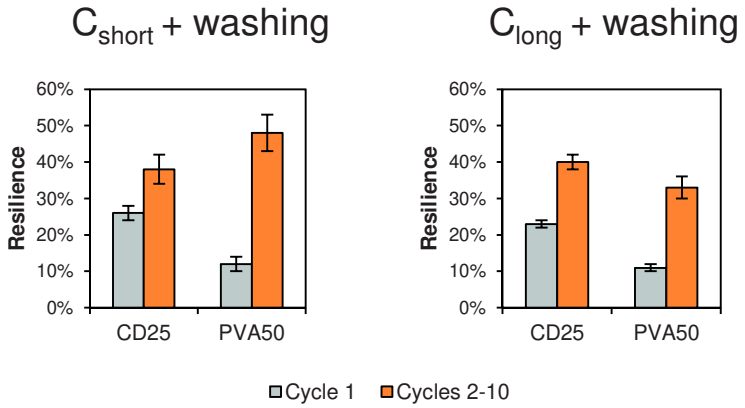

Figure 4.13. Energy recovery of dry membranes after the first cycle and mean energy recovery during cycles 2 to 10. The given value is the average resilience value for 3 samples with the standard deviation.

Finally, both materials show similar behavior under repeated solicitation except during the first extension of the material: PVA50 underwent more important irreversible structural modifications. The morphology of the fibrous samples can help to justify this result. Indeed, as PVA50's fibers are better defined and include a lower density of fixed contact points, they can move with higher amplitudes, these displacements being permanent. On the contrary, washed CD25-C_{short} sample comprises a high density of fixed contact points and shows thus less irreversible deformation.

The cyclic mechanical tests were also conducted on CD25-C wet samples. The curves comprised again a lot of noise, but the stretching and releasing curves clearly overlap at each cycle (Figure 4.14 after smoothing), confirming the observation made thanks to the tensile test curves: at wet state, the elasticity is almost perfect. Finally, from a mechanical point of view, the membranes prepared here seem to be suitable for cardiac tissue engineering.

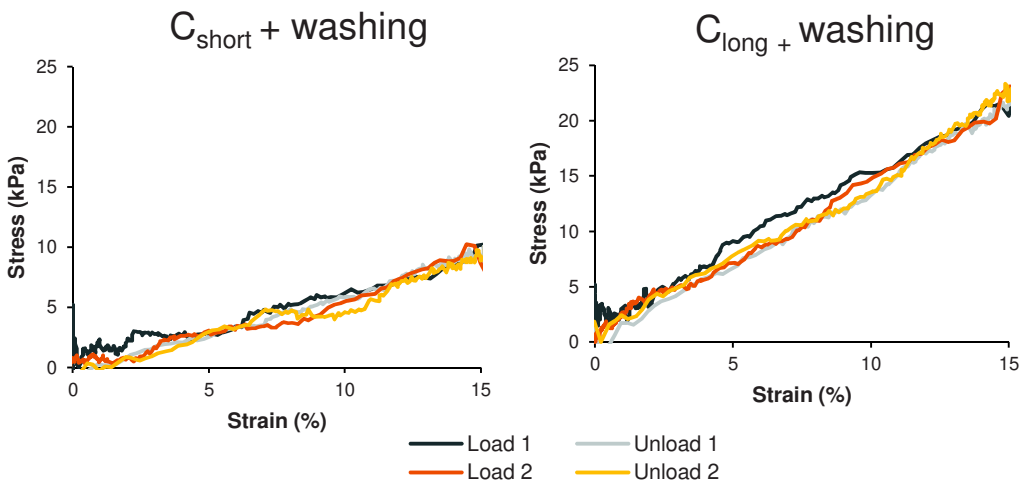

Figure 4.14. Stress-strain curve obtained for CD25-C_{long} washed and hydrated between 0 and 15% of strain for 2 cycles. Curves were smoothed with the moving average window over 20 points.

3.4.1. Dye removal

Besides its mechanical properties, CD25 scaffold can have an additional interest if therapeutic molecules can be encapsulated in the membrane thanks to the beneficial presence of cyclodextrins. However, infra-red analysis showed that the washing step lead to a reduction of the HPβCD content. It is important to prove that enough cyclodextrin molecules remain for encapsulation. For this purpose, methylene blue (MB) removal experiments were carried out by immersion of membranes in a MB solution. After 24h, the membrane is blue (Figure 4.15.(B)) and the solution is lighter (Figure 4.15.(A)), showing that MB was adsorbed on the membrane. However, the same phenomenon was observed for PVA50, showing that MB can be adsorbed on PGS without the help of cyclodextrins. This is possible because as a cationic molecule, MB can adsorb on PGS thanks to ionic exchanges with COO^- groups. Nevertheless, if HPβCD in CD25 create inclusion complexes with the dye, the concentration of the soaking solution should be lower in CD25 because both samples contain a similar amount of PGS.

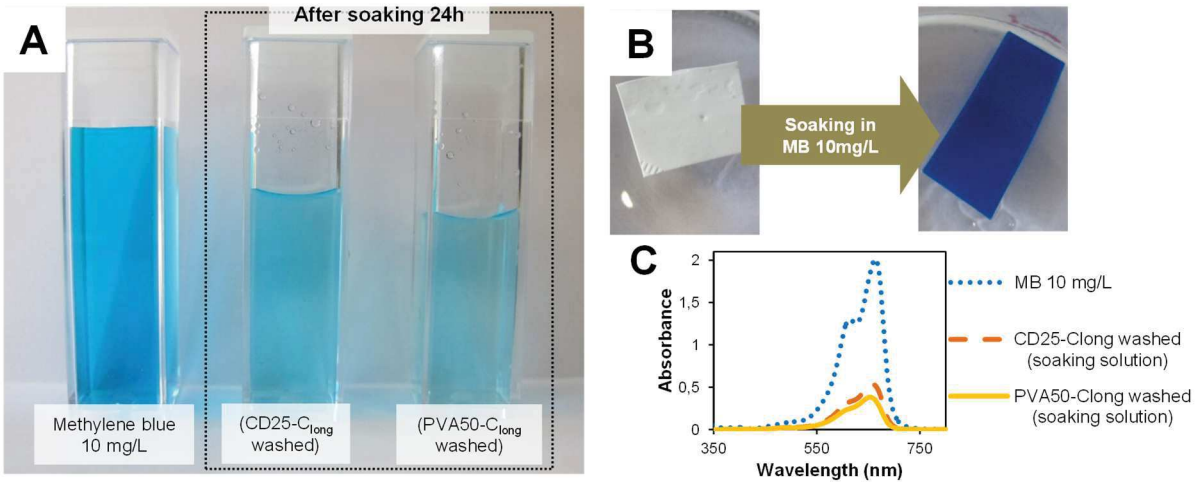

Figure 4.15. ***Methylene blue removal.*** **(A)** Soaking solution after 24h. **(B)** Color change of CD25 after soaking. **(C)** UV-vis spectra of MB 10 mg/L solution and soaking solution for CD25 and PVA50.

The UV-vis spectra of the MB solution at initial state, after immersion of washed CD25-C_{long} and after immersion of washed PVA50-C_{long} are thus compared on Figure 4.15.(C). A decrease of the signal at 664 nm, corresponding to MB, is observed for both soaking solutions. However, the intensity of the signals is very similar for both samples. It is even slightly lower for PVA50, what can be explained by a visibly higher porosity and a resulting larger exchange surface. But it seems that CD25 does not absorb more methylene blue. Finally, the potential use of cyclodextrin included in CD25 could here not be proved. Such experiment should be repeated with a non-cationic dye.

3.4.2. Cell culture results and deductions

Few cell culture experiments with washed CD25-C were conducted. No matter the tested curing step, cell attachment was very poor and cell did not show an elongated morphology, despite a Matrigel coating. This phenomenon could be explained by the high acidity induced by the material in the culture medium; the acidity breaking bindings between cells and their substrate. Indeed, Matrigel preparation contains phenol red, a pH indicator with transition between pH 6.6 and 8.2. The solution is normally pink, but it turns yellow in acidic media: this happened with CD25. Our samples containing carboxylic acids, the decrease of the pH is not totally surprising. However, this result was unexpected because PGS-based patches – even after shorter curing steps – were already successfully used for cell culture (see Chapter 3).

It was hypothesized that the type of PGS was important for a biological point of view. Indeed, for the study dedicated to PLA/PGS fibers (Chapter 3), a 1/1 pPGS was used. This type of PGS contains a lower proportion of carboxylic groups, what could explain the better cell attachment. To confirm this hypothesis, patches with the same dimension as for cell culture were cut in CD25-C_{long} washed and the corresponding sample prepared with a pPGS 1/1 cured and washed (labeled $Blend_{1/1}$ in appendix 2). These patches were immersed in distilled water during one day. Then, a small amount of bromothymol blue (with transition from yellow to blue between pH 6.0 and 7.6) was added in each solution. The soaking solution from CD25 turned yellow, not the solution from PEx4, as shown in Figure 4.16:

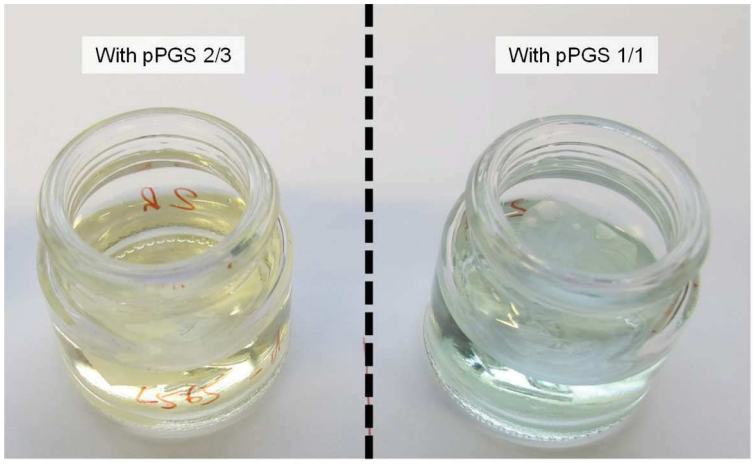

Figure 4.16. Result after soaking of membranes made of 50% PGS, 25% PVP and 25% HPβCD after curing and washing during one day and addition of bromothymol blue. Comparison with a pPGS prepared with a G/SA ratio 2/3 (left) and 1/1 (right).

These results indicate that PGS-based membranes should be prepared from 1/1 pPGS for better interactions with cells.

4. Conclusion

In this work, PGS-based membranes were successfully prepared using a 50/50 blend of PVP and HPβCD as carrier materials. Two strategies were tested. First, the coaxial method allowed the fabrication of core-shell fibers. After crosslinking of the PGS core, the fibers were washed but no pure PGS fibers could be obtained. As the process was complex, efforts were focused on blend electrospinning. For this second technic, preliminary experiments showed that better results in term of fibers morphology could be obtained with the use of a 2/3 pPGS with a DE of 72% (appendix 2). Blend fibers with 50% of pPGS, 25% of PVP and 25% of HPβCD were electrospun, cured and washed. For comparison, fibers with 50% of PGS and 50% of PVA were also electrospun and post-treated in the same way. In both cases, the washing step did not lead to pure PGS fibers. Washing was however slightly more efficient for materials prepared from the PVP/HPβCD blend. Mechanical characterization showed that both types of membranes can be stretched at strains larger than 100% after washing in the dry state but their moduli are higher than 2 MPa. Mats prepared from PVA are slightly stiffer. In wet state, both kinds of membranes show linear elasticity with moduli in the range 100-200 kPa. Finally, cyclic mechanical tests showed that samples prepared from PVP/HPβCD blends have a good resilience, making them good candidates for soft tissue engineering. Unfortunately, it has not been possible to demonstrate that cyclodextrins could be advantageously used to encapsulate molecules of therapeutic interest. In addition, the use of 2/3 pPGS ensuring the best fibrous morphology led to scaffolds inducing high acidity in culture media inducing toxicity for cells. These materials should thus be improved by the use of 1/1 pPGS. It can be assumed that to achieve the goal, prepolymer pPGS should have a very high DE, and some work should be done to find the right conditions. But this modification should be beneficial for both biological and mechanical properties, 1/1 PGS being softer.

References

1. You, Z.-R.; Hu, M.-H.; Tuan-Mu, H.-Y.; Hu, J.-J. Fabrication of poly(glycerol sebacate) fibrous membranes by coaxial electrospinning: Influence of shell and core solutions. *Journal of the Mechanical Behavior of Biomedical Materials* **2016**, *63*, 220–231.
2. Xu, B.; Li, Y.; Zhu, C.; Cook, W.D.; Forsythe, J.; Chen, Q. Fabrication, mechanical properties and cytocompatibility of elastomeric nanofibrous mats of poly(glycerol sebacate). *European Polymer Journal* **2015**, *64*, 79–92.
3. Peijs, T.; van Vught, R.J.M.; Govaert, L.E. Mechanical properties of poly(vinyl alcohol) fibres and composites. *Composites* **1995**, *26*, 83–90.
4. Jeffries, E.M.; Allen, R.A.; Gao, J.; Pesce, M.; Wang, Y. Highly elastic and suturable electrospun poly(glycerol sebacate) fibrous scaffolds. *Acta Biomaterialia* **2015**, *18*, 30–39.
5. Saudi, A.; Rafienia, M.; Kharazi, A.Z.; Salehi, H.; Zarrabi, A.; Karevan, M. Design and fabrication of poly (glycerol sebacate)-based fibers for neural tissue engineering: Synthesis, electrospinning, and characterization. *Polymers for Advanced Technologies 0*.
6. Keirouz, A.; Fortunato, G.; Zhang, M.; Callanan, A.; Radacsi, N. Nozzle-free electrospinning of Polyvinylpyrrolidone/Poly(glycerol sebacate) fibrous scaffolds for skin tissue engineering applications. *Medical Engineering & Physics* **2019**.
7. Uyar, T.; Balan, A.; Toppare, L.; Besenbacher, F. Electrospinning of cyclodextrin functionalized poly(methyl methacrylate) (PMMA) nanofibers. *Polymer* **2009**, *50*, 475–480.
8. Kayaci, F.; Uyar, T. Electrospun zein nanofibers incorporating cyclodextrins. *Carbohydrate Polymers* **2012**, *90*, 558–568.
9. Séon-Lutz, M.; Couffin, A.-C.; Vignoud, S.; Schlatter, G.; Hébraud, A. Electrospinning in water and in situ crosslinking of hyaluronic acid / cyclodextrin nanofibers: Towards wound dressing with controlled drug release. *Carbohydrate Polymers* **2019**, *207*, 276–287.
10. Otero-Espinar, F.J.; Torres-Labandeira, J.J.; Alvarez-Lorenzo, C.; Blanco-Méndez, J. Cyclodextrins in drug delivery systems. *Journal of Drug Delivery Science and Technology* **2010**, *20*, 289–301.
11. Bellani, C.; Yue, K.; Flaig, F.; Hébraud, A.; Ray, P.; Annabi, N.; Selistre Sobreiro de Araújo, H.; Branciforti, M.C.; Minarelli Gaspar, A.M.; Shin, S.-R.; et al. Suturable elastomeric tubular grafts with patterned porosity for rapid vascularization of 3D constructs. *Submitted to ACS Biomaterials Science & Engineering*.
12. Zhu, C.; Rodda, A.E.; Truong, V.X.; Shi, Y.; Zhou, K.; Haynes, J.M.; Wang, B.; Cook, W.D.; Forsythe, J.S. Increased Cardiomyocyte Alignment and Intracellular Calcium Transients Using Micropatterned and Drug-Releasing Poly(Glycerol Sebacate) Elastomers. *ACS Biomater. Sci. Eng.* **2018**, *4*, 2494–2504.
13. Veress, A.I.; Gullberg, G.T.; Weiss, J.A. Measurement of Strain in the Left Ventricle during Diastole with cine-MRI and Deformable Image Registration. *J Biomech Eng* **2005**, *127*, 1195–1207.
14. Zhao, R.; Wang, Y.; Li, X.; Sun, B.; Wang, C. Synthesis of β-Cyclodextrin-Based Electrospun Nanofiber Membranes for Highly Efficient Adsorption and Separation of Methylene Blue. *ACS Appl. Mater. Interfaces* **2015**, *7*, 26649–26657.
15. Zhao, F.; Repo, E.; Yin, D.; Meng, Y.; Jafari, S.; Sillanpää, M. EDTA-Cross-Linked β-Cyclodextrin: An Environmentally Friendly Bifunctional Adsorbent for Simultaneous Adsorption of Metals and Cationic Dyes. *Environ. Sci. Technol.* **2015**, *49*, 10570–10580.
16. Celebioglu, A.; Yildiz, Z.I.; Uyar, T. Electrospun crosslinked poly-cyclodextrin nanofibers: Highly efficient molecular filtration thru host-guest inclusion complexation. *Sci Rep* **2017**, *7*.
17. Dogan, Y.E.; Satilmis, B.; Uyar, T. Crosslinked PolyCyclodextrin/PolyBenzoxazine electrospun microfibers for selective removal of methylene blue from an aqueous system. *European Polymer Journal* **2019**, *119*, 311–321.
18. Chen, Q.-Z.; Bismarck, A.; Hansen, U.; Junaid, S.; Tran, M.Q.; Harding, S.E.; Ali, N.N.; Boccaccini, A.R. Characterisation of a soft elastomer poly(glycerol sebacate) designed to match the mechanical properties of myocardial tissue. *Biomaterials* **2008**, *29*, 47–57.
19. Lee, K.H.; Kim, H.Y.; Ryu, Y.J.; Kim, K.W.; Choi, S.W. Mechanical behavior of electrospun fiber mats of poly(vinyl chloride)/polyurethane polyblends. *Journal of Polymer Science Part B: Polymer Physics* **2003**, *41*, 1256–1262.

CHAPTER 5

Structured scaffolds with organized fibers

The previous chapter aims to fabricate scaffolds mimicking cardiac tissue by their mechanical properties. However, we have seen that they should also mimic the tissues by their structure. Indeed, the extracellular matrix of cardiac tissue is not only fibrous, but also hierarchically structured.

In the present chapter, various methods will be tested to fabricate scaffolds with a structure closer to the cardiac tissue's one. First, PLA fibers will be combined with PGS electrospray to make more porous scaffolds. Then, aligned PLA and PLA/PGS fibers will be electrospun. Finally, both methods will be combined, and scaffolds based on aligned PLA fibers and PGS/HPβCD particles and having a structure comparable to cardiac tissue's one will be achieved. The mechanical properties of the membranes will be compared.

CHAPTER 5

Structured scaffolds with organized fibers

1. Objectives and possible approaches

Electrospinning allows the fabrication of scaffolds made of fibers mimicking collagen fibers found in living tissues. However, the latter are much more complex, as they are structured in 3D, at different levels. In particular, myocardial tissue shows a hierarchical structure with aligned fibrous cells embedded into 3D honeycomb-like micro-patterns formed by undulated perimysial collagen fibers [1,2], as already described in Chapter 1. Unfortunately, electrospun mats are made of randomly deposited fibers and have pores too small to let the cells penetrate inside the scaffold. Starting from these observations, it seems important to find methods to introduce organization and structuration in electrospun scaffolds and to create larger pores.

1.1. Alignment of the fibers

A first way to organize the fibers deposition is their alignment in one direction. This method allows to mimic the structural and mechanical anisotropy of cardiac tissue. Several works showed that the alignment of electrospun fibers enhances the attachment, orientation, alignment, contraction ability, elongation and maturation of muscle cells, and more specifically of cardiomyocytes [3–8]. This alignment can be obtained by two types of methods: mechanical methods or electrostatic methods.

A first simple mechanical method is the use of a cylindrical collector rotating at high speed. As shown by Matthews *et al.* [9], when the tangential velocity of the collector reaches the velocity of the landing jet fiber, alignment occurs perpendicularly to the axis of the cylindrical collector. Many examples of this method can be found in the literature. For example, it was used to electrospin aligned fibers based on TPU [10], PCL for muscle tissue engineering [5], PLGA and polyaniline for cardiac application [11], PLA [12,13] or PGS [14,15]. Another mechanical method consists of stretching while heating the randomly deposited fibers close to their melting temperature. For such post-processing step, alignment is kept after cooling as seen for example for PCL fibers heated and stretched at 55°C [7].

Other methods exploit electrostatic forces. Li *et al.* [16] studied this possibility by electrospinning onto two parallel conductive stripes acting as electrodes. They found that the fibers sections deposit perpendicularly to the electrodes and form consequently a membrane made of aligned fibers. The authors explain this result by the electrostatic forces. They calculated that the electric field near the electrode (see vectorial field represented on Figure 5.1.(A)) is such that each

extremity of a section of fiber approaching the conductive stripes is attracted by the closest electrode. In addition to that, the fiber deposits perpendicular to the electrode in order to minimize the repulsion due to the charges remaining on the hanging section of the fiber. This principle was used in many works [6,17–20]. The process was improved by Katta *et al.* [21] who constructed a drum collector composed of wires parallel to the rotation axis and regularly disposed around the latter (see Figure 5.1.(B)). The same principle allows aligning the fibers circumferentially to the drum. Another variation of the principle involves a wire disposed along the circumference of a rotating insulating cylinder [22]. In this case, the polymer jet is attracted by the thin wire, and because the cylinder is rotating, the fiber aligns on the circumferential wire, in the direction of rotation of the cylinder. A similar method was developed by Theron *et al.* [23] who used a rotating disc with a sharp edge. Again, the fiber is strongly attracted by the edge of the disc and land therefore on it, in the direction of the rotation.

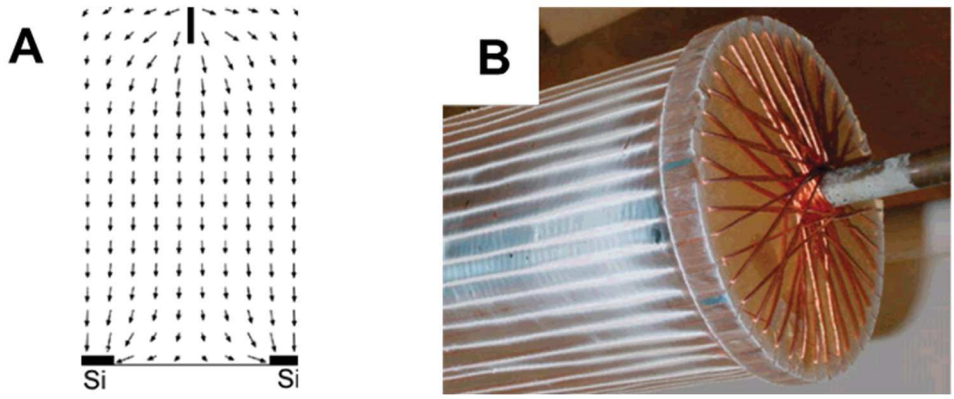

Figure 5.1. (A) Electric field vectors between the needle and the collector composed of two parallel silicon bars calculated by Li *et al.* [16]. **(B)** Collector drum composed of parallel wires developped by Katta *et al.* [21].

Some of these methods where used to align PGS fibers. High speed rotation of the collector was used in order to prepare anisotropic scaffolds based on acrylated PGS for cardiac tissue engineering [24]. PLA/PGS coaxial fibers were also aligned by this method [15]. It allowed also preparing aligned PGS fibers after electrospinning of (PLA+POE)/PGS coaxial fibers, curing and elimination of the shell [14]. The post-treatments decreased the degree of alignment but the authors found that the process still improve orientation of smooth muscle cells. Parallel electrodes were used by Kenar *et al.* [17,25] to fabricate a complex cardiac patch composed of aligned fibers based on poly(3-hydroxybutyrate-*co*-3-hydroxyvalerate), PLA and pPGS (maximum 4%). The same kind of collector was used by Kharaziha *et al.* [6] for cardiac tissue engineering to align pPGS/gelatin fibers where carbon nanotubes were incorporated. They found that the presence of the carbon nanotubes improves fibers alignment, and that both carbon nanotubes and fibers alignment enhance cardiomyocytes alignment. Two parallel electrodes were also used to align pPGS/PCL fibers for valvular tissue engineering [19] and corneal repair [20,26], cornea being a tissue presenting also a strong anisotropy.

1.2. Structuration of the mats

Control of the fibers deposition by monitoring the electrostatic field can also be employed to make more complex structures, in particular for scaffolds comprising large pores able to allow cells migration. Conductive and dielectric areas can be created on the collector with rings, polygonal, strips, blocks or holes shapes possibly arranged in patterns. Globally, depending on the size of the

pattern, fibers deposit preferentially on the conductive parts and minimize the electrostatic forces by landing strained on the dielectric parts [27,28]. For example, on Figure 5.2, a patterned collector with conductive blocks is represented. If the ratio height of the block over the distance between two blocks is high enough, fibers land strained and keep their charges, making repulsive areas (Figure 5.2.(A)). If the ratio is lower, fibers can touch the conductive bottom of the collector (Figure 5.2.(B)).

Figure 5.2. ***Schematic representation of fibers deposition on conductive blocks.*** **(A)** When height/distance is high, fibers stay hanged over the holes and charges are not dissipated. **(B)** When height/distance is low, fibers deposit on the flat area of the collector between the blocks. Blue arrows indicate the dissipation of the charges through the collector.

Tallawi *et al.* [29] used for example patterned collectors to electrospin pPGS/PCL fibers with a controlled topography. They tried with parallel grooves disposed regularly or not and windows-like square patterns. The topography of the face of the mat in contact with the collector was affected by the pattern. It results in a better elongation and alignment of fibroblasts cultured on regular parallel lines and also a better maturation and cell-to-cell communication.

However, such a method can lead to the apparition of large repulsive areas, due to the impossibility for fibers to discharge through the contact with a conductive surface. As a result, no thick scaffolds can be fabricated. Besides, thick deposits made of self-organized fibers can be achieved for fibers presenting a bimodal distribution of the fiber diameter [30–33]. Examples of honeycomb patterns that can be obtained in this way are given on Figure 5.3.

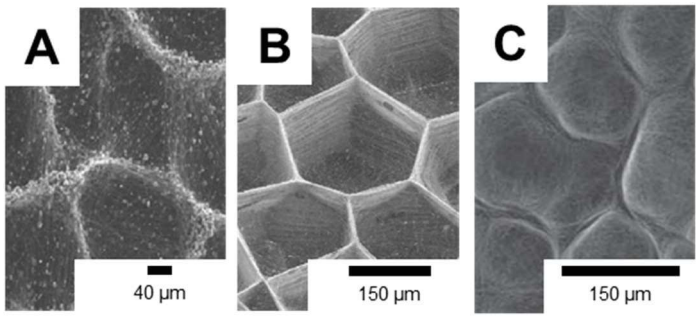

Figure 5.3. ***Examples of self-assembled honeycomb patterns.*** **(A)** With polyurethane fibers [31]. **(B)** With PVA fibers [32]. **(C)** With PCL fibers [33].

The construction of such structures can be explained by a similar argumentation than for organization of fibers on patterned collectors. When a fiber comprising beads or thicker portions is deposited, the thicker parts, containing residual solvent, touch the collector, while the thinner parts are suspended between two thick parts (Figure 5.4.(A)). As a result, thick parts get discharged whereas the thinner parts stay charged, creating repulsive areas. The distribution of these thick and thin areas forms an electrostatic template, acting as a patterned collector. Next fibers land preferentially on discharged areas, forming the honeycomb-like pores. In this way, the electrospun scaffold comprises a two-scales porosity. Moreover, the vertical walls of these pores are good paths for discharge. It avoids the quick formation of a globally repulsive deposit and allows thus the continuation of the process until a cm-thick scaffold is obtained (Figure 5.4.(B)).

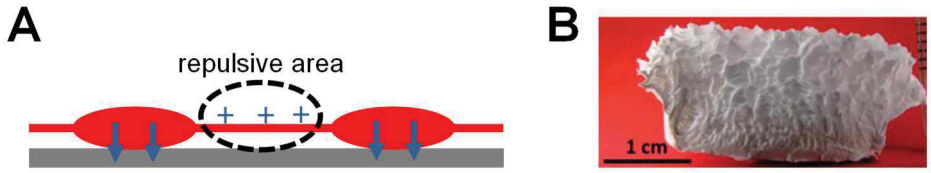

Figure 5.4. ***Self-assembling of fibers.*** **(A)** Schematic representation of deposition on a flat collector of a beaded fiber (in red). Blue arrows indicate the dissipation of the charges through the collector. **(B)** Cross-section of a scaffold obtained after five hours of PCL electrospinning [33].

Nevertheless, this technique is only feasible in certain conditions, when a bi-modal distribution of the fibers diameter is possible. To cope with this limitation, it is possible to replace beaded fibers by monodisperse fibers associated with particles. In this way, the combination of electrospinning and electrospraying allows the fabrication of composite scaffolds that can have a real interest for tissue engineering. Indeed, the presence of particles brings new properties coming from the material they are made of and also offers the possibility to encapsulate molecules of therapeutic interest [34,35]. But most importantly, thanks to this procedure, it is possible to benefit from the self-organization of a wide variety of materials able to form fibers or particles. For example, honeycomb-like structures were fabricated by electrospinning of PLA and electrospraying of microparticles made polyethylene glycol (PEG) [36] (Figure 5.7.(A)). PEG particles are here interesting because they increase the hydrophilicity of the mat. Fibers and particles layers were successively deposited thanks to the rotation of the cylindrical collector, with the corresponding needles placed on two opposite sides of the collector (Figure 5.5).

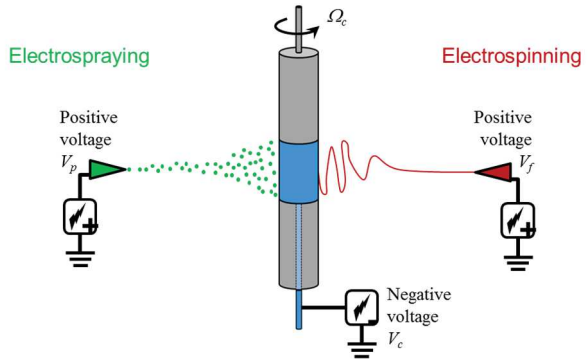

Figure 5.5. Set-up used to alternate fibers and particles deposition by continuous rotation of the collector.

The resulting structure can be explained with the same argumentation than for non-monodisperse fibers, with the aggregates of particles playing the role of the thick parts of the fibers. These aggregates are thus attractive areas, where next particles and fibers deposit preferentially. On the other hand, between two aggregates, the fibers land strained and create repulsive areas. In this way, large pores are created, with diameters ranging from a few micrometers to hundreds of micrometers.

In order to better control the deposition of fibers and particles, it is possible to combine the use of a patterned collector and the method based on electrospinning/electrospraying. PLA fibers were for example electrospun alternatively with PEG or PCL particles on a honeycomb-patterned silicon wafer [37]. In this way, more than 200 µm thick membranes could be fabricated. These membranes include large pores with columnar structure (Figure 5.7.(B)) where the walls are composed of fibers and particles. However, this structure is lost above a certain thickness produced. It was noticed that without particles, no columnar structure was observed and the

thickness of the mat remained low (45 µm). Moreover, without fibers, particles deposit everywhere. The interaction between electrospinning and electrospraying is thus of great importance. Numerical simulation showed that the first fibers hanged above the holes of the patterns create highly repulsive areas that rejects the particles and very attractive areas above the walls of the collector where the particles land and evacuate their charges, allowing the next fibers to land as represented on Figure 5.6:

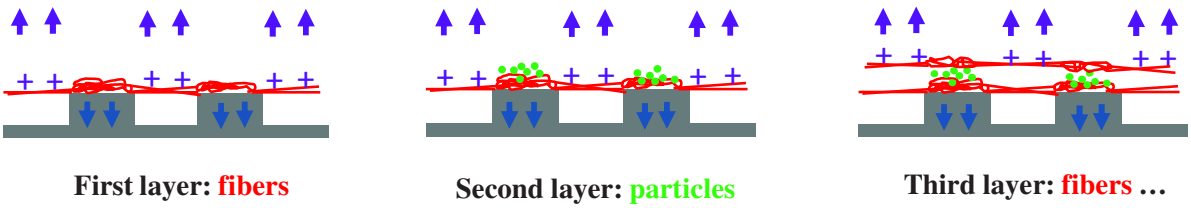

Figure 5.6. Representation of the mechanism of structuration by alternate deposition of fibers and particles on a patterned collector. Blue arrows indicate the dissipation of the charges through the collector. Purple arrows indicate the repulsion due to remaining charges.

An electrostatic template is actually created, allowing the formation of the interesting fibrous structure. However, above a certain thickness produced, the structure is lost certainly because the charges cannot dissipate efficiently anymore. This critical thickness is increased when the particles wet the fibers, what improves the electrical contact. This Electrostatic Template Assisted Deposition (ETAD) method can be used for different patterns [38] and with various materials. Scaffolds for bone cells culture were for example prepared from electrospinning of PCL and electrospraying of hydroxyapatite onto a honeycomb pattern. Six fibers/particles bilayers allowed the formation of a material that helps bone cells differentiation. Moreover, cells were able to proliferate in honeycomb-like cavities [39].

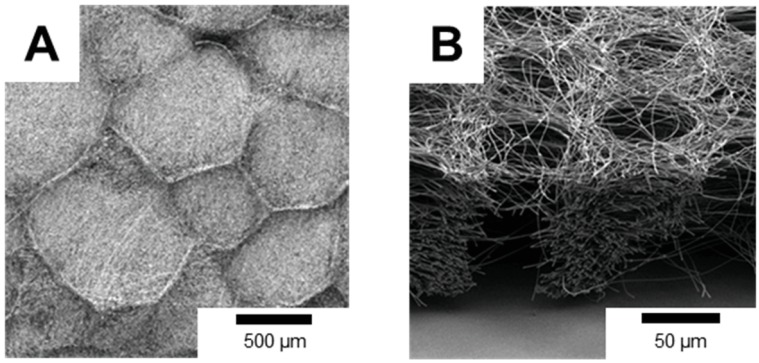

Figure 5.7. ***Example of structuration of fibrous mats by combination of electrospinning of PLA fibers and electrospraying of PEG particles.*** **(A)** On a flat collector [40]. **(B)** On a patterned collector with honeycomb structures 80 µm large (side view) [37].

It should here be underlined that this process is possible thanks to the charges remaining on the hanging fibers. Therefore, it is not possible with conductive fibers that would let the charges dissipate towards the walls of the structure.

In the present work, the objective was to mimic the hierarchical structure and anisotropy of the cardiac tissue. For this purpose, three different strategies were experimented:

***Strategy A**: Combination of electrospinning and electrospraying*. This strategy aims to prepare porous scaffolds. For this purpose, PLA or PLA/pPGS fibers electrospinning and pPGS electrospraying were alternated. Results for both kind of fibers deposited on a structured or a smooth collector were compared.

***Strategy B**: Alignment of the fibers*. The goal of this strategy is to mimic the anisotropy of cardiac tissue by alignment of the fibers. PLA and PLA/PGS fibers were aligned thanks to high-speed rotation of the collector. The mechanical behavior was studied to determine the effect of the alignment.

***Strategy C:** Combination of aligned fibers and electrospray*. In this strategy, the two previous ones are combined. PLA fibers aligned by high-speed rotation of the collector were electrospun while pPGS/HPβCD particles were electrosprayed. The internal structure and the mechanical properties of such membranes were investigated and compared to scaffolds without particles.

2. Materials and methods

2.1. Materials

Poly(D-lactic acid) (PLA, Ingeo 7000D, NatureWorks), dimethylformamide (DMF, >99.8%, Sigma-Aldrich), dichloromethane (DCM, >99.8%, Carlo Erba), hydroxypropyl-β-cyclodextrin (HPβCD, 97%, Acros Organics) and absolute anhydrous ethanol (>=99,9%, Carlo Erba) were used as received. pPGS was synthesized with the microwave procedure presented in Chapter 1. The ratio of reactant G/SA and degree of esterification are given below for each case.

2.2. Method for strategy A: combination of electrospinning and electrospraying

Electrospinning and electropraying were combined by alternated deposition of PLA or PLA/PGS fibers and pPGS electrospray.

The alternated deposition was performed using a home-made horizontal set-up with a rotating cylindrical collector at low rotation speed. Two 18-gauge needles were disposed on either side of the collector to deliver fibers and particles, as represented on Figure 5.5. The collector was 5 cm-wide and covered by an aluminum foil or a metallic grid when a patterned collector was required. A negative voltage of -5 kV was applied to it. Two kinds of grids were used: with square holes (represented on Figure 5.8.(A) and (C)) and with rectangular holes (represented on Figure 5.8.(B) and (D)). Apart from the geometry of the holes, the two kinds of grids differ by the warp and weft arrangement, as shown on the side views on Figure 5.8.(C) and (D). The blue stars represent the highest parts of the collector, which are the equivalent of the tops the blocks on patterned collectors described above: the fibers and the particles should preferentially land on these locations. In Figure 5.8.(D), it can be observed that the red wire is never at the top of the pattern. Consequently, the arrangement of the tops is different on the rectangular grids, what is important for the final pattern.

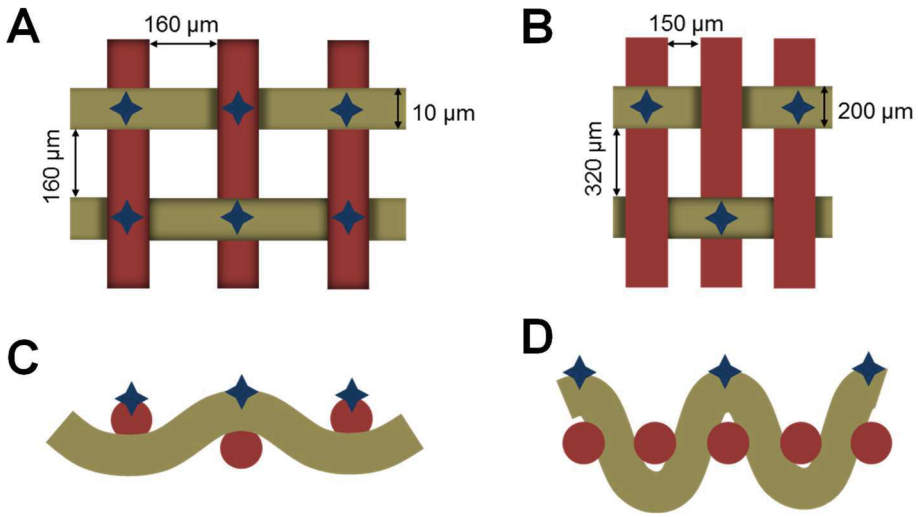

Figure 5.8. ***Metallic grids used as patterned collectors***. **(A-B)** Top view. **(C-D)** Side view. **(A-C)** With square holes. **(B-D)** With rectangular holes.

With PLA fibers

Electrospinning solution was prepared at 10 wt% PLA in DCM/DMF 6/4 (w/w) 24h prior to electrospinning. It was injected at 1.6 mL/h. Electrospraying solution was composed of 15 wt% of pPGS (prepared from a ratio G/SA = 2/3, DE = 65%) in ethanol at least one day prior to electrospinning and was injected at 1mL/h. A high voltage of 15 kV was applied to the electrospinning needle which was 18 cm away from the collector. A high voltage of 17,5 kV was applied to the electrospraying needle 18 cm away from the collector. The collector was rotating at 150 rpm.

Two different 1h-lasting experiments were carried out: one with an aluminum foil at the surface of the collector, the second one with a grid with rectangular holes (represented on Figure 5.8.(B) and (D)). For both experiments, fibers and particles were produced continuously but deposited alternatively thanks to the rotation of the collector.

The resulting membranes were visibly structured on the top side and could be easily peeled from the aluminum or the grid. They were cured 2 days at 120°C under vacuum (below 10^{-2} mbar) in order to crosslink the PGS and were further used for biological tests.

With PLA/PGS fibers

Electrospinning solution was prepared at 7 wt% PLA and 3 wt% pPGS (1/1, 85%) in DCM/DMF 6/4 (w/w) injected at 1.3 mL/h. Electrospraying solution was composed of 15 wt% of pPGS (prepared from a ratio G/SA = 2/3, DE = 65%) in ethanol and was injected at 1mL/h. A high voltage of 13 kV was applied to the electrospinning needle which was 18 cm away from the collector. A high voltage of 17,5 kV was applied to the electrospraying needle 18 cm away from the collector.

A first experiment was performed during one hour with the collector covered by a metallic grid with rectangular holes. The latter was rotating at 150 rpm, allowing the alternated deposition of fibers and particles which were produced continuously. In a second experiment, the collector was motionless; fibers were deposited during 30s on a metallic grid with square holes, and then particles were deposited directly on the fibers during 30s.

2.3. Method for strategy B: alignment of the fibers

PLA and PLA/PGS fibers were aligned by rotation of the collector at high speed, using a horizontal electrospinning set-up. To achieve this goal, a nude large collector (diameter: 13 cm; height: 3 cm) connected to electrical ground was rotated at 3000 rpm by a motor (EUROSTAR 20 high speed digital, IKA). The corresponding surface linear speed is 20 m/s.

With PLA fibers

PLA fibers were electrospun from solutions concentrated at 10 wt% in DCM/DMF 6/4 (w/w) injected at 1.4 mL/h through a needle 16 cm away from the collector. A high voltage of 16 kV was applied to the needle.

With PLA/PGS fibers

PLA/PGS fibers were electrospun from solutions concentrated at 7 wt% PLA and 3 wt% pPGS (1/1, 2/3) in DCM/DMF 6/4 (w/w) injected at 1 mL/h through a needle 16 cm away from the collector. A high voltage of 15 kV was applied to the needle.

Both kinds of samples were fabricated in one hour. The anisotropic membranes could be peeled from the collector and cured 48h at 120°C under vacuum. For this step, they were hold in the longitudinal direction to avoid shrinkage in this direction. They were however subjected to a strong shrinkage in the transversal direction. They were then used for mechanical and biological tests.

2.4. Method for strategy C: Combination of aligned fibers and electrospray

Aligned fibers and particles were combined by electrospinning of a solution of PLA at 10 wt% in DCM/DMF 6/4 (w/w) and electrospraying of a solution of pPGS (1/1, 85%) at 15 wt% and HPβCD at 15 wt% in ethanol/DMF 7/3 (w/w). Two needles placed side-by-side were used to produce the particles. The flow rate at each needle was 0.5 mL/h. Electrospinning solution was injected at 1.4 mL/h.

To ensure the alignment of the fibers, a nude large collector (diameter: 13 cm; height: 3 cm) connected to electrical ground was rotated at 3000 rpm by a motor (EUROSTAR 20 high speed digital, IKA). The corresponding surface linear speed is 20 m/s. 14 kV were applied to the electrospinning needle and 15 kV to the electrospraying needle. They were placed on either side of the collector, respectively 16 cm and 18 cm away from the collector.

The production of these membranes was divided in two steps. First, particles and fibers were deposited simultaneously on the collector at a rotation speed of 3000 rpm during 2 minutes. Then, particles were deposited alone at the same speed of rotation during 1 minute. This two-steps cycle was repeated 30 times, the result corresponding to a fibers deposition time of one hour.

The obtained membranes were visibly structured at their surface. They were peeled and cured 48h at 120°C under vacuum, hold in the longitudinal direction to avoid shrinkage. They were subjected to a weak shrinkage in the transversal direction. They were then used for mechanical characterization.

2.5. Voltage measurement during electrospinning

Voltage measurements were performed at the surface of the smooth collector during electrospinning. A probe connected to an electrostatic voltmeter (Trek Model 347) was approached close to the surface of the collector. With this set-up, it was possible to follow the accumulation of charges, resulting in voltage, during electrospinning. PLA and PLA/PGS fibers were electrospun during 10 minutes with this equipment.

2.6. Characterizations of the membranes

The surface of the membrane was observed by scanning electron microscopy (SEM) after coating by a thin layer of gold. The SEM (Vega 3, Tescan) was used in high vacuum mode with a voltage of 5 kV. Mean diameter of aligned fibers was calculated over 100 diameters measurements using ImageJ software. The mean values are given with the standard deviation. The degree of alignment of PLA and PLA/PGS fibers produced by high speed rotation of the collector was also evaluated using ImageJ. The angle formed by the fibers and the horizontal border of the picture was compared to the mean angle value. SEM observations were also done to show the internal organization of the structured membranes. For this, the membranes were immersed in liquid nitrogen and then directly cut with a razor blade. The cut section was then observed.

Uniaxial tensile tests were conducted with the Linear Tension Geometry of a rheometer (Discovery HR3, TA Instruments) on samples made of aligned fibers with or without particles. The tests were done in the longitudinal and transversal direction, before and after crosslinking. Rectangular samples were cut with 5 mm width and about 20 mm long. The samples were fixed in the clamps with an initial gap of 10 mm and stretched at 100 μm/s until breaking. 5 measurements were performed for each type of samples except PLA/PGS fibers in the transversal direction, because these thin samples were very difficult to handle. Only one value was measured in this precise case. Young's modulus, ultimate tensile stress (UTS) and maximal strain were calculated from the stress-strain curves. The mean values are given with their standard deviation.

The internal structure of a membrane composed of aligned fibers and particles was investigated by X-ray micro-tomography (EasyTom 150/160, RXSolutions). A rectangular sample of approximatively 3x20x0.2 mm^3 was fixed on the holder. Tomographical reconstruction was carried out with the software myVGL by a filtered back projection. Beam power and energy ranged from 4 W and 70 kV for lowest resolution (10 μm) to 0.8 W and 50 kV for highest resolution (0.5 μm). The images were reconstructed after one rotation, from 2016 projections at 6 fps for the lowest resolution and 1600 projections at 0.6 fps for the higher resolution.

3. Results

3.1. Strategy A: combination of electrospinning and electrospraying

Structured scaffolds were prepared by combination of electrospinning of PLA fibers and electrospraying of pPGS particles

3.1.1. With PLA fibers

Alternate depositions of PLA fibers and pPGS spray onto a smooth cylindrical collector covered by an aluminum foil lead to the formation of thick and visibly structured membranes, typical of self-organized fibers, after 30 min (Figure 5.9.(A)).

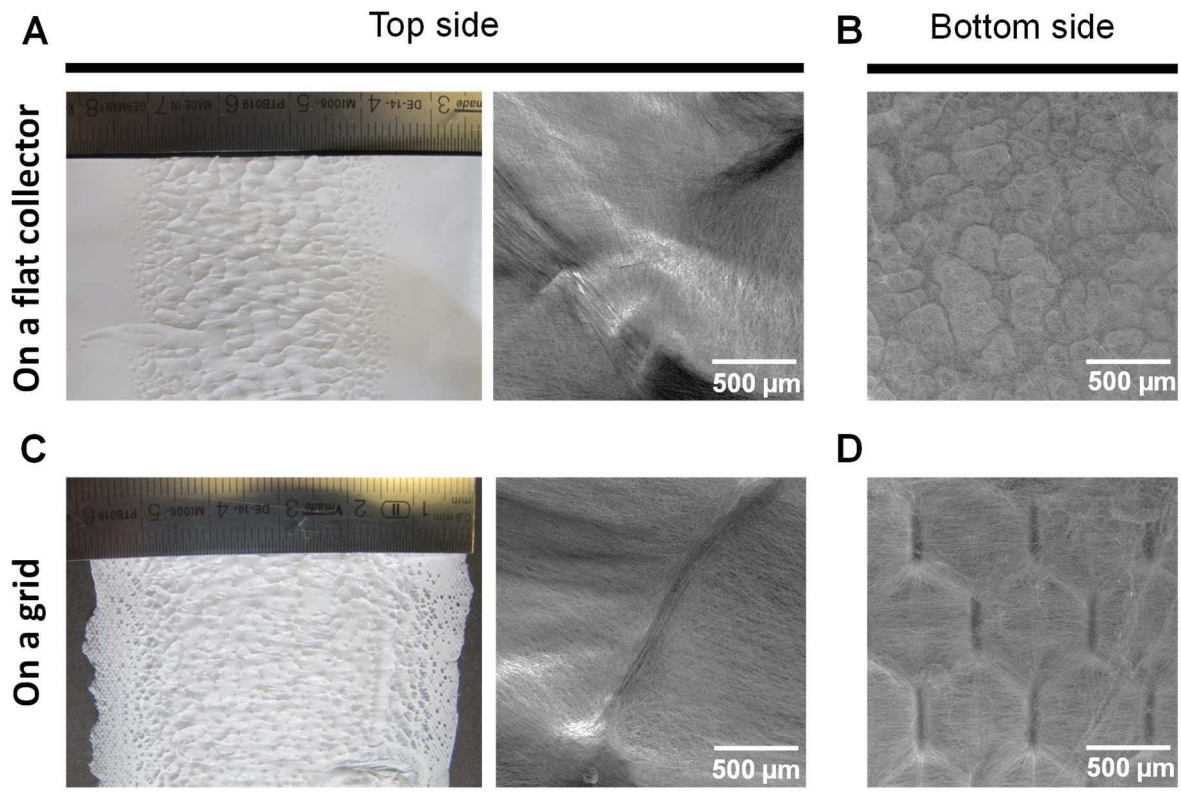

Figure 5.9. Pictures of PLA fibers and pPGS spray electrospun onto **(A-B)** a flat collector (aluminum foil) and **(C-D)** a structured collector (metallic grid) taken with a camera and the SEM on **(A-C)** top surface side and **(B-D)** bottom surface.

This hexagonal structure is obtained thanks to the structure of the grid described in Figure 5.8.(B) and (D) which allows the fibers to deposit mainly as schematized on Figure 5.10.

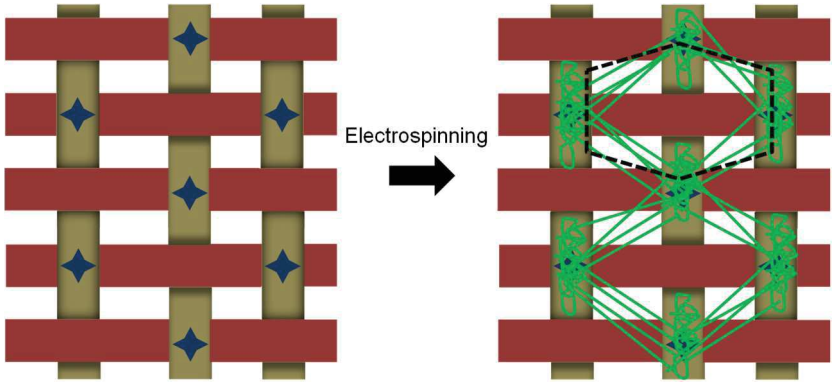

Figure 5.10. Representation of the apparition of hexagonal structures after electrospinning on a grid. The preferential disposition of the fibers is represented in green.

From Figure 5.9.(A), it can be noticed that the pattern is large in the middle and becomes smaller at the borders. Moreover, the patterns are smaller at the beginning of the production (Figure 5.9.(B): observation on the bottom side) than at the end (Figure 5.9.(A): observation on the top side). This evolution has already been observed for the alternative electrospinning and electrospraying of PLA fibers with PEG particles [40] leading to the self-organization of the fibers. It can be understood by the mechanism of construction of these pores made of hanging fibers and particles-based walls. These pores become larger during time because sometimes, a hanging fiber can land overhead a too short wall, as represented on the Figure 5.11.(A). Afterward, the wall is

hidden, and a new bigger pore grows up. It results in a pore size gradient in the thickness of the scaffold. Pores stay smaller at the border of the sample because the scaffold is thinner in this area.

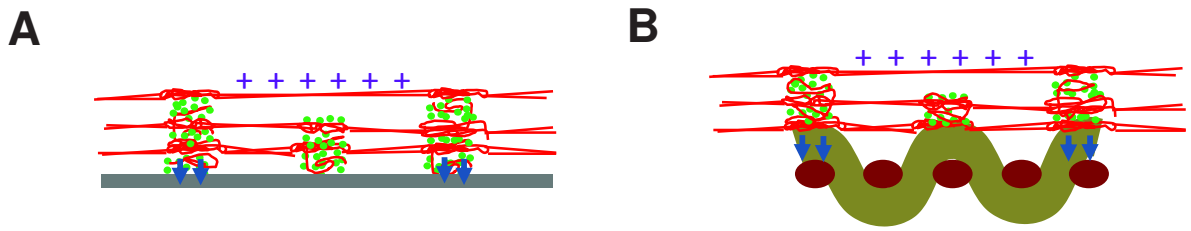

Figure 5.11. ***Schematic representation of the mechanism of expansion of a pore.*** **(A)** On a smooth collector. **(B)** On a metallic grid.

The same process conducted with a collector covered by the grid with rectangular holes gave similar results (Figure 5.9.(C)). The geometry of the pores is initially better controlled (Figure 5.9.(D)): thanks to the structure of the grid, honeycomb patterns are created. The Figure 5.12 shows the presence of pPGS spray on the walls of the honeycomb-like pores. However, this shape is lost during time due to the same phenomenon as explained above.

A closer look at the wall of the pattern shows that pPGS spray results in semi-liquid particles that wet the fibers, allowing a good dissipation of the electrical charges towards the collector and the formation of an electrical template (Figure 5.12). Moreover, after 2 days of curing at 120°C, the crosslinked PGS consolidates the walls of the pore and increases the cohesion of the membrane.

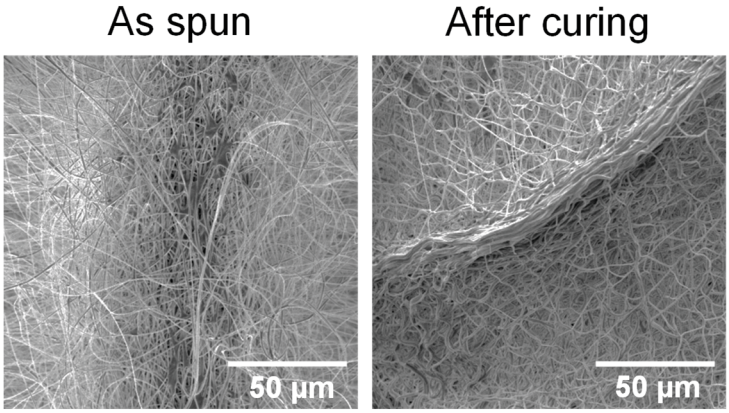

Figure 5.12. SEM pictures of the wall of a pore made of PLA fibers and PGS spray before and after curing.

The internal organization of such samples is interesting, as the objective is to fabricate a loose structure allowing the cells migration. SEM images taken after slicing in liquid nitrogen show that the membranes are crossed by dense columns and large pores (Figure 5.13). The pores seem disposed slightly more regularly for membrane electrospun with a patterned collector, but the difference remains not clear. However, preliminary cell culture experiments showed that cells can migrate more deeply in samples prepared with the grid (70 µm deep) than in samples prepared without (less than 50 µm after 48h of culture) after seeding on bottom surface. Indeed, pores on this side of membranes prepared on aluminum are too small. Finally, the method with the grid leads to the fabrication of scaffolds promoting cells penetration thanks to pores with a low density of fibers.

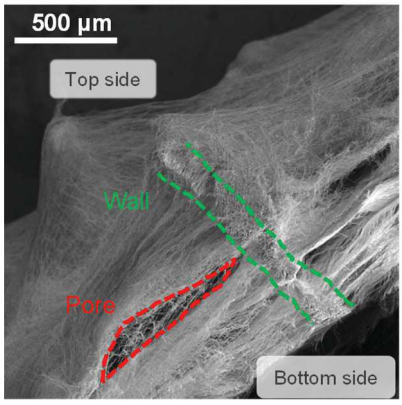

Figure 5.13. Cross-sectional view of a membrane composed of PLA fibers and pPGS spray deposited on a grid. Large pores and walls are visible.

3.1.2. With PLA/pPGS fibers

These first results being promising, it was intended to improve these scaffold properties by employing PLA/pPGS fibers instead of pure PLA fibers. The same kind of experience was thus repeated: alternate deposition of PLA/pPGS fibers and of pPGS spray onto a grid with rectangular holes. Unfortunately, in this case a different result was obtained with no structuration appearing at the surface of the membrane after one hour of production. The SEM image taken on collector side shows that an initial organization exists (Figure 5.14: bottom side). It is however less clear and obviously rapidly lost.

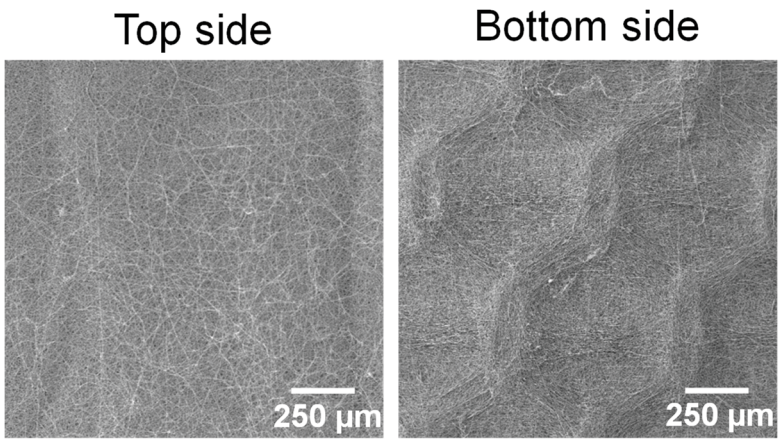

Figure 5.14. SEM pictures of a membrane made of PLA/PGS fibers and pPGS spray prepared on a grid.

In order to better understand this result, a bi-layer sample was prepared on a grid. Here, fibers are deposited during 30 s and then the spray is directly deposited during 30 s on the fibers. To have a good organization, most of the fibers should be deposited at the crossovers on the grid, with some segments strained over the holes. These few fibers segment hanging in air should keep their electrical charge, resulting in a repulsive interaction with the arriving particles. Therefore, the particles should exclusively deposit on the crossovers covered by the fibers, as explained above (Figure 5.6). The result for PLA/pPGS fibers and pPGS spray is here shown for a grid with square holes in Figure 5.15. It can be seen that the spray is deposited on the grid but also on the fibers over the holes. In this case, the formation of an electrical template with attractive and repulsive

areas does not seem to arise. Then, because of this material accumulation over the whole surface of the collector, no walls can grow and create pores.

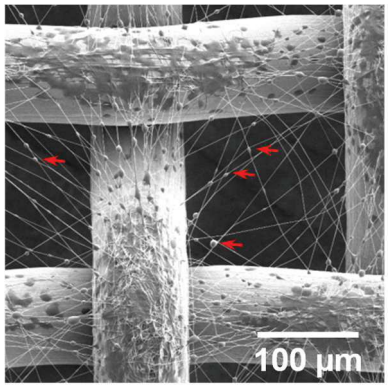

Figure 5.15. SEM picture of a first layer of PLA/pPGS fibers deposited on a grid covered by a second layer of pPGS spray. Red arrows indicate particles deposited over the hole.

In order to test this hypothesis, the electric potential at the surface of the sample was measured during electrospinning using an electrostatic voltmeter. In these experiments, the capacity of the electrospun fibers to accumulate charges was compared between PLA fibers or PLA/pPGS fibers. Indeed, during the process, fibers land charged on the smooth collector. If these charges are not dissipated, the electric potential increases at the surface of the mat during electrospinning. Its evolution is compared for PLA and PLA/pPGS fibers electrospun in the same conditions (Figure 5.16). It shows that while the voltage increases fast for PLA fibers, it increases very slowly for PLA/pPGS fibers, proving that only few charges accumulate on PLA/pPGS mat. From this result, it can be assumed that pPGS makes fibers conductive enough to let the charges dissipate, certainly because of its –COOH groups.

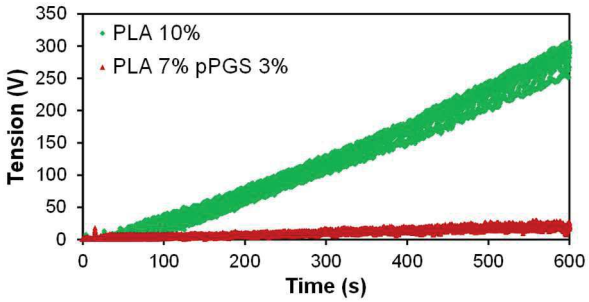

Figure 5.16. Evolution of the voltage at the surface of the collector during electrospinning of PLA and PLA/PGS fibers.

As a result, when PLA/pPGS fibers are electrospun onto a patterned collector, the hanging fibers do not keep their charges. Thus, no repulsive area appears, and particles can land everywhere resulting in a rapid loss of the organization of the scaffold.

Finally, structuration by combination of electrospinning and electrospraying is not possible for PGS-containing fibers. However, PGS can still be used for this kind of samples in the electrospray, its presence offering hydrophilic areas with available –OH groups and elastomeric points of attachment between fibers.

3.2. Strategy B: Aligned fibers

Fibrous scaffolds with aligned PLA or PLA/PGS fibers were obtained by electrospinning on a high-speed rotating collector. They were then cured at 120°C for 48h under vacuum.

3.2.1. Morphology of the scaffolds

SEM images of the scaffolds were taken for comparison before and after the curing step (Figure 5.17). PLA and PLA/PGS fibers were aligned by rotation of a large collector at 3000 rpm. This rotation rate corresponds to a surface moving at 20 m/s. As can be seen on Figure 5.17.(A), PLA and PLA/PGS fibers were relatively well aligned.

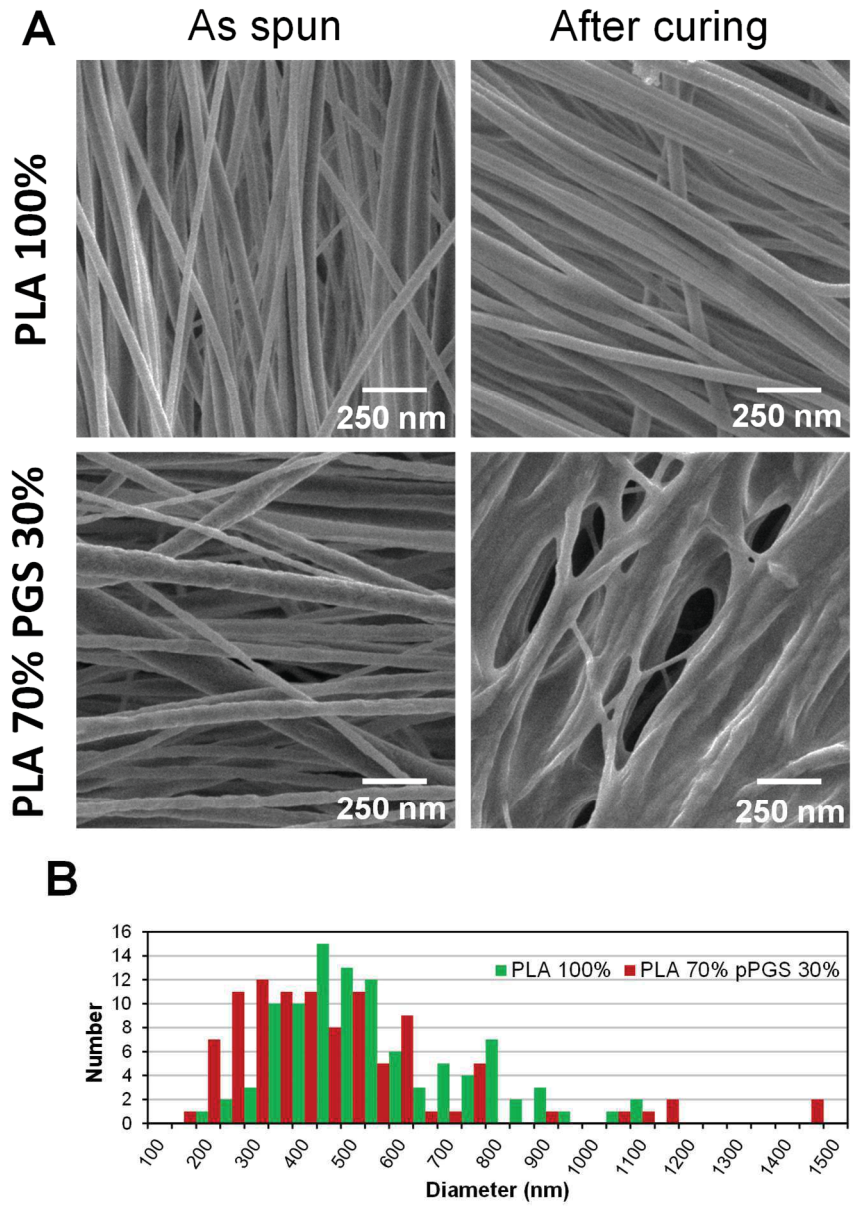

Figure 5.17. ***Morphology of the aligned fibers.*** **(A)** SEM pictures after electrospinning and after curing. **(B)** Diameter distribution after electrospinning.

For PLA fibers, 74% of the fibers forms an angle within ± 15° of the mean angle. PLA/PGS fibers are less well aligned, with only 54% of the angles being within ± 15° of the mean angle. It should be remarked that the samples analyzed here were detached from their support,

allowing them to move from their initial position. In particular, they are slightly wavy, and this can explain a degree of alignment slightly lower than expected. Moreover, experiments conducted at 4000 rpm gave a better alignment but led to defaults in the fibers. Finally, the alignment of the fibers should be improved if used on a heart, thanks to movement of the muscle.

Because of the alignment of the fibers, the membranes look quite dense with only few small pores. Moreover, the diameter distribution after electrospinning is given for both aligned sample in Figure 5.17.(B). In the case of aligned PLA fibers, the mean diameter of 526 ± 200 nm is similar to the mean diameter of non-aligned PLA fibers (see Chapter 3) showing that the collector speed does not have an important influence on the formation of the fibers. However, in the case of aligned PLA/PGS fibers, the mean diameter is lower than for the corresponding randomly deposited fibers (PLA/PGS_{thin} in Chapter 3 have a mean diameter of 532 ± 130 nm) with 443 ± 250 nm. This could indicate that due to the pPGS, PLA/PGS fibers were easier to stretch by high-speed rotation of the collector.

After curing, the mats look even denser (Figure 5.9.(A)). PLA fibers are a little bit wavier. Because of the high density of such membranes and of the proximity of the surface of neighboring fibers, it seems that some PLA fibers become attached together. This slight fusion is possible because the curing temperature is higher than the T_g of PLA. For PLA/PGS fibers, the result is much more pronounced: they clearly merge during curing. A lot of pores are thus closed after curing. Fibers are slightly less parallel, but the topography with grooves at the surface globally remains, what is interesting to guide the cells. Moreover, in contrast with other scaffolds with grooves at the surface [41], some pores, useful for nutriments or blood carriage, remain.

3.2.2. Mechanical properties

Mechanical properties of materials made of aligned fibers are of course very different in the direction of the fibers and in the direction perpendicular to the fibers. Measurements were thus performed for both directions and results are given in Figure 5.18. In the longitudinal direction, there is little contribution of interaction between the fibers to the measured stress. Yet, this contribution increases after curing, when fibers are merged together. In the transversal direction, fibers are very little solicited. The stress corresponds mainly to bending of fibers and fiber-fiber friction.

In the longitudinal direction

For the results in the longitudinal direction, the first observation that can be done is the high values of modulus and UTS, especially after curing. For example, aligned PLA fibers cured 48h at 120°C have a Young's modulus of 746 MPa. For comparison, the Young's modulus of dry randomly deposited PLA fibers cured two days at 120°C was found close to 150 MPa [42]. The alignment offers a high mechanical strength in the direction of the fibers. As explained above, in the anisotropic case, almost no friction at contact points contributes to the initial modulus. It corresponds exclusively to the deformation of the material the fibers are made of. However, the modulus found for aligned fibers remains lower than for a non-porous PDLLA film, which has a Young's modulus measured between 1 and 3.45 GPa [43], because of the lower density of the fibrous sample. On the contrary, in the case of randomly depostied fibers, displacement of the fibers in the direction of the mechanical force and resulting friction forces contribute to the measured Young's modulus before their elongation. Consequently, the modulus measured in the longitudinal direction is largely too high for cardiac tissue. From the typical stress-strain curves

given in Figure 5.18.(A), it should be noticed that the rupture is often not abrupt: the fracture spreads progressively while the fibers break successively. It is particularly visible for as spun PLA fibers. PLA/PGS fibers, especially after curing, form more cohesive membranes that break more abruptly.

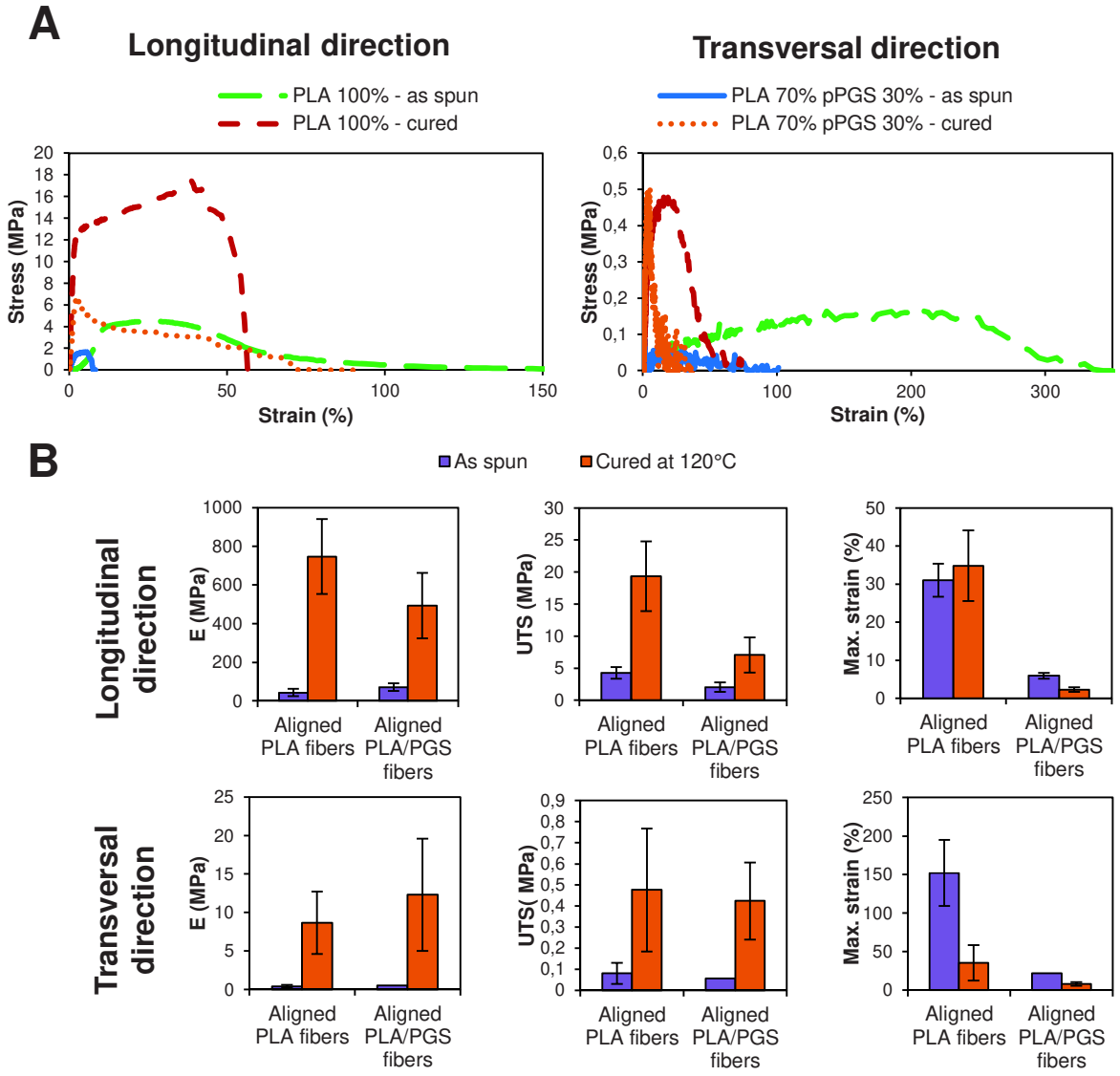

Figure 5.18. ***Mechanical properties of aligned PLA and PLA/PGS fibers in dry state.*** **(A)** Typical stress-strain curves in the longitudinal and transversal directions before and after curing. **(B)** Results after tensile tests in the longitudinal and transversal directions before and after curing. The error bars correspond to the standard deviation.

After curing, Young's modulus and UTS of both type of membranes increase, just like for randomly deposited fibers. This can be explained by changes in the material, namely crystallization of PLA and crosslinking of PGS.

The presence of the soft PGS in the fibers has the effect to decrease the rigidity of the membranes: the Young's modulus, the UTS and the strain at break are lower for PLA/PGS fibers. This difference is more particularly clear after crosslinking. The same tendency was not observed for wet randomly deposited PLA and PLA/PGS fibers (see PLA/PGS_{thin} in Chapter 3) where the contribution of the interaction between fibers was more important: PGS increases the cohesion between fibers, which increases the strength of the fibrous material. But this phenomenon has less

effect for aligned fibers stretched in the longitudinal direction. Moreover, it was inferred from SEM pictures of as spun aligned fibers that PLA/pPGS fibers may be more affected by the strong stretching. This is visible because some of the fibers are thinner than on randomly deposited mats. So, after crosslinking, PLA/PGS fibers are maybe weakened by the stronger stretching they undergo due to the high-speed rotation.

In the transversal direction

The force measured in the transversal direction was measurable but very low; the data comprise thus a lot of noise. It corresponds to friction forces and bending of the fibers. Under the action of friction forces, fibers are dragged during stretching of the membrane, which allows high strains before the break point, where no fibers are in contact anymore.

As in the longitudinal direction, the Young's modulus and the UTS increase after curing. The strain at break tends to decrease. Here, crystallization of PLA and crosslinking of PGS should play a very minor role. These results are however easy to justify for PLA/PGS fibers because of the merging of the fibers during curing. The same evolution of the properties in the pure PLA case indicates that some stronger interactions appear also between PLA fibers during curing, as observed on the SEM pictures. Moreover, crystallization and thus stiffening of PLA during curing makes fibers more difficult to bend.

In the transversal direction for as spun fibers, the mechanical behavior is not very dependent to the presence of PGS. The only noticeable difference relies on the strain at break, which is much higher for PLA fibers. This could be explained by the weaker interactions between PLA fibers that allow them to be bended more easily. Surprisingly, after curing, the Young's modulus of PLA/PGS fibers is not significantly higher and the strain at break not significantly lower than for PLA fibers, despite the partial merging of the fibers. This may be related to the low precision of the measurement, as the force is very low.

To conclude, the tensile tests confirmed the anisotropy of the mechanical properties, which is interesting for the intended application. These membranes are however very weak in the transversal direction. In order to improve this point, multilayer scaffolds could be prepared with randomly oriented fibers in-between two layers of aligned fibers, as it was proposed by Belanger *et al.* [44].

3.2.3. Biological results

The biological properties of the aligned scaffolds in vitro and in vivo are currently under investigation and until now, results were only obtained for a first culture test on PLA aligned fibers. Cardiomyocytes were seeded on PLA aligned fibers or PLA randomly oriented fiber for comparison. Both scaffolds were coated with Matrigel prior to cell seeding. After 3 days of culture, the cells were stained and observed by microscopy. Figure 5.19 gives optical images of the seeded scaffolds after staining of the cardiomyocytes. It can be seen that the cells are clearly better aligned on aligned fibers than on random fibers, thus proving the ability of the aligned fibers to guide the cell proliferation.

These first results are thus promising, however because of the very high density of the aligned fibers, the cells will proliferate only on the surface of the scaffold. In order to improve the migration inside of the scaffolds, a larger porosity should be obtained.

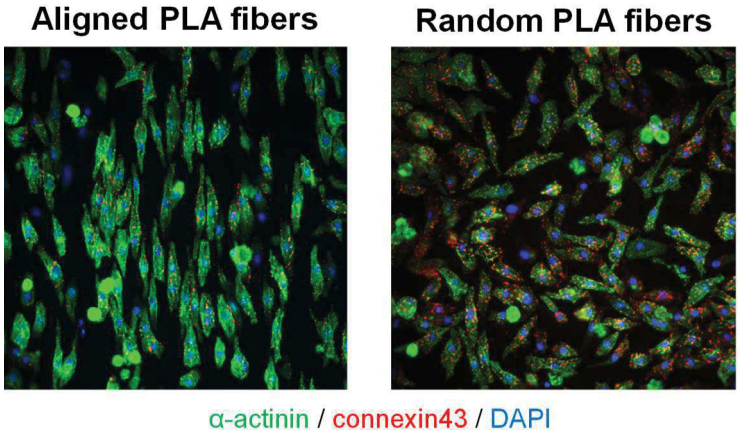

Figure 5.19. Immunofluorescence results after 3 days of culture of cardiomyocytes on PLA fibers aligned and randomly deposited both cured.

3.3. Strategy C: combination of aligned fibers and electrospraying

Starting from the previous results, it was decided to combine the aligned fibers able to guide cells and the incorporation of particles to make less dense scaffolds. The objective was here the separation of the layers of fibers rather than a well-controlled organization of the fibers. For this purpose, well-defined particles were needed. As it was not possible to make "solid" particles from only pPGS. But with the addition of HPβCD and after optimization of the concentrations in the spray solution, it was possible to make almost spherical particles. Cyclodextrin was chosen to have the possibility to encapsulate molecules of therapeutic interest able to diffuse from the clusters of particles in the scaffold. It can also be bonded to PGS during curing. Moreover, to enhance the separation between the layers of fibers, the amount of particles was maximized. Indeed, two phases were alternated. During the first phase, fibers and particles were deposited alternatively thanks to the rotation of the collector. In the second phase, only particles are deposited, to make a larger separation before the next fibers deposition. In addition, two needles were used for electrospraying in order to increase the global particles flow rate.

3.3.1. Morphology of the scaffolds

After the equivalent of one hour of fibers deposition, a thick membrane is fabricated with visible structuration at the surface, as shown on Figure 5.20. SEM observations confirm that on top surface, long clusters of particles are visible (encircled in yellow on Figure 5.21)), surrounded by well-aligned fibers. However, on the bottom surface, particles are dispersed all over the bottom surface, forming no big clusters: as observed for strategy A, the patterns increase in size during the production.

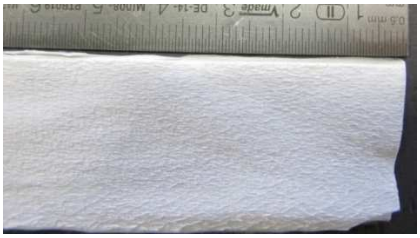

Figure 5.20. Picture of a membrane made of aligned PLA fibers and pPGS/HPβCD particles.

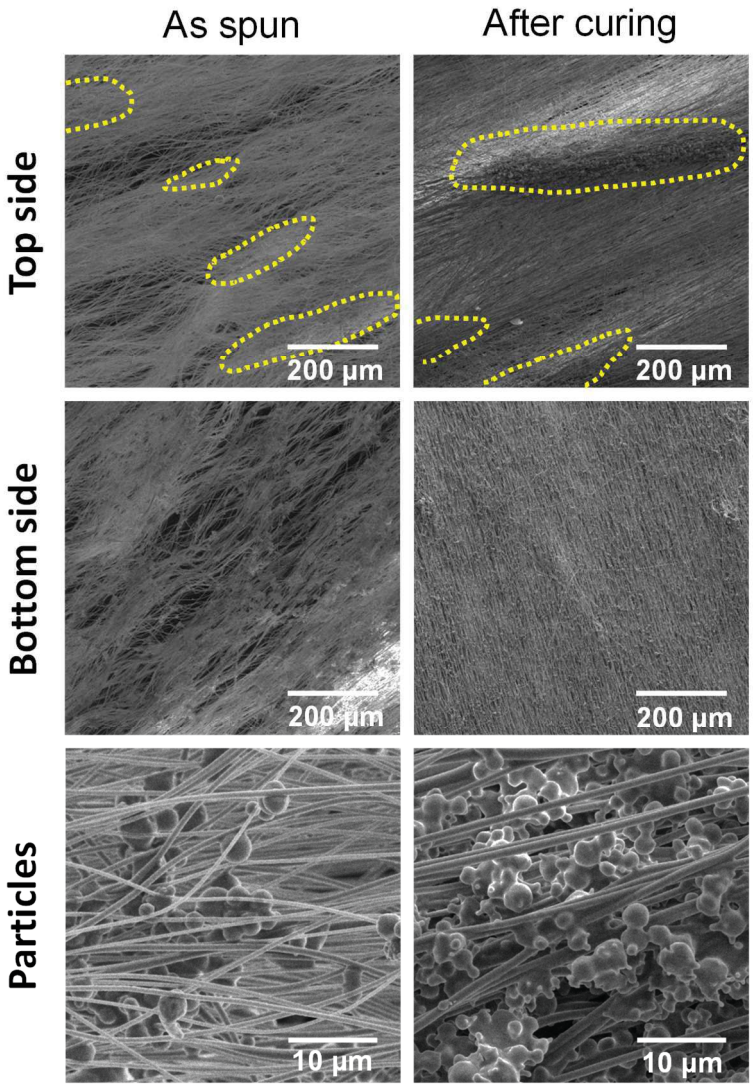

Figure 5.21. SEM pictures of a membrane made of aligned PLA fibers and PGS/HPβCD particles. Particles clusters are encircled in yellow on the top side view.

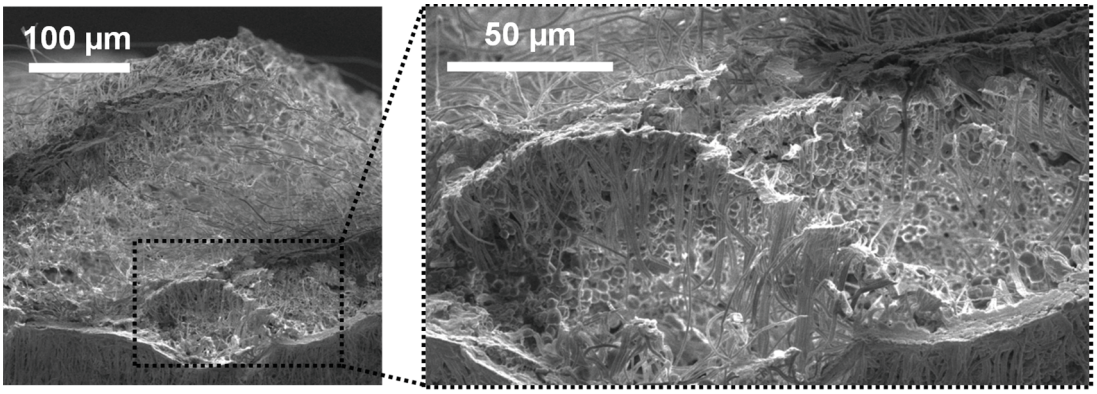

Figure 5.22. Cross-sectional view of a membrane made of aligned PLA fibers and PGS/HPβCD particles, with a zoom on two pores.

After two days of curing at 120°C to crosslink the PGS in the particles, the same organization is still visible (Figure 5.21). Curing also leads to the merging of the particles, what allows a better cohesion of the material: it is then easier to handle and it was possible to cut it in liquid nitrogen in order to observe their cross-section perpendicular to the direction of the fibers (Figure 5.22). These observations allowed to confirm the low density and the high thickness of such samples. Indeed, they are about 300 µm thick as spun for only about 150 µm for aligned PLA fibers produced during the same time without particles. Figure 5.22 shows that the membrane is composed of small domains delimited by dense lines composed of particles and aligned fibers. This organization can be compared to the structure found in the heart tissue, which is also composed of large pores surrounded by aligned collagen fibers.

To complete the SEM observations, the internal structure of these samples composed of aligned PLA fibers and PGS/HPβCD particles cured was analyzed by tomography. Despite the similar atomic composition of fibers and particles, the contrast was sufficient to observe areas with particles and areas with fibers (Figure 5.23). This may be explained by the high density of oxygen atoms in cyclodextrins (about one over three) compared to PLA (one over four).

On Figure 5.23.(A), a plane close to the top (last layers deposited) is compared to a plane close to the bottom (first layers deposited). With these two images at the same scale, it is clearly visible that the pattern becomes larger during the process, confirming what was observed on SEM pictures.

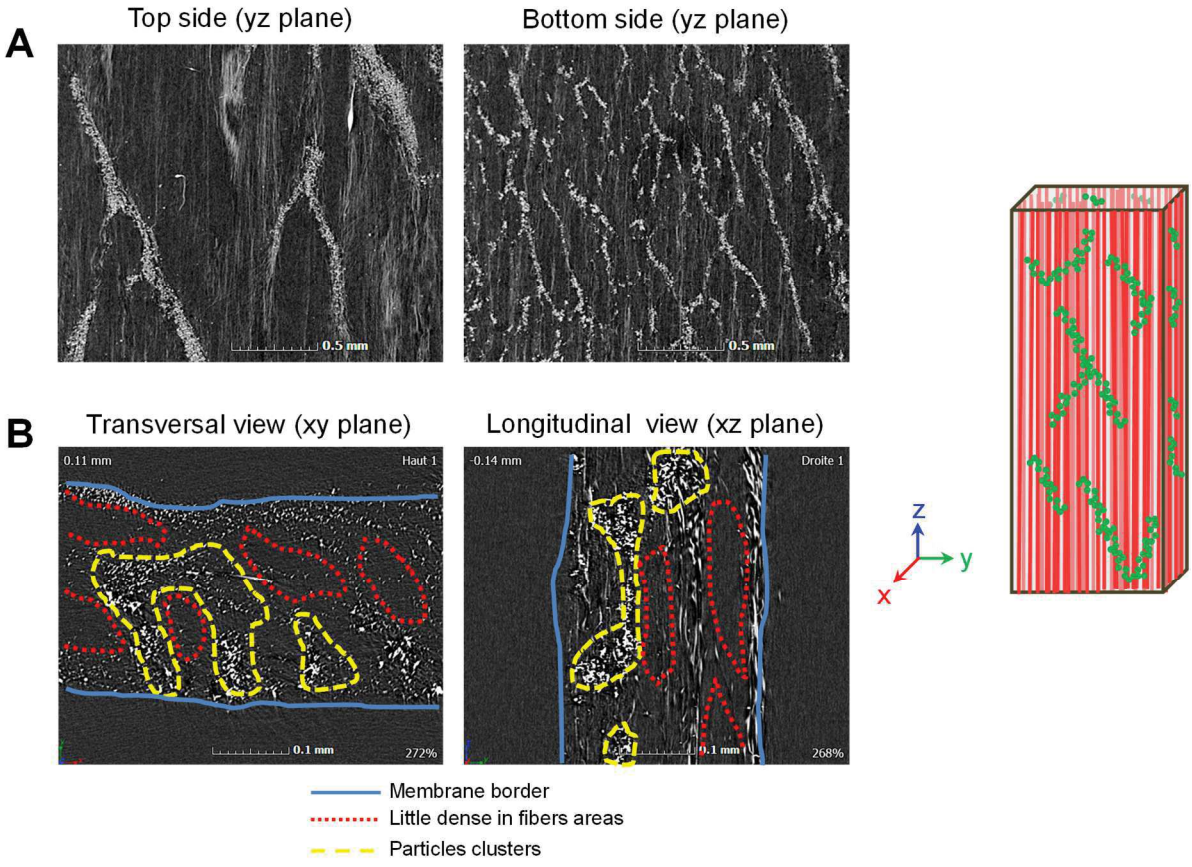

Figure 5.23. X-ray micro-*tomography images.* (A) Observation in the plane parallel to the surface (yz) of the sample. On the left, a slide close to the top surface; on the right, a plane close to the bottom surface (resolution: 2 µm). **(B)** Transversal (xy plane) and longitudinal (xz plane) views. The clusters of particles are surrounded (resolution: 0.5 µm).

On Figure 5.23.(B), we can observe on a transversal and a longitudinal cut some areas with few particles (dark areas) surrounded by clusters of particles.

The tomography method can thus help us to observe the pores present in the scaffolds. In order to make a better reconstruction of the organization of the pores, it could be interesting to add a contrast agent to separate the fibers areas from the particles areas.

3.3.1. Mechanical properties

As for aligned fibers without particles, mechanical properties of such materials are very different in the longitudinal and in the transversal direction: both were tested before and after curing, and the results are given in Figure 5.24. The Young's moduli and UTS are much lower in the transversal direction, while high ultimate strains can be reached. Again, this is due to the low contribution of interactions between fibers in the longitudinal direction, whereas there are dominant in the transversal direction.

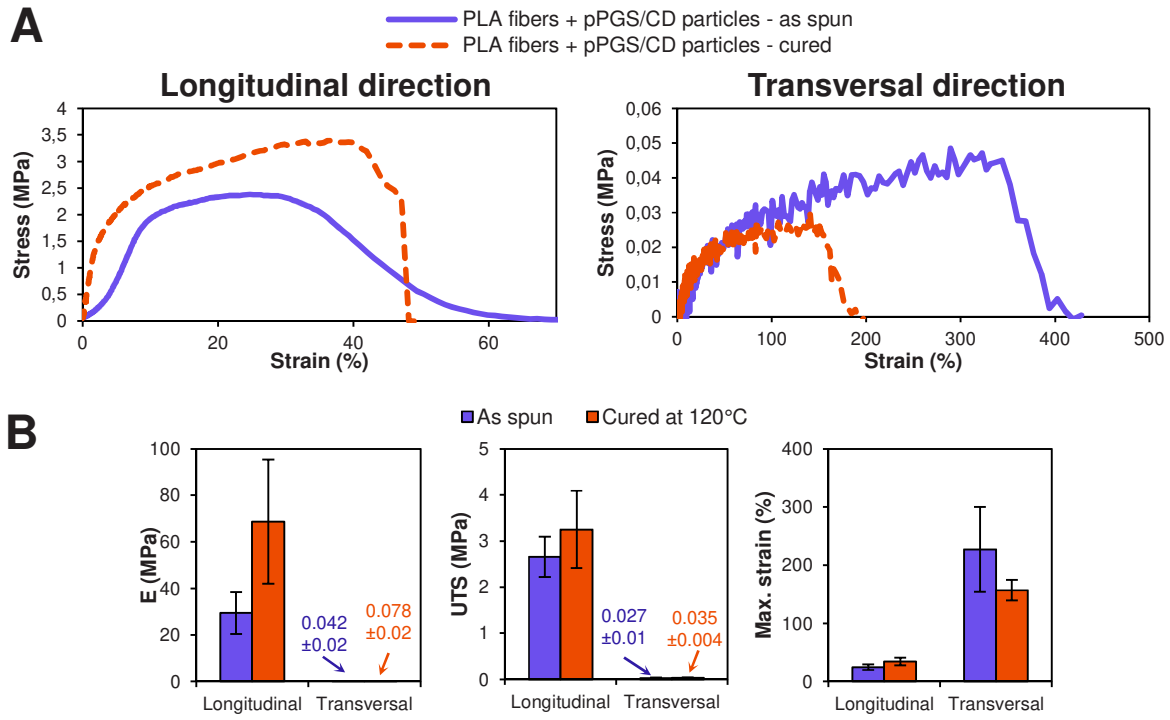

Figure 5.24. ***Mechanical properties of aligned PLA fibers structured with pPGS/HPBCD particles at dry state.*** **(A)** Typical stress-strain curves in the longitudinal and transversal directions. **(B)** Results after tensile tests in the longitudinal and transversal directions before and after curing. The error bars correspond to the standard deviation.

The curing has also the same effect as in the absence of particles: it tends to increase the Young's modulus and the UTS in the direction of the fibers because of the crystallization of PLA. Moreover, the crosslinking of PGS located in the particles clusters improves the cohesion of the membrane which leads to an increase of the Young's modulus and the UTS in the perpendicular direction too.

The Young's moduli and UTS are globally lower for the samples with particles than for aligned PLA fibers alone (Table 5.1). This tendency is stronger after curing. This could be explained by the lower density of samples with particles. Indeed, the same total fiber length should be deposited in both cases during the electrospinning experience because the final production time was equivalent. However, the thickness is much higher when particles are included among the

fibers (240 µm versus 120 µm without particles, as shown on Table 5.1). After curing, this difference is more pronounced because while PLA fibers collapse under the effect of the temperature, the structure is well conserved when particles are present. Samples with particles are thus less dense in term of fibers and the apparent stress is thus lower.

However, this observation is not sufficient to explain the large difference after curing. Indeed, the presence of the particles increases the interaction between fibers. Friction forces located in the particles areas contribute to the stress. Moreover, the particles clusters provide a better cohesion of the material, especially in the transversal direction, that allows higher strains at break. This is mostly true after crosslinking of PGS.

Table 5.1. Characteristics of PLA and PLA/PGS aligned fibers and aligned PLA fibers organized by pPGS/HPβCD particles. Mechanical properties correspond to the measurements in the longitudinal direction at dry state.

		Thickness (µm)	E (MPa)	UTS (MPa)	ε_{break} (%)
Aligned PLA fibers	as spun	118±26	44±20	4±1	31±4
	cured	50±11	746±194	19±5	35±9
Aligned PLA/PGS fibers	as spun	43±17	72±20	2±1	6±1
	cured	28±17	493±169	7±3	2±1
Aligned PLA fibers + pPGS/CD particles	as spun	240±18	29±9	3±0.4	25±5
	cured	254±75	69±27	3±1	34±6

Finally, the inclusion of particles among the aligned PLA fibers has an effect on the mechanical properties of the scaffolds. A strong anisotropy is still observed, but higher strains can be reached for lower apparent moduli, what is interesting for soft tissue engineering: after curing, the modulus in the longitudinal direction is about 70 MPa and the strain at break 30% versus about 100 kPa and 150% in the transversal direction. It could be interesting to perform a deeper analysis of the mechanical behavior of such structures by making SEM observation during tensile tests in order to understand the movement of the fibers and clusters.

To conclude this part, by combination of aligned fibers and particles, it was possible to obtain structures that resemble the cardiac tissue, with interesting mechanical properties. Moreover, the formulation of the particles was chosen to combine the advantageous properties of PGS and the possibility of encapsulation offered by the cyclodextrin, making these scaffolds promising. Biological investigation of the ability of the scaffolds to be used as matrix for cardiac tissue regeneration are currently performed and should confirm the interest of these membranes.

4. Conclusion

In this chapter, several strategies were investigated in order to structure electrospun membranes designed for cardiac tissue engineering. In a first strategy, electrospinning and electrospraying were combined to apply the ETAD process. This process exploits the electrostatic template created thanks to the spray. Unfortunately, this method did not work with PLA/PGS fibers because of their electrical conductivity. However, good results were obtained with PLA fibers and PGS spray and scaffolds including large pores able to promote cell penetration were fabricated using both flat and structured collectors. The control of the porosity and the resulting cell penetration were better when a pattern was used.

In a second strategy, the rotation of the collector at high velocity allowed to align PLA or PLA/PGS fibers in one direction, in order to mimic the structural and mechanical anisotropy of the cardiac tissue. We can assume that PLA/PGS aligned fibers have a good potential for cardiac tissue engineering. Indeed, it was shown in Chapter 3 that PLA/PGS fibers can enhance cardiac regeneration. In addition, first results with aligned PLA fibers showed that cardiomyocytes seeded on them get a good phenotype. Biological tests such as cardiomyocytes culture and *in vivo* implantation are currently carried out in order to prove the interest of such membranes in comparison to random fibers or pure PLA aligned fibers. If the results are promising, these scaffolds could be used *in vivo* to test their ability to help the regeneration of a defective heart. They could also have a great interest for *in vitro* phenotypic analyses with cardiomyocytes. These scaffolds were however very dense, especially PGS-containing membranes. Such structures are thus interesting to guide the cells at the surface but tend to hinder a deep migration in the scaffolds.

For this reason, a third strategy was carried out. Scaffolds with large pores and aligned fibers were obtained by electrospinning of PLA fibers and electrospraying of pPGS/HPβCD particles onto a high speed-rotating collector. These structures mimic well heart tissue. It is too early to confirm their therapeutic interest, but their high porosity makes them promising, especially concerning cell penetration. Moreover, these membranes could be exploited for drug delivery as encapsulation could be performed thanks to the presence of cyclodextrins.

References

1. Macchiarelli, G.; Ohtani, O.; Nottola, S.; Stallone, T.; Camboni, A.; M Prado, I.; M Motta, P. A micro-anatomical model of the distribution of myocardial endomysial collagen. *Histol Histopathol* **2002**, *17*, 699–706.
2. Engelmayr Jr, G.C.; Cheng, M.; Bettinger, C.J.; Borenstein, J.T.; Langer, R.; Freed, L.E. Accordion-like honeycombs for tissue engineering of cardiac anisotropy. *Nature Materials* **2008**, *7*, 1003–1010.
3. Huang, N.F.; Patel, S.; Thakar, R.G.; Wu, J.; Hsiao, B.S.; Chu, B.; Lee, R.J.; Li, S. Myotube Assembly on Nanofibrous and Micropatterned Polymers. *Nano Lett.* **2006**, *6*, 537–542.
4. Kai, D.; Prabhakaran, M.P.; Jin, G.; Ramakrishna, S. Guided orientation of cardiomyocytes on electrospun aligned nanofibers for cardiac tissue engineering. *Journal of Biomedical Materials Research Part B: Applied Biomaterials* **2011**, *98B*, 379–386.
5. Guex, A.G.; Kocher, F.M.; Fortunato, G.; Körner, E.; Hegemann, D.; Carrel, T.P.; Tevaearai, H.T.; Giraud, M.N. Fine-tuning of substrate architecture and surface chemistry promotes muscle tissue development. *Acta Biomaterialia* **2012**, *8*, 1481–1489.
6. Kharaziha, M.; Shin, S.R.; Nikkhah, M.; Topkaya, S.N.; Masoumi, N.; Annabi, N.; Dokmeci, M.R.; Khademhosseini, A. Tough and flexible CNT–polymeric hybrid scaffolds for engineering cardiac constructs. *Biomaterials* **2014**, *35*, 7346–7354.
7. Wanjare, M.; Hou, L.; H. Nakayama, K.; J. Kim, J.; P. Mezak, N.; J. Abilez, O.; Tzatzalos, E.; C. Wu, J.; F. Huang, N. Anisotropic microfibrous scaffolds enhance the organization and function of cardiomyocytes derived from induced pluripotent stem cells. *Biomaterials Science* **2017**, *5*, 1567–1578.
8. Liu, Y.; Wang, S.; Zhang, R. Composite poly(lactic acid)/chitosan nanofibrous scaffolds for cardiac tissue engineering. *International Journal of Biological Macromolecules* **2017**, *103*, 1130–1137.
9. Matthews, J.A.; Wnek, G.E.; Simpson, D.G.; Bowlin, G.L. Electrospinning of Collagen Nanofibers. *Biomacromolecules* **2002**, *3*, 232–238.
10. Courtney, T.; Sacks, M.S.; Stankus, J.; Guan, J.; Wagner, W.R. Design and analysis of tissue engineering scaffolds that mimic soft tissue mechanical anisotropy. *Biomaterials* **2006**, *27*, 3631–3638.
11. Hsiao, C.-W.; Bai, M.-Y.; Chang, Y.; Chung, M.-F.; Lee, T.-Y.; Wu, C.-T.; Maiti, B.; Liao, Z.-X.; Li, R.-K.; Sung, H.-W. Electrical coupling of isolated cardiomyocyte clusters grown on aligned conductive nanofibrous meshes for their synchronized beating. *Biomaterials* **2013**, *34*, 1063–1072.
12. Ribeiro, C.; Sencadas, V.; Costa, C.M.; Gómez Ribelles, J.L.; Lanceros-Méndez, S. Tailoring the morphology and crystallinity of poly(L-lactide acid) electrospun membranes. *Sci. Technol. Adv. Mater.* **2011**, *12*.
13. Valente, T.A.M.; Silva, D.M.; Gomes, P.S.; Fernandes, M.H.; Santos, J.D.; Sencadas, V. Effect of Sterilization Methods on Electrospun Poly(lactic acid) (PLA) Fiber Alignment for Biomedical Applications. *ACS Appl. Mater. Interfaces* **2016**, *8*, 3241–3249.
14. Wu, H.-J.; Hu, M.-H.; Tuan-Mu, H.-Y.; Hu, J.-J. Preparation of aligned poly(glycerol sebacate) fibrous membranes for anisotropic tissue engineering. *Materials Science and Engineering: C* **2019**, *100*, 30–37.
15. Xu, B.; Cook, W.D.; Zhu, C.; Chen, Q. Aligned core/shell electrospinning of poly(glycerol sebacate)/poly(l-lactic acid) with tuneable structural and mechanical properties. *Polym. Int.* **2016**, *65*, 423–429.
16. Li, D.; Wang, Y.; Xia, Y. Electrospinning of Polymeric and Ceramic Nanofibers as Uniaxially Aligned Arrays. *Nano Lett.* **2003**, *3*, 1167–1171.
17. Kenar, H.; Kose, G.T.; Hasirci, V. Design of a 3D aligned myocardial tissue construct from biodegradable polyesters. *J Mater Sci: Mater Med* **2010**, *21*, 989–997.
18. Orlova, Y.; Magome, N.; Liu, L.; Chen, Y.; Agladze, K. Electrospun nanofibers as a tool for architecture control in engineered cardiac tissue. *Biomaterials* **2011**, *32*, 5615–5624.
19. Masoumi, N.; Larson, B.L.; Annabi, N.; Kharaziha, M.; Zamanian, B.; Shapero, K.S.; Cubberley, A.T.; Camci-Unal, G.; Manning, Keefe.B.; Mayer, J.E.; et al. Electrospun PGS:PCL Microfibers Align Human Valvular Interstitial Cells and Provide Tunable Scaffold Anisotropy. *Advanced Healthcare Materials* **2014**, *3*, 929–939.
20. Salehi, S.; Bahners, T.; Gutmann, J.S.; Gao, S.-L.; Mäder, E.; Fuchsluger, T.A. Characterization of structural, mechanical and nano-mechanical properties of electrospun PGS/PCL fibers. *RSC Adv.* **2014**, *4*, 16951–16957.

21. Katta, P.; Alessandro, M.; Ramsier, R.D.; Chase, G.G. Continuous Electrospinning of Aligned Polymer Nanofibers onto a Wire Drum Collector. *Nano Lett.* **2004**, *4*, 2215–2218.
22. Bhattarai, N.; Edmondson, D.; Veiseh, O.; Matsen, F.A.; Zhang, M. Electrospun chitosan-based nanofibers and their cellular compatibility. *Biomaterials* **2005**, *26*, 6176–6184.
23. Theron, A.; Zussman, E.; Yarin, A.L. Electrostatic field-assisted alignment of electrospun nanofibres. *Nanotechnology* **2001**, *12*, 384–390.
24. Ifkovits, J.L.; Wu, K.; Mauck, R.L.; Burdick, J.A. The Influence of Fibrous Elastomer Structure and Porosity on Matrix Organization. *PLOS ONE* **2010**, *5*, e15717.
25. Kenar, H.; Kose, G.T.; Toner, M.; Kaplan, D.L.; Hasirci, V. A 3D aligned microfibrous myocardial tissue construct cultured under transient perfusion. *Biomaterials* **2011**, *32*, 5320–5329.
26. Salehi, S.; Fathi, M.; Javanmard, S.H.; Bahners, T.; Gutmann, J.S.; Ergün, S.; Steuhl, K.P.; Fuchsluger, T.A. Generation of PGS/PCL Blend Nanofibrous Scaffolds Mimicking Corneal Stroma Structure. *Macromolecular Materials and Engineering* **2014**, *299*, 455–469.
27. Li, D.; Ouyang, G.; McCann, J.T.; Xia, Y. Collecting Electrospun Nanofibers with Patterned Electrodes. *Nano Lett.* **2005**, *5*, 913–916.
28. Lavielle, N.; Hébraud, A.; Mendoza-Palomares, C.; Ferrand, A.; Benkirane-Jessel, N.; Schlatter, G. Structuring and Molding of Electrospun Nanofibers: Effect of Electrical and Topographical Local Properties of Micro-Patterned Collectors. *Macromolecular Materials and Engineering* **2012**, *297*, 958–968.
29. Tallawi, M.; Dippold, D.; Rai, R.; D'Atri, D.; Roether, J.A.; Schubert, D.W.; Rosellini, E.; Engel, F.B.; Boccaccini, A.R. Novel PGS/PCL electrospun fiber mats with patterned topographical features for cardiac patch applications. *Materials Science and Engineering: C* **2016**, *69*, 569–576.
30. Deitzel, J.M.; Kleinmeyer, J.; Harris, D.; Beck Tan, N.C. The effect of processing variables on the morphology of electrospun nanofibers and textiles. *Polymer* **2001**, *42*, 261–272.
31. Thandavamoorthy, S.; Gopinath, N.; Ramkumar, S.S. Self-assembled honeycomb polyurethane nanofibers. *Journal of Applied Polymer Science* **2006**, *101*, 3121–3124.
32. Yan, G.; Yu, J.; Qiu, Y.; Yi, X.; Lu, J.; Zhou, X.; Bai, X. Self-Assembly of Electrospun Polymer Nanofibers: A General Phenomenon Generating Honeycomb-Patterned Nanofibrous Structures. *Langmuir* **2011**, *27*, 4285–4289.
33. Ahirwal, D.; Hébraud, A.; Kádár, R.; Wilhelm, M.; Schlatter, G. From self-assembly of electrospun nanofibers to 3D cm thick hierarchical foams. *Soft Matter* **2013**, *9*, 3164–3172.
34. Bock, N.; Dargaville, T.R.; Woodruff, M.A. Electrospraying of polymers with therapeutic molecules: State of the art. *Progress in Polymer Science* **2012**, *37*, 1510–1551.
35. Guarino, V.; Altobelli, R.; Cirillo, V.; Cummaro, A.; Ambrosio, L. Additive electrospraying: a route to process electrospun scaffolds for controlled molecular release. *Polymers for Advanced Technologies* **2015**, *26*, 1359–1369.
36. Lavielle, N.; Popa, A.-M.; de Geus, M.; Hébraud, A.; Schlatter, G.; Thöny-Meyer, L.; Rossi, R.M. Controlled formation of poly(ε-caprolactone) ultrathin electrospun nanofibers in a hydrolytic degradation-assisted process. *European Polymer Journal* **2013**, *49*, 1331–1336.
37. Wittmer, C.R.; Hébraud, A.; Nedjari, S.; Schlatter, G. Well-organized 3D nanofibrous composite constructs using cooperative effects between electrospinning and electrospraying. *Polymer* **2014**, *55*, 5781–5787.
38. Nedjari, S.; Hébraud, A.; Eap, S.; Siegwald, S.; Mélart, C.; Benkirane-Jessel, N.; Schlatter, G. Electrostatic template-assisted deposition of microparticles on electrospun nanofibers: towards microstructured functional biochips for screening applications. *RSC Adv.* **2015**, *5*, 83600–83607.
39. Garcia Garcia, A.; Hébraud, A.; Duval, J.-L.; Wittmer, C.R.; Gaut, L.; Duprez, D.; Egles, C.; Bedoui, F.; Schlatter, G.; Legallais, C. Poly(ε-caprolactone)/Hydroxyapatite 3D Honeycomb Scaffolds for a Cellular Microenvironment Adapted to Maxillofacial Bone Reconstruction. *ACS Biomater. Sci. Eng.* **2018**, *4*, 3317–3326.
40. Lavielle, N.; Hébraud, A.; Schlatter, G.; Thöny-Meyer, L.; Rossi, R.M.; Popa, A.-M. Simultaneous Electrospinning and Electrospraying: A Straightforward Approach for Fabricating Hierarchically Structured Composite Membranes. *ACS Appl. Mater. Interfaces* **2013**, *5*, 10090–10097.
41. Zhu, C.; Rodda, A.E.; Truong, V.X.; Shi, Y.; Zhou, K.; Haynes, J.M.; Wang, B.; Cook, W.D.; Forsythe, J.S. Increased Cardiomyocyte Alignment and Intracellular Calcium Transients Using Micropatterned and Drug-Releasing Poly(Glycerol Sebacate) Elastomers. *ACS Biomater. Sci. Eng.* **2018**, *4*, 2494–2504.

42. You, Z.-R.; Hu, M.-H.; Tuan-Mu, H.-Y.; Hu, J.-J. Fabrication of poly(glycerol sebacate) fibrous membranes by coaxial electrospinning: Influence of shell and core solutions. *Journal of the Mechanical Behavior of Biomedical Materials* **2016**, *63*, 220–231.
43. Farah, S.; Anderson, D.G.; Langer, R. Physical and mechanical properties of PLA, and their functions in widespread applications — A comprehensive review. *Advanced Drug Delivery Reviews* **2016**, *107*, 367–392.
44. Belanger, K.; Schlatter, G.; Hébraud, A.; Marin, F.; Testelin, S.; Dakpé, S.; Devauchelle, B.; Egles, C. A multi-layered nerve guidance conduit design adapted to facilitate surgical implantation. *Health Sci Rep* **2018**, *1*.

General conclusion and perspectives

General conclusion and perspectives

The objective of this thesis was to prepare nanofibrous elastomeric and biomimetic scaffolds able to help cardiac tissue regeneration. This goal was a real challenge because elastomers cannot be electrospun as they are insoluble. The elastomer chosen here, poly(glycerol sebacate), was processed as a prepolymer of low molar mass. It required thus the use of a carrier polymer for the electrospinning and crosslinking steps. Different methods were explored. Composite scaffolds and elastomeric ones were fabricated. Membranes could be organized in structures that should promote the cardiomyocytes growth.

PGS synthesis was first investigated in order to understand the effect of the reaction conditions on the properties of the material. Prepolymers (pPGS) and elastomers were characterized. It was found that the kinetic of the reaction could be accelerated by an increase of the temperature, but above all by microwave heating. The glycerol/sebacic acid ratio was also found of great importance. Indeed, the degree of crosslinking of the elastomer, and thus the mechanical properties depend on this ratio: a stoichiometric ratio (glycerol/sebacic acid = 2/3) leads to a stiffer elastomer. The synthesis was controlled by the degree of esterification calculated after NMR analyses. It allowed characterizing the prepolymers used for electrospinning and choosing the pPGS the most adapted for the application.

A pPGS synthesized from a glycerol/sebacic acid ratio equal to 1/1 (giving a more hydrophilic and softer elastomer) was employed to functionalize PLA fibers. The addition of PGS allowed an increase of the hydrophilicity of the membranes and thus a better functionalization by Matrigel, which helps cell attachment. No significant difference was identified for PGS contents of 30% or 40%. The curing of the membranes led to their stiffening because of the crosslinking of PGS, the crystallization of PLA, and the merging of the fibers at the contact points. However, an efficient curing of PLA/PGS membranes (at 120°C instead of 90°C) ensure a lower cytotoxicity, certainly thanks to a lower carboxylic acids content. In addition, by adjusting the solvent mixture for electrospinning solutions, it has been possible to fabricate fibers with small (500 nm) and large (1500 nm) average diameters, and to show that the thinner ones allow a better cardiomyocytes spreading. Finally, implantation of PLA and PLA/PGS patches cured at 120°C and composed of thin fibers on mice's hearts proved that the presence of PGS (30%) allows a lower inflammatory response and a better vascularization of the surrounding tissue after 28 days. This result indicates that these scaffolds are good candidates to help cardiac regeneration.

These fibers being not elastomeric, the method was improved to strive to make pure PGS fibers. For this aim, a pPGS close to its gel point (prepared from a 2/3 ratio and with high degree

of esterification equal to 72%) was used to ensure an efficient crosslinking. Here, fibers were electrospun with a high PGS content (50%) and the help of PVP and HPβCD as carrier material. It was proven that PVP alone cannot guarantee thermomechanical properties of the fibers that avoid their melting during curing. Moreover, due to HPβCD, the membranes can potentially be used for encapsulation of molecules of therapeutic interest. Crosslinking of PGS was successfully achieved thanks to the carrier material that was then partially removed by washing in water. This method led to membranes with moduli comprised between 2 and 10 MPa and strain at break higher than 100% at dry state. The mechanical properties could be modulated by adjusting the curing conditions. When hydrated, the membranes had a high resilience and a modulus between 100 and 200 kPa, which is interesting for soft tissues applications. It was however hypothesized that such scaffolds could be improved be using a 1/1 G/SA ratio. In this way, the material could be softer and have better interactions with cells thanks to a lower –COOH content. Unfortunately, first trials indicated that such a modification in the process requires some optimization. In particular, it would be necessary to use a prepolymer of higher degree of esterification.

This method led to the fabrication of scaffolds mimicking the myocardium by its mechanical properties. However, a good imitation of the cardiac tissue should also rely on its organization. Because the PGS-containing fibers are enough electrically conducting regarding the process of electrospinning, it was difficult to control their deposition through an electrostatic template assisted deposition (ETAD) strategy. However, the combination of electrosprayed PGS microparticles and PLA electrospinning led to structured membranes comprising large pores with a low density of fibers thanks to the ETAD strategy. These membranes allow an enhanced penetration of the cells. Moreover, PLA/PGS as well as PLA fiber alignment was possible mechanically using a collector rotating at high velocity. In the case of PLA, membranes help to guide cardiomyocytes: the cells align themselves along the fibers to form an organized tissue. Finally, scaffolds mimicking well the cardiac tissue structure were prepared by combining aligned PLA fibers and PGS/HPβCD electrosprayed microparticles. In this method, both ETAD strategy and mechanical alignment were combined. The resulting membranes have both aligned fibers and large pores. It is expected that such structures can enhance cell orientation, elongation, and migration in the scaffold.

To conclude, we can say that this project is not over. Indeed, many biological experiments should still be carried out. PLA/PGS scaffolds showed a good potential for cardiac application. However, this result should be completed. First, their ability to help the regeneration of a defective heart should be tested in future *in vivo* experiments. Moreover, good results found *in vitro* for these scaffolds and for aligned PLA fibers indicate that the combination of both should lead to scaffolds with a real interest for cardiac tissue engineering. Experiments will be carried out soon and it is expected that PLA/PGS aligned fibers induce a good phenotypic development of cardiomyocytes.

Regarding more specifically the material engineering side, focus could be done in the future on the structured scaffolds based on fibers and particles. The combination of electrospinning and electrospraying to make organized membranes is an original method developed in our team since several years. In the context of the MimHeart project, the mechanisms responsible for the controlled deposition of fibers and particles were studied by another PhD student. These results are important to provide a better control of the technic. Besides, the combination of aligned fibers and particles is really promising. To the best of our

knowledge, it is the first time that the drawback of aligned fibers, namely their high density, was compensated by the inclusion of clusters of particles. This strategy could thus be examined further by employing other materials for the fibers and the particles.

Finally, a dimension that was only shortly considered in this work was the functionalization of the scaffolds. Here, PLA/PGS fibers were functionalized by a Matrigel coating before cell seeding. This method was essential for cell attachment, but it raises some concerns. Indeed, Matrigel is a protein mixture obtained from mice's cancerous cells and can trigger an immunological response. However, the use of PGS comprising free –OH in these fibers offers large possibilities of functionalization. The availability of these hydroxyl groups could first be verified by grafting fluorescein isothiocyanate and verifying the fluorescent activity. If the potential use of these groups were confirmed, it would be possible to graft proteins at the surface of the fibers. A procedure was already developed by our team to make this functionalization in water and without the help of any toxic catalyst using click chemistry [1]. This is possible by bonding to –OH groups an amino-bicyclononyne in two steps (Figure 1). The nonyne group can then react with the azide groups of proteins.

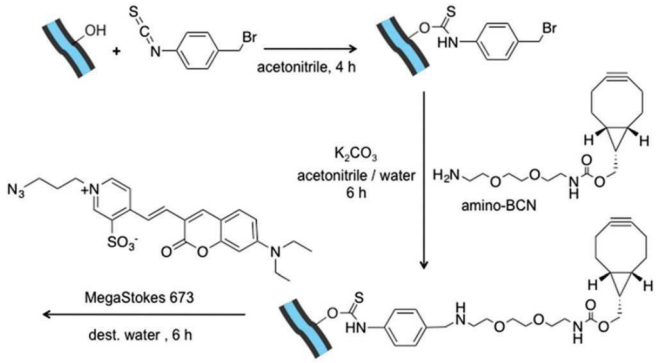

Figure 1. Description of the steps allowing the grafting of proteins at the surface of fibers comprising –OH groups. In this example, a fluorescent dye is grafted on the nonyne group instead of a protein (last step) in order to visualize the efficiency of the procedure [1].

Elastomeric fibers prepared using PVP and HPβCD as carrier material can be functionalized by the same method: hydroxyl groups are numerous in these materials, thanks to PGS but also cyclodextrin. But the latter can also be exploited for encapsulation of molecules such as drugs [2–5], biocides [6], antioxydants [7] or growth factors [8] able to promote tissue development. The same kind of functionalization can be intended for scaffolds comprising PGS/HPβCD particles. In this case, the diffusion of the molecules of interest would start from precise locations in the scaffold, which allows a better control. All these functionalization possibilities suggest that the therapeutic potential of PGS-based scaffolds can be largely expanded.

References:

1. Oster, M.; Schlatter, G.; Gallet, S.; Baati, R.; Pollet, E.; Gaillard, C.; Avérous, L.; Fajolles, C.; Hébraud, A. The study of the pseudo-polyrotaxane architecture as a route for mild surface functionalization by click chemistry of poly(ε-caprolactone)-based electrospun fibers. *J. Mater. Chem. B* **2017**, *5*, 2181–2189.
2. Shelley, H.; Babu, R.J. Role of Cyclodextrins in Nanoparticle-Based Drug Delivery Systems. *Journal of Pharmaceutical Sciences* **2018**, *107*, 1741–1753.
3. Gidwani, B.; Vyas, A. A Comprehensive Review on Cyclodextrin-Based Carriers for Delivery of Chemotherapeutic Cytotoxic Anticancer Drugs. *Biomed Res Int* **2015**, *2015*.
4. Challa, R.; Ahuja, A.; Ali, J.; Khar, R.K. Cyclodextrins in drug delivery: An updated review. *AAPS PharmSciTech* **2005**, *6*, E329–E357.
5. Uekama, K.; Hirayama, F.; Irie, T. Cyclodextrin Drug Carrier Systems. *Chem. Rev.* **1998**, *98*, 2045–2076.
6. Nardello-Rataj, V.; Leclercq, L. Encapsulation of biocides by cyclodextrins: toward synergistic effects against pathogens. *Beilstein J. Org. Chem.* **2014**, *10*, 2603–2622.
7. Pinho, E.; Grootveld, M.; Soares, G.; Henriques, M. Cyclodextrins as encapsulation agents for plant bioactive compounds. *Carbohydrate Polymers* **2014**, *101*, 121–135.
8. Ma, D.; Zhang, H.-B.; Tu, K.; Zhang, L.-M. Novel supramolecular hydrogel/micelle composite for co-delivery of anticancer drug and growth factor. *Soft Matter* **2012**, *8*, 3665–3672.

APPENDIX 1:
Synthesis and electrospinning of PGS-*co*-PEG[1]

In order to fabricate longer and more linear prepolymer chains potentially more efficient for electrospinning, PGS-*co*-PEG copolymers were designed. It was expected that thanks to a higher molar mass, they could form fibers more easily than pPGS, meaning that less carrier polymer would be necessary. A better resistance of the fibers during curing was also expected.

For this study, PEG of two different molar mass (200 and 400 g/mol) were used to test variations on the length of the linear segments. In a first step, PEG and sebacic acid reacted together under microwave irradiations (Figure A1.1.). Two ratios PEG/sebacic acid were tested: 1/2 and 2/3. The linear molecule obtained after this first step is named lin-SPEG. In a second step, glycerol reacted with the linear segments. The amount of glycerol was chosen to have the same total number of –OH and of –COOH introduced. In the third step, the branched prepolymer was cured under vacuum to verify if a crosslinked elastomer could be fabricated.

On the other hand, branched prepolymers were used for electrospinning with a carrier polymer to test the possibility to make fibers and the resistance to curing of these latter.

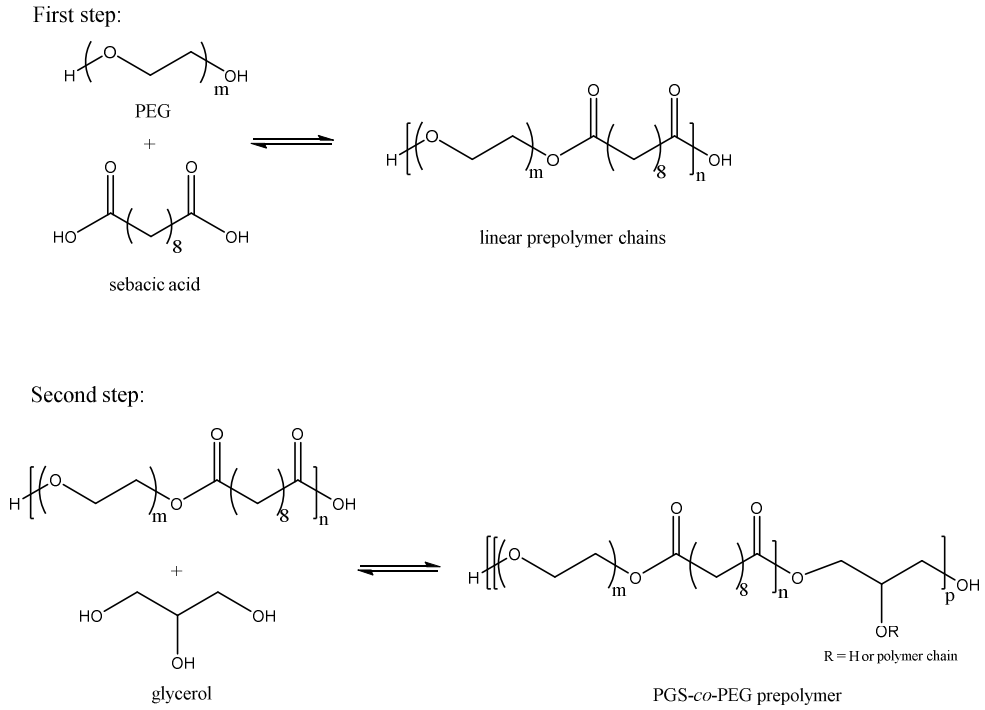

Figure A1.1. Chemical scheme describing PGS-*co*-PEG synthesis.

[1] This part was largely done by Alfred Bazin and Mathilde Guillaumond, ECPM students who did a two-weeks lab internship under my supervision.

1. Materials and methods

1.1. Materials

Same sebacic acid and glycerol as for PGS synthesis were used, with PEG200 (200 g/mol, Sigma-Aldrich) and PEG400 (400 g/mol, Sigma-Aldrich). Polyvinylpyrrolidone (PVP, 1300000g/mol, Aldrich), dimethylformamide (DMF, >99.8%, Sigma-Aldrich) and absolute anhydrous ethanol (>=99,9%), Carlo Erba) were used as received.

1.2. Microwave synthesis and corresponding characterization

The procedure for microwave synthesis of linear segments was similar to pPGS synthesis at 150°C during 180 minutes. For the second step, a known amount of linear prepolymer was put in a flask and the corresponding amount of glycerol was added before microwave heating at 150°C during 120 minutes. For crosslinking, the prepolymer was poured in a Teflon dish and heated at 160°C under vacuum during five days.

The esterification of the first two steps was followed by ^{1}H NMR. For the first step, –COOH are introduced in excess. The conversion rate can thus be calculated as:

$$p_1(\%) = \frac{I_E}{I_E + I_A} \times \frac{n_{AS}}{n_{PEG}} \times 100$$

with I_{acids} and I_{esters} the integration of the peaks on the spectra obtained by ^{1}H NMR, respectively at 2.18 ppm for the carboxylic acids (–C**H**$_2$–COOH) and 2.28 ppm for the esters (–C**H**$_2$–COOR) and n_{AS}/n_{PEG} the ratio between the amount of sebacic acid and of PEG.

The degree of polymerization can be calculated from p_1 using Carothers equation. The corresponding number average molar mass value was calculated. For comparison, SEC analysis was done in chloroform with a Shimadzu liquid chromatograph with PLGel Mixed-C and PLGeL 100 Å columns and a refractive index detector. PEG standards were used for calibration. M_n and polydispersity index (PDI) of linear segments were determined.

After the second step, all the proportions are stoichiometric. The extend of reaction corresponds then to the degree of esterification as defined before:

$$p_2(\%) = DE\ (\%) = \frac{I_E}{I_E + I_A} \times 100$$

and was determined by NMR.

1.3. Electrospinning

pPGS-*co*-PEG were solubilized in various proportions with PVP in DMF/ethanol 3/7. The total concentration of solid in the solution was fixed at 10%. The solutions were stirred overnight before use.

Short electrospinning experiences were carried out in order to verify the electrospinnability of the blends and then to verify how the fibrous deposits can resist when heated. A home-made vertical electrospinning set-up was used. One metallic 18 gauge needle was fed with the solution at 1.2 mL/h-1.5 mL/h by a syringe pump (PHD 2000, Hardvard Apparatus). The collector was placed 18.5 cm from the tip of the needle and rotated at 80 rpm. High voltage was applied to the

needles (13-14.5 kV) by a power supply (SL10, Spellman). Samples were electrospun during 10 minutes with a temperature of 22°C and a dew point between -3 and -5°C.

1.4. Heat resistance tests

Heat resistance of the most fibrous samples was tested. Electrospinning deposits still attached to the aluminum foil were put in contact to a surface heated at 120°C during more than 1h. To ensure a homogenous temperature on both sides on the sample, they were covered in order to create a heating chamber.

1.5. SEM observations

The surface of the as spun and heated deposits was observed by scanning electron microscopy after coating by a thin layer of gold. The SEM (Vega 3, Tescan) was used in high vacuum mode with a voltage of 5 kV.

2. Results

2.1. Molecular weight of prepolymers and crosslinking

Four kinds of PGS-*co*-PEG were synthesized, with various PEG size and ratio PEG/SA. Resulting lin-SPEG were analyzed by NMR and SEC to characterize their extend of reaction and M_n. Results are given in Table A1.1. It can be seen that the extend of reaction after the first step remains quite low: only dimers or trimers are synthesized. SEC results give a little higher molar mass values; however, it does not correspond to significantly long molecules. Concretely, the molar mass is not high enough for electrospinning. However, the second step should lead to branched prepolymers with higher molar mass that could potentially be employed for electrospinning.

Table A1.1. Results obtained after the first, the second, the third step of copolymerization of sebacic acid, PEG and glycerol.

M_n PEG (g/mol)	$\frac{n_{SA}}{n_{PEG}}$	1st step					2nd step	3rd step
		$p_1(\%)$	$\overline{DP_n}$	Theoretical M_n (g/mol)	SEC M_n (g/mol)	PDI	$p_2(\%)$	$p_3(\%)$
200	3/2	77%	2.6	524	636	1.32	60%	87%
	2/1	99%	2.9	583	608	1.37	63%	Gel
400	3/2	76%	2.6	718	788	1.41	65%	91%
	2/1	87%	2.4	717	800	1.43	58%	85%

The last step of curing allows verifying the possibility to crosslink the material into an insoluble and infusible elastomer. After five days of curing, only one material gelified: the use of PEG200 with SA/PEG 2/1 gave a transparent yellowish elastomeric film (Figure A1.2.). The others were solubilized in d-DMSO to be characterized by NMR. The corresponding extend of reaction was calculated in the same way than p_2. It was not possible to crosslink PGS-*co*-PEG made from PEG400, certainly because of the too long distance between the crosslinking points.

Moreover, the ratio SA/PEG 2/1 with PEG200 did not lead to an infusible gel. This can be explained by the large amount of PEG used. Statistically, sebacic acids units are surrounded by more PEG before reacting with glycerol. Again, the distance between crosslinking points is large, making gelification difficult.

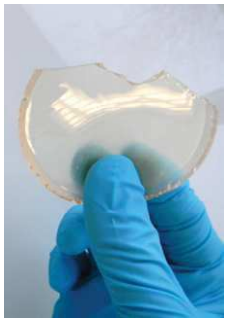

Figure A1.2. PGS-*co*-PEG made from PEG200 and SA/PEG 2/1 after crosslinking.

Two branched prepolymers were selected for electrospinning. pPGS-*co*-PEG for which crosslinking was successful (made from PEG200 and SA/PEG 2/1) was firstly used. A longer prepolymer, made from PEG400 after the 3 steps of synthesis (including unsuccessful curing), was also tested, as its molar mass was high. Indeed, SEC measurements were done on this copolymer. Despite its branched structure, it can give an idea of its molecular weight. The values are given in Table A1.2, compared with the result for a simple pPGS synthesized in the same conditions as the pPGS used for electrospinning. PGS-*co*-PEG have much higher M_n, what could be promising for electrospinning.

Table A1.2. SEC results for long PGS-*co*-PEG.

	SA/PEG	SEC M_n (g/mol)	PDI
pPGS	-	612	1.35
PGS-*co*-PEG400-1	2/1	2771	6.07

2.2. Electrospinning

For formulations with 50% or more of PVP, the jet is quite stable. When there is less PVP, the jet is very discontinuous and a lot of droplets are projected, which is a first proof that the carrier polymer remains essential for electrospinning of PGS-*co*-PEG. SEM images just after electrospinning are shown in Figure A1.3. SEM pictures of PGS-co-PEG/PVP electrospun fibers, as spun and after heating at 120°C.

For the sample with the prepolymer made from PEG200, with only 10% of PVP, a very diffuse deposit is produced. When the amount of PVP is increased, more spots are visible, and at 50% of PVP, spread fibers can be seen. With 40% of PVP, fibers are still merged together. And finally, with 30% of PVP, beaded fibers are obtained. This PVP proportion is similar to the minimal proportion required for pPGS electrospinning. In addition, it can be seen on the SEM picture after heating that the fibers cannot resist to curing.

The prepolymer made from PEG400 was then electrospun. A better result was expected as its molar mass is higher. Indeed, fibers are obtained even with only 50% of carrier polymer. However, they did not resist well to heating, even when the amount of PVP was increased to 70%, where the fibers collapsed.

3. Conclusion

To conclude, the $\overline{DP_n}$ of the linear chains of these copolymers stayed very low. After addition of glycerol, more interesting molar mass could be reached for pPGS-*co*-PEG. Finally, it was possible to decrease the proportion of carrier polymer only if the prepolymer used was long enough – here synthesized from PEG400 – while the use of shorter prepolymers requires the same amount of PVP than simple pPGS to make fibers. However, these fibers did not resist to heating. Indeed, PEG moieties have a low melting point. The elastomer can thus not be crosslinked in the fibers. Moreover, these long prepolymers are difficult to crosslink. So, no further work dedicated to PGS-*co*-PEG was done.

Prepolymer used	Prepolymer /PVP	Result as spun	Result after heating
PGS-*co*-PEG200	9/1	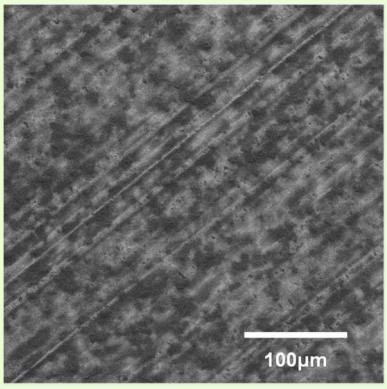	
	7/3	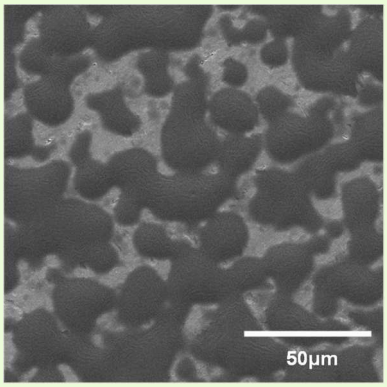	
	5/5	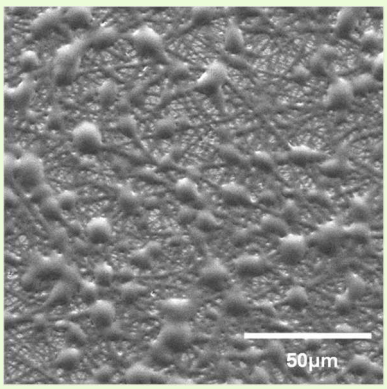	
	4/6	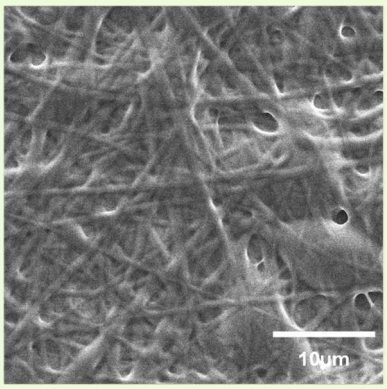	

Prepolymer used	Prepolymer /PVP	Result as spun	Result after heating
PGS-*co*-PEG200	3/7	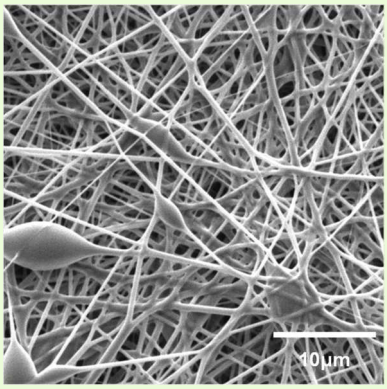	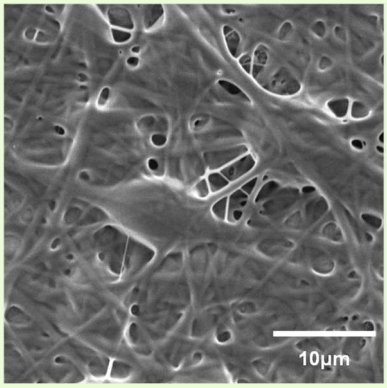
PGS-*co*-PEG400-1	5/5	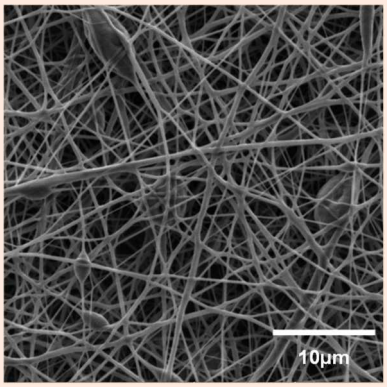	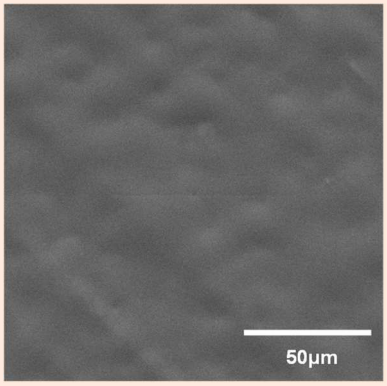
	4/6	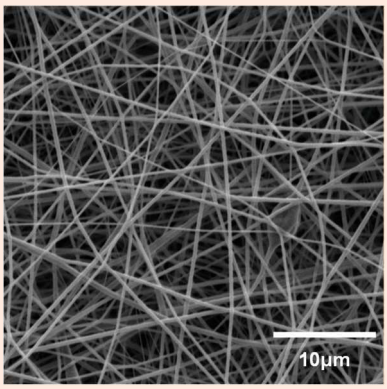	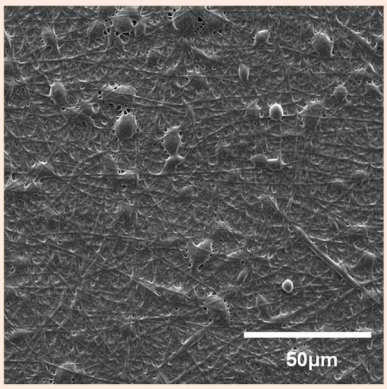
	3/7	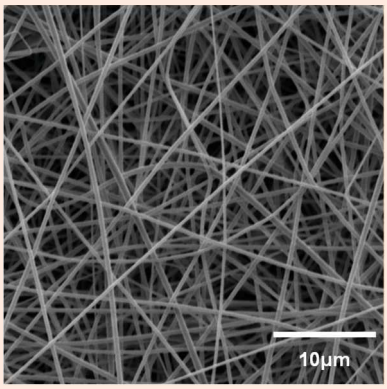	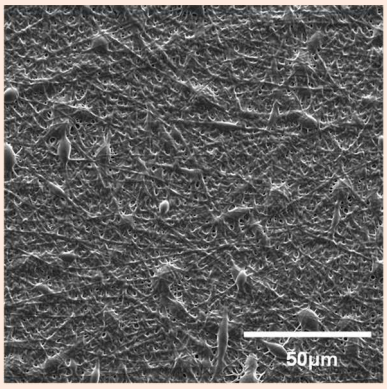

Figure A1.3. SEM pictures of PGS-*co*-PEG/PVP electrospun fibers, as spun and after heating at 120°C.

APPENDIX 2:

Effect of the type of pPGS on the morphology of PGS/PVP/HPβCD fibers after curing

The short experiments presented here are a part of the work aiming to prepare PGS-based elastomeric fibers with the help of PVP and HPβCD as carrier materials. Here, different types of pPGS were electrospun mixed with the carrier materials. The fibers were then cured in order to identify in which cases they resist to the curing temperature.

1. Materials and methods

1.1. Materials

Polyvinylpyrrolidone (PVP, 1300000g/mol, Aldrich), hydroxypropyl-β-cyclodextrin (HPβCD, 97%, Acros Organics), dimethylformamide (DMF, >99.8%, Sigma-Aldrich) and absolute anhydrous ethanol (>=99,9%, Carlo Erba) were used as received. Glycerol (>99.96%, Fisher Chemicals) and sebacic acid (98%, ACROS Organics) were employed to synthesized pPGS in various conditions according to the microwave procedure presented in Chapter 1. G/SA ratio chosen and DE of each pPGS employed here are given in each case.

1.2. Electrospinning

The effect of the esterification degree of the employed pPGS was first studied. Two solutions with 5 wt% of pPGS, 4 wt% of PVP and 4 wt% of HPβCD in DMF/ethanol 3/7 (w/w) were prepared. In both cases, the pPGS was synthesized from a G/SA ratio 2/3. However, in the first case ($Blend_{64\%}$), its DE was 64% while for the second case ($Blend_{71\%}$), its DE was 71%. For electrospinning, a horizontal set-up with a cylindrical rotating collector covered by an aluminum foil was used. A 18 gauge needle 18 cm away from the collector was fed by the solution. High voltage was applied to the needle (12 kV) by a power supply (SL10, Spellman). The injection flow rate was fixed at 3.3 mL/h for $Blend_{64\%}$ and 1.5 mL/h for $Blend_{71\%}$ by a syringe pump (PHD 2000, Hardvard Apparatus). The membranes were produced after about 1h of electrospinning. All the parameters are given in Table A2.1.

After electrospinning, the membranes were peeled and cut in the appropriate shape to be placed between two frames tight together before being placed in a pre-heated vacuum oven (Vacutherm VT6025, Fisher Scientific). The curing step was then conducted under a pressure bellow 10^{-2} mbar during 24h at 130°C and 72h at 160°C.

The effect of the G/SA ratio was also analyzed. For this purpose, two solutions with 6.5 wt% of pPGS, 3.25 wt% of PVP and 3.25 wt% of HPβCD in DMF/ethanol 3/7 (w/w) were prepared. Here, the G/SA ratio and the DE of the pPGS were different. In the first case ($Blend_{1/1}$), a pPGS 1/1 with a DE of 85% was used. In the second case ($Blend_{2/3}$), the prepolymer had a DE of 72% with G/SA equal to 2/3. However, they both have a theoretical degree of polymerization of 7 according to Carothers' equation (for details, see Chapter 2). For electrospinning, a vertical set-up with a cylindrical rotating collector covered by an aluminum foil was used. A 18 gauge needle 16 cm away from the collector was fed by the solution at a flow rate fixed at 2.5 mL/h by a syringe pump. High voltage was applied to the needle (15 kV). The membranes were produced after about 5h of electrospinning. All the parameters are given in Table A2.1.

After electrospinning, the membranes were peeled and cut in the appropriate shape to be placed between two frames tight together before being placed in a pre-heated vacuum oven (Vacutherm VT6025, Fisher Scientific). The curing step was then conducted under a pressure bellow 10^{-2} mbar during 24h at 120°C plus 48h at 140°C and 24h at 170°C.

Table A2.1. Summary of electrospinning parameters used for preliminary blend electrospinning experiments.

	$Blend_{64\%}$	**$Blend_{71\%}$**	**$Blend_{1/1}$**	**$Blend_{2/3}$**
pPGS type (G/SA, DE, $\overline{DP_n}$)	2/3, **64%**, 5	2/3, **71%**, 7	**1/1**, 85%, 7	**2/3**, 72%, 7
%pPGS in solution	5%	5%	6.5%	6.5%
%PVP in solution	4%	4%	3.25%	3.25%
% HPβCD in solution	4%	4%	3.25%	3.25%
Solvent: DMF/ethanol (w/w)	2/8	2/8	3/7	3/7
Flow rate	3.3 mL/h	1.5 mL/h	2.5 mL/h	2.5 mL/h
Set-up	Horizontal	Horizontal	Vertical	Vertical
Voltage at needle	12 kV	12 kV	15 kV	15 kV
Distance needle-collector	18 cm	18 cm	16 cm	16 cm

1.3. SEM observations

The surface of the as-spun, cured, and cured and purified mats was observed by scanning electron microscopy (SEM) after coating by a thin layer of gold. The SEM (Vega 3, Tescan) was used in high vacuum mode with a voltage of 5 kV.

2. Results and discussion

2.1. Effect of the degree of esterification

Samples labeled $Blend_{64\%}$ and $Blend_{71\%}$ allowed us to study the effect of the degree of esterification of the pPGS on the fibers morphology after curing. As shown on Table A2.1, DE is the main difference between these samples. On Figure A2.1.A, it can be seen that fibers were successfully electrospun in both cases. However, the fibers on $Blend_{64\%}$ did not resist during the curing step: its pores are largely closed after curing, indicating that pPGS could flow out of the fibers during heating. On the contrary, $Blend_{71\%}$ is still porous after curing: fibers are only little melted. This result indicates that a high extend of reaction is required. Indeed, it is important to use a pPGS close to its gel point. In this way, its viscosity can increase fast enough during curing to reach the threshold where it cannot flow anymore. It was thus determined that a minimal DE value of 71% was required for a pPGS 2/3. The pPGS 2/3 used for the next experiments has a DE of 72%.

2.2. Effect of the G/SA ratio

However, the same DE value cannot be taken for 1/1 pPGS, as the gel point is reached at higher DE for the latter (see Chapter 2). It was thus decided to make the experiment with a pPGS 1/1 having a similar theoretical $\overline{DP_n}$. $Blend_{1/1}$ and $Blend_{2/3}$ were thus fabricated with pPGS having different DE but same $\overline{DP_n}$ (equal to 7) according to Carothers' equation. Whereas the fibers on $Blend_{2/3}$, prepared from a pPGS 2/3, kept their shape during curing, the fibers of $Blend_{1/1}$ totally melt: a nearly continuous film is obtained (Figure A2.1.B). Again, it can be explained by the time needed to reach the gel point. pPGS 1/1 used for $Blend_{1/1}$ has a high $\overline{DP_n}$ close to the theoretical gel point value. But we have seen in Chapter 2 that during synthesis, the increase of $\overline{DP_n}$ occurs slower in the 1/1 case. Thus, more time is needed until the viscosity of the pPGS in the fibers reaches the threshold avoiding the flow of the prepolymer. To conclude, to make membranes with pPGS 1/1, it is necessary to use a pPGS with a higher $\overline{DP_n}$.

3. Conclusion

Taking into account the result of these preliminary experiments, it was decided to prepare the membranes with a pPGS synthesized from a G/SA ratio equal to 2/3 and a DE of 72%, corresponding to a $\overline{DP_n}$ of 7. It is expected, that such parameters should avoid the loss of the fibrous structure during curing, even at high pPGS amounts in the fibers. Actually, the use of a pPGS synthesized from a G/SA ratio equal to 1/1 may be possible but would need adjustments. In particular, a decrease of the pPGS content in the solution may be necessary. Moreover, a very high degree of esterification is certainly required. This would raise difficulties because it is difficult to approach the gel point without synthesizing an insoluble material.

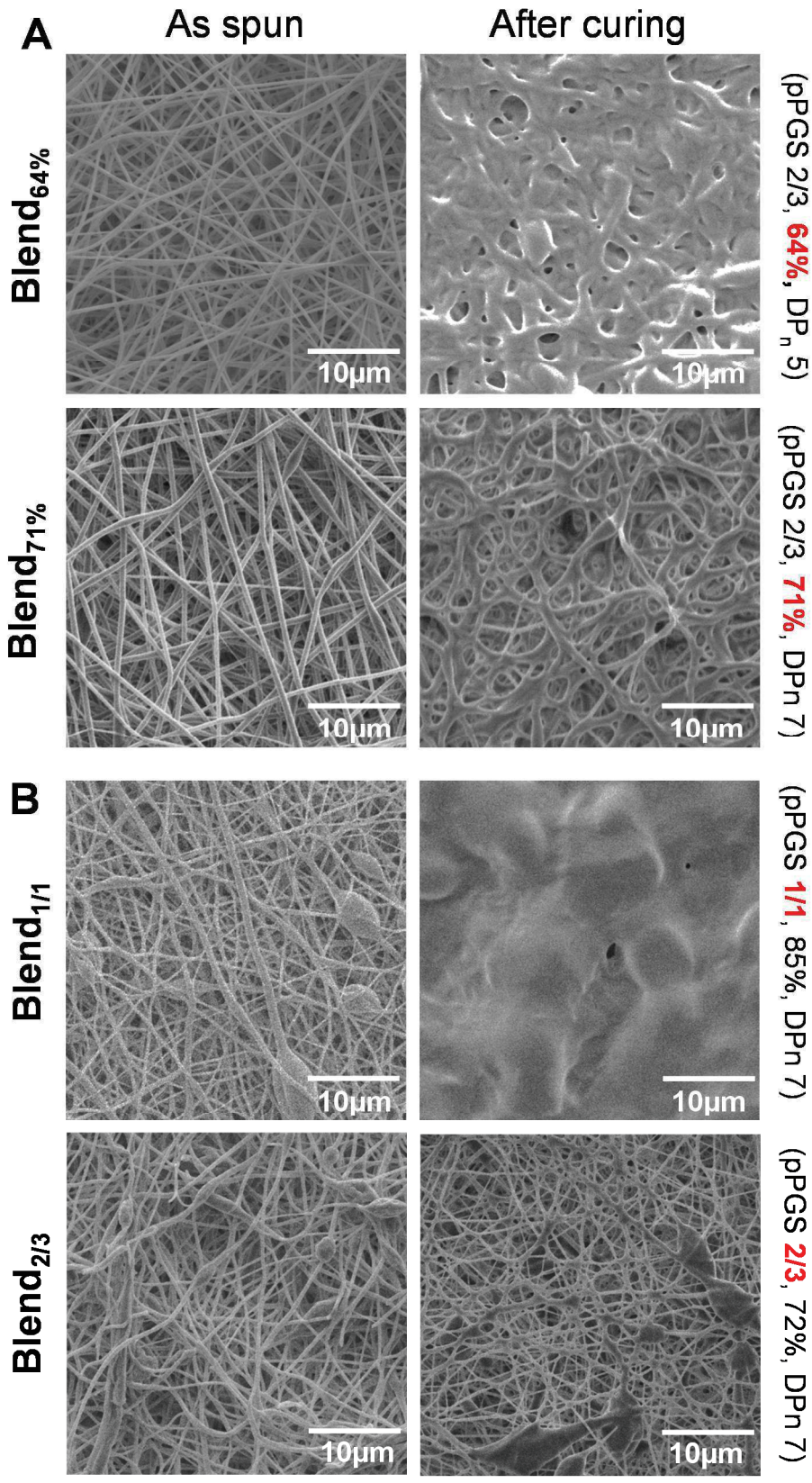

Figure A2.1. ***Resistance to curing of blend fibers with various types of pPGS.*** **(A)** Influence of DE. **(B)** Influence of G/SA.

APPENDIX 3:

Suturable elastomeric tubular grafts with patterned porosity for rapid vascularization of 3D constructs

(Submitted to *ACS Biomaterials & Engineering*)

Caroline Faria Bellani[†#×§⊥‖*], *Kan Yue*[⊥‖], *Florence Flaig*[‡], *Anne Hébraud*[‡], *Pengfei Ray*[⊥‖], *Nasim Annabi*[⊥‖¶Δ], *Heloísa Selistre Sobreiro de Araújo*[§], *Márcia Cristina Branciforti*[†¤]; *Ana Maria Minarelli Gaspar*[♣], *Su-Ryon Shin*[⊥‖♦], *Ali Khademhosseini*[⊥‖¶Δ♥♠], *Guy Schlatter*[‡*]

† Bioengineering Department, Sao Carlos School of Engineering, University of Sao Paulo, Sao Carlos, SP, Brazil.

CAPES (Coordination for the Improvement of Higher Level Personnel), Brasilia, DF, Brazil.

‡ Institut de Chimie et Procédés pour l'Energie, l'Environnement et la Santé (ICPEES), UMR 7515 CNRS-University of Strasbourg, ECPM, Strasbourg, France.

§ Laboratory Biochemistry and Molecular Biology, Physiological Sciences Department, Federal University of Sao Carlos, Sao Carlos, Brazil.

⊥ Harvard-Massachusetts Institute of Technology, Division of Health Sciences and Technology, Massachusetts Institute of Technology, Cambridge 02139, MA, USA.

‖ Biomaterials Innovation Research Center, Division of Biomedical Engineering, Department of Medicine, Brigham and Women's Hospital, Harvard Medical School, Boston 02139, MA, USA.

¶ Department of Chemical and Biomolecular Engineering, University of California – Los Angeles, Los Angeles, CA 90095, USA.

Δ Center for Minimally Invasive Therapeutics (C-MIT), California NanoSystems Institute (CNSI), University of California – Los Angeles, 570 Westwood Plaza, Los Angeles, CA 90095, USA.

¤ Materials Engineering Department, Sao Carlos School of Engineering, University of Sao Paulo, Sao Carlos, SP, Brazil.

♣ Department of Morphology, School of Dentistry at Araraquara, São Paulo State University (UNESP), Araraquara, SP, Brazil.

♦ Department of Medicine, Division of Engineering in Medicine, Brigham and Women's Hospital, Harvard Medical School, Cambridge, MA, 02139 USA

♥ Department of Bioengineering, University of California - Los Angeles, Los Angeles, CA, 90095 USA

♠ Department of Radiology, David Geffen School of Medicine, University of California-Los Angeles, Los Angeles, CA, 90095 USA

Keywords: Electrospinning; PGS; laser micromachining; vascularization; biofabrication.

ABSTRACT

Vascularization is considered to be one of the key challenges in engineering functional 3D tissues. Engineering suturable vascular grafts containing pores with diameter of several tens of microns in tissue engineered constructs may provide an instantaneous blood perfusion through the grafts improving cell infiltration and thus, allowing rapid vascularization and vascular branching. Here, tubular grafts with customizable shapes (tubes, Y-shape capillaries) and controlled diameter ranging from several hundreds of microns to few mm are fabricated based on poly(glycerol sebacate) (PGS) / poly(vinyl alcohol) (PVA) electrospun scaffolds. Furthermore, a network of pore channels of diameter in the order of 100 μm was machined by laser femtosecond ablation in the tube wall. Both non-machined and laser machined tubular scaffolds elongated more than 100% of their original size have shown suture retention, being 5.85 and 3.96 N/mm^2 respectively. To demonstrate the potential of application, the laser machined porous grafts were embedded in gelatin methacryloyl (GelMA) hydrogels, resulting in elastomeric porous tubular graft/GelMA 3D constructs. These constructs were then dynamically co-seeded with osteoblast-like cells (MG-63) at the external side of the graft and with endothelial cells (HUVEC) inside, forming thus a bone osteon model. The laser machined pore network allowed an immediate endothelial cell flow towards the osteoblasts enabling osteoblasts and endothelial cells to interact and form complex 3D structures. This rapid vascularization approach can be potentially applied not only for bone tissue regeneration, but also for an extend variety of tissues and organs.

1. INTRODUCTION

Vascularization is considered to be one of the key challenges in tissue engineering,[1] and remains the principle obstacle that impedes the translation of most tissue engineered constructs to clinical practice.[2] After construct implantation, the delivery of nutrients to cells on a biomaterial is limited beyond a thickness of approximately 200 μm and occurs via interstitial fluid diffusion.[3–5] Most tissue regeneration applications require considerably thicker engineered constructs, as for example in the case of regeneration after tumor surgery. Spontaneous vascular ingrowth is often limited to several tenths of micrometers per day,[6,7] which is too slow to provide adequate nutrients to cells in the interior part of implant, leading to compromised healing results.[8]

Biofabrication strategies have been used to pre-vascularize tissue constructs. These strategies employ hydrogels associated with cells and encompass the creation of hollow channels within the hydrogel itself that can be latter perfused with vascular cells.[2] However, the most fundamental question for clinically translation of these constructs is how to connect such delicate networks with the host blood vessels. Even a microsurgical connection is not achievable due to insufficient mechanical properties of the biofabricated vessel network made from hydrogels.[2] Thus, a strategy to overcome these issues may be to include a stronger vascular graft with pore channels inside the biofabricated construct, enabling the direct connection of the construct with the host blood stream, providing an immediate blood flow inside the construct.

The success of a vascular graft allowing the rapid vascularization of biofabricated constructs is governed by several characteristics: i) to mimic the extracellular matrix (ECM), providing an adequate environment site for the cells;[9] ii) to have a small diameter in order to be better integrated inside biofabricated tissues, increasing the vascularization area;[2] ii) to be biodegradable in order to be remodeled into a new vessel;[10] iii) to be suturable, so it can be anastomosed with the host vasculature providing an anchor site to the biofabricated graft;[2] iv)

and to have an open porosity with pores diameter in the order of 100 μm to allow vascular cell migration and thus, favoring the vascular branching towards biofabricated tissues.[2] An attractive approach to obtain vascular grafts with these features is based on the use of decellularized ECM [11]. However, such strategy requires to harvest the suitable vessel according to the host site and furthermore, the decellularization protocols can be challenging and time consuming.[11,12] Therefore, there is a need for techniques that allow the fabrication of customized vascular grafts with these characteristics.

The electrospinning technique is based on the stretching of a viscoelastic solution into nano/microfibers using a high electrostatic force[13] and offers a valuable tool to produce biomimetic tubular scaffolds with similar architecture to the ECM for tissue engineering.[13–15] However, the traditional approach to elaborate electrospun tubular grafts is based on direct electrospinning over a conducting rotating collector[13,16,17] which mostly consists in a cylindrical mandrel. The mandrel should be pre-coated to allow removing of fibers as they usually stick on the collector surface.[18–20] Furthermore, it is worth noting that the process of electrospinning does not lead to an efficient fiber deposition in the case of cylindrical collectors having a small diameter.[20,21] Thus, the fabrication of tubular scaffolds by the direct electrospinning on a mandrel with diameter smaller than few mm is not possible. Another limitation in electrospinning is the formation of fibrous scaffolds with pore diameters smaller than few microns, which does not allow the cell infiltration through the scaffolds. To increase the pore size of electrospun scaffolds, various techniques have been investigated, including the incorporation of porogens,[22] the use of patterned collectors,[23,24] modification of fiber diameter[25] ultraviolet radiation treatment [26], and electrospinning with sacrificial fibers [27]. Though interesting, these approaches do not offer a perfect control of the pore patterning or size and thus, they cannot be devoted for the fabrication of scaffolds ensuring the function of ideal vascular branching. To address this limitation, laser femtosecond micro-ablation or laser machining can be used. Indeed, this technique is considered as a promising tool to rapidly create complex hollow microstructures on electrospun scaffolds,[28–30] as the material is removed with minimal thermal damage.[28,31]

Poly(glycerol sebacate) (PGS), is a synthetic elastomer which can degrade rapidly *in vivo* into glycerol and sebacic acid, metabolites that naturally exist in the body, minimizing the duration of host inflammatory response.[32,33] However, the direct electrospinning of the crosslinked PGS is challenging due to its insolubility resulting from its 3D macromolecular network structure. The pre-polymer of PGS (pPGS) can be easily dissolved to obtain a electrospinning solution,[32] however, the pPGS molecular weight is not suitable to produce the molecular entanglements necessary to obtain pPGS only electrospun fibers.[34] Consequently, the pPGS must be associated with a carrier polymer to be firstly processed by electrospinning. Then, a post-treatment is required to crosslink the pPGS in order to obtain elastomeric PGS-based fibrous scaffolds. Jeffries *et al.*[35] developed a simple method for electrospinning pPGS scaffolds using poly(vinyl alcohol) (PVA) as the carrier polymer, which also maintains the fibrous morphology after the crosslinking step. Furthermore, PVA is highly water-soluble and most of PVA can be removed by simple washing the scaffold in water, enabling to obtain a PGS blend tubular scaffold with properties as close as possible the non-modified PGS.[35]

The aim of this work was to develop suturable vascular tubular scaffolds with small inner diameter to be integrated in biofabricated tissue engineered constructs. The tubular scaffolds were developed to connect the constructs to the vascular network providing an immediate blood perfusion. We employed PGS combined with PVA to obtain a biodegradable tubular scaffold with suitable elastomeric mechanical properties for application as vascular graft. We described a

fast and simple technique that enables the fabrication of vascular grafts from electrospinning with controlled diameter as low as few hundreds of microns. Furthermore, a network of pore channels was also machined by femtosecond laser micro-ablation, intended to facilitate the endothelialization/vascularization from the vascular graft to the biofabricated construct. The grafts were characterized regarding their morphology, thermal and mechanical properties and their *in vitro* toxicity. To demonstrate the potential of application of such tubular grafts, the architecture of an osteon (the bone unity constituted of bone layers around a longitudinal vascular channel[36,37]) was simulated: 3D osteon-like constructs were obtained from the co-culture of osteoblast-like cells (MG63) and endothelial cells (HUVECs) in a composite made of gelatin methacryloyl hydrogels (GelMA)/tubular graft system.

2. EXPERIMENTAL SECTION

2.1. pPGS Synthesis

We performed the pPGS synthesis assisted by microwave. Briefly, a 1:1 molar ratio of glycerol (4.55 g, 99%, Sigma-Aldrich) and sebacic acid (10 g, 99%, Sigma-Aldrich) were mixed together, at room temperature, inside a glass round-bottom flask connected to a glass tube to allow the evaporation of the water which would be resulted from the pPGS synthesis. This opening allows also limited evaporation of the glycerol. The mixture was placed in a microwave oven (Discover SP®, CEM™) and the synthesis was carried during 180 minutes at 180°C at a maximal power of 200 W under stirring. After this time, a transparent pale yellow slightly viscous liquid was obtained and allowed to cool until becoming a white waxy paste. The obtained pPGS was stored at room temperature.

2.2. Pre-GelMA synthesis

The GelMA prepolymer (Gelatin Methacryloyl) was prepared as published before.[38] Briefly, the GelMA was fabricated by the direct reaction of the gelatin (previously diluted at 10% in Dulbecco's Phosphate Buffered Saline (DPBS) during one hour at 50°C) with the methacrylic anhydride (MA) in PBS at 50°C for two hours. The reaction was interrupted by diluting the obtained product 5 times in PBS. The solution was dialyzed in ultrapure water with a porous membrane of 12-14 kDa to remove low molecular impurities (i. e. free MA). The material was allowed to be dialyzed for 5 days, at 60°C. Following, the solution was lyophilized and the GelMA was stored at -80°C until utilization.

2.3. Fibrous scaffolds and fibrous tubular scaffolds manufacturing

2.3.1. Electrospinning

Due to its low molecular weight, the pPGS must be electrospun with a carrier polymer that has a higher molecular weight.[39] Since it is necessary to further crosslink the pPGS into PGS after electrospinning, the carrier polymer of choice must have the following criteria: melting temperature above of PGS crosslink temperature; dissolution in a solvent which is common to the pPGS. As suggested in the work of Jeffries et al., we employed PVA as carrier polymer (Gohsenol®, as a generous donation from Nippon Gohsei™, MW ≈ 20,000), because it has a higher melting point than the one required for the crosslink process of PGS, and it is easily removable by water.[35] Additionally, if some PVA remains, it is a non-toxic and non-carcinogenic

material.[40] Finally, we employed the hexafluorisopropanol (HFIP, Covachem, Ref. 12206-25) as the common solvent for both pPGS and PVA to prepare a solution for electrospinning.

The electrospinning solution was prepared as suggested by Jeffries et al.,[35] with some modifications. The pPGS/PVA at a 55:45 (w/w) ratio were diluted at 10% (w/v) in HFIP, and the solution was kept in magnetic stirring at room temperature overnight, prior to electrospinning. We employed an electrospinning machine assembled in house with a rotating collector (Figure 2A). A voltage of 20 kV has been applied through a positive electrode connected to the tip of the spinneret (electrospinning needle), and -1 kV to the collector, which was positioned at 18 cm of distance from the spinneret. The solution was put inside a syringe which has been connected to the spinneret by a polytetrafluoroethylene (PTFE) tube. The flow rate was kept by a syringe pump (Harvard Apparatus™) at 2 ml/hour, controlling the humidity at around 40% with dry air injection inside the electrospinning cabin, if necessary. The pPGS/PVA fibers were collected over parchment paper (Figure 2A and B). The standard time of collection for samples assembled in tubes was 30 minutes.

2.3.2. Assembly and Crosslink of the Scaffolds

We took advantage of the feature of the non-crosslinked pPGS to stack various layers of electrospun scaffolds together to assembly tubular scaffolds by simply rolling the electrospun pPGS/PVA scaffolds (10 cm width x 20 cm length) around PTFE rods (Figure 2B) of 0.75, 2 and 3 mm of diameter. In order to assess mechanical and in vitro properties (cytotoxicity), flat samples have been also crosslinked: the assembled scaffolds obtained from the electrospun scaffolds were placed in a vacuum oven (Heraeus, Thermo Scientific™) at 150°C for 48 hours (Figure 2C), under the minimum pressure achieved assisted by a suction pumping (value between 6 – $7x10^{-3}$ mbars, as measured by a pressure transducer). We also crosslinked samples at 120°C for 24h, then for 150°C for 24h for comparison purposes.

2.3.3. Samples purification

The samples were washed by immersion in distillated water with gentle agitation at room temperature for 24 hours to remove the PVA (the carrier polymer). Then, to remove the non-crosslinked PGS (i.e. the pPGS), the samples were washed in ethanol 100%, then in distillated water. For storage and/or analyses, the samples were lyophilized (Figure 2D).

2.3.4. Laser Micro-ablation

In order to pattern the tubular scaffolds with porous structures allowing endothelial cells migration, we employed a 1030 nm femtosecond laser (Amplitude Systèmes) to perform laser micro-ablation (or laser machining) and creation of the pores. Samples were loaded in a rotor stage, and synchronized in a computer software (Optec Laser Systems) to fully pattern the tubular scaffold (Figure 2F). The laser energy employed was 1.9 W, with a frequency of 100 kHz and laser beam scanning speed of 250 mm/s. The pores drilling has been performed by pathing a circle of 100 μm of diameter approximately by laser beam pulses (size spot around 30 μm of diameter) for 20 times for complete drilling.

2.4. Characterization

2.4.1. Proton Nuclear Magnetic Resonance (^{1}H NMR) analysis

To determine the advancement of the esterification reaction, samples of the pPGS as synthesized were solubilized in deuterated dimethyl sulfoxide (d-DMSO) and analyzed by ^{1}H NMR. The degree of esterification (DE) was calculated, as proposed by Li et al. [41], according to Equation 1 :

$$DE = \frac{I_E}{I_E + I_A}$$

Equation 1. Degree of Esterification

where I_E is the integration of the 2.28 ppm peak for the esters (—C$\underline{H_2}$—COOR), and the I_A is the integration of the 2.17 peak for the carboxylic acids (—C$\underline{H_2}$—COOH). The higher the degree of esterification, the higher the polymerization PGS. In this study, we aimed to achieve an ideal degree of esterification equivalent to a pre-polymer of PGS (pPGS), suitable for dilution and for further crosslinking.

2.4.2. Scanning Electron Microscopy (SEM)

Morphological aspects of the electrospun scaffolds and of the tubular constructs were analyzed by SEM Vega 3 TESCAN™. Samples were cut and placed over aluminum stubs with conductive adhesive tape, then they were coated with gold. The average fiber diameter was obtained by analysis using ImageJ software (Wayne Hasband, National Institut of Health, USA). An average over 50 measurements for each picture/condition was considered.

2.4.3. Mass Loss

We evaluated the removal of PVA and pPGS by mass loss. Samples were weighted after the crosslinking, then after the different washing steps, and the mass was compared.

2.4.4. Mechanical Properties

Mechanical properties of electrospun PGS/PVA blends were measured by uniaxial tensile testing until their rupture using a hybrid rheometer (Discovery HR-3, TA Instruments), with a pre-load of 0.010 N and speed of 50 μm/s at room temperature. Crosslinked and purified tubular samples were longitudinally opened, and carefully cut in order to obtain samples of 10 mm length and 4 mm width. Sample thickness was measured with a caliper. Four specimens of each sample were obtained and hydrated prior to the measurements. Suture retention strength (SRS) was measured by inserting a 4-0 suture 2mm from the edge of the long axis of 4mm x 10mm samples and strained to rupture. Suture retention strength was calculated as maximum load/(suture diameter x sample thickness) in N/mm^2.

To test the interfacial adhesion of the electrospun layers, as employed for the tubular scaffolds, the samples for delamination characterization were fabricated by direct electrospinning or stacking the electrospun scaffolds. For the direct electrospinning samples, the electrospinning scaffolds were collected over parchment paper for 20 minutes, then, a stripe of parchment paper was placed longitudinally to the collector over the sample. The electrospinning was carried for more 20 minutes. For the stacked samples, an electrospun layers were stacked, with a parchment paper stripe between the layers. These samples were subject to curing with glass weight overt

them, and with parchment paper between the weight and the samples. The samples were cured in a vacuum oven at 150°C for 48h and then purified as described. Prior to mechanical testing, the parchment paper was removed and the samples obtained had at 3D T-shape. Delamination tests were performed on the hydrated T-peel samples.

2.4.5. Thermogravimetric Analysis (TGA)

To establish if the samples could be autoclaved, their thermal stability was analyzed by thermogravimetric analyses (TGA) using a Perkin-Elmer thermo-analyzer model Pyris 1. Thermograms were recorded from room temperature to 700°C at a heating rate of 10°C/min under nitrogen flow of 20 mL/ min.

2.5. Cell proliferation/cytotoxicity

Cell proliferation/cytotoxicity was measured by resazurin (Cat. No R7017, Sigma-Aldrich®), a compound that is reduced and fluoresces in the presence of viable cells and continuous cell proliferation.[42] To prepare the resazurin solution, 1g of resazurin powder was diluted in 100 ml of ultrapure water in magnetic stirring overnight, producing the first resazurin stock solution. We diluted then the first stock solution at 10% in ultrapure water, then filtering it, creating a second stock solution, ready to employ when diluted at 5% (v/v) in cell culture media. The cell viability/cytotoxicity test was performed according the ISO 10993-5 standard, with biomaterials extract. The extract was prepared by incubating overnight 20 mg of autoclaved PGS/PVA scaffolds per mL of cell culture media, at 37°C. Human Umbilical Vein Endothelial Cells (HUVEC) were trypsinized, counted and resuspended at 1 x 10^4 cells/well. Cells were incubated in DMEM (Vitrocell®, EmbriolifeTM) supplemented with 10% fetal bovine serum, 1% penicillin, and 1% streptomycin (100 mg/mL) for 3 hours at 37°C, 5% CO_2. Following, cells were incubated with the scaffolds extract or DMEM only (negative control) or methanol (positive control for cytotoxicity). The extract, or cell medium or methanol was changed at each 2 days. The cell proliferation assay was performed by incubation of resazurin final stock solution diluted at 5% in DMEM at 100 µL per well. We employed four wells for each PGS extract, positive and negative control, and three independent assays (triplicate). Two empty wells were used as reagent blanks (control of the resazurin). The cells were incubated at 37 °C in atmosphere supplemented with 5% of CO_2 for 4 h. After incubation, 30 µL of medium was transferred into a 96-well TCPS plate, and 30 µL of 100% reduced (fluorescent) resazurin (obtained by autoclaving, as described) was used as reference of the assay. We measured the fluorescence according the Equation 2. The assay was done at 1, 3, 5 and 7 days after cell seeding.

$$Relative\ Fluorescence\ (\%) = \frac{(Sample\ value - blank)}{(100\%\ fluorescent\ resazurin - blank)}$$

Equation 2. Calculation of relative fluorescence of resazurin.

2.6. GelMA polymerization

Prior to the polymerization, the photoinitiator solution (PI) was prepared by adding 10 mg of 2-Hydroxy-4'-(2-hydroxyethoxy)-2-methylpropiophenone (Sigma-Aldrich 410896-10G) in 1 ml of ultrapure water, vortexing the solution and keeping it at 37°C. Following, the pre-GelMA was diluted at 10% (m/v) in PBS, and this solution was also kept at 60°C for, at least, 1 hour, in order to completely dissolve the pre-GelMA, creating the stock pre-GelMA. Following the dissolution

steps, all solutions were kept at 37°C. The final pre-GelMA solution was made by mixing the PI solution, the pre-GelMA stock solution and EBM-2 + bullet kit cell culture media (Lonza®), with a final pre-GelMA solution at pre-GelMA at 5% (m/v) with 0.1% (m/v) of PI read to employ. The pre-GelMA final solution was put inside the wells of a 96-well transparent TCPS plate (40 μl/well). The plate was placed inside a UV curing chamber (375 nm, 36 w) and the polymerization was proceeded for 15 minutes.

2.7. HUVEC/MG-63 3D co-culture on GelMA

First, in order to determine which kind of interactions we would observe and/or expect from 3D co-culturing MG-63 and HUVEC cells, though this interaction is widely reported.[43–47] The GelMA was previously polymerized as described. First, we prepared 3D monocultures of osteoblasts and endothelial cells directly on the previously polymerized GelMA. Following, to simulate the dynamic seeding which would be performed for the assembly of vascular grafts + GelMA, osteoblasts were first seeded at 1 x 10^4 suspended at 40 μl of EBM-2 bullet kit media, then allowed to adhere on GelMA for 1 hour. Finally, the cell media was removed and the HUVEC cells were seeded at 2 X 10^4 cell/well (with the half of the cell concentration of the MG-63 because the HUVEC is a less proliferative cell lineage compared to the MG-63[45]). This amount of HUVEC was, initially, suspended in 15 μl of media. They were allowed to attach for 30 minutes (to permit cell adhesion and, at the same time, to prevent cell dehydration) and, then, the wells were completed with 120 μl of cell culture media. These steps were made in order to keep the majority of HUVECs in the middle of the hydrogel, so we could create a gradient of HUVECs towards the osteoblasts. After 48 hours, the constructs were fixed and stained as it will be explained.

2.8. Fluorescent Staining

Cells were fixed with 4% of paraformaldehyde in PBS for 10 minutes and washed twice with PBS. To increase the permeability of the cells, a solution of 0.1% of triton x-100 in PBS was used for 5 minutes. The wells were washed two times with PBS, and DAPI (provided by Sigma-Aldrich) and Phalloidin (CytoPainter Phalloidin-iFluor 488, Cat. Nº 176753, Abcam™) staining was diluted in PBS with 1% of BSA as the manufacturer's recommendations. After 10 minutes, the samples were washed twice with PBS, but, at the last wash, some PBS was left to prevent samples dehydration. The light and fluorescence images from samples were taken from a Zeiss Axio Vert.A1 inverted microscope with AxioCam software. The images were superimposed according to the desirable (DAPI and GFP filters and their superimposition with the light microscopy images, as illustrated on Figure S1). Noise reduction and contrast improvement filters were applied.

2.9. Endothelial Cells Seeding from the Vascular Graft: an *in vitro* model of bone vascularization (osteon-like) from the PGS vascular grafts embedded in GelMA

As one of the hypotheses of this work is the porous structure created by laser ablation on the fibrous PGS/PVA scaffolds allows the endothelialization from the scaffold towards a bone-like tissue engineering construct, we created an *in vitro* model which simulates the rapid cell perfusion from the vascular scaffolds to an 3D bone construct, in order to observe how endothelial cells can migrated and/or interact towards a 3D bone-like biofabricated construct. Osteoblast-like MG-63 cells and HUVEC cells as endothelial cells were employed. MG-63 is derived from a

malignant tumor and possess osteoblastic features,[48] often employed for studies with different materials and it is a stable, immortal lineage, which is a positive feature for its use for in vitro assays.[49] HUVEC cells are widely employed as angiogenesis model for vascularization in vitro.[50]

This experiment was designed to be an osteon-like,[36,37] which contain the central blood capillary – represented by the vascular graft and the vascular endothelial cells (HUVECs) - and the concentric osseous lamellae – represented by the osteoblast-like cells (MG-63). An overview of the experiment assembly is given on Figure 1. First, transversal sections of non-patterned (without micropores) and laser patterned scaffolds (with micropores) were embedded inside non-crosslinked GelMA (pre-GelMA) in well of a 96 well-plate (Figure 1A and B). The GelMA was allowed to crosslink for 15 minutes, fixing the tubular scaffold (Figure 1C). Suspended MG-63 were seeded at 1 x 10^4 per well (40 µl), over GelMA, outside the graft. The MG-63 were allowed to adhere at GelMA substrates for 30 minutes prior to HUVEC seeding (2 x 10^4/well, suspended in 15 µl of cell culture media), creating again a gradient of HUVECs and MG-63 (Figure 1D). For the machined scaffolds, it is worth pointing that, inevitably, HUVECs got out from the scaffold and MG-63 got in through the micropores during seeding. After 48 hours, the constructs were fixed and stained with phalloidin and DAPI, as reported, and, then, observed by a fluorescence microscope.

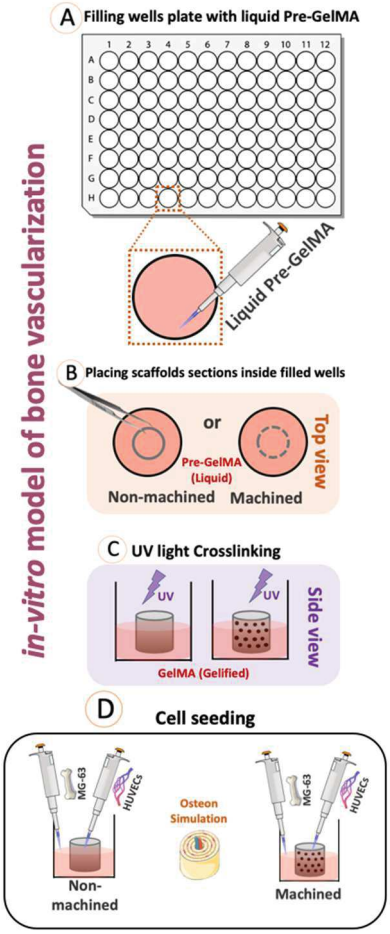

Figure 1. ***In vitro model of bone vascularization (osteon-like) from the PGS vascular grafts embedded in GelMA:*** **(A)** First, empty TCPS wells of a 96-wells plate were filled with liquid GelMA prepolymer. **(B)** Then, transversal cuts of the tubular scaffolds (non-machined and machined), were embedded into liquid GelMA, placed at the middle of the well. **(C)** Following, the GelMA was crosslinked by UV light with the scaffold inside. **(D)** Dynamic cell seeding, as simulation of an osteon: the endothelial cells were seeded inside the tubular scaffold, while the osteoblasts were seeded at the external side of the scaffold (considering proper times for cells to adhere, as described).

2.10. Statistical Analysis

Statistical comparisons were performed using two-way ANOVA carried out with GraphPad Prism® software and the Bonferroni multiple comparisons test. P-values < 0.05 were considered statistically significant (n=4).

3. RESULTS

3.1. Fabrication of vascular graft overview

In the context of rapid vascularization in tissue engineering, vascular grafts, which are embedded in complex biofabricated 3D constructs, must ensure immediate blood flow from the host to the whole construct. Thus, in this work, we propose the elaboration of fibrous tubular elastomeric vascular grafts with pores of diameter in the order of 100 μm. The several steps allowing the fabrication of a tubular graft are depicted in the Figure 2.

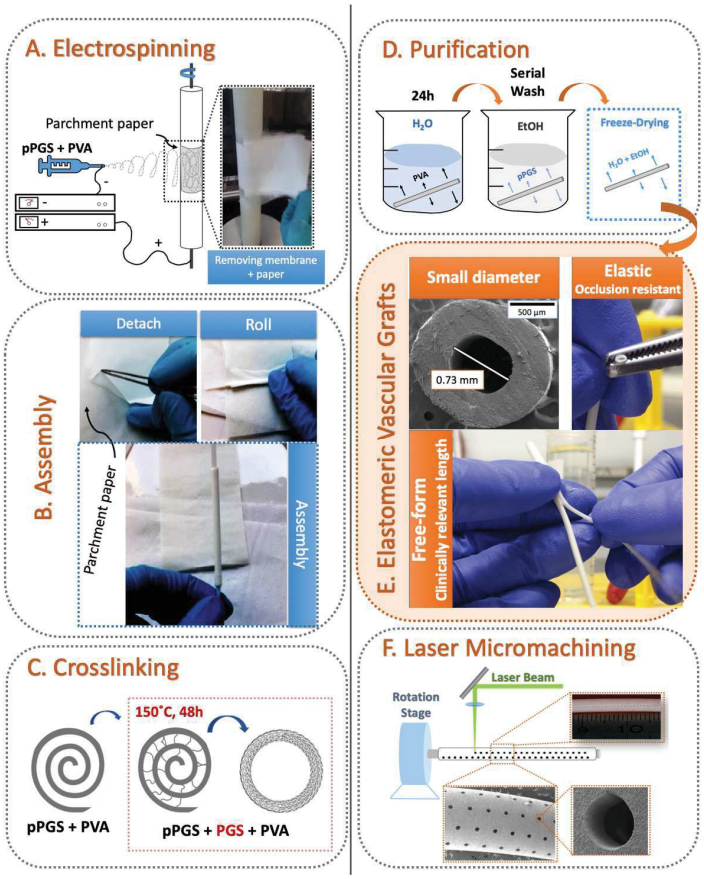

Figure 2. ***Overview of the fabrication process of bioabsorbable and elastomeric vascular grafts.*** **(A)** Electrospinning of pPGS and PVA on a non-sticky parchment paper using a rotating collector insuring the homogeneity of the scaffold. **(B)** Assembly of the tubular scaffolds by detaching the electrospun scaffolds and rolling them around PTFE mandrels. **(C)** Crosslinking the pPGS into PGS, which also leads to the fusing of electrospun layers of the scaffold. **(D)** Purification of the scaffolds by dH2O, to remove the PVA, then by serial washing with ethanol to remove possible traces of pPGS, followed by freeze-drying the obtained scaffolds. **(E)** The obtained tubular scaffolds can have very small inner diameters, clinically relevant lengths and some liberty of forms (Y-shape). **(F)** Laser femtosecond micro-ablation post-processing, which does not melt the fibers. Through this process, tubular scaffolds with a patterning of porous at the microscale were produced.

Briefly, a nanofibrous scaffold was first elaborated by electrospinning a solution of a pre-polymer of PGS (pPGS) and poly (vinyl alcohol) (PVA) as a carrier polymer, using a rotating collector insuring a homogeneous deposition of the fibers (Figure 2A). Following, the tube was assembled

by rolling the fibrous scaffold around a PTFE mandrel with different diameters (Figure 2B) and, eventually, in a Y-shape (Figure 2E and Movie S1). The presence of pPGS, which is slightly adhesive, allowed a simple assembling of the tube while keeping its shape after its manufacturing. Then, the assembled tubes were thermally crosslinked under vacuum in order to cure the pPGS into PGS, which also leads to the welding of the electrospun layers of the scaffold (Figure 2C). The obtained tubes were washed in dH_2O to remove the carrier polymer (PVA) and in ethanol to remove possible traces of pPGS. The tubes were then freeze-dried (Figure 2D). Elastomeric fibrous tubular scaffolds with various calibers - as small as 0.73 mm – and clinically relevant lengths could easily be obtained thanks to the described assembly process, which also allows some liberty of forms, e.g. the illustrated Y-shape tubular scaffold (Figure 2E). Finally, laser micromachining post-processing was performed in order to create a network of pore channels of diameter in the order of 100 μm to potentially promote vascular branching inside biofabricated constructs (Figure 2F). Through this process, fibrous elastomeric tubes with a patterning of pores having diameter in the range of 100 μm were produced. The detailed results of each of these steps will then be described.

3.2. Characterization of elastomeric PGS fibrous scaffolds

3.2.1. PGS fibrous scaffolds crosslinking optimization

A poly (glycerol sebacate) prepolymer (pPGS) with a soft wax aspect, as described by Li et. al.[41] was synthesized, with a estimated degree of esterification of 51%, as measured by ^{1}H NMR (see Figure S2). Following, pPGS was employed to produce pPGS/PVA (55/45 weight ratio) fibrous scaffolds by electrospinning from 10% (w/v) solutions in hexafluoroisopropanol (HFIP).

The morphology of the electrospun scaffolds were observed by SEM after their collection on parchment paper (Figure 3A), their crosslinking in different conditions (Figure 3B, C and D) followed by their dH2O and serial EtOH washings to remove PVA and uncrosslinked pPGS chains. The conditions allowing the crosslinking of PGS/PVA scaffolds were adapted from the work reported by Jeffries et al., who reported various curing temperature and time to crosslink their PGS/PVA membranes under vacuum. They concluded that the best condition, in terms of mechanical properties and integrity of fibers preservation, was 120°C for 48h 35. We investigated this crosslinking condition in our lab, as well as curing at 120°C for 24h, followed by 150°C for 24 more hours, or curing at 150°C for 48 h. In our case, only a curing step of 48h at 150°C allowed to obtain samples with a uniform morphology and preserved porosity (Figure 3D), while a film or fused fibers were obtained for the two other tested conditions (Figure 3B, C, respectively). Therefore, all the following fibrous scaffolds described in this work were crosslinked under vacuum at 150°C for 48h.

The PVA purification efficiency was estimated by mass loss, from the different crosslinking conditions (Figure 3E). The remaining mass at 150ºC, 48 h condition was higher than for 120ºC-24 h and 150ºC-24 h, after both water and ethanol washes, indicating that a significant amount of mass remained after the water washing for the 150°C 48h condition in comparison with the 120°C-24h, 150°C-24h condition. This thermal annealing may contribute for PVA insolubility[51] due to its possible crosslinking with the residual carboxylic groups of the pPGS.[35] For both crosslinking conditions, the most significant mass loss was measured after water washing, which most likely removes the PVA, due to its solubility in water. A significant amount of mass remained after the water washing for the 150°C 48h condition in comparison with the 120°C-24h, 150°C-24h condition. Finally, the mass loss after washing in ethanol is also

lower in the case of crosslinking reaction at 150°C for 48 h indicating that less uncrosslinked pPGS has been removed at this step.

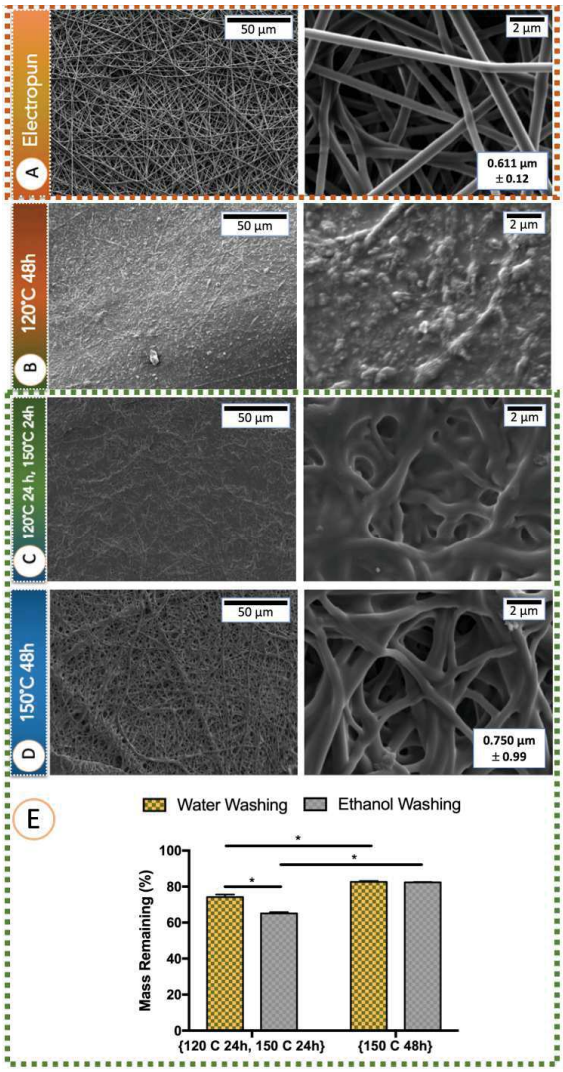

Figure 3. ***SEM images*** of **(A)** electrospun pPGS/PVA scaffolds; and crosslinked and purified at different conditions: **(B)** 120°C 48h; **(C)** 120° 24h, then 150°C 24h; and **(D)** 150°C 48h. The overall morphology of the scaffolds is shown. At the square on electrospun and crosslinked at 150°C 48 h images, the average diameter ± Standard Deviation of the Mean are displayed. **(E)** ***Scaffolds purification efficiency*** calculated by the average remaining mass (%, n=3) after each washing step (water washing and ethanol serial washing) in comparison with the crosslinked samples. Error bars represent the Standard Error of the Meaning. *n<0.05.

3.2.2. Elastomeric tubular grafts from fibrous scaffolds with patterned porosity from laser phemtosecond ablation

Electrospun sheets of 10 cm x 20 cm were fabricated in order to produce tubes of 10 cm length. By simply rolling the electrospun pPGS/PVA scaffold around various PTFE rods, followed by the curing step, tubes with various internal diameter and thickness were obtained. A SEM image of the transversal cut (Figure 4A) shows how the welding of consecutives electrospun layers occurred (connections highlighted in red dashed lines): the pPGS flowed through within the layers and was crosslinked during scaffold curing, resulting in a monolithic tubular scaffold from the electrospun scaffolds stacking. Cross-sections of tubular scaffolds of 0.73, 1.35 and 1.75 mm

are shown on Figure 4B (i, ii and iii, respectively). Also from this technique, Y-shape tubular scaffolds, inspired on the GORE TEX® PTFE vascular grafts commercially available from Gore Medical (which are neither biodegradable, nor mimics the native ECM), was easily produced, as it can be seen on Figure 2E and on Movie S1.

The abluminal (the external side of the tubular scaffold) and the luminal (the inner side) surfaces were also analyzed through SEM (Figure 4C and D, respectively). On the abluminal side, a fibrous architecture with a preserved architecture of fibers and porosity after crosslinking was observed (Figure 4C(i)). The smooth surface of the luminal side (Figure 4E) in comparison with the surface of the abluminal side, is probably due to the contact with the PTFE surface during curing.

A pattern of pore channels has been created by laser microablation as seen on Figure 4C (i and ii). More morphological aspects of the pores are shown on Figure 4E, showing the pores are in the range of 100 microns, with diameters of 150 μm for the abluminal (external) side of the tube (Figure 4(i)) and 130 μm for the luminal (internal) side of the tube (Figure 4(ii)), with drop shapes (as displayed by the red dashed forms). The laser ablation process did not affect the fibrous structure or melted the polymer at the edge of the created pore (Figure 4E (iii)). More SEM images showing these and more morphological features closer can be checked at Figures S3, S4 and S5.

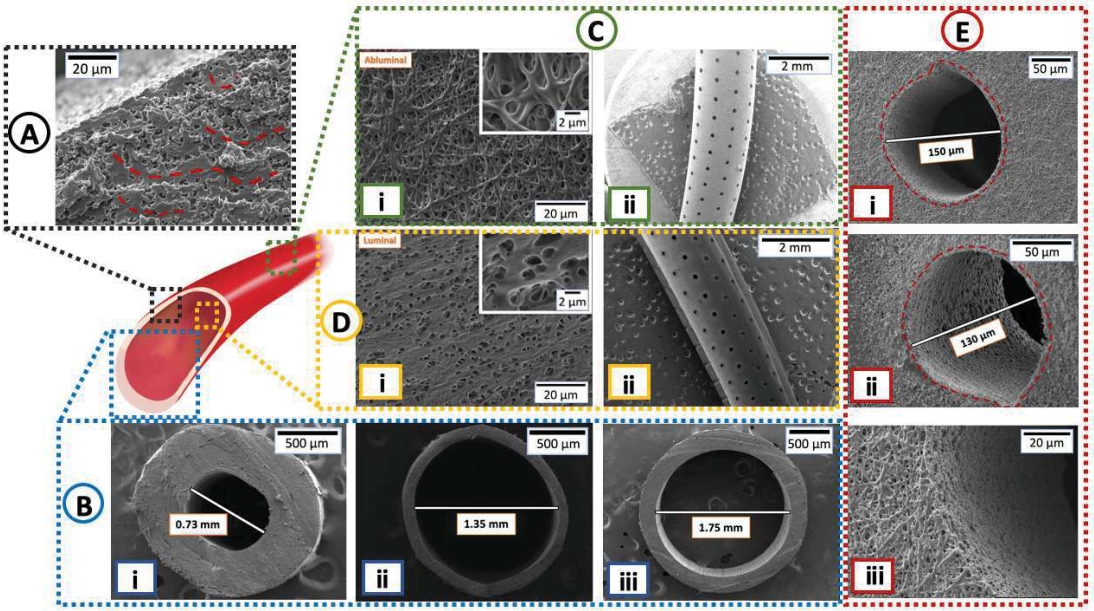

Figure 4. ***Morphological properties of the tubular scaffolds according to the SEM images.*** **(A)** A cross-section of a tubular scaffold, showing its inner porosity and the interlayer connection between the layers, highlighted by red dashed lines. **(B)** Cross-sections of tubular grafts with inner diameter of i) 0.73 mm; ii) 1,35 mm and iii) 1,75mm - as result from the electrospun scaffolds wrapping around TPFE mandrels – are shown. **(C)** The abluminal (external) surface (i), and the pores pattern resulting from the laser machining (ii). **(D)** The luminal (internal) surface (i) and the internal pattern of machined pores (ii). **(E)** The abluminal (i) and the luminal pore face (ii), respectively; (iii)The pore edge (external), evidencing the laser does not melt or fuse the fibers on their edges.

Therefore, the PGS/PVA tubular grafts machined by laser photoablation have two major levels of porosity: (i) the porosity from the electrospun fibers allowing the nutrients and growth factors exchange[52] and (ii) the porosity from the laser machining allowing cell migration[28,53] and, potentially, a vascular branching towards biofabricated constructs.

3.2.3. Mechanical and thermal characterizations of the vascular grafts

Mechanical tests were performed in order to determine the mechanical properties of the PGS/PVA tubular scaffolds, to evaluate their suturability and to verify the scaffold layers bonding. We also characterized the effect of the laser ablation on these properties. It is worth noting that the properties discussed here were obtained from hydrated scaffolds, as they will be hydrated in the organism after implantation.

Delamination tests were first carried out with T-peel samples, simulating either the interactions inside electrospun scaffolds or the bonding between two stacked scaffolds (Figure 5A). The stacked and the directly electrospun scaffolds did not present significant differences, both resting delamination up to 5 mN/mm, demonstrating the effectiveness of the bonding between the layers of the assembled scaffolds.

The tubular scaffolds behave as elastomeric materials (Figure 5B, Movies S1 and S2). Non-machined and laser ablated samples, characterized by tensile tests, have presented no significant difference regarding their ultimate tensile stress at breaking, both with 1.5 MPa approximately (Figure 5C). Both scaffolds are highly elastic, and elongated for more than 100% their original size, though the elongation at breaking of the ablated scaffolds (140%) increased from the non-machined scaffold (107%). The presence of pores in the laser ablated sample obviously decreased its apparent Young modulus from 3.11± 0.9 MPa (non-machined) to 1.99 MPa ± 0.2 MPa (machined). Some of the mechanical behavior when handling is show on Movie S3.

Finally, both non-machined and machined tubular scaffolds have shown suture retention, independently of the caliber of the tube (Figure 5D). However, the suture retention for the laser machined scaffolds is smaller in comparison with the non-machined scaffolds (3.96 ± 0.52 N/mm^2 and 5.85 ± 0.46 N/mm^2, respectively), which was attributed to the porous structure facilitating the tearing due to force from the suture.

Prior to biological assays, in order to evaluate the suitability of the vascular grafts for autoclaving, scaffolds were analyzed by thermal gravimetric analysis (TGA) (Figure 5E). The material degradation started at 200°C, and its carbonization begun at around 430°C. As the autoclave sterilizes materials under a vapor temperature of 120°C, the TGA analysis indicates that the scaffolds are suitable for autoclaving. Therefore, this was our sterilization method prior to the biological assays. The mechanical behavior of the vascular grafts after autoclaving, when handled, can be seen at Movie S4.

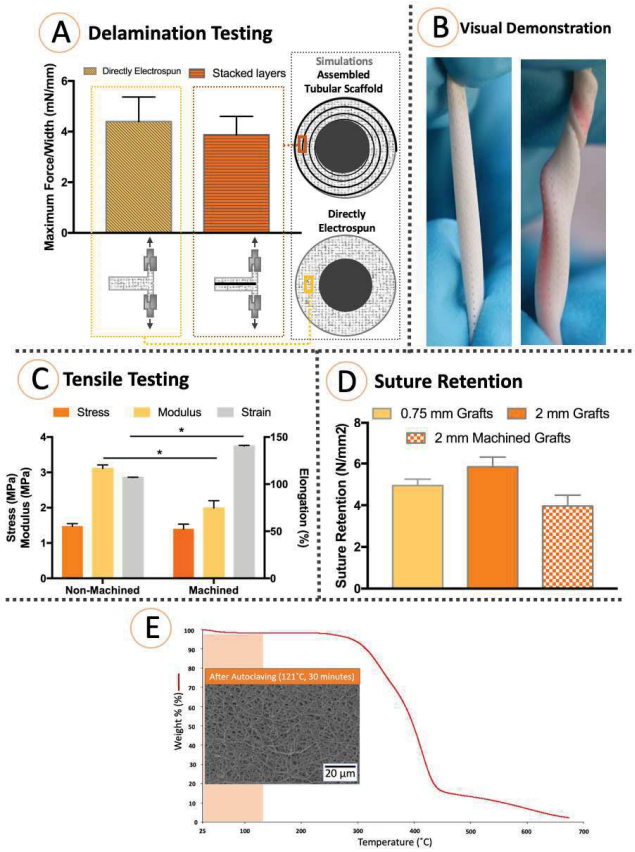

Figure 5. ***Thermo-mechanical properties of the elastomeric tubular scaffolds.*** **(A)** Delamination testing by uniaxial tensile assay of directly electrospun and stacked layers T-peel samples, as illustrated, simulating directly electrospun scaffolds or assembled by layers fusing, respectively. **(B)** Visual demonstration of the laser ablated scaffolds elasticity through gross images. The vascular graft deformation is demonstrated by a red-line **(C)** Stress, modulus (young's modulus) and strain data, also obtained from uniaxial tensile testing, of non-machined and laser-machined grafts. Error bars represent Standard Error of the Mean. *P-values < 0.05. **(D)** Suture retention strength from uniaxial tensile testing of very small (0.73 mm), small (2 mm) and small machined PGS/PVA tubular grafts (2 mm). **(E)** Thermogravimetric Analysis (TGA) of the suturable grafts, which demonstrates the polymer degradation (PGS/PVA) starts from 230°C approximately, indicating the scaffolds can be sterilized by autoclaving (121°C, 20 minutes). The orange band indicates the temperature ranging of a conventional vapor autoclave. The SEM picture, obtained from an autoclaved scaffold, confirmed the scaffold structure it is not affected by autoclaving.

3.3. Cell proliferation/cytotoxicity characterization

For the cell proliferation/cytotoxicity characterization, results shown that endothelial cells (HUVECs) proliferated over time with both PGS/PVA scaffolds extracts and cell culture media, proving that PGS/PVA does not release armful compounds and, therefore, has no cytotoxic effects, corroborating with the analysis of Jeffries et al. with 3T3 cells,[35] as seen on Figure 6. Until the day 3, the culture was maintained stable, which was expected for both PGS/PVA extracts and control, since we started with a relatively high cell density (1 x 10^4 cells/well from a 96-well plate). However, at day 5 from cell seeding, the HUVEC proliferation rate was significantly higher for the PGS/PVA extracts than for the control. At day 7, once the HUVEC cells cultured with PGS/PVA extracts filled the well, the cell proliferation stabilized, probably because of the limited space of the well, while the HUVECs in non-modified media continued to proliferate and reached a similar proliferation in comparison with the PGS/PVA extracts. HUVEC cells cultured directly on PGS/PVA membranes can be seen on Figure S6.

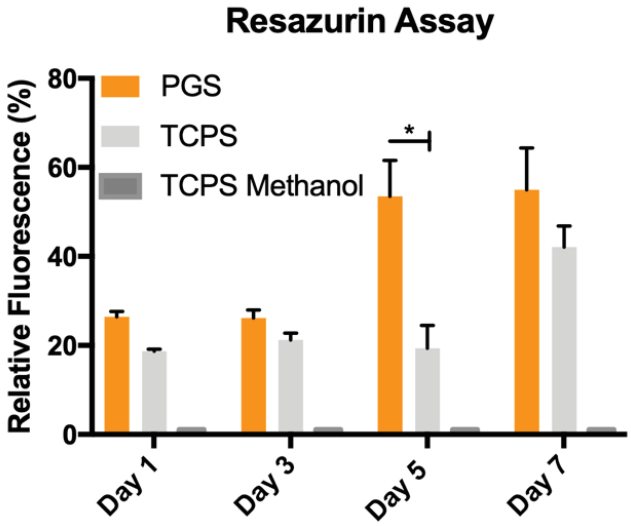

Figure 6. Resazurin cell viability assay for the HUVEC proliferation with PGS extracts. The error bars represent the Standard Error of the Meaning. *n<0.05, comparing the PGS extracts with non-modified cell culture medium.

3.4. Application of the vascular graft: an *in vitro* osteon-like model

3.4.1. Co-culture of HUVEC and MG-63 in GelMA alone: determining the expecting cell interactions

Before studying the behavior of the osteon-like model, HUVEC and MG-63 cells were co-cultured in GelMA alone. Prior to seeding, MG-63 osteoblasts were maintained in EBM-2 + bullet kit media in order to verify if the MG-63 would survive in the same media as endothelial cells, in which both cells would be co-cultured. By observations at microscope, which was performed after, at least, 4 passages continually, it was confirmed that the osteoblasts survived and proliferated at same rate if cultured in DMEM media. Following, we proceed with the MG-63/HUVEC co-culture system in the EBM-2 culture media.

In order to determine the *in vitro* interaction of the HUVEC (endothelial) and the MG-63 (osteoblasts-like) co-cultured in GelMA and to predict their behavior with the tubular scaffolds embedded in GelMA hydrogels, HUVECs and MG-63 were firstly 3D co-cultured on the scaffold-free hydrogels. After 2 days of cell culture (48 h), the endothelial cells alone formed their typical tubular structure[54] as shown in Figure 7(1A), with some of the tubes indicated by arrows, while the osteoblasts alone were organized in islets Figure 7(1B). This was, thus, the expected behavior for dynamic seeding experiments with tubular scaffolds without the micropatterned pores or, in other words, seeding the endothelial cells (HUVECs) isolated from the osteoblasts (MG-63) by the tubular scaffold. However, the HUVEC and MG-63, when co-cultured, associated together in clusters (Figure 7(1C), interconnected by HUVEC branches, highlighted at Figure 7(1C.1), indicated by arrows. These observations corroborate with the work of Fuchs et al. of a morphological assessment of endothelial networks formed by outgrowth endothelial cells and MG-63.[43] Thus, we expected, for the experiments with tubular scaffolds with laser-ablated pores integrated on GelMA, that the HUVECs and MG-63 would assembly into particular 3D structures thanks to the endothelial cell flow towards the osteoblasts and their consequent synergistic interaction.

3.4.2. Osteon-like model

A 3D osteon-like construct was prepared, composed of a vascular graft embedded in gelatin methacryloyl (GelMA) hydrogels, then seeded with MG-63 (osteoblasts-like) at the exterior of the vascular graft and seeded with HUVECs (endothelial cells) at the interior of the vascular graft (Figure 1). Two kinds of osteon models were studied. The first one was built with a vascular graft without pore channels and the second was built with a laser-machined vascular graft.

For the non-machined scaffolds, due to the absence of pores, the HUVECs remained trapped inside the tubular scaffold (Figure 7(2A)), forming some tubes, indicated by an arrow at its zoomed square at Figure 7(A.1). However, due to the high cell density (equally employed for all experiments), the cells preferably aggregated into large structures than capillaries[54] inside the vascular graft. At the external side of the vascular graft region, the MG-63 remained aggregated into clusters or islets (highlighted at the Figure 7(2B), which detail is magnified at Figure 7(2B.1)), which was also observed on Figure 7(1B) for the osteoblasts seeded on GelMA without the tubular grafts. Therefore, due to the absence of machined pores, the observed structures from the HUVECs and MG-63 were similar as observed for these cell types when cultured separately.

However, when the scaffold had pores that allowed the endothelial cell to flow, these cells permeated the external surface of the hydrogel and, then, interacted with the osteoblasts at the external side (Figure 7(2C), magnified at Figure 7(2C.1)). We can observe how the MG-63 sprout when around the HUVECs spheroids (Figure 7(2D)). The white square, zoomed at Figure 7(D.1) shows the close cell–cell contacts, suggesting the formation of specialized unions within the osteoblasts and HUVECs, observed by their aggregation in clusters. HUVECs can be seen as cuboid cells which organizes in clusters, and MG-63 as spindle-like cells[45,55,56] (Figure 7(2D.1)). Therefore, the laser ablated pores pattern over the vascular graft is pivotal for the endothelial cell flow and their consecutive interaction with the cells in the biofabricated interface.

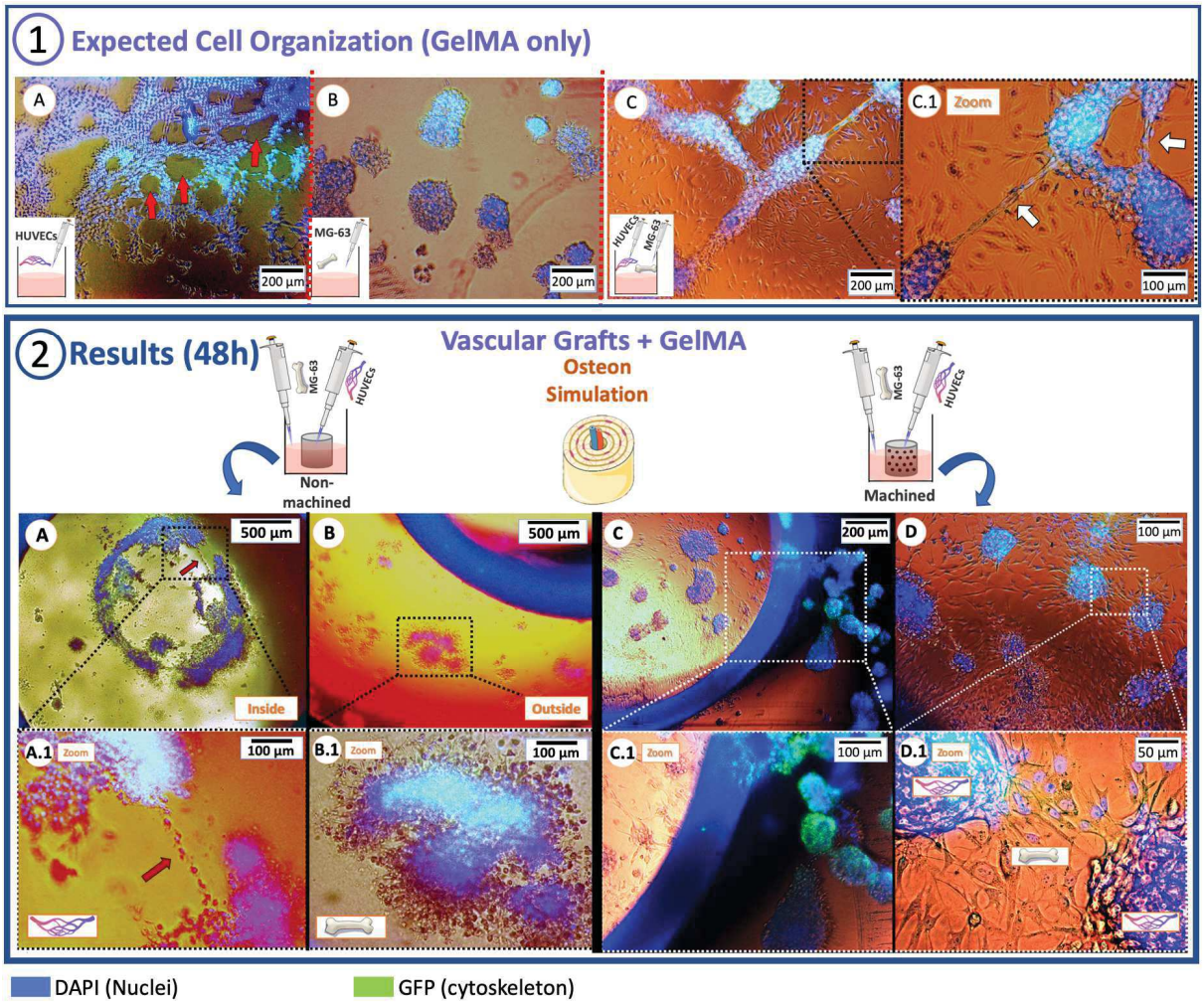

Figure 7. (*1) 3D culture in GelMA constructs, in order to define the expected 3D structures of:* **(A)** HUVEC cells only, with their characteristic tube formation (with some of them indicated by red arrows): **(B)** MG-63 osteoblasts-like only, forming circular colonies; **(C)** HUVEC + MG-63 co-cultures, with the association of colonies + tubular formation; **(C.1)** Image zoomed from the dashed area in **(C)**, evidencing the structure which connects the cell colonies by white arrows. **(2)** After 48h of cell incubation, the structures were observed in an inverted microscope. For the non-machined scaffolds, **(A)** at the inner side of the scaffold, seeded by endothelial cells, the dashed square is amplified at **(A.1)**, showing the typical structure formed by the HUVECs 3D culture (pointed by red arrows); **(B)** At the external side of the scaffold, the expected 3D structures (islets), from osteoblasts only, are highlighted at the dashed black square, zoomed on **(B.1).** For the machined scaffolds, where the endothelial cells were allowed to flow towards the osteoblasts through the machined channels, exclusive structures from the interaction of endothelial cells and osteoblasts are observed on **(C)** and **(B)** and amplified on **(C.1)** and **(D.1)** respectively.

4. DISCUSSION

The current strategies to create vascular networks in biofabricated tissues encompasses the creation of hollow channels comprised by the association of cells and hydrogels.[57–59] However, the anastomose of these channels with the host vasculature, in order to enable an instantaneous blood perfusion inside these channels, is generally not possible because of the lack of mechanical properties of hydrogels.[2]

In our study, we proposed the fabrication of a small suturable vessel graft based on the elastomeric and biodegradable PGS/PVA composites, obtained by electrospinning. By

embedding these elastomeric tubular grafts in biofabricated tissues, an anastomosis between the engineered tissue and the host vasculature may be possible.

The electrospinning enables the fabrication of tubular structures with a fibrous structure similar to the native ECM and improved mechanical strength to PGS/PVA, particularly the suture retention.[35] However, to obtain such tubular structures through electrospinning with a diameter smaller than 1 mm, that can be better embedded in microfabricated tissues, is challenging. Here, we addressed this issue by electropinning over a non-sticky surface (parchment paper) and then rolling the obtained fibrous mats around PTFE templates. The consecutive PGS curing also bonds the successive layers of the tubular grafts.

The fibers collection over parchment paper allowed to detach 100% of the scaffolds for the purpose of production of tubular scaffolds, without tearing the fibers (Figure 2B). Scaffolds fabricated over conductive surfaces (metal mandrels or aluminum foil, for example) cannot be detached without leaving a large amount of the product over the surface. Due to this reason, when directly electrospinning a tubular scaffold, a pre-coating step of mandrels is commonly applied.[20] Here, this step is not necessary. This strategy is more efficient in terms of productivity when compared with electrospinning directly on a small cylindrical collector, allowing the fabrication of a tube with the desired thickness, which can be controlled by the number of electrospun layers employed. It highlights the easily customizable feature of this strategy, allowing to obtain tubular scaffolds with internal diameter ranging from 0.73 mm (see the Movie S2) to beyond (Figure 4B) and diverse shapes, as demonstrated by the fabrication of the Y-shape tube (Figure 2B and the Movie S1), and clinically relevant lengths (10 cm for our prototypes, which is considered clinically relevant ($\geq$ 3 cm)[60]). This is of crucial importance for the clinical application of these vascular grafts, either for its potential application for rapid vascularization of tissue engineered grafts, or to treat vascular injuries, since the scaffold caliber can be easily customized according to the vascular host site. Still, it may be possible to employ larger electrospun scaffolds to obtain longer tubes, or potentially bond various sheets to create continuous tubular scaffolds, which can be cut and employed by the surgeon according to surgery site need.

Regarding the final composition of the tubular scaffolds, though we intended to fabricate them with the most similar properties of PGS as possible, the mass loss analysis indicated that an amount of PVA remained even after the purification of the scaffolds in water (Figure 3E), which results corroborate with the work of Jeffries et. al.[35] As also they pointed, it is difficult to quantify the remaining PVA employing traditional analysis as FT-IR spectra, since the PVA and PGS spectra are quite similar.[35] It is worth pointing out the remaining PVA is not harmful for cells,[61–63] as it is the PGS. PVA is non-toxic, biodegradable, and does not degrade in any harm compound to the cells.[64–67] Those are essential features, as the scaffold are intended to be applied as bioabsorbable vascular grafts.

To promote a vascular branching from the vascular graft towards the interior of the biofabricated tissue, we created a pattern of pore channels across the wall of the tubular grafts through laser femtosecond ablation, or laser machining (Figure 4C, D and E; and Movie S3). Since endothelial cells have 13.2 ± 4.1 μm width and 25.8 ± 8.5 μm length,[68] these pores dimensions ($\cong$ 150 μm) can, therefore, support endothelial cell migration and potentially allow blood flow and thus create a vascular micronetworking from the vascular graft to the biofabricated implant. However, it is worth to questioning how the vascular grafts with the patterned pores will behave once it is connected to the host vasculature in order to allow the angiogenesis inside the fabricated tissue engineering construct. We hypothesized that, as the blood flows outside and goes in contact with the external tissue, it will coagulate the pores, as the

coagulum formation is part of the dynamics of angiogenesis process.[69] Though the coagulation inside the machined pores can be beneficial concerning the dynamic of angiogenesis and vascular branching, however, for *in vivo* studies, we suggest to previously soak these tubular scaffolds in heparin, an anticoagulant that can prevent blood clot formation inside the lumen of the vascular grafts as natural response from the organism at the implant site and that can also enhance endothelial cell recruitment.[70] The smooth luminal surface at the interior of the tubular scaffolds can be an interesting feature (Figure 4D), since the scaffolds are intended to be immediately employed as vascular grafts, potentially helping to prevent turbulent blood flow after the first days from the graft implantation, as we hypothesize. Moreover, because there is a crescent clinical need of small diameter vascular grafts (D < 6 mm) for treatments for vascular diseases, as for coronary artery bypass grafting and some peripheral vascular diseases71,20,72, the scaffolds without the ablated pores can potentially be applied as small-diameter vascular grafts for some vascular treatments.

The causes of the increase in cell proliferation for HUVEC cells, treated with PGS extracts for 5 days (Figure 6), remains unclear. For future works, we suggest deeper investigations at molecular level (e.g. qPCR) in order to stablish a hypothesis for this observation.

To demonstrate the potential of application of the vascular grafts and the laser machined pores networking for the task of rapid vascularization of biofabricated constructs, we created an osteon-like *in vitro* model which simulates the rapid endothelial cell perfusion from the vascular scaffolds, through the pores, towards a 3D bone-like biofabricated construct (Figure 1). From the observations on MG-63 and HUVECs co-cultured on GelMA hydrogels without the vascular graft (Figure 7(1C and D)), compared with the two cell types cultured separately on GelMA (Figure 7A and B), we hypothesized that both cell types would interact and form exclusive aggregations from their interactions thanks to laser-machined pores that would allow the endothelial cells, which were seeded at inside of the vascular graft, to flow towards the osteoblasts seeded at the exterior of the vascular graft. Confirming our assumptions, the endothelial cells permeated the external surface of the hydrogel and, then, interacted with the osteoblasts at the external side, forming connected clusters (Figure 7(2C and 2C.1)), with sprout MG-63 around the HUVEC clusters (Figure 7(2D.1)). These interactions are pivotal for the proliferation and survival of both cell types:[2,6] according to Shi et. al.,[45] the MG-63 play a positive role in HUVEC cells proliferation, while endothelial cells are known to secret osteogenic growth factors which enhance the survival and the proliferation of osteoblasts.[73] On the other hand, osteoblasts secrets VEGF in enough quantities to increase the cell proliferation and survival of endothelial cells.[74] It is likely probable the permeability of the vascular grafts allows the crosstalk of cell-secreted growth factors from MG-63 and HUVECs which stimulates the cell migrations, while the laser machined pores allow the cell flows/migrations. Therefore, regarding potential applications in bone tissue engineering, when inserting the elastomeric tubular grafts with laser machined pores in biofabricated bone, the presence of a vascular networking may increase the bone formation, while the bone cells may contribute to improve the construct vasculature in a dynamic effect.[75,76] Moreover, it has been reported that not only the growth factors, but also the direct contact with endothelial cells has a positive effect on the alkaline phosphatase activity of osteoblasts.[77] Complex crosstalks occurs in a complex way in the organism, with hundreds of cell types regulating each other in harmony.[36] The importance to reproduce these crosstalks on in vitro models leads to an increasing in the employment of co-culture systems.[78] Besides, this vascular network can later serve as template for ossification, which happens thanks to the synergistic interactions between osteoblasts and endothelial cells.[79]

It is also worthy to point out that, in the lumen of the scaffolds, we can find some clusters associations of HUVECs/MG-63 (Figure 7(2C)), though less developed than at the external side. Inevitably, during the MG-63 seeding, some cells can also go into the lumen through the laser machined pores. In order to avoid this association, for further works, we suggest to bioprint the bone construct with a bioink from the association of GelMA and osteoblasts (or another bioink of interest), embedding the tubular scaffold inside the structure and to perfuse the endothelial cells by through a bioreactor, controlling the spatial distribution of both cell lines. For further studies, we also suggest to localize the two cell-types by immunofluorescence with specific cell markers for each cell type. We also suggest to investigate this interaction at the molecular level (i.e. Polymerase Chain Reverse Transcription, or PCR-rt) to better understand how this crosstalk works and, therefore, to better predict this behavior once the constructs are sutured into the host.

This work gives an example of application through the creation of an osteon-like construct as model of rapid in vitro vascularization/cell migration. Furthermore, combining our machined vascular grafts with other biofabrication and/or bioprinting techniques such as Freeform Reversible Embedding of Suspended Hydrogels (FRESH)[80] or integrated tissue–organ printer (ITOP),[81] more complexed structures could even be explored.

5. CONCLUSION

We developed a small, suturable, biodegradable and biomimetic vascular tubular scaffold to be integrated in 3D biofabricated tissue engineered grafts to potentially provide an anchor site to the biofabricated graft and an immediate blood perfusion. We described a simple and fast method to produce elastomeric and biodegradable PGS/PVA vascular grafts from electrospinning that can be customizable regarding their inner diameter (being as small as 0.73) mm, wall thickness, length, and even their shape (simple tube and Y-shape). Pore channels of diameter of 100 microns were machined by laser femtosecond photoablation across the wall of the tubular scaffold. These pore channels were opened in order to provide an immediate blood perfusion and also rapid vascularization. The tubular scaffolds have a biomimetic architecture that resembles the native extracellular matrix. They stand the mechanical requirements for suturability and elasticity to be applied as vascular grafts, being suitable to be incorporated into tissue engineered grafts and to be directly connected within the host blood stream. Moreover, they could also be applied as bypass conduit to treat vascular diseases, as there is a crescent clinical need of small diameter vascular grafts. To demonstrate the potential of application, an osteon-like model for rapid endothelialization was assembled from the integration of the vascular grafts inside 3D GelMA hydrogels which was dynamically seeded with endothelial cells inside the graft and osteoblasts outside. Thanks to the laser machined pores, the endothelial cells can permeate to the external side of the vascular grafts and interact with the 3D culture of osteoblasts, generating new 3D structures. Therefore, the customizable, bioabsorbable and biomimetic suturable vascular grafts developed in this work, with an engineered pattern of laser micro-ablated pores, can be embedded into biofabricated 3D tissue engineered constructs, in order to potentially promote a vascular branching inside the constructs and serving as anchor site, improving the integration of tissue engineering constructs with the host. This approach offers new prospects to tissue engineers to improve the survival and to advance the clinical translation of biofabricated tissues.

ASSOCIATED CONTENT

Supporting Information

The Supporting Information is available free of charge on the ACS Publications website at DOI: [[[To be defined]]]

Schematic of fluorescent images assembly, NMR+ analysis of the pPGS (1:1 molar rate) employed, SEM images of the tubular scaffold processed by laser microablation, SEM images of details of the laser machined pores created, SEM pictures from the details of the laser machined tubular scaffolds, optical microscopy images of PGS membranes cultured with HUVEC cells (PDF)

Movie S1, Bioresorbable Bifurcated Vascular Grafts obtained from Electrospinning (MPG).

Movie S2, Super Small PGS Vessel Graft (MPG).

Movie S3, Laser Machined Vascular Grafts (MPG).

Movie S4, PGS Vascular Grafts Mechanical Behavior after Autoclaving (MPG).

Corresponding Author

*E-mail: carolbellani@usp.br (C.F.B)

*E-mail: guy.schlatter@unistra.fr (G.S.)

Funding Sources

This work has been financed by the Fundação de Amparo à Pesquisa do Estado de São Paulo (FAPESP, process nº 2014/17939-0 and process nº 2016/04418-8), by the Coordenação de Aperfeiçoamento de Pessoal de Nível Superior – Brasil (CAPES) – Finance Code 001, by funds from the Agence Nationale de la Recherche (MimHeart project ANR-15-CE08-0010-02) and from Institut Carnot MICA (project ElectrATPulp).

ACKNOWLEDGMENT

We would like to thank Frédéric Mermet from IREPA LASER (Strasbourg, France) for the laser micromachining of the tubular constructs.

REFERENCES

(1) Novosel, E. C.; Kleinhans, C.; Kluger, P. J. Vascularization Is the Key Challenge in Tissue Engineering. *Advanced drug delivery reviews* **2011**, *63* (4–5), 300–311. https://doi.org/10.1016/j.addr.2011.03.004.

(2) Rouwkema, J.; Khademhosseini, A. Vascularization and Angiogenesis in Tissue Engineering: Beyond Creating Static Networks. *Trends in biotechnology* **2016**, *34* (9), 733–745. https://doi.org/10.1016/j.tibtech.2016.03.002.

(3) Carmeliet, P. Mechanisms of Angiogenesis and Arteriogenesis. *Nature medicine*. 2000, pp 389–395. https://doi.org/10.1038/74651.

(4) Jain, R. K.; Au, P.; Tam, J.; Duda, D. G.; Fukumura, D. Engineering Vascularized Tissue. *Nat Biotech* **2005**, *23* (7), 821–823.

(5) Kannan, R. Y.; Salacinski, H. J.; Sales, K.; Butler, P.; Seifalian, A. M. The Roles of Tissue Engineering and Vascularisation in the Development of Micro-Vascular Networks: A Review. *Biomaterials* **2005**, *26* (14), 1857–1875. https://doi.org/10.1016/j.biomaterials.2004.07.006.

(6) Rouwkema, J.; Rivron, N. C.; van Blitterswijk, C. A. Vascularization in Tissue Engineering. *Trends in biotechnology* **2008**, *26* (8), 434–441. https://doi.org/10.1016/j.tibtech.2008.04.009.

(7) Clark, E. R.; Clark, E. L. Microscopic Observations on the Growth of Blood Capillaries in the Living Mammal. *American Journal of Anatomy* **1939**, *64* (2), 251–301. https://doi.org/10.1002/aja.1000640203.

(8) Jafarian, M.; Eslaminejad, M. B.; Khojasteh, A.; Mashhadi Abbas, F.; Dehghan, M. M.; Hassanizadeh, R.; Houshmand, B. Marrow-Derived Mesenchymal Stem Cells-Directed Bone Regeneration in the Dog Mandible: A Comparison between Biphasic Calcium Phosphate and Natural Bone Mineral. *Oral surgery, oral medicine, oral pathology, oral radiology, and endodontics* **2008**, *105* (5), e14-24. https://doi.org/10.1016/j.tripleo.2008.01.010.

(9) Barnes, C. P.; Sell, S. A.; Boland, E. D.; Simpson, D. G.; Bowlin, G. L. Nanofiber Technology: Designing the next Generation of Tissue Engineering Scaffolds. *Advanced drug delivery reviews* **2007**, *59* (14), 1413–1433. https://doi.org/10.1016/j.addr.2007.04.022.

(10) Langer, R.; Vacanti, J. P. Tissue Engineering. *Science* **1993**, *260* (5110), 920–926. https://doi.org/10.1126/science.8493529.

(11) Hoshiba, T. Cultured Cell-Derived Decellularized Matrices: A Review towards the next Decade. *Journal of Materials Chemistry B* **2017**, *5* (23), 4322–4331. https://doi.org/10.1039/c7tb00074j.

(12) Simsa, R.; Padma, A. M.; Heher, P.; Hellström, M.; Teuschl, A.; Jenndahl, L.; Bergh, N.; Fogelstrand, P. Systematic in Vitro Comparison of Decellularization Protocols for Blood Vessels. *PloS one* **2018**, *13* (12), e0209269. https://doi.org/10.1371/journal.pone.0209269.

(13) Hasan, A.; Memic, A.; Annabi, N.; Hossain, M.; Paul, A.; Dokmeci, M. R.; Dehghani, F.; Khademhosseini, A. Electrospun Scaffolds for Tissue Engineering of Vascular Grafts. *Acta biomaterialia* **2014**, *10* (1), 11–25. https://doi.org/10.1016/j.actbio.2013.08.022.

(14) Shin, N. G. R. and C. S. S. and H. Current Approaches to Electrospun Nanofibers for Tissue Engineering. *Biomedical Materials* **2013**, *8* (1), 14102.

(15) Jia, L.; Prabhakaran, M. P.; Qin, X.; Ramakrishna, S. Stem Cell Differentiation on Electrospun Nanofibrous Substrates for Vascular Tissue Engineering. *Materials science & engineering. C, Materials for biological applications* **2013**, *33* (8), 4640–4650. https://doi.org/10.1016/j.msec.2013.07.021.

(16) Abdal-hay, A.; Bartnikowski, M.; Hamlet, S.; Ivanovski, S. Electrospun Biphasic Tubular Scaffold with Enhanced Mechanical Properties for Vascular Tissue Engineering. *Materials Science and Engineering: C* **2018**, *82*, 10–18. https://doi.org/10.1016/j.msec.2017.08.041.

(17) Wu, H.; Fan, J.; Chu, C.-C.; Wu, J. Electrospinning of Small Diameter 3-D Nanofibrous Tubular Scaffolds with Controllable Nanofiber Orientations for Vascular Grafts. *Journal of Materials Science: Materials in Medicine* **2010**, *21* (12), 3207–3215. https://doi.org/10.1007/s10856-010-4164-8.

(18) Ferrari, P. F.; Aliakbarian, B.; Lagazzo, A.; Tamayol, A.; Palombo, D.; Perego, P. Tailored Electrospun Small-Diameter Graft for Vascular Prosthesis. *International Journal of Polymeric Materials and Polymeric Biomaterials* **2017**, *66* (12), 635–643. https://doi.org/10.1080/00914037.2016.1252361.

(19) Marcolin, C.; Draghi, L.; Tanzi, M.; Faré, S. Electrospun Silk Fibroin–Gelatin Composite Tubular Matrices as Scaffolds for Small Diameter Blood Vessel Regeneration. *Journal of Materials Science: Materials in Medicine* **2017**, *28* (5), 80. https://doi.org/10.1007/s10856-017-5884-9.

(20) Rocco, K. A.; Maxfield, M. W.; Best, C. A.; Dean, E. W.; Breuer, C. K. In Vivo Applications of Electrospun Tissue-Engineered Vascular Grafts: A Review. *Tissue Engineering Part B: Reviews* **2014**, *20* (6), 628–640. https://doi.org/10.1089/ten.teb.2014.0123.

(21) Kishan, A. P.; Cosgriff-Hernandez, E. M. Recent Advancements in Electrospinning Design for Tissue Engineering Applications: A Review. *Journal of Biomedical Materials Research Part A* **2017**. https://doi.org/10.1002/jbm.a.36124.

(22) Nam, J.; Huang, Y.; Agarwal, S.; Lannutti, J. Improved Cellular Infiltration in Electrospun Fiber via Engineered Porosity. *Tissue engineering* **2007**, *13* (9), 2249–2257.

(23) Wittmer, C. R.; Hébraud, A.; Nedjari, S.; Schlatter, G. Well-Organized 3D Nanofibrous Composite Constructs Using Cooperative Effects between Electrospinning and Electrospraying. *Polymer* **2014**, *55* (22), 5781–5787. https://doi.org/10.1016/j.polymer.2014.08.044.

(24) Garcia Garcia, A.; Hébraud, A.; Duval, J.-L.; Wittmer, C. R.; Gaut, L.; Duprez, D.; Egles, C.; Bedoui, F.; Schlatter, G.; Legallais, C. Poly(ε-Caprolactone)/Hydroxyapatite 3D Honeycomb Scaffolds for a Cellular Microenvironment Adapted to Maxillofacial Bone Reconstruction. *ACS Biomater. Sci. Eng.* **2018**, *4* (9), 3317–3326. https://doi.org/10.1021/acsbiomaterials.8b00521.

(25) Soliman, S.; Sant, S.; Nichol, J. W.; Khabiry, M.; Traversa, E.; Khademhosseini, A. Controlling the Porosity of Fibrous Scaffolds by Modulating the Fiber Diameter and Packing Density. *Journal of Biomedical Materials Research Part A* **2011**, *96* (3), 566–574.

(26) Yixiang, D.; Yong, T.; Liao, S.; Chan, C. K.; Ramakrishna, S. Degradation of Electrospun Nanofiber Scaffold by Short Wave Length Ultraviolet Radiation Treatment and Its Potential Applications in Tissue Engineering. *Tissue Engineering Part A* **2008**, *14* (8), 1321–1329.

(27) Baker, B. M.; Gee, A. O.; Metter, R. B.; Nathan, A. S.; Marklein, R. A.; Burdick, J. A.; Mauck, R. L. The Potential to Improve Cell Infiltration in Composite Fiber-Aligned Electrospun Scaffolds by the Selective Removal of Sacrificial Fibers. *Biomaterials* **2008**, *29* (15), 2348–2358.

(28) Lee, B. L.-P.; Jeon, H.; Wang, A.; Yan, Z.; Yu, J.; Grigoropoulos, C.; Li, S. Femtosecond Laser Ablation Enhances Cell Infiltration into Three-Dimensional Electrospun Scaffolds. *Acta Biomaterialia* **2012**, *8* (7), 2648–2658. https://doi.org/10.1016/j.actbio.2012.04.023.

(29) Lim, Y. C.; Johnson, J.; Fei, Z.; Wu, Y.; Farson, D. F.; Lannutti, J. J.; Choi, H. W.; Lee, L. J. Micropatterning and Characterization of Electrospun Poly (E-caprolactone)/Gelatin Nanofiber Tissue Scaffolds by Femtosecond Laser Ablation for Tissue Engineering Applications. *Biotechnology and bioengineering* **2011**, *108* (1), 116–126.

(30) McCullen, S. D.; Gittard, S. D.; Miller, P. R.; Pourdeyhimi, B.; Narayan, R. J.; Loboa, E. G. Laser Ablation Imparts Controlled Micro-Scale Pores in Electrospun Scaffolds for Tissue Engineering Applications. *Annals of Biomedical Engineering* **2011**, *39* (12), 3021. https://doi.org/10.1007/s10439-011-0378-2.

(31) Srinivasan, R. Ablation of Polymers and Biological Tissue by Ultraviolet Lasers. *Science* **1986**, *234* (4776), 559–565.

(32) Rai, R.; Tallawi, M.; Grigore, A.; Boccaccini, A. R. Synthesis, Properties and Biomedical Applications of Poly(Glycerol Sebacate) (PGS): A Review. *Progress in Polymer Science* **2012**, *37* (8), 1051–1078. https://doi.org/10.1016/j.progpolymsci.2012.02.001.

(33) Wang, Y.; Ameer, G. A.; Sheppard, B. J.; Langer, R. A Tough Biodegradable Elastomer. *Nat Biotech* **2002**, *20* (6), 602–606.

(34) Shenoy, S. L.; Bates, W. D.; Frisch, H. L.; Wnek, G. E. Role of Chain Entanglements on Fiber Formation during Electrospinning of Polymer Solutions: Good Solvent,

Non-Specific Polymer–Polymer Interaction Limit. *Polymer* **2005**, *46* (10), 3372–3384. https://doi.org/10.1016/j.polymer.2005.03.011.

(35) Jeffries, E. M.; Allen, R. A.; Gao, J.; Pesce, M.; Wang, Y. Highly Elastic and Suturable Electrospun Poly(Glycerol Sebacate) Fibrous Scaffolds. *Acta Biomaterialia* **2015**, *18*, 30–39. https://doi.org/10.1016/j.actbio.2015.02.005.

(36) Alberts, B.; Bray, D.; Hopkin, K.; Johnson, A.; Lewis, J.; Raff, M.; Roberts, K.; Walter, P. *Essential Cell Biology*; Garland Science, 2013.

(37) Weiner, S.; Wagner, H. D. The Material Bone: Structure-Mechanical Function Relations. *Annual review of materials science* **1998**, *28* (1), 271–298. https://doi.org/10.1146/annurev.matsci.28.1.271.

(38) Yue, K.; Trujillo-de Santiago, G.; Alvarez, M. M.; Tamayol, A.; Annabi, N.; Khademhosseini, A. Synthesis, Properties, and Biomedical Applications of Gelatin Methacryloyl (GelMA) Hydrogels. *Biomaterials* **2015**, *73*, 254–271.

(39) McKee, M. G.; Wilkes, G. L.; Colby, R. H.; Long, T. E. Correlations of Solution Rheology with Electrospun Fiber Formation of Linear and Branched Polyesters. *Macromolecules* **2004**, *37* (5), 1760–1767. https://doi.org/10.1021/ma035689h.

(40) Chaouat, M.; Le Visage, C.; Baille, W. E.; Escoubet, B.; Chaubet, F.; Mateescu, M. A.; Letourneur, D. A Novel Cross-Linked Poly(Vinyl Alcohol) (PVA) for Vascular Grafts. *Advanced Functional Materials* **2008**, *18* (19), 2855–2861. https://doi.org/10.1002/adfm.200701261.

(41) Li, X.; Hong, A. T.-L.; Naskar, N.; Chung, H.-J. Criteria for Quick and Consistent Synthesis of Poly(Glycerol Sebacate) for Tailored Mechanical Properties. *Biomacromolecules* **2015**, *16* (5), 1525–1533. https://doi.org/10.1021/acs.biomac.5b00018.

(42) Czekanska, E. M. Assessment of Cell Proliferation with Resazurin-Based Fluorescent Dye. In *Mammalian Cell Viability*; Springer, 2011; pp 27–32.

(43) Fuchs, S.; Hofmann, A.; Kirkpatrick, C. J. Microvessel-like Structures from Outgrowth Endothelial Cells from Human Peripheral Blood in 2-Dimensional and 3-Dimensional Co-Cultures with Osteoblastic Lineage Cells. *Tissue engineering* **2007**, *13* (10), 2577–2588.

(44) Kyriakidou, K.; Lucarini, G.; Zizzi, A.; Salvolini, E.; Mattioli Belmonte, M.; Mollica, F.; Gloria, A.; Ambrosio, L. Dynamic Co-Seeding of Osteoblast and Endothelial Cells on 3D Polycaprolactone Scaffolds for Enhanced Bone Tissue Engineering. *Journal of bioactive and compatible polymers* **2008**, *23* (3), 227–243.

(45) Shi, B.; Andrukhov, O.; Berner, S.; Schedle, A.; Rausch-Fan, X. The Angiogenic Behaviors of Human Umbilical Vein Endothelial Cells (HUVEC) in Co-Culture with Osteoblast-like Cells (MG-63) on Different Titanium Surfaces. *Dental Materials* **2014**, *30* (8), 839–847.

(46) Unger, R. E.; Sartoris, A.; Peters, K.; Motta, A.; Migliaresi, C.; Kunkel, M.; Bulnheim, U.; Rychly, J.; Kirkpatrick, C. J. Tissue-like Self-Assembly in Cocultures of Endothelial Cells and Osteoblasts and the Formation of Microcapillary-like Structures on Three-Dimensional Porous Biomaterials. *Biomaterials* **2007**, *28* (27), 3965–3976. https://doi.org/10.1016/j.biomaterials.2007.05.032.

(47) Zhang, Y.; Schedle, A.; Matejka, M.; Rausch-Fan, X.; Andrukhov, O. The Proliferation and Differentiation of Osteoblasts in Co-Culture with Human Umbilical Vein Endothelial Cells: An Improved Analysis Using Fluorescence-Activated Cell Sorting. *Cellular & molecular biology letters* **2010**, *15* (4), 517.

(48) Clover, J.; Gowen, M. Are MG-63 and HOS TE85 Human Osteosarcoma Cell Lines Representative Models of the Osteoblastic Phenotype? *Bone* **1994**, *15* (6), 585–591.

(49) Masters, J. R. Human Cancer Cell Lines: Fact and Fantasy. *Nature reviews Molecular cell biology* **2000**, *1* (3), 233.

(50) Goodwin, A. M. In Vitro Assays of Angiogenesis for Assessment of Angiogenic and Anti-Angiogenic Agents. *Microvascular research* **2007**, *74* (2–3), 172–183.

(51) Hassan, C.; Peppas, N. Structure and Applications of Poly (Vinyl Alcohol) Hydrogels Produced by Conventional Crosslinking or by Freezing/Thawing Methods. *Biopolymers· PVA Hydrogels, Anionic Polymerisation Nanocomposites* **2000**, 37–65.

(52) Ngadiman, N. H. A.; Noordin, M. Y.; Idris, A.; Kurniawan, D. A Review of Evolution of Electrospun Tissue Engineering Scaffold: From Two Dimensions to Three Dimensions. *Proceedings of the Institution of Mechanical Engineers, Part H: Journal of Engineering in Medicine* **2017**, *231* (7), 597–616.

(53) Hollister, S. J. Porous Scaffold Design for Tissue Engineering. *Nature materials* **2005**, *4* (7), 518.

(54) Arnaoutova, I.; George, J.; Kleinman, H. K.; Benton, G. The Endothelial Cell Tube Formation Assay on Basement Membrane Turns 20: State of the Science and the Art. *Angiogenesis* **2009**, *12* (3), 267–274.

(55) Hofmann, A.; Ritz, U.; Verrier, S.; Eglin, D.; Alini, M.; Fuchs, S.; Kirkpatrick, C. J.; Rommens, P. M. The Effect of Human Osteoblasts on Proliferation and Neo-Vessel Formation of Human Umbilical Vein Endothelial Cells in a Long-Term 3D Co-Culture on Polyurethane Scaffolds. *Biomaterials* **2008**, *29* (31), 4217–4226. https://doi.org/10.1016/j.biomaterials.2008.07.024.

(56) PAUTKE, C.; SCHIEKER, M.; TISCHER, T.; KOLK, A.; NETH, P.; MUTSCHLER, W.; MILZ, S. Characterization of Osteosarcoma Cell Lines MG-63, Saos-2 and U-2 OS in Comparison to Human Osteoblasts. *Anticancer research* **2004**, *24* (6), 3743–3748.

(57) Moroni, L.; Burdick, J. A.; Highley, C.; Lee, S. J.; Morimoto, Y.; Takeuchi, S.; Yoo, J. J. Biofabrication Strategies for 3D in Vitro Models and Regenerative Medicine. *Nature Reviews Materials* **2018**, *3* (5). https://doi.org/10.1038/s41578-018-0006-y.

(58) Clyne, A. M.; Swaminathan, S.; Lantada, A. D. Biofabrication Strategies for Creating Microvascular Complexity. *Biofabrication* **2019**, *11* (3), 032001. https://doi.org/10.1088/1758-5090/ab0621.

(59) Gao, G.; Kim, B. S.; Jang, J.; Cho, D.-W. Recent Strategies in Extrusion-Based Three-Dimensional Cell Printing toward Organ Biofabrication. *ACS Biomaterials Science & Engineering* **2019**, *5* (3), 1150–1169. https://doi.org/10.1021/acsbiomaterials.8b00691.

(60) L'Heureux, N.; Dusserre, N.; Konig, G.; Victor, B.; Keire, P.; Wight, T. N.; Chronos, N. A. F.; Kyles, A. E.; Gregory, C. R.; Hoyt, G.; et al. Human Tissue-Engineered Blood Vessels for Adult Arterial Revascularization. *Nat Med* **2006**, *12* (3), 361–365.

(61) Mathews, D. T.; Birney, Y. A.; Cahill, P. A.; McGuinness, G. B. Vascular Cell Viability on Polyvinyl Alcohol Hydrogels Modified with Water-Soluble and -Insoluble Chitosan. *Journal of Biomedical Materials Research Part B: Applied Biomaterials* **2008**, *84B* (2), 531–540. https://doi.org/10.1002/jbm.b.30901.

(62) Fatih Canbolat, M.; Tang, C.; Bernacki, S. H.; Pourdeyhimi, B.; Khan, S. Mammalian Cell Viability in Electrospun Composite Nanofiber Structures. *Macromolecular Bioscience* **2011**, *11* (10), 1346–1356. https://doi.org/10.1002/mabi.201100108.

(63) Mahmoud, K. A.; Mena, J. A.; Male, K. B.; Hrapovic, S.; Kamen, A.; Luong, J. H. T. Effect of Surface Charge on the Cellular Uptake and Cytotoxicity of Fluorescent Labeled Cellulose Nanocrystals. *ACS Applied Materials & Interfaces* **2010**, *2* (10), 2924–2932. https://doi.org/10.1021/am1006222.

(64) Baker, M. I.; Walsh, S. P.; Schwartz, Z.; Boyan, B. D. A Review of Polyvinyl Alcohol and Its Uses in Cartilage and Orthopedic Applications. *Journal of Biomedical Materials Research Part B: Applied Biomaterials* **2012**, *100* (5), 1451–1457.

(65) Burstein, N. L. Corneal Cytotoxicity of Topically Applied Drugs, Vehicles and Preservatives. *Survey of ophthalmology* **1980**, *25* (1), 15–30.

(66) DeMerlis, C. C.; Schoneker, D. R. Review of the Oral Toxicity of Polyvinyl Alcohol (PVA). *Food and Chemical Toxicology* **2003**, *41* (3), 319–326.

(67) Wang, M.; Li, Y.; Wu, J.; Xu, F.; Zuo, Y.; Jansen, J. A. In Vitro and in Vivo Study to the Biocompatibility and Biodegradation of Hydroxyapatite/Poly (Vinyl Alcohol)/Gelatin Composite. *Journal of Biomedical Materials Research Part A* **2008**, *85* (2), 418–426.

(68) Garipcan, B.; Maenz, S.; Pham, T.; Settmacher, U.; Jandt, K. D.; Zanow, J.; Bossert, J. Image Analysis of Endothelial Microstructure and Endothelial Cell Dimensions of Human Arteries–a Preliminary Study. *Advanced Engineering Materials* **2011**, *13* (1-2).

(69) Browder, T.; Folkman, J.; Pirie-Shepherd, S. The Hemostatic System as a Regulator of Angiogenesis. *Journal of Biological Chemistry* **2000**, *275* (3), 1521–1524.

(70) Sarkar, S.; Sales, K. M.; Hamilton, G.; Seifalian, A. M. Addressing Thrombogenicity in Vascular Graft Construction. *Journal of Biomedical Materials Research Part B: Applied Biomaterials* **2007**, *82* (1), 100–108.

(71) Seifu, D. G.; Purnama, A.; Mequanint, K.; Mantovani, D. Small-Diameter Vascular Tissue Engineering. *Nature Reviews Cardiology* **2013**, *10* (7), 410. https://doi.org/10.1038/nrcardio.2013.77.

(72) Bouchet, M.; Gauthier, M.; Maire, M.; Ajji, A.; Lerouge, S. Towards Compliant Small-Diameter Vascular Grafts: Predictive Analytical Model and Experiments. *Materials Science and Engineering: C* **2019**, *100*, 715–723. https://doi.org/10.1016/j.msec.2019.03.023.

(73) Villars, F.; Bordenave, L.; Bareille, R.; Amedee, J. Effect of Human Endothelial Cells on Human Bone Marrow Stromal Cell Phenotype: Role of VEGF? *Journal of cellular biochemistry* **2000**, *79* (4), 672–685.

(74) Furumatsu, T.; Shen, Z. N.; Kawai, A.; Nishida, K.; Manabe, H.; Oohashi, T.; Inoue, H.; Ninomiya, Y. Vascular Endothelial Growth Factor Principally Acts as the Main Angiogenic Factor in the Early Stage of Human Osteoblastogenesis. *Journal of biochemistry* **2003**, *133* (5), 633–639.

(75) Kang, Y.; Kim, S.; Fahrenholtz, M.; Khademhosseini, A.; Yang, Y. Osteogenic and Angiogenic Potentials of Monocultured and Co-Cultured Human-Bone-Marrow-Derived Mesenchymal Stem Cells and Human-Umbilical-Vein Endothelial Cells on Three-Dimensional Porous Beta-Tricalcium Phosphate Scaffold. *Acta biomaterialia* **2013**, *9* (1), 4906–4915. https://doi.org/10.1016/j.actbio.2012.08.008.

(76) Nguyen, L. H.; Annabi, N.; Nikkhah, M.; Bae, H.; Binan, L.; Park, S.; Kang, Y.; Yang, Y.; Khademhosseini, A. Vascularized Bone Tissue Engineering: Approaches for Potential Improvement. *Tissue Engineering Part B: Reviews* **2012**, *18* (5), 363–382. https://doi.org/10.1089/ten.teb.2012.0012.

(77) Stahl, A.; Wenger, A.; Weber, H.; Stark, G. B.; Augustin, H. G.; Finkenzeller, G. Bi-Directional Cell Contact-Dependent Regulation of Gene Expression between Endothelial Cells and Osteoblasts in a Three-Dimensional Spheroidal Coculture Model. *Biochemical and biophysical research communications* **2004**, *322* (2), 684–692.

(78) Kirkpatrick, C. J.; Wagner, M.; Hermanns, I.; Klein, C. L.; Köhler, H.; Otto, M.; Van Kooten, T. G.; Bittinger, F. Physiology and Cell Biology of the Endothelium: A Dynamic Interface for Cell Communication. *International Journal of Microcirculation* **1997**, *17* (5), 231–240.

(79) Vattikuti, R.; Towler, D. A. Osteogenic Regulation of Vascular Calcification: An Early Perspective. *American Journal of Physiology-Endocrinology And Metabolism* **2004**, *286* (5), E686–E696.

(80) Hinton, T. J.; Jallerat, Q.; Palchesko, R. N.; Park, J. H.; Grodzicki, M. S.; Shue, H.-J.; Ramadan, M. H.; Hudson, A. R.; Feinberg, A. W. Three-Dimensional Printing of Complex Biological Structures by Freeform Reversible Embedding of Suspended Hydrogels. *Science advances* **2015**, *1* (9), e1500758. https://doi.org/10.1126/sciadv.1500758.

(81) Kang, H.-W.; Lee, S. J.; Ko, I. K.; Kengla, C.; Yoo, J. J.; Atala, A. A 3D Bioprinting System to Produce Human-Scale Tissue Constructs with Structural Integrity. *Nature Biotechnology* **2016**, *34*, 312. https://doi.org/10.1038/nbt.3413.

(82) Hospodiuk, M.; Dey, M.; Sosnoski, D.; Ozbolat, I. T. The Bioink: A Comprehensive Review on Bioprintable Materials. *Biotechnology Advances* **2017**, *35* (2), 217–239. https://doi.org/10.1016/j.biotechadv.2016.12.006.

Abbreviations

aCA	Apparent contact angle
ATR	Attenuated total reflectance
DCM	Dichloromethane
DE	Degree of esterification
DMF	*N,N*-dimethylformamide
DMSO	Dimethyl sulfoxide
$\overline{\mathbf{DP_n}}$	Number-average degree of polymerization
DSC	Differential scanning calorimetry
ECM	Extracellular matrix
FDA	Food and drug administration
FTIR	Fourier-transform infrared spectroscopy
G/SA	Molar ratio glycerol/sebacic acid
HFIP	1,1,1,3,3,3-hexafluoro-propan-2-ol
HPβCD	Hydroxypropyl-β-cyclodextrin
NMR	Nuclear magnetic resonance
PCL	Poly-ε-caprolactone
PEG	Polyethylene glycol
PGS	Poly(glycerol sebacate) (elastomer)
PLA	Poly(acid lactic)
pPGS	Poly(glycerol sebacate) (prepolymer)
PVP	Polyvinylpyrrolidone
PVA	Polyvinyl alcohol
SEC	Size exclusion chromatography
SEM	Scanning electron microscope
$\mathbf{T_g}$	Glass transition temperature
THF	Tetrahydrofuran

TPE	Thermoplastic elastomer
TPU	Thermoplastic polyurethane
UTS	Ultimate tensile strength
UV	Ultraviolet
wt%	Weight percentage

Communications

Publications:

- F. Flaig, H. Ragot, A. Simon, G. Revet, M. Kitsara, L. Kitasato, A. Hébraud, O. Agbulut, G. Schlatter*, « Design of functional electrospun scaffolds based on poly(glycerol sebacate) elastomer and poly(lactic acid) for cardiac tissue engineering »*, submitted to ACS Biomaterials Science & Engineering.
- C. F. Bellani, K. Yue, F. Flaig, A. Hébraud, P. Ray, N. Annabi, H. S. S. de Araújo, M. C. Branciforti, A. M. Minarelli Gaspar, S.-R. Shin, A. Khademhosseini, G. Schlatter, *« Suturable elastomeric tubular grafts with patterned porosity for rapid vascularization of 3D constructs »*, submitted to ACS Biomaterials Science & Engineering.
- F. Flaig, Ö. Uyumaz, C. F. Bellani, A. Hébraud, G. Schlatter, *« Fully crosslinked elastomeric nanofibrous scaffolds based on poly(glycerol sebacate) and cyclodextrin matching the mechanical properties of the myocardial tissue »*, under preparation.

Oral communications:

- F. Flaig, A. Hébraud, G. Schlatter, « *Synthèse, caractérisation et mise en œuvre du poly(sébaçate de glycérol) pour l'ingénierie cardiaque »*, **45èmes Journées d'Études des Polymères**, Gravelines, France, october 2017.
- F. Flaig, A. Hébraud, G. Schlatter, « *Nanofibrous bio-inspired scaffolds for cardiac engineering »*, **ED182 PhD student's Congress**, Strasbourg, France, nevember 2017.
- G. Schlatter, F. Flaig, M. Liang, A. Hébraud, *« 2D and 3D controlled deposition of electrospun nanofibers: from the mechanisms to the applications »*, **Europolymer Conference (EUPOC)**, Como, Italy, may 2019.
- F. Flaig, A. Hébraud, G. Schlatter, « *Nanofibrous bio-inspired elastomeric scaffolds based on poly(glycerol sebacate) for cardiac tissue engineering »*, **European Polymer Congress EPF 2019**, Hersonissos, Greece, june 2019.
- F. Flaig, A. Hébraud, G. Schlatter, « Vers des élastomères nanofibreux pour l'ingénierie tissulaire cardiaque*»*, **Journée Scientifique et Technique de l'ICPEES,** Strasbourg, France, july 2019.

Florence FLAIG

École doctorale
Physique, chimie-physique
ED 182
Université de Strasbourg

Elaboration of nanofibrous biomimetic materials based on poly(glycerol sebacate) for cardiac tissue engineering

Résumé

L'ingénierie tissulaire cardiaque permet de promouvoir la régénération du cœur. Cette technique repose sur l'utilisation d'un substrat où se développent les cellules. Pour être performant, ce substrat doit mimer les propriétés mécaniques et structurelles du myocarde. Pour cette thèse, le poly(sébaçate de glycérol) (PGS), un élastomère biocompatible, a été choisi comme matériau de base. Sa synthèse a été étudiée, montrant quels sont les paramètres à contrôler pour obtenir les propriétés attendues. En particulier, des propriétés mécaniques adaptées au muscle cardiaque peuvent être obtenues. La méthode de mise œuvre choisie est l'élelectrofilage, qui permet la fabrication de mats nanofibreux imitant la structure des tissus biologiques. Comme la mise en forme du PGS est rendue difficile par son insolubilité, il a été électrofilé à l'état de prépolymère, mélangé à un autre polymère. Des patchs cardiaques à base d'acide polylactique et de PGS ont pu être fabriqués. Par ailleurs, en mélangeant le PGS à de la polyvinylpyrrolidone et de la cyclodextrine, des membranes élastomères aux propriétés mécaniques adaptées au cœur ont pu être préparées. Enfin, le PGS a été utilisé sous forme de particules afin d'organiser des dépôts de fibres de PLA en structures capables d'améliorer le développement des cellules et des tissus.

Mots-clés : *ingénierie tissulaire, substrats nanofibreux, électrofilage, électrospraying, élastomère, biopolyester*

Abstract

Cardiac tissue engineering aims to regenerate the heart. This technic relies on the use of a scaffold where the cells can proliferate. To be efficient, this scaffold should mimic mechanical and structural properties of the myocardium. In this thesis, poly(glycerol sebacate) (PGS) was chosen as building material. Its synthesis was studied, showing which parameters should be controlled in order to get the expected properties. In particular, mechanical properties fitting cardiac muscle's ones can be obtained. Electrospinning was chosen as process method. This method allows the fabrication of nanofibrous mats mimicking biological tissues structure. As PGS processing is difficult because it is insoluble, it was electrospun at the prepolymer state, blended with another polymer. In this way, cardiac patches composed of poly(lactic acid) and PGS were fabricated. Furthermore, PGS was blended with polyvinylpyrrolidone and cyclodextrin to prepare elastomeric membranes with mechanical properties adapted to the heart. Finally, PGS was used in particles in order to organize PLA fibers deposits into structures able to improve cells and tissues development.

Keywords: *tissue engineering, nanofibrous scaffolds, electrospinning, electrospraying, biopolyester, elastomer*